Exploring exotic states with twisted boundary conditions

Dissertation
zur
Erlangung des Doktorgrades (Dr. rer. nat.)
der
Mathematisch-Naturwissenschaftlichen Fakultät
der
Rheinischen Friedrich-Wilhelms-Universität Bonn

von
Dimitri Agadjanov
aus
Tbilisi, Georgien

Bonn, 2017

Dieser Forschungsbericht wurde als Dissertation von der Mathematisch-Naturwissenschaftlichen Fakultät der Universität Bonn angenommen und ist auf dem Hochschulschriftenserver der ULB Bonn `http://hss.ulb.uni-bonn.de/diss_online` elektronisch publiziert.

1. Gutachter:	Prof. Dr. Ulf-G. Meißner
2. Gutachter:	PD. Dr. Akaki Rusetsky
Tag der Promotion:	11.09.2017
Erscheinungsjahr:	2017

Abstract

The goal of this thesis is to develop methods to study the nature and properties of exotic hadrons from lattice simulations. The main focus lies in the application of twisted boundary conditions. The thesis consists of a general introduction and the collection of three papers, represented respectively in three chapters. The introduction of the thesis reviews the theoretical background, which is further used in the rest of the thesis. Further, in Chapter 1, implementing partially twisted boundary conditions in the scalar sector of lattice QCD is studied. In Chapter 2, we develop a method to study the content of the exotic hadrons by determining the wave function renormalization constant from lattice simulations, exploiting the dependence of the spectrum on the twisted boundary conditions. Finally, Chapter 3 deals with a novel method to study the multi-channel scattering problem in a finite volume, which is relevant for exotic states. Its key idea is to extract the complex hadron-hadron optical potential, avoiding the difficulties, accociated with the solution of the multi-channel Lüscher equation.

Acknowledgements

First of all, I express my deep gratitude to Prof. Dr. Ulf-G. Meißner and PD Dr. Akaki Rusetsky for giving me the opportunity to work on this fascinating project in one of the world-leading theory groups. I thank them for their excellent supervision and constant support during the years of PhD work.

I thank further, my colleagues, former office mates and simply good friends Dr. Maxim Mai and Dr. Michael Döring for their support in scientific matters and beyond.

Needless to say, it is the people who create the scientific atmosphere. I thank all members of the theory division for that.

I also thank all my friends both in Germany a nd Georgia.

Finally, I am very thankful to my brother Andrei and my parents Giorgi and Tamara, for their understanding, support and motivation.

I thank the Sino-German CRC 110: "Symmetries and the Emergence of Structure in QCD " and the Bonn-Cologne Graduate School of Physics and Astronomy for financial support.

Contents

CHAPTER 1

Introduction

1.1 Quantum Chromodynamics

According to the current physical picture there exist four fundamental forces in Nature which describe all possible interactions between elementary particles. These are the strong, electromagnetic, weak and gravitational forces. The first three are unified in the so-called Standard Model (SM) of particle physics, whereas gravity, for a number of reasons, is not. The Standard model is a gauge field theory, in which the building blocks are *matter fields* and interactions are mediated by *gauge bosonic fields*. The Standard Model is considered to be extremely successful in describing a large number of experiments in elementary particle physics.The masses of gauge bosons are essentially generated through the Higgs mechanism. The resent discovery of Higgs particle has confirmed the validity of the SM [1].

In the present thesis we will focus on the strong sector of the Standard Model, i.e. Quantum Chromodynamics (QCD). It is a theory that describes the interaction between spin $1/2$ quark fields and spin-1 massless gauge fields, called gluons. The underlying gauge group is colour $SU(3)$. The QCD Lagrangian has the following form:

$$\mathcal{L} = -\frac{1}{4}F^{a,\alpha\beta}F_a^{\alpha\beta} + \bar{q}_f^i(i\gamma^\mu D_{\mu,ij} - \delta_{ij}m_f)q_f^j, \tag{1.1}$$

where the spinors q represent quark fields and the indices $i, j, ...$ run over the colour degrees of freedom (these are r, b, g). Summation over flavor index corresponds to six quark flavours f={u, d, s, c, t, b } with corresponding masses m_f. In addition, quarks of flavour d, c and b carry an electric charge $-1/3$, whereas u, c, and t quarks have charge $+2/3$ in units of the elementary charge. Further, $F^a_{\alpha\beta}$ is the field strength tensor, derived from the gluon field A^a_α,

$$F^a_{\alpha\beta} = \partial_\alpha A^a_\beta - \partial_\beta A^a_\alpha - g f^{abc} A^b_\alpha A^c_\beta \tag{1.2}$$

and D is the gauge-covariant derivative

$$D_{\mu,ij} = \delta_{ij}\partial_\mu + igt^a_{ij}A^a_\mu, \tag{1.3}$$

where g denotes the coupling constant, which determines the strength of the interaction and f^{abc} are structure constants of the $SU(3)$ Lie algebra $[t^a, t^b] = if^{abc}t^c$, with the generator $t^a = \lambda^a/2$ (λ^a denote the Gell-Mann matrices).

In this thesis, we will be mainly interested in QCD at low energies. Note that, due to loop corrections, the coupling g depends on the renormalization scale, i.e. on the typical energy in the system in question

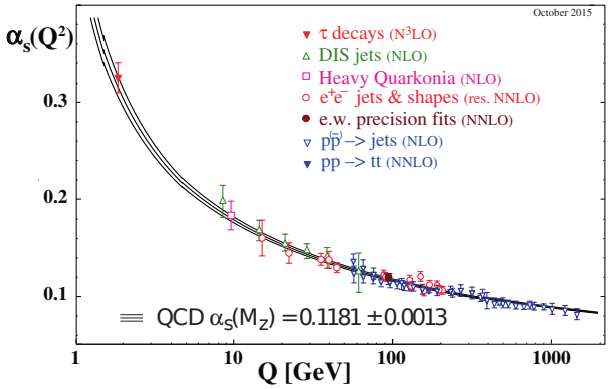

Figure 1.1: Running coupling constant as a function of transfer momentum Q, [2]

(see Fig. (1.1)). In the high-energy regime of about few GeV, quarks and gluons interact weakly and one speaks about the *asymptotic freedom* [3, 4]. In this case, the coupling is small enough and perturbative methods lead to consistent physical results. On the other hand, at energies below one GeV, the perturbative series no longer converge and the theory has no predictive power. Physically, at low energies, quarks and gluons are bound into hadrons, which become effective dynamical degrees of freedom. Now, the question arises, whether we can formulate a most general quantum field theory (in terms of hadronic degrees of freedom) which shares all symmetries of underlying theory (QCD) and correctly describes the low-energy dynamics. A theorem by Weinberg gives positive answer to this question and provides a recipe to costruct such a theory [5]:

"...if one writes down the most general possible Lagrangian, including all terms consistent with assumed symmetry principles, and then calculates matrix elements with this Lagrangian to any given order of perturbation theory, the result will simply be the most general possible S-matrix consistent with analyticity, perturbative unitarity, cluster decomposition and the assumed symmetry principles"

Using this guiding principle, we will see in the next section, how to construct the effective field theory of QCD, called Chiral Perturbation Theory (ChPT). But before proceeding further, let us have closer a look at the underlying symmetries of QCD.

The masses of u, d and s quarks are much smaller than the typical low-energy scale Λ_χ=1 GeV. Therefore let us consider the massless limit of the QCD containing only light quarks

$$\mathcal{L}_0 = -\frac{1}{4}F^{a,\alpha\beta}F_a^{\alpha\beta} + \bar{q}_f^i(i\gamma^\mu D_{\mu,ij})q_f^j. \tag{1.4}$$

The Lagrangian is invariant under left- and right- hand chiral transformations of quark fields, given by

$$q_R = \frac{1}{2}(1+\gamma_5)q, \qquad q_L = \frac{1}{2}(1-\gamma_5)q. \tag{1.5}$$

The kinetic term may be written as:

$$\bar{q}(i\gamma^\mu D_\mu)q = \bar{q}_L(i\gamma^\mu D_\mu)q_L + \bar{q}_R(i\gamma^\mu D_\mu)q_R. \tag{1.6}$$

We see that components with different chirality decouple in the kinetic term. Note that the opposite is

true for the mass term. It is clear that $\mathcal{L}_0$ is invariant under independent unitary transformations of the left- and right-handed quark fields $R \in U(3)_R$ and $L \in U(3)_L$:

$$q_R \to Rq_R, \quad q_L \to Lq_L \tag{1.7}$$

The decomposition of the the full symmetry group has the form :

$$U(3)_L \times U(3)_R = U(1)_A \times U(1)_V \times SU(3)_V \times SU(3)_A, \tag{1.8}$$

where the subscripts V and A denote vector ($R + L$) and axial-vector ($R - L$) transformations correspondingly. The subgroup $U_A(1)$ is not a symmetry of the quantum theory due to an anomaly: even though the action remains invariant, the measure of the path integral is not [6–8]. Furthermore, the $U_V(1)$ symmetry is responsible for the baryon number conservation. The question to be answered to is how the remaining part $SU(3)_V \times SU(3)_A = SU(3)_L \times SU(3)_R$, called chiral symmetry, is realized in Nature. Note that, according to the Vafa-Witten theorem, $SU(3)_V$ cannot be spontaneously broken in QCD [9]. Furthermore, there is a strong evidence that the $SU(3)_R \times SU(3)_L$ is spontaneously broken down to the vectorial subgroup $SU(3)_V$. Otherwise, there would be observed parity doublets in the hadronic spectrum, which is not the case. In other words, the symmetry is realized in the Nambu-Goldstone mode rather then Wigner-Weyl one, and therefore there schould exist massless spin zero particles, called Goldstone bosons [10–12]. According to Goldstone's theorem, the number of such particles is given by the number of generators of the broken symmetry group, which is in our case eight. This picture corresponds to the octet of pseudoscalar mesons (π, η, K), whose finite masses can be traced back to the explicit symmetry breaking due to non-vanishing quark masses.

Another non-perturbative approach to get insight into the low-energy hadron interactions is Lattice QCD. Its idea is to evalute QCD the path integral numerically on a discretized space-time lattice. We will outline this method in sec. 1.3.

1.2 Chiral perturbation theory

As we have seen in the previous section, the interactions between quarks and gluons, ruled by QCD, are highly non-perturbative at the energies below the breaking scale of chiral symmetry $\Lambda_\chi \approx 1\text{GeV}$. This makes any description of the low-energy hadronic world in terms of quark and gluons very difficult. On the other hand, it is an experimental fact that the low-energy spectrum of the theory contains only the octet of the light pseudoscalar mesons (π, K, η) and they interact weakly, both among themselves and with the nucleons. We can expect that the pseudoscalar mesons are the relevant degrees of freedom at low energies and it is possible to construct such an effective field theory that makes possible to analyse the low energy structure of QCD.

As mentioned earlier, the theoretical basis, which determined a successful application of such effective field theories was formulated by Weinberg [5] as well as by Gasser and Leutwyler, Refs. [13–15]. Chiral perturbation theory (ChPT) provides a systematic method for discussing the consequences of the global flavour symmetries of QCD at low energies by means of an effective field theory. At very low energies, the corresponding Lagrangian is expressed in terms of the members of the octet of the light pseudoscalar mesons. Such an effective field theory is called the ChPT for mesons. We will outline its construction, following the works by Gasser and Leutwyler [14, 15].

In order to relate the effective theory with underlying theory, consider the generating functional of QCD in the presence of external fields. Let us promote the global $\text{SU}(3)_L \times \text{SU}(3)_R$ to a local symmetry. In order to do so, we equip the QCD Lagrangian Eq. (1.4) with external fields $v^\mu(x), a^\mu(x), s(x), p(x)$,

coupled to the currents $V^{\mu,a}$,V^{μ}, $A^{\mu,a}$, associated with the global symmetry, as well as scalar $S = \bar{q}q$ and pseudoscalar $P = i\bar{q}\gamma^5 q$ densities:

$$\mathcal{L} = \mathcal{L}_0 + \mathcal{L}_{ext} = \mathcal{L}_0 + \bar{q}\gamma_\mu(v^\mu + \gamma_5 a^\mu)q - \bar{q}(s - i\gamma_5 p)q. \tag{1.9}$$

The singlet scalar source a_μ^0 is assumed to be zero in order to avoid the discussion of the anomalous sector of the the theory. Note that external fields are color-neutral hermitian matrices. Then the generating functional, which is a vacuum-to-vacuum transition amplitude in the presence of external fields, has the form:

$$\begin{aligned}\exp[iZ(v,a,s,p)] &= \langle 0;\mathrm{o}ut|0;\mathrm{i}n\rangle_{v,a,s,p} = \langle 0|T\exp\left[i\int d^4x\mathcal{L}_{ext}(x)\right]|0\rangle \\ &= \langle 0|T\exp\left(i\int d^4x\bar{q}(x)\{\gamma_\mu[v^\mu(x) + \gamma_5 a^\mu(x)] - (s(x) - i\gamma_5 p(x))\}q(x)\right)|0\rangle, \\ &.\end{aligned} \tag{1.10}$$

The quark mass matrix M =diag(m_u, m_d, m_s) is contained in the scalar field $s(x)$. The Green functions formed with the current operators of massless QCD are obtained by expanding the generating functional around $v^\mu = v^\mu_{(s)} = a^\mu = s = p = 0$, whereas for the real world one has to expand around $v^\mu = v^\mu_{(s)} = a^\mu = p = 0$, $s(x) = M$. In the absence of anomalies, the Ward identities, which express the symmetry properties of the theory in terms of the Green functions, are equivalent to gauge invariance of the generating functional under local transformations of the external fields given by

$$\begin{aligned} r_\mu &\mapsto Rr_\mu R^\dagger + iR\partial_\mu R^\dagger, \\ l_\mu &\mapsto Ll_\mu L^\dagger + iL\partial_\mu L^\dagger, \\ s + ip &\mapsto R(s + ip)L^\dagger, \\ s - ip &\mapsto L(s - ip)R^\dagger, \end{aligned} \tag{1.11}$$

where $R(x)$ and $L(x)$ are space-time-dependent SU(3) matrices and $r_\mu = v_\mu + a_\mu, \quad l_\mu = v_\mu - a_\mu$.

Now, in accordance with Weinberg's conjecture the QCD generating functional can be expressed through the effective Lagrangian $\mathcal{L}_{eff}$ with the same external fields v^μ, a^μ, p, s:

$$\exp[iZ(v,a,s,p)] = \int [dU]\exp\left(i\int d^4x\mathcal{L}_{eff}(U,v,a,s,p)\right) \tag{1.12}$$

This formula provides a link between the underlying (QCD) and the effective theory (ChPT). While the left-hand side represents the generating functional for the Green functions of the underlying theory, the right-hand side only involves the effective Lagrangian.

It should be stressed out that Eq. (1.12) is valid only, when the typical momenta in processes are small, $q \ll \Lambda_\chi$ (the low energy sector of the theory). Only with this condition, the Green functions can be expanded in powers of the external momenta. This amounts to an expansion in derivatives of the external fields. However, the low-energy expansion is not a simple Taylor expansion ,since the Goldstone bosons generate poles at $q^2 = 0$ (in the chiral limit) or $q^2 = M_\pi^2$ (for finite quark masses, M_π is the pion mass). The low-energy expansion involves two small parameters, the external momenta q and the quark masses M. Then, one expands in powers of these with the ratio M/q^2 fixed . Therefore we can approximate the

underlying generating functional in the following way :

$$Z_{QCD}(v,a,s,p) = Z_{eff}(v,a,s,p)^{(2)} + Z_{eff}(v,a,s,p)^{(4)} + ..., \tag{1.13}$$

Note that the Goldstone fields enter the measure $[dU]$ and effective Lagrangian in path integral (see Eq.(1.12)) in a peculiar way. While the external fields transform according to Eq. (1.11, the meson fields ϕ^a, which we associate with the Goldstone bosons, transform with a nonlinear representation of $G = \mathrm{SU}(3)_L \times \mathrm{SU}(3)_R$, spontaneously broken down to $H = SU(3)_V$. According to formalism developed in Refs. [16, 17] , the meson fields lie in the so-called coset space G/H. We collect them in a unitary matrix field $U(\phi)$ transforming as

$$U(\phi) \mapsto RU(\phi)L^\dagger \tag{1.14}$$

under local chiral rotations $\mathrm{SU}(3)_L \times \mathrm{SU}(3)_R$. There are different parametrizations of $U(\phi)$ corresponding to different choices of coordinates for the coset space. For convenience,we choose the matrix $U(x) \equiv U(\phi(x))$ to be the SU(3) matrix:

$$U(x) = \exp\left(i\frac{\phi(x)}{F_0}\right),$$

where

$$\phi(x) \quad = \quad \sum_{a=1}^{8} \lambda_a \phi_a(x) \equiv \begin{pmatrix} \pi^0 + \frac{1}{\sqrt{3}}\eta & \sqrt{2}\pi^+ & \sqrt{2}K^+ \\ \sqrt{2}\pi^- & -\pi^0 + \frac{1}{\sqrt{3}}\eta & \sqrt{2}K^0 \\ \sqrt{2}K^- & \sqrt{2}\bar{K}^0 & -\frac{2}{\sqrt{3}}\eta \end{pmatrix}. \tag{1.15}$$

The local nature of G requires the introduction of a covariant derivative

$$d_\mu U = \partial_\mu U - ir_\mu U + iUl_\mu, \;\; d_\mu U \xrightarrow{\mathrm{G}} V_R d_\mu U V^\dagger \tag{1.16}$$

Finally, we introduce the linear combination

$$\chi = 2B_0(s + ip),$$

with the scalar and pseudoscalar external fields, where B_0 is a constant which can be related to the quark condensate. The effective Lagrangian consists of the infinite string of terms, containing the building blocks U, v, a, s, p and multiple derivatives acting on it. In accordance with Eq. (1.13), the Lagrangian is ordered, according to powers of the expansion parameter, which is equal to the number of the derivatives in a given term. To construct each term in $\mathcal{L}_{eff}$, building blocks should be counted as:

$$U = O(1),\; D_\mu U = O(p),\; r_\mu, l_\mu = O(p),\; \chi = O(p^2). \tag{1.17}$$

From Lorentz invariance, we conclude that only the terms with even number of derivatives can appear in the effective Lagrangian:

$$\mathcal{L}_{eff} = \mathcal{L}_2 + \mathcal{L}_4 + \mathcal{L}_6 + ... \tag{1.18}$$

The $\mathcal{L}_2$ contains either two derivatives, or one quark mass term. In other words, $\mathcal{L}_2$, called the leading-order Lagrangian, contains terms of the chiral order p^2; $\mathcal{L}_4$ contains terms of chiral order p^4 etc.

From the building blocks, specified in Eq. (1.17), one constructs the most general, Lorentz,-C, -P

invariant local effective Lagrangian at leading order :

$$\mathcal{L}_2 = \frac{F_0^2}{4}\mathrm{Tr}[d_\mu U (d^\mu U)^\dagger] + \frac{F_0^2}{4}\mathrm{Tr}[\chi U^\dagger + U\chi^\dagger]. \tag{1.19}$$

Here, $\mathcal{L}_2$ contains two free parameters, called low-energy constants, F_0 and B_0. In order to determine the constant F_0, note that the Noether currents $V^{\mu,a}, A^{\mu,a}$ from $\mathcal{L}_2$ are given by

$$V^{\mu,a} = -i\frac{F_0^2}{4}\mathrm{Tr}\left(\lambda_a[U, \partial^\mu U^\dagger]\right), \tag{1.20}$$

$$A^{\mu,a} = -i\frac{F_0^2}{4}\mathrm{Tr}\left(\lambda_a\{U, \partial^\mu U^\dagger\}\right). \tag{1.21}$$

Then, to find the leading term, one should expand $A^{\mu,a}$ in the meson fields,

$$A^{\mu,a} = -i\frac{F_0^2}{4}\mathrm{Tr}\left(\lambda_a\left\{1 + \cdots, -i\frac{\lambda_b \partial^\mu \phi_b}{F_0} + \cdots\right\}\right) = -F_0 \partial^\mu \phi_a + \cdots$$

such that we can calculate the matrix element of the axial current between a one-boson state and the vacuum,

$$\begin{aligned}\langle 0|A^{\mu,a}(x)|\phi^b(p)\rangle &= \langle 0| - F_0 \partial^\mu \phi_a(x)|\phi^b(p)\rangle \\ &= ip^\mu F_0 \exp(-ip\cdot x)\delta^{ab}.\end{aligned}$$

Thus, the F_0 can be identified with the pion (meson) decay constant F_π in the chiral limit, which is measured in pion decay $\pi^+ \to \ell^+ \nu_\ell$, $F_0 = F_\pi[1 + O(M)]$. The constant B_0, which appears in the field χ, is related to the explicit symmetry breaking. One can choose $p = 0$ and $s = M$ ($\chi = 2B_0 M$), and expand the symmetry breaking part of $\mathcal{L}_2$ in powers of the meson fields

$$\mathcal{L}_2^{SB} = \frac{1}{2}F_0^2 B_0 \mathrm{Tr}[M(U + U^\dagger)] = (m_u + m_d + m_s)B_0[F_0^2 - \frac{\phi^2}{2} + \frac{\phi^4}{24F_0^2} + \cdots], \tag{1.22}$$

where the superscript SB refers to symmetry breaking. The first term in the right hand side of Eq.(1.22) is related to the vacuum energy, while the second and the third are meson mass and interaction terms, respectively. One can show that B_0 is proportional to vacuum expectation value of quark condensate:

$$\langle 0|\bar{q}q|0\rangle = -3F_0^2 B_0[1 + O(M)]. \tag{1.23}$$

Furthermore, the meson masses, calculated from Eq. (1.22), in the case of isospin symmetry ($m_u = m_d = m$) are given by

$$\begin{aligned}M_\pi^2 &= 2mB_0[1 + O(M)], \\ M_K^2 &= (m + m_s)B_0[1 + O(M)], \\ M_\eta^2 &= \frac{2}{3}(m + 2m_s)\, B_0[1 + O(M)].\end{aligned} \tag{1.24}$$

Those results, in combination with Eq.1.23, are referred to as the Gell-Mann-Oakes-Renner relations

[18]. Moreover, the linear combination of above masses yields the Gell-Mann-Okubo relation [19]

$$4M_K^2 = 4B_0(m + m_s) = 2B_0(m + 2m_s) + 2B_0 m = 3M_\eta^2 + M_\pi^2, \tag{1.25}$$

which is found to be fulfilled in Nature to a 7% accuracy.

So far, we have only considered the chiral Lagrangian for mesons at leading order, i.e. $O(p^2)$. Going to higher orders will systematically improve the accuracy of calculations. Moreover, it is even necessary to include higher orders, since tree level contributions from $\mathcal{L}_2$ violate unitarity. Indeed, consider pion-pion scattering to leading order. The scattering amplitude in the isospin limit, $m_u = m_d$, can be decomposed as

$$M(\pi^a\pi^b \to \pi^c\pi^d) = \delta^{ab}\delta^{cd}A(s,t,u) + \delta^{ac}\delta^{bd}A(t,u,s) + \delta^{ad}\delta^{bc}A(u,s,t)\ ,$$

where u, s, t are the so-called Mandelstam variables and $A(s,t,u)$ is the invariant amplitude. The tree-level amplitude $A(s,t,u)$, calculated from $\mathcal{L}_2$,

$$A(s,t,u) = \frac{s - M_\pi^2}{F^2}\ ,$$

is real-valued. However, the unitarity requires the partial waves t_l^I to obey

$$\mathrm{Im}\, t_\ell^I = \sqrt{1 - \frac{4M_\pi^2}{s}}\left|t_\ell^I\right|^2\ .$$

Here, I denotes the isospin $I = 0, 1, 2$ and l is the angular momentum $l = 0, 1, 2, \cdots$.The correct imaginary parts are only generated perturbatively by loops. Corresponding UV-divergences can be absorbed into the couplings of the effective Lagrangian. In order to implement this procedure in a self-consistent way, one needs some ordering scheme, known in ChPT as Weinberg's power counting [5].

Consider an arbitrary loop diagram based on the general effective Lagrangian $\mathcal{L}_{eff} = \sum_n \mathcal{L}_n$, where n denotes the chiral power of the various terms. Then, the amplitude $\mathcal{A}$ of a diagram with L loops , I internal lines, and V_n vertices of order n behaves in expansion of powers of momenta as

$$\mathcal{A} \propto \int (d^4p)^L \frac{1}{(p^2)^I} \prod_n (p^n)^{V_n}\ . \tag{1.26}$$

Then $\mathcal{A}$ is of chiral dimension $\mathcal{D} = 4L - 2I + \sum_n nV_n$. Using the topological identity $L = I - \sum_n V_n + 1$ to eliminate I, we find

$$\mathcal{D} = \sum_n V_n(n-2) + 2L + 2\ . \tag{1.27}$$

Note that, since the chiral Lagrangian starts with $\mathcal{L}_2$, i.e. $n \geq 2$, the right-hand-side of Eq. (1.27) is a sum of non-negative terms. Consequently, for fixed $\mathcal{D}$, there is only a finite number of combinations with L, V_n that can contribute. In other words, only a finite number of terms in the $\mathcal{L}_{eff}$ are needed to work to a fixed order in p. To illustrate this scheme, consider again $\pi\pi$ scattering. At $O(p^2)$, only tree level diagrams, composed of vertices of $\mathcal{L}_2$, contribute ($V_{n>2} = 0, L = 0$). At $O(p^4)$, there are two possibilities: either one-loop graphs, composed only of lowest-order vertices ($V_{n>2} = 0$, $L = 1$), or tree graphs with exactly one insertion from $\mathcal{L}_4$ ($V_4 = 1$, $V_{n>4} = 0$, $L = 0$). The low-energy constants, which are the coefficients at local terms, absorb loop divergences order by order.

Calculating loop graphs, we might expect that a given amplitude is proportional to some power of the

parameter p/Λ. There is an estimate of Λ based on loop expansion [20]:

$$\Lambda \sim 4\pi F_0 \approx 1.2 \text{ GeV}, \tag{1.28}$$

In addition, note that the effective theory contains Goldstone bosons as the only dynamical degrees of freedom. Therefore, it must fail once the energy reaches the resonance region, hence for $p^2/\Lambda^2 \approx p^2/M_{res}^2 \approx 1$. The lightest narrow resonance, observed in $\pi\pi$ scattering in the $I = l = 1$ channel is the ρ resonance: $M_{res} = M_\rho = 770$MeV. It is therefore appropriate to choose

$$\Lambda \sim M_\rho \approx 770\text{MeV}, \tag{1.29}$$

which is consistent with the estimate in Eq. (1.28).

In this section, based on the general formalism, we have just outlined how one can construct the effective Lagrangian at higher orders from building blocks in Eq.(1.17). However, the number of independent terms and corresponding low-energy constants (LECs) increases rapidly at higher orders. For example, at $O(p^4)$, the Lagrangian $\mathcal{L}_4$ contains 10 chiral operators and the same number of LECs [14, 15]. ChPT provides no information about the low-energy constants. Essentially, they should be fixed, using experimental input or from lattice QCD simulations.

1.3 Lattice QCD

In this section, we will consider another powerful non-perturbative method, which deals with the formulation of QCD in a finite discretized Euclidean space-time.The key idea of this approach, referred to as lattice QCD (LQCD), is that the QCD observables can be determined from Euclidean correlation functions, which are evaluated numerically from the path integral [21]. To illustrate this idea , consider the behaviour of the correlation function of a particle with creation/annihilation opeartors $\hat{O}^\dagger\hat{O}$ for large Euclidean time separation T

$$\lim_{T\to\infty}\langle O(t)O^\dagger(0)\rangle_T = \lim_{T\to\infty}\frac{1}{Z_T}\text{Tr}[\text{e}^{-(T-t)\hat{H}}\hat{O}\text{e}^{-t\hat{H}}\hat{O}^\dagger] = \sum_n \langle 0|\hat{O}|n\rangle\langle n|\hat{O}^\dagger|0\rangle \text{e}^{-tE_n},\ |t| \ll T \tag{1.30}$$

where $Z_T = \text{Tr}[\text{e}^{-t\hat{H}|}]$ is the partition function and n labels the eigenstates $|n\rangle$ and eigenvalues E_n of the QCD Hamiltonian $\hat{H}$ and $O(t)$ is a c-number, corresponding to the operator $\hat{O}$. For a given choice of the operator $\hat{O}^\dagger$, at large t, due to the exponential factor in the sum, only the lowest lying state, which has the quantum number of $\hat{O}^\dagger$ will survive.

On the other hand, the correlation function can be expressed through the path integral

$$\frac{1}{Z_T}\text{Tr}[\text{e}^{-(T-t)\hat{H}}\hat{O}\text{e}^{-t\hat{H}}\hat{O}^\dagger] = \frac{1}{Z_T}\int [DA, Dq, D\bar{q}]\, O(t)O^\dagger(0)\, \text{e}^{-S_E} \tag{1.31}$$

where S_E is the Euclidean QCD action. The crucial point is that the numerical evaluation of the path integral, using Monte Carlo methods together with the spectral decomposition Eq. (1.30), allows to determine the spectrum of the underlying theory. Moreover, the Osterwalder-Schrader theorem ensures that the correlation functions in Minkowski space can be reconstructed from finite-volume Euclidean correlation functions [22, 23].

The implementation of program just outlined proceeds through the few steps which we consider below.

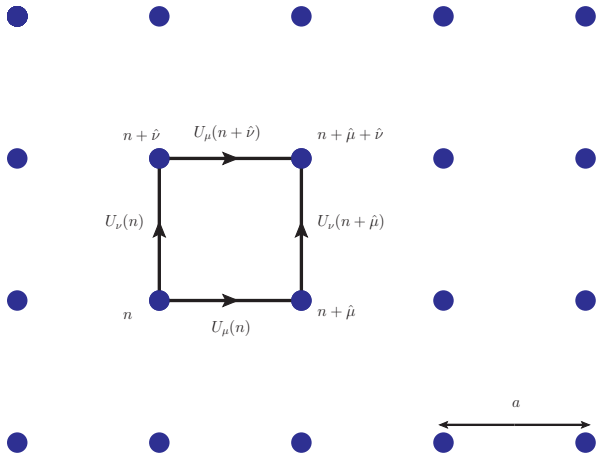

Figure 1.2: two-dimentional slice of the lattice with elementary plaquette

1.3.1 Disretization of QCD

The numerical evalution of the path integral in Eq. (1.31) is possible, only when the path integral is defined on a finite Eucledean space-time lattice. The distance beteween neighboring lattice sites, the so-called *lattice spacing*, denoted by a, plays a role of the UV-regulator. In its simplest realization, the lattice has a form of a hypercube with a spatial size L and equal lattice spacing in all directions. Physically, it is clear that the lattice cutoff should be small, compared to the hadronic scale $a \ll \Lambda_{QCD}^{-1}$, in order to include the nonperturbative dynamics. Furthermore, the spatial extent should be much larger than the correlation length in the theory, which is the inverse of the mass of the lightest particle in the spectrum, (i.e., pion), $L \gg m_\pi^{-1}$. From these two requirements it follows that the number of lattice points should be large enough.

We now turn to the problem of discretization of the fermionic and gauge actions. The quark fields, which are defined on the lattice sites (see Fig.1.2), transform under the gauge group $SU(3)$ in the same way as in the continuum

$$q(x) \to \Omega(x)q(x) \qquad \bar{q}(x) \to \bar{q}(x)\Omega\dagger(x) \tag{1.32}$$

with $\Omega(x) \in SU(3)$ and $x = x_\mu = n_\mu a^{(\mu)}$ ($n_\mu \in \{0, ..., N_\mu - 1\}$). If we discretize the fermionic continuum action by doing a sum instead of an integral and replace the derivative $\partial_\mu q$ in Eq.(1.3) by lattice finite difference

$$\partial_\mu q(x) \to \frac{1}{2a}(q(n+\hat{\mu}) - q(n-\hat{\mu})), \tag{1.33}$$

we see that the terms of the form $\bar{q(n)}q(n+\hat{\mu})$ appear, which are not gauge-invariant. To make the discretized fermionic action gauge-invariant, we introduce a new field $U_\mu(n)$, entering bilinear as $\bar{q(n)}U_\mu(n)q(n+\hat{\mu})$, with the following transformation property

$$U_\mu(n) \to U'_\mu(n) = \Omega(n)U_\mu(n)\Omega^\dagger(n+\hat{\mu}) \tag{1.34}$$

The field $U_\mu(n)$, called *link variable*, connects lattice sites n and $n+\hat{\mu}$ as depicted on Fig.1.2. Note that $U_\mu(n)$ are the elements of gauge group $SU(3)$, whereas the gauge fields A_μ are the elements of the Lie algebra. In the continuum, the object, which has the same transformation property as the gauge link, is

the *gauge transporter*

$$G(x,y) = P\exp\left(ig\int_{C_{xy}} A\cdot ds\right) \tag{1.35}$$

$$G(x,y) \to \Omega(x)G(x,y)\Omega^{\dagger}(y) \tag{1.36}$$

which is defined as a path-ordered (P) integral of the gauge field A_μ along the path C_{xy} from x to y. Thus, the gauge link acts as a gauge transporter connecting the points $x = an$ and $y = a(n+\hat{\mu})$. From Eq. (1.35), it follows

$$U_\mu(n) = G(x,y) = \exp(igaA_\mu n) + O(a^2). \tag{1.37}$$

Having introduced the link variables as building blocks, we can construct the lattice version of the gauge action, which recovers the action in of Eq. (1.1) in the continuum limit. To this end, we choose the minimal closed loop on the lattice called *plaquette* (see Fig. 1.2), which is a product of four link variables

$$\begin{aligned} U_{\mu\nu} &= U_\mu(n)U_\nu(n+\hat{\mu})U_{-\mu}(n+\hat{\mu}+\hat{\nu})U_{-\nu}(n+\hat{\nu}) \\ &= U_\mu(n)U_\nu(n+\hat{\mu})U_\mu(n+\hat{\mu})^{\dagger}U_\nu(n)^{\dagger}. \end{aligned} \tag{1.38}$$

With the transformation property in Eq. (1.34) it is clear that the trace of the plaquette $\mathrm{Tr}[U_{\mu\nu}]$ is gauge-invariant. Then, the lattice gauge action that has the correct continuum limit is a sum over all plaquettes [21]

$$S_G[U] = \frac{2}{g^2}\sum_{n,\mu<\nu}\mathrm{Re}\,\mathrm{Tr}[1-U_{\mu\nu}] = \frac{a^4}{2g^2}\sum_{n,\mu<\nu}\mathrm{Tr}[F_{\mu\nu}(n)^2] + O(a^6) \tag{1.39}$$

The so-called *naive discretization* of the fermion action, which we have introduced earlier (see Eq.(1.33)) leads to the well-known *fermion doubling problem*. To have a closer look at this issue, consider the lattice Dirac operator $D(n|m)$ in a momentum space for the trivial choice of gauge fields $U_\mu(n) = 1$

$$\tilde{D}(\mathbf{p}) = m + \frac{i}{a}\sum_{\mu=1}^{4}\gamma_\mu \sin(p_\mu a) \tag{1.40}$$

The *quark propogator* defined as inverse of the Dirac operator $D^{-1}(n|m)$ is given by

$$\tilde{D}^{-1}(\mathbf{p}) = \frac{m - ia^{-1}\sum_\mu \gamma_\mu \sin(p_\mu a)}{m^2 + a^{-2}\sum_\mu \sin^2(p_\mu a)} \tag{1.41}$$

Apart from the physical pole at $p^2 = -m^2$, the lattice quark propagator has 15 unphysical poles called *doublers* at

$$p = (\pi/a,0,0,0),(0,\pi/a,0,0),...,(\pi/a,\pi/a,\pi/a,\pi/a) \tag{1.42}$$

Thus, the theory on the lattice has the unphysical states in the spectrum on the lattice. The physical reason for such a behaviour is related to the axial anomaly in lattice regulated theory. That is, unlike in the continuum, the axial-vector current is conserved, i.e. the anomaly of the physical fermion is cancelled by the anomaly of the doublers [24]. Furthermore, according to the Nielsen-Ninomiya theorem [25], it is not possible to construct the lattice fermion action that is both:

1. *local* i.e., Dirac opeartor $D(n|m)$ vanishes exponentialy for $|n-m| \to 0$ or in momentum space $D\tilde{(\mathbf{p})}$

is a periodic, analytic function of p except $p = 0$;

2. *free of doublers and has the correct continuum limit* i.e., $\tilde{D}(\mathbf{p}) \propto \gamma_\mu p_\mu$ as $ap \ll 1$;

3. *chirally symmetric in the continuum* i.e., $\{\gamma_5, \tilde{D}(\mathbf{p})\} = 0$.

The way to remove the doublers, as suggested by Wilson, is to add a discretized Laplacian term $\bar{q}\frac{r}{2}\Delta q$ to the naive fermion action. Effectively, the doublers acquire a mass of the order $O(1/a)$ and thus become heavy, decoupling from the theory in the continuum limit. The corresponding massless Wilson Dirac operator, which reads

$$\tilde{D}_W(\mathbf{p}) = \frac{i}{a}\sum_{\mu=1}^{4}\gamma_\mu \sin(p_\mu a) + \frac{1}{a}\sum_{\mu=1}^{4}\gamma_\mu(1-\cos(p_\mu a)) \tag{1.43}$$

fulfils the conditions 1. and 2., but breaks chiral symmetry, being γ_5-Hermitian, i.e.,$\gamma_5 D\gamma_5 = D^\dagger$ [21] The vacuum expectation value of any operator $\hat{O}$ in the so-called Wilson formulation of lattice QCD has the form

$$\langle B\rangle = \frac{1}{Z}\int \mathcal{D}[q,\bar{q}]\,\mathcal{D}[U]\,e^{-S_G[U]-S_F[q,\bar{q},U]}\,B[q,\bar{q},U], \tag{1.44}$$

where the gauge action $S_G[U]$ is given in Eq. (1.39) and the fermion action is

$$S_F[q,\bar{q},U] = a^4\sum_{f,n,m}\bar{q}^{(f)}(n)\,D_W^{(f)}(n|m)\,q^{(f)}(m). \tag{1.45}$$

The Wilson Dirac opeartor is the one in Eq. (1.43) in coordinate space

$$D_W^{(f)}(n|m) = \left(m^{(f)} + \frac{4}{a}\right)\delta_{n,m} - \frac{1}{2a}\sum_{\mu=\pm1}^{\pm4}(1-\gamma_\mu)U_\mu(n)\delta_{n+\hat{\mu},m}. \tag{1.46}$$

Note that the absence of the doublers in Wilson formulation is directly related to the breaking of chiral symmetry. Nevertheless, it is possible to construct the fermionic action that possesses both chiral symmetry in the continuum limit and is free of doublers. As was shown by Ginsparg and Wilson, the corresponding lattice Dirac operator should satisfy the relation [26]

$$\{\gamma_5, D\} = aD\gamma_5 D, \tag{1.47}$$

known as the Ginsparg-Wilson relation. Furthermore, one can write down the modified chiral transformation on the lattice, which is an exact symmetry for fermions, satisfying the above relation [27]. The small explicit chiral symmetry breaking, necessary to avoid Nielsen-Ninomiya theorem does not affect the spectrum extracted from the two-point functions. The chiral anomaly and index theorem are also reproduced [28].

There are two particular types of fermions, satisfying the Ginsparg-Wilson relation, which are used in modern simulations. These are *overlap fermions* and *domain wall fermions*. The overlap fermions are defined through the overlap operator [29, 30]

$$D_{ov} = \frac{1}{a}(1+\gamma_5\,\mathrm{sign}[H]) = \frac{1}{a}(1+\gamma_5\frac{H}{\sqrt{H^2}}), \qquad H = \gamma_5 A, \tag{1.48}$$

where A denotes an appropriate γ_5-hermitian "kernel" Dirac operator with possible choice of Wilson-Dirac operator defined in Eq. 1.46

$$A = a\, D_W. \tag{1.49}$$

Rewriting the Ginsparg-Wilson condition for γ_5-Hermitian operators as

$$aDD^\dagger = D + D^\dagger \tag{1.50}$$

it is straightforward to check that it is satisfied by overlap operator. Furthermore, by expanding D_{ov} for small a, one can show that it has correct continuum limit $\tilde{D}_{ov} \approx i\gamma_\mu p_\mu + O(p^2)$. Note that, due to term $(\gamma_5 A \gamma_5 A)^{-1/2}$, the overlap operator does not vanish between all lattice points, i.e., it is not *ultralocal* which is case with the D_W. It is this property (which is also true for any other formulation of chirally symmetric fermions [31, 32]) that makes the numerical calculations with chiral fermions extremely cost-demanding, compared to Wilson-type fermions. What, however, must hold true is the *locality* in the sense of exponential decay of the Dirac operator with a rate, proportional to the cut-off $1/a$. In that sense, the overlap operator is local [33].

Another type of Wilson-Ginsparg fermions are *domain wall fermions*. [34–37]. They are defined in the five-dimensional space with chiral fermions, localized on the opposite boundaries of this space. They satisfy the Ginsparg-Wilson condition only for infinite extension of the fictitious fifth dimension. In real simulations, this dimension should be truncated, leading to a controllable violation of chiral symmetry.

1.3.2 Generation of gauge-field configurations

Having outlined the discretization of the QCD action, we now discuss the numerical techniques for evaluation of the path intergral. The starting point is the Eq. (1.44) for vacuum expectation value, which for a generic Dirac operator D, is rewritten as follows

$$\langle B \rangle = \frac{1}{Z} \int \mathcal{D}[q, \bar{q}]\, \mathcal{D}[U]\, e^{-S_G[U] - \bar{q} D(U) q}\, B[q, \bar{q}, U], \tag{1.51}$$

Since the observable B is a fermion multilinear, one can explicitly integrate over fermioin fields with corresponding Wick contractions (denoted by the overbar) of the quark fields

$$\langle B \rangle = \frac{1}{Z} \int \mathcal{D}[U] \prod_f \det D_f(U)\, \overline{B}[U]\, e^{-S_G[U]} \tag{1.52}$$

Having performed the fermionic part of the path integral, the reminder can be performed using Monte Carlo techniques. To this end, one should generate a finite sample of *gauge field configurations* $\{U_1, U_2, ..., U_N\}$ of size N according to the probability distribution $\frac{1}{Z}\det D_f(U)\, e^{-S_G[U]}$. Then, the expectation value is approximated by an average over the generated configuration :

$$\langle B \rangle = \frac{1}{N} \sum_i^N \bar{B}[U_i]. \tag{1.53}$$

In the dynamical simulations, the computationally demanding part is the calculation of the fermionic determinant, which should be updated together with the gauge part to generate the next configuration. The reason for high computational cost is that fermionic determinant is a large matrix with dimensionality $(12L^3T)^2$. In the earlier era of LQCD, the way to avoid that issue was to the set the determinant to unity. Unfortunately, such a uncontrolled *quenched* approximation describes the theory with infinitely heavy

quarks in loops. Nowadays, thanks to the growth of computational resources and improved algorithms, it became possible to perform many important calculations with dynamical quarks.

1.3.3 Partial quenching and PQChPT

Before we proceed further, it is necessary to introduce partially quenched QCD and the corresponding effective field theory, which will be used in the next chapter of the thesis. We start by considering explicitly the 2-point correlation function of the pion in QCD

$$\begin{aligned} C_\pi &= -\left\langle \sum_{\mathbf{x}} \bar{u}\gamma_5 d(\mathbf{x},t)\bar{d}\gamma_5 u(0) \right\rangle \\ &= -\frac{1}{Z}\int \mathcal{D}U \prod_q \mathcal{D}[q,\bar{q}] e^{-S_G - \int \sum_q \bar{q}(\hat{D}+m_q)q} \sum_{\mathbf{x}} \bar{u}\gamma_5 d(\mathbf{x},t)\bar{d}\gamma_5 u(0) \\ &= -\frac{1}{Z}\int \mathcal{D}U \prod_q \det(\hat{D}+m_q) e^{-} S_G \sum_{\mathrm{x}} \mathrm{tr}[\gamma_5(\hat{D}+m_d)^{-1}(x,0)\gamma_5(\hat{D}+m_u)^{-1}(0,x)]. \end{aligned} \tag{1.54}$$

We see from the last line of this equation, where the Wick contractions have been performed, that the masses of the quarks entering the determinant (so-called *sea* or *dynamical* quark masses) and the masses of the quark in propagators (*valence* quark masses) can be put by hand to be different. On the technical level, such a procedure, called *partial quenching*, is relatively cheap to implement, since the computation of propagators is much less expensive as compared to the calculation of the fermionic determinant [38–40]. The validity of the partial quenching boils down to the question: is it possible to extract physical results from such unphysical calculations? One may build a QCD-like theory (the so called partially quenched QCD or PQQCD) for valence and sea quarks, having different masses and try to relate its properties to those of QCD. However, the PQQCD is an unphysical theory, because it breaks unitarity and there appear double poles in propagators. Nevertheless, the QCD should be included into PQQCD with $m_{val} = m_{sea}$ as a physical subspace. This is provided with help of partially quenched chiral perturbation theory or PQChPT. It is an effective field theory which shares the symmetries of PQQCD and reproduces the dynamics of usual ChPT in physical subspace of quark masses. As was rigorously shown in Ref. [41], it is indeed possible to formulate such an effective field theory.

In order to formulate PQChPT, we explore the possibility that the masses of the valence and sea quarks can be chosen different. One way to do this is to introduce commuting spin-1/2 fields or *ghost* quarks, denoted by $\tilde{q}$, which have the masses equal to those of valence quarks [42]. The crucial observation is that the determinant with ghost quarks cancels that from valence quark:

$$\int \mathcal{D}[q,\bar{q}] e^{-\bar{q}(\hat{D}+m_q)q} = \det(\hat{D}+m_q), \qquad \int \mathcal{D}[\tilde{q},\tilde{q}^\dagger] e^{-\tilde{q}^\dagger(\hat{D}+m_q)\tilde{q}} = \frac{1}{\det(\hat{D}+m_q)} \tag{1.55}$$

In general, there are three types of quarks: N_V number of valence quarks q_V, N number of sea quarks q_S and N_V number of ghost quarks $\tilde{q_S}$. Then, the action of PQQCD looks like a generalized version of

QCD action:

$$\begin{aligned} S_{PQ} &= S_G + \int \bar{Q}(\hat{D} + \mathcal{M})Q \\ Q^T &= (\underbrace{q_{V_1}, ..., q_{V_{N_V}}}_{valence}, \underbrace{q_{S_1}, ..., q_{S_N}}_{sea}, \underbrace{q_{\tilde{V}_1}, ..., q_{\tilde{V}_{N_V}}}_{ghost}) \\ \mathcal{M} &= (\underbrace{m_{V_1}, ..., m_{V_{N_V}}}_{valence}, \underbrace{m_{S_1}, ..., m_{S_N}}_{sea}, \underbrace{m_{\tilde{V}_1}, ..., m_{\tilde{V}_{N_V}}}_{ghost=valence}) \end{aligned} \tag{1.56}$$

Furthermore, with the corresponding extended measure in the path integral, one can see that the partition function of PQQCD, Z_{PQ}, is reduced to that of the QCD thanks to the cancellation of determinants:

$$\begin{aligned} Z_{PQ} &= \int DU\, D\bar{Q}DQ\; e^{-S_{PQ}} \\ &= \int DU\, e^{-S_G} \prod_{i=1}^{N_V} \left(\frac{\det(\hat{D} + m_{V_i})}{\det(\hat{D} + m_{V_i})}\right) \prod_{j=1}^{N} \det(\hat{D} + m_{S_j}) \\ &= \int DU\, e^{-S_G} \prod_{j=1}^{N} \det(\hat{D} + m_{S_j}) = Z_{QCD}. \end{aligned} \tag{1.57}$$

The field theoretical formulation of PPQCD, we have just outlined, is well-defined in Euclidean space. Nevertheless, the theory remains unphysical, as can be shown by going back to Minkowski space and observing the violation of spin-statistics theorem. In addition, PQQCD does not satisfy reflection positivity, i.e. one cannot construct a physical Hilbert space. However, that should not possess a problem as long as we are concerned about QCD and use PQQCD in Euclidean space.

In the limit of vanishing quark masses, the action of PQQCD turnes out to be invariant under a *graded extension* of chiral symmetry transformations of all types of quarks

$$Q_{L,R} \longrightarrow U_{L,R} Q_{L,R},\ \bar{Q}_{L,R} \longrightarrow \bar{Q}_{L,R} U^{\dagger}_{L,R},\ U_{L,R} \in SU(N_V + N \mid N_V) \tag{1.58}$$

and the apparent symmetry is $SU(N_V + N \mid N_V)_L \times SU(N_V + N \mid N_V)_R \times U(1)_V$. Here, graded Lie groups are defined as group matrices $U \in SU(N_V + N \mid N_V)$ that contain both commuting and anticommuting elements written in the block form

$$U = \begin{pmatrix} A & B \\ \underbrace{C}_{N_V+N} & \underbrace{D}_{N_V} \end{pmatrix}, \tag{1.59}$$

where A and D contain commuting elements whereas B and C contain anticommuting ones. Furthermore, the usual trace is substituted by the *supertrace* defined as

$$\mathrm{str} = \mathrm{tr}A - \mathrm{tr}D \;\Rightarrow\; \mathrm{str}(U_1 U_2) = \mathrm{str}(U_2 U_1) \tag{1.60}$$

and the determinant is generelized to the *superdeterminant*

$$\mathrm{sdet}U = \exp[\mathrm{str}(\ln U)] = \det(A - BD^{-1}/C)/\det(D), \tag{1.61}$$

which obeys the condition $\mathrm{sdet}(U_1 U_2) = \mathrm{sdet}(U_1)\mathrm{sdet}(U_2)$. Therefore, the matrices $U \in SU(N_V+N \mid N_V)$ are unitary graded matrices with $\mathrm{sdet}U = 1$.

Since QCD is a limiting case of PQQCD, as $m_{sea} \to m_{val}$, we *assume* that there exists a local effective field theory of PQQCD [41]. Indeed, setting the quarks masses in the valence and sea sectors equal, one gets correlation functions of QCD as a subset of correlation functions of PQQCD, and a corresponding chiral symmetry breaking pattern takes place in sea sector. Furthermore, it is reasonable to assume that the EFT framework can be extended for the case $m_{val} \neq m_{sea}$ and the corresponding Ward identities can be derived for arbitrary order correlation functions as generalizations of those in QCD.

Based on above arguments, the construction of partially quenched ChPT (PQChPT) goes in analogy with construction of ChPT. Namely, the expansion proceeds around the chiral limit $\mathcal{M} = 0$, where the exact symmetry group is $G = SU(N_V+N \mid N_V)_L \times SU(N_V+N \mid N_V)_R$. Futheremore, this exact symmetry is spontaneously broken down to the graded vector symmetry $G \to H = SU(N_V + N \mid N_V)_V$. The corresponding nonlinear field Σ lives in the coset space G/H and transforms under the group G as

$$\Sigma = \exp[2i\Phi/f], \quad \Sigma \to U_L \Sigma U_R^{\dagger}. \tag{1.62}$$

According to Goldstone theorem there are $(N + 2N_V)^2 - 1$ pseudoscalar mesons, composed from sea, valence and ghost quarks and antiquarks and Φ has a block form:

$$\Phi = \begin{pmatrix} \phi & \eta_1 \\ \eta_2 & \tilde{\phi} \end{pmatrix}, \tag{1.63}$$

where ϕ contains quark-antiquark Goldstone bosons, $\tilde{\phi}$ are made of ghost-antighost bosons, and $\eta_{1,2}$ are quark-ghost fermions (or vice versa). The condition $\mathrm{sdet}(\Sigma) = 1$ implies that $\mathrm{str}\,\Phi = \mathrm{tr}\phi - \mathrm{tr}\tilde{\phi} = 0$. The building blocks are Σ, graded generalization of the covariant derivative $D_\mu\Sigma$ and $\chi = 2B_0(s + ip)$ (one must set $p = 0$ and $s = \mathcal{M}$ at the end). Since the power counting rules are the same as in ChPT, we are in the position to write down the leading order Lagrangian in PQChPT

$$\mathcal{L}^{(2)}_{PQ} = \frac{f^2}{4}\mathrm{str}(D_\mu\Sigma D_\mu\Sigma^{\dagger}) - \frac{f^2}{4}\mathrm{str}(\chi^{\dagger}\Sigma + \Sigma^{\dagger}\chi) \tag{1.64}$$

One may proceed further and construct the chiral Lagrangian at NLO and so on. They all contain the low-energy constans and the crucial point is that *this low-energy constants are identical* to those of ChPT [1].

1.3.4 Lattice spectroscopy

As the next step of the lattice calculation, we are interested in the n - point Green functions of hadrons. In accordance with Eq.(1.30), one can extract masses and energy levels from their large-time behaviour. For the 2-point Green functon, playing the central role in LQCD, we have $\hat{B} = \hat{O}\hat{O}^{\dagger}$. Here the $\hat{O}$ and $\hat{O}^{\dagger}$ denote *interpolating* operators which correspondingly create and annihilate hadron states from the vacuum of QCD. It is clear, that the interpolating operators must share the quantum numbers with the hadron in question. For example, it can be easily checked that that the general form of interpolating operators for flavour non-singlet pseudoscalar mesons have a form

$$\hat{O} = \bar{q}_1(x)\gamma_5 q_2(x), \tag{1.65}$$

[1] The *number* of LECs in PQChPT can, however, exceed that of ChPT. This happens because extra operators can appear in the Lagrangian from supertrace identities, already at $O(p^4)$ order. Of course, their contribution vanish for sea and valence quarks having equal masses [43]

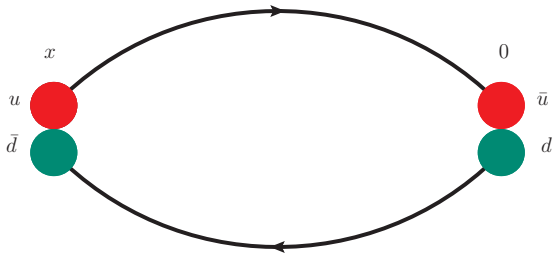

Figure 1.3: π^+ 2-point correlation function

Figure 1.4: One piece of a disconnected contribution to 2-point Green function of π^0

whereas for the singlet one

$$\hat{O} = \bar{q_f}(x)\gamma_5 q_f(x), \tag{1.66}$$

where $q(x)$ denotes quark field.

Let us consider, in particular, the pions. They are represented by the following interpolators:

$$O^{\pi^+} = \bar{d}\gamma_5 u, \quad O^{\pi^0} = \frac{1}{\sqrt{2}}(\bar{u}\gamma_5 u - \bar{d}\gamma_5 d), \quad O^{\pi^-} = \bar{u}\gamma_5 d \tag{1.67}$$

To see, how the observables are constructed from these operators, consider the 2-point correlation function of the π^+:

$$C_{\pi^+}(t,0) = \langle O^{\pi^+}(x) O^{\pi^+\dagger(0)}\rangle = -\int \mathcal{D}U e^{-S_G} \mathrm{Tr}[D_u^{-1}(x,0)\gamma_5 D_d^{-1}(x,0)\gamma_5], \tag{1.68}$$

where the Wick contractions have been performed and the pion is created at the origin and annihilated at coordinate x. We see that the quark propagators, which are the inverse of the Dirac operator D_f^{-1}, enter the equation. The inversions must be performed for each step of the gauge field configuration. The correlation function of flavor non-singlet propogator, such as π^+, contains only *"connected"* contribution schematically depicted on Fig 1.3. In case of flavour-singlet interpolating operator of π^0, there appear additional contributions to the 2 -pont Green function:

$$C_{\pi^0}(t,0) = \langle O^{\pi^0}(x) O^{\pi^{0\dagger}}\rangle = \int \mathcal{D}U e^{-S_G}\{-\frac{1}{2}\mathrm{Tr}[D_u^{-1}(x,0)\gamma_5 D_u^{-1}(x,0)\gamma_5] \tag{1.69}$$

$$+\frac{1}{2}\mathrm{Tr}[D_u^{-1}(x,x)\gamma_5 D_u^{-1}(0,0)\gamma_5] - \frac{1}{2}\mathrm{Tr}[D_u^{-1}(x,x)\gamma_5 D_d^{-1}(0,0)\gamma_5] + u \leftrightarrow d\}, \tag{1.70}$$

which contain propagators from one lattice point to itself (the so-called *all-to-all* propagators). This type of *disconnected* contribution, depicted on Fig. 1.4, are particularly challenging to calculate on the lattice. Nevertheless, substantial progress has been made in recent years in that direction [44–47].

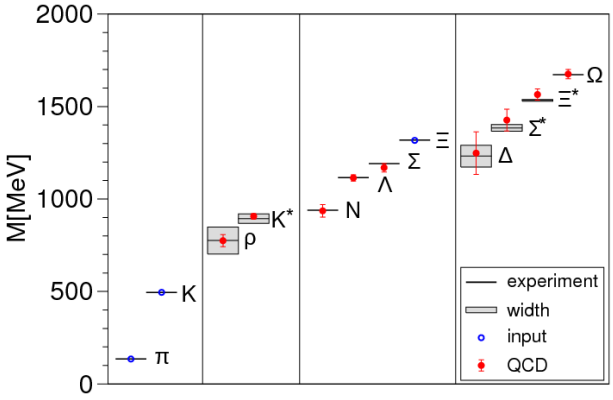

Figure 1.5: Light hadron spectrum, [50]

Having outlined the construction of the interpolators and corresponding Green functions, we discuss now, how to extract the lowest energy levels. Consider first the projection of the 2-point correlation function to a momentum **P**:

$$C(\mathbf{P},t) = \sum_{\mathbf{x}} e^{i\mathbf{P}\mathbf{x}} \langle \hat{O}(\mathbf{x},t)\hat{O}^{\dagger}(\mathbf{0},0)\rangle \tag{1.71}$$

Repeating the steps as in Eq.(1.30), we see that only the exponent with lowest energy eigenvalue dominates the spectral representation of the 2-point Green function in the limit of a large Euclidean time:

$$C(\mathbf{P},t) \xrightarrow{t\to\infty} \frac{\langle 0|\hat{O}|n\rangle\langle n|\hat{O}^{\dagger}|0\rangle}{2E(\mathbf{P})} e^{-E(\mathbf{P})t}, \tag{1.72}$$

where $E(\mathbf{P})$ is energy of lowest state in the spectrum. From Eq. (1.72), one can extract the mass of the hadron and the product of matrix elements $\langle 0|\hat{O}|n\rangle\langle n|\hat{O}^{\dagger}|0\rangle$. Even though one cannot go to asymptotic times, it clear that high energy states will be exponentially suppressed for sufficiently large Euclidean times on a finite lattice. The time, at which the contributions of the excited states start to be negligible, is called the *plateau region*. On the technical level, one introduces the so-called effective mass, defined as

$$m_{eff}(t+a/2) = \ln \frac{C(\mathbf{P},t+a)}{C(\mathbf{P},t)} \tag{1.73}$$

Once the system approaches the ground state, this quantity becomes constant, defining the plateau. Furthermore, excited energy states can be extracted by applying larger basis of interpolating operators. For details see, Refs. [48, 49].

The question now is, how the infinite-volume observables can be extracted from energy levels obtained through the approach outlined above. What are measured in the lattice calculations, are dimensionless quantities. Therefore, one has fix the scale, in order to get a prediction for a dimensionful observable in question. Scale setting can be achieved through fixing the lattice spacing a, which is equivalent to fixing the bare gauge coupling. Furthermore, the input parameters in any lattice calculation are N_f bare quark masses and the gauge coupling. Then, one can in principle, extract any observable for several values of the lattice spacing and, finally, using relevant interpolation function (which depends on the particular form of action, etc.) find its value in continuum limit $a = 0$. However, one cannot implement the above program, since lattice input parameters cannot be measured by experiment. Experimental observables, such as hadron masses, are related to the bare parameters in a unknown way that must

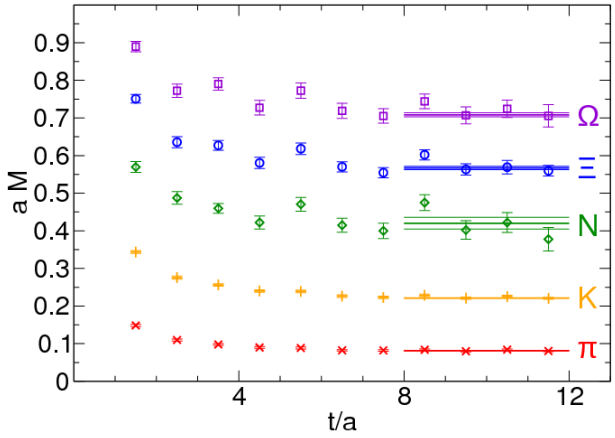

Figure 1.6: Effective mass as a function of time. Horizontal colored line are the masses with corresponding error bars [50]

be itself determined from lattice QCD. The way to overcome this issue is to tune the bare parameters. Particularly, we can set the scale $1/a$ using the experimental value of the mass of the hadron M_h by means of relation $a = (aM_h)_{lat}/(M_h)_{exp}$. For this purpose, one widely uses the mass of the Ω^- baryon as a scale setting observable [50, 51]. Before applying the last equation, one must tune the light, strange and charm quark masses to their physical values. This is achieved by tuning the light quark masses so, that the ratios $M_\pi/M_\Omega, M_K/M_\Omega$ acquire physical values [52]. However, when simulations are performed with unphysical light quark masses, one must extrapolate the results to the physical point with chiral EFT. Note that, nowadays, more and more simulations are done with light quarks having masses close to physical. In the next step, one has to remove the cutoff. i.e., one must extrapolate to the continuum $a \to 0$. This procedure depends on a particular choice of the fermionic action, as well as on the combination of the scale setting observable and measured observable. The last step of any lattice calculation consists of extrapolation of the results to the infinite-volume limit $L \to \infty$.

We would like to show an impressive example of a lattice calculation of the light hadron spectrum, performed by the Budapest-Marseille-Wuppertal Collaboration [50]. The simulations were done with pion mass $M_\pi = 190$MeV and subsequent extrapolation to the physical point. The lattice size was chosen to be $a = 4/M_\pi$ so that finite-volume effects are under control. Furthermore, three lattice spacings were used for the continuum extrapolation. The effective mass plots are depicted in Fig.1.6. The light hadron spectrum, shown on Fig.1.5, agrees with high precision with the experiment and thus confirms the validity of QCD as the theory of strong interactions. We have just shown the case of lattice calculation of the *stable* particles spectrum. Hovewer, most hadron observed in experiments, are rather *resonances* and thus *unstable*. The above method for the extraction of masses is not applicable for the reasons that will be discussed in the subsequent section. As it will turn out, finite-volume effects play a key role in the study of the nature and properties of resonances in lattice QCD.

1.4 Nonrelativistic EFT

Below we shall consistently use the so-called nonrelativistic EFT. In a number of hadronic systems at low energies, the S-matrix is expressed only through measurable observables, such as scattering length, effective range, etc. The key idea a of such a theory is that, when the three-momentum of the particles in

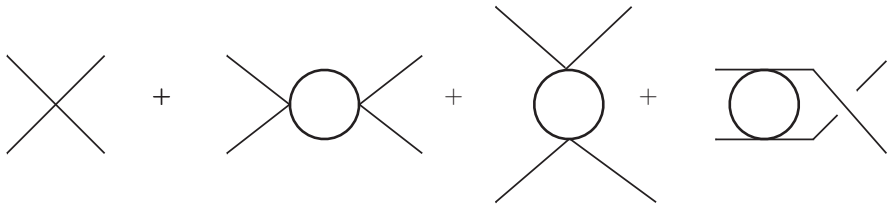

Figure 1.7: one-loop scattering amplitude in full theory

a given process is much smaller then its mass and thus no creation/annihilation of particles/antiparticles occurs, the analytical structure of the S-matrix is much simplified, compared to the full relativistic theory. It means that the S-matrix contains only poles, located close to the elastic cut, and distant singularities can be Taylor-expanded in external momenta [53]. The effective Lagrangian that corresponds to this expansion, consists of tower of derivative operators, multiplied with unknown coupling constants. The renormalization program in the NREFT is highly non-trivial, since the matrix elements diverge at high enough order of the perturbative expansion and one has to deal with "power counting" problem. At low energies, the non-relativistic theory is physically equivalent to relativistic one and the couplings in NREFT are fixed through the *matching procedure*. The power of the non-relativistic theory lies in the fact that one can analytically sum up all diagrams in the four-point Green function to get an exact amplitude. In what follows, we will only consider the 2-body sector.

In order to construct the most general non-relativistic Lagrangian, one has to exploit the symmetry principles. Most important are particle number conservation, Galilean invariance and P, T symmetries. Furthermore, we have to specify the counting scheme. If v is the velocity of the massive particle (of the mass M) then: each 3-momentum $\mathbf{p}$ and space derivative ∇ is counted as $O(v)$ and the kinetic energy $p^0 - M$ as $O(v^2)$. The non-relativistic Lagrangian in the 2-body sector has the form

$$\begin{aligned} \mathcal{L}_{NR} &= \sum \Phi^\dagger \left(i\partial_t - M + \frac{\Delta}{2M} + \frac{\Delta^2}{8M^3} + ... \right) \Phi + \frac{g_1}{4M^2} (\Phi^\dagger \Phi^\dagger)(\Phi\Phi) \\ &+ \frac{g_2}{16M^4} \{ (\Phi^\dagger \overleftrightarrow{\Delta} \Phi)^\dagger (\Phi\Phi) + h.c. \} + \frac{g_3}{8M^4} (\Phi^\dagger \Phi) \overleftrightarrow{\Delta} (\Phi^\dagger \Phi) + ..., \end{aligned} \tag{1.74}$$

where Φ ($\Phi^\dagger$) denotes the non-relativistic operator that annihilates(creates) a particle from the vacuum and the g_i are non-relativistic couplings. The free non-relativistic propagator is given by

$$i\langle 0|T\Phi(x)\Phi^\dagger(0)|0\rangle = \int \frac{d^4p}{(2\pi)^4} \frac{\mathrm{e}^{-ipx}}{M + \frac{\mathbf{p}^2}{2M} - p^0 - i0}. \tag{1.75}$$

Indeed, this propagator corresponds to the non-relativistic dispersion relation $p^0 = M + \mathbf{p}^2/2M$, whereas the terms of the order $\Delta^2/8M^3$ and higher orders amount to the relativistic corrections and must be summed up. In other words, the relativistic effects in NREFT are of pure kinematic nature, while low-energy constants contain information about the short-range dynamics and thus depend on the system under consideration.

We wish to demonstrate, how to match the NREFT with the well-studied scalar ϕ^4 theory, containing a

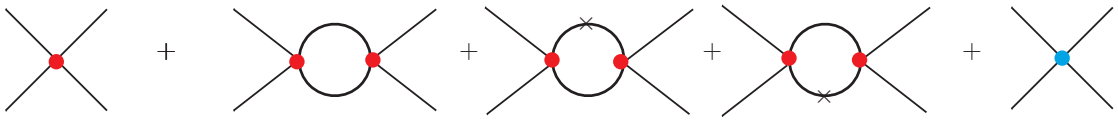

Figure 1.8: Diagrams contributing to the one-loop matching of the 2-particle scattering amplitude in the NR theory. Red dots denote g_1 vertices,crosses relativistic vertices and green dot the derivative one

massive scalar spin-0 field ϕ with physical mass M. Its Lagrangian is given by

$$\mathcal{L} = \frac{1}{2}(\partial_\mu \phi)^2 - \frac{M_r^2}{2}\phi^2 - \frac{\lambda_r}{4!}\phi^4 + counterterms, \tag{1.76}$$

where the renormalized mass is $M_r = M_r(\mu_0)$ and the coupling is $\lambda_r = \lambda_r(\mu_0)$. Here, μ_0 denotes the renormalization scale in $\overline{MS}$ scheme with dimensional regularisation. Before we discuss the matching procedure of a scalar field theory with the NREFT, whose Lagrangian is given by Eq. (1.74), let us discuss some important properties and the nonrelativistic limit. Scalar ϕ^4 theory belongs to non-asymptotically free theories. Its crucial feature is *triviality*, which means that the coupling λ must vanish when the theory supposed to be valid down to the arbitrarily short distances. As was shown using the Lippmann-Schwinger formalism, the relativistic ϕ^4 theory is indeed trivial in the nonrelitivistic limit [54]. It means that, in the nonrelativistic limit, one has only a contact interaction with $\delta^3(\mathbf{r})$ potential and the S-matrix is unity. However, it is clear that, physically, one can cannot have the theory with a zero-range potential, since it is impossible to probe two nonrelativistic particles at distances smaller than Compton wavelength. Therefore, the typical interaction range of the ϕ^4 interaction is not zero but rather $1/M$. Translating this into the language of the effective field theory, we can say that the absence of zero-range interaction is related to the fact that the effective theory can be valid only up to some scale Λ (cut-off), equal to the inverse of the interaction range. In our case, $\Lambda \propto M$. The power of the NREFT approach is the simplification of the loop calculations as compared to the full relativistic scalar ϕ^4 theory. A large class of diagrams vanish in the nonrelativistic limit. Thanks to particle conservation, the two-body amplitude reduces to the *bubble chain sum* with the single loop entering the chain as depicted on Fig. 1.8. Furthermore, it should be pointed out that the non-relativistic EFT is essentially equivalent to the effective range expansion. This statement stems from the fact that in a hadronic processes with particle momenta much smaller than their masses, the scattering amplitude can be expressed through effective range parameters and therefore the couplings in the NREFT are directly related to these parameters.

The matching procedure implies that the non-relativistic couplings g_i can be expressed through the parameters M, λ_r and the scale μ_0. Generally,the matching condition in the 2-body sector is expressed through the equality of the non-relativistic T_{NR} and relativistic T scattering amplitudes with different normalization of the asymptotic states taken into account

$$T(\mathbf{p}_1, \mathbf{p}_2; \mathbf{q}_1, \mathbf{q}_2) = \prod_{i=1}^{2} (2\omega(\mathbf{p}_i))^{1/2} (2\omega(\mathbf{q}_i))^{1/2} T_{NR}(\mathbf{p}_1, \mathbf{p}_2; \mathbf{q}_1, \mathbf{q}_2)\,, \tag{1.77}$$

where $\mathbf{p}_1, \mathbf{p}_2$ and $\mathbf{q}_1, \mathbf{q}_1$ are 3-momenta of particles in the initial and final states, respectively. Note that this condition should hold order by order in the expansion in $\mathbf{p}_i/M, \mathbf{q}_i/M$.

Let us illustrate the matching procedure, considering the S-wave scattering in the relativistic ϕ^4 theory and, correspondingly, in the NREFT. We expand first the non-relativistic amplitude, in powers of v, using

Eq. (1.77) in the CM frame with the tree level amplitude from Eq. (1.76)

$$\frac{T(\mathbf{p}_1,\mathbf{p}_2;\mathbf{q}_1,\mathbf{q}_2)}{2\omega(\mathbf{p})2\omega(\mathbf{q})} = \lambda_r \frac{1}{2\omega(\mathbf{p})2\omega(\mathbf{p})} = \frac{\lambda_r}{4M^2} - \frac{\lambda_r}{4M^2}\mathbf{p}^2 + O(\frac{1}{M^6}). \tag{1.78}$$

On the other hand, we can read off the non-relativistic amplitude from the Lagrangian in Eq.(1.74)

$$T_{NR}(\mathbf{p}_1,\mathbf{p}_2;\mathbf{q}_1,\mathbf{q}_2) = \frac{g_1}{M^2} - \frac{g_2}{M^4}\mathbf{p}^2 - \frac{g_3(\mathbf{p}-\mathbf{q})^2}{M^4} + O(\mathbf{p}^4). \tag{1.79}$$

By comparing two last equations, we arrrive at values of couplings at tree level

$$g_1 = \frac{\lambda_r}{4} + O(\lambda_r^2),\;\; g_2 = \frac{\lambda_r}{4} + O(\lambda_r^2),\;\; g_3 = O(\lambda_r^2) \tag{1.80}$$

Going beyond the tree level requires the calculation of the loops. The corresponding relativistic and non-relativistic one loop amplitudes that should be matched, are shown on Fig.1.7 and Fig. 1.8, respectively. We see that the non-relativistic amplitude contains a single loop plus relativistic and derivative 4-body vertices. The single loop, which enters the bubble chain, is given in the CM frame by

$$\begin{aligned} J(P^0) &= \int \frac{d^D l}{(2\pi)^D i} \frac{1}{M + \frac{\mathbf{l}^2}{2M} - P^0 + l^0 - i0} \frac{1}{M + \frac{\mathbf{l}^2}{2M} - l^0 - i0} \\ &= \frac{iM}{4\pi}(M(P^0 - 2M))^{1/2},\;\; D \to 4, \end{aligned} \tag{1.81}$$

where $P^\mu = p_1^\mu + p_2^\mu$. The loop containing derivative couplings and relativistic vertices is calculated in a similar manner. Note that the loop integral with arbitrary derivative vertex factorizes into the same power of external momentum $|\mathbf{p}|$ multiplied by $J(P^0)$. It is this property that makes it possible to sum up the amplitude to all orders in the perturbative expansion. Note that only a finite number of non-relativistic loops contribute at a given order in v. We arrive finally at the following expansion of the non-relativistic amplitude in the CM frame

$$T_{NR} = M^{-2}\left(h_0 + h_1\frac{|\mathbf{p}|}{M} + h_2\frac{|\mathbf{p}|^2}{M^2} + h_3\frac{\mathbf{pq}}{M^2} + ...\right), \tag{1.82}$$

where the coefficients h_i are finite polynomials in g_i. Here, only the odd powers of $|\mathbf{p}|$ contribute the the non-analytic piece of the non-relativistic amplitude. The crucial point is that this non analytic piece reproduces the one of the full relativistic theory. To show this, we consider the scattering amplitude in ϕ^4 theory at one loop (see Fig. 1.7)

$$\begin{aligned} T(s,t,u) &= \text{const} + \lambda_r^2(\bar{J}(s) + \bar{J}(t) + \bar{J}(u)) + O(\lambda_r^3), \\ \bar{J}(x) &= \frac{1}{16\pi^2}\left(\sigma_x \ln\frac{\sigma_x - 1}{\sigma_x + 1} + 2\right),\;\; \sigma_x = \sqrt{1 - \frac{4M^2}{x}}, \end{aligned} \tag{1.83}$$

where s,t,u are Mandelstam variables. Since we are considering the vicinity of the threshold, the

expansion of $\bar{J}(s), \bar{J}(t), \bar{J}(u)$ around $s = 4M^2, t = 0, u = 0$ takes the form [55]

$$\begin{aligned} 16\pi^2 \bar{J}(s) &= 2 + \frac{i\pi|\mathbf{p}|}{M} - \frac{2|\mathbf{p}|^2}{M^2} + O(v^3), \\ 16\pi^2 \bar{J}(t) &= -\frac{(\mathbf{p}-\mathbf{q})^2}{6M^2} + O(v^4), \\ 16\pi^2 \bar{J}(u) &= -\frac{(\mathbf{p}+\mathbf{q})^2}{6M^2} + O(v^4) \end{aligned} \tag{1.84}$$

Let us now demonstrate that the non-relativistic amplitude in Eq. (1.82) correctly reproduces the non-analytic piece which is generated only by the s-channel contribution. To check this, consider one-loop diagram without derivative vertices. The amplitude is given by

$$T_{NR} = \frac{g_1^2}{M^4} J(P_0) = \frac{g_1^2}{M^3} \frac{i}{4\pi} |\mathbf{p}|. \tag{1.85}$$

Substituting the value of g_1 from the tree-level matching we get

$$T_{NR} = \frac{i\lambda_r^2}{64\pi M^3} |\mathbf{p}|. \tag{1.86}$$

On the other hand, taking into account the matching condition, which takes the form $4M^2 T_{NR} = T_R$ and the explicit expansion of relativistic loop finction $\bar{J}(s)$ from Eq.(1.84) , we see directly that the non-analytic piece from NREFT is the same as in the full relativistic theory.
In the framework of NREFT, the relativistic corrections must be summed up to all orders, to get the relativistic amplitude with particles having the relativistic dispersion law. Furthermore, this issue affects the matching condition Eq.(1.77). Due to non-relativistic normalization of the states, leading to the factors $2\omega(\mathbf{p_i})^{1/2}$ in the matching condition, one has to sum up contributions of higher order operators to fulfil Lorentz invariance. However, in the so-called *covariant NREFT* one can modify the above framework such that the Lorentz invariance is maintained from the beginning by construction [56]. To this end, let us rescale the non-relativistic field as $\Phi(x) \to \sqrt{2\Omega}\Phi(x)$, where $\Omega = \sqrt{M^2 - \Delta}$. Then, one can write down the Lagrangian with the rescaled field

$$\mathcal{L} = \Phi^\dagger 2\Omega(i\partial_t - \Omega)\Phi + G(\Phi^\dagger)^2\Phi^2 + ..., \tag{1.87}$$

where G is the lowest-order coupling and the higher-order derivative terms are omitted in the expression. The corresponding propagator has the form

$$i\langle|T\Phi(x)\Phi^\dagger(0)|\rangle = \int \frac{d^4p}{(2\pi)^4} \frac{\mathrm{e}^{-ipx}}{2\omega(\mathbf{p})(\omega(\mathbf{p}) - p_0 - i\epsilon)}, \tag{1.88}$$

whereas the loop integral, entering all loop diagramms, is given by

$$J(P^0, \mathbf{P}) = \int \frac{d^D k}{(2\pi)^D i} \frac{1}{2\omega(\mathbf{k})2\omega(\mathbf{P}-\mathbf{k})(\omega(\mathbf{k}) - k^0)(\omega(\mathbf{P}-\mathbf{k}) - P^0 + k^0)} \tag{1.89}$$

and dimensional regularization is implied. At this point, we mention that the loop integral violates the power counting rules, which require that $J(P^0, \mathbf{P})$ is counted as $O(v^{d-2})$. The reason for this is related to the presence of heavy mass scale M in the integrand of Eq.(1.89). Since the integration in Eq.(1.89) is performed up to infinity, it is clear that at momenta of the order of M and higher, when effective

theory breaks down, the integration procedure is no longer valid. However, there is a way to remove the high-energy contributions to the integral through the so-called *threshold expansion* [55, 57, 58]. The main idea of this prescription is to expand the integrand in Eq.(1.89) in powers of $1/M$, integrate each term of the expansion and then resum. Performing the threshold expansion in the above integral and doing the momentum integration, one arrives at the following expression of the loop integral

$$J(P^0, \mathbf{P}) = \int \frac{d^D k}{(2\pi)^D} \frac{1}{2P^0} \frac{1}{\mathbf{k}^2 - (\mathbf{kP}/P^0)^2 - q_0^2} = \frac{i}{16} \sqrt{1 - \frac{4M^2}{s}}. \tag{1.90}$$

Note that it is equivalent to the relativistic one loop integral. We see that the threshold expansion leads to the correct relativistic result and loops preserve the power counting rules, i.e., J is counted as $O(v)$.

1.5 Finite-volume formalism

In the previous section, we mentioned already that the resonances require a special treatment in lattice QCD. The reason, why it is impossible to gain any information about resonances from large- time behaviour of Euclidean correlators (as it is the case with stable particles), is the following. In order to calculate scattering parameters from lattice QCD, one has to Wick-rotate the Euclidean n-point function back to Minkowski space. Such continuum reconstruction, indeed, would be possible according to the Osterwalder-Schrader theorem, which however requires the *continuity* of the lattice. Since the lattice momentum takes only *discrete* values, $p = 2\pi n/L, n \in \mathcal{N}$, it is not possible to perform the analytical continuation. The statement that infinite volume scattering parameters cannot be directly determined from Euclidean lattice correlators goes under the name of Maiani-Testa theorem [59]. However, as we will discuss below, the *finite volume* effects of two interacting particles on the lattice, whose interaction range is much smaller than the box size, contain information about their infinite-volume scattering amplitudes. Historically, the above mentioned idea appeared in the work by Huang and Yang [60], who considered the interaction of two hard spheres in a box and found the relation between the energy shift due to interaction and the scattering length in the infinite volume. The other pioneering work is by DeWitt [61], who also established connection between discrete spectrum and scattering parameters. Years later, there was the first attempt of lattice determination of the $\pi - \pi$ and $\pi - N$ scattering lengths by Guagnelli, Marinari and Parisi [62]. However, it was Martin Lüscher, who systematically addressed this problem in a series of papers [48, 63, 64].

Physically, there are two types of finite volume-effects. One is due to the polarization effects of individual particles "around the world". Such effects are exponentially suppressed in volume size as $e^{-M_\pi L}$. Another finite-volume effect results from direct interaction of the particles with each other and is not exponentially suppressed, but rather has a power law dependence on the box size. This can be seen from the following quantum-mechanical consideration. The probability that two particles in the finite volume interact at rest is proportional to inverse of the volume V^{-1}, but equal to zero in the infinite volume. Thus in the cubic box of the size L, the finite-volume effect due to interaction is $1/L^3$ at leading order. The 2-particle energy shift in a finite box due to this effect is related to the scattering phase shift in the infinite volume. Of course, for a precise determination of phase shift, the box must be large enough, so that polarization effects can be neglected. In other words, one must exploit lattices with the length L much bigger than the interaction range R. We focus below first on the elastic 2-body scattering and then consider the coupled-channel formalism.

1.5.1 Elastic scattering

The mapping between the 2-particle energy shift in a finite volume and the infinite-volume phase shift was initially derived by Lüscher in the non-relativistic-quantum mechanics and then proved in a quantum field theory [63, 64]. We treat first the non-relativistic case. [2] To this end, let us consider the simple case of non-relativistic scattering of two spin-0 particles with equal masses, which interact through a short-range potential V in 3 dimensions and in the CM frame. We write first the scattering T-matrix given by the Lippmann-Schwinger (LS) equation, which has the following momentum-space representation :

$$\langle\, \mathbf{q}' \,|\, T(E) \,|\, \mathbf{q} \,\rangle = \langle\, \mathbf{q}' \,|\, V(E) \,|\, \mathbf{q} \,\rangle + \int \frac{d^3\mathbf{k}}{(2\pi)^3} \langle\, \mathbf{q}' \,|\, V(E) \,|\, \mathbf{k} \,\rangle \frac{1}{\frac{\mathbf{k}^2}{2\mu} - E - i\epsilon} \langle\, \mathbf{k} \,|\, T(E) \,|\, \mathbf{q} \,\rangle, \tag{1.91}$$

where $E = q_0^2/2\mu$ is the full CM energy of the incoming particles and μ is the reduced mass. The corresponding partial wave expansions of V and T have the well-known form:

$$\begin{aligned} \langle\, \mathbf{q}' \,|\, T(E) \,|\, \mathbf{q} \,\rangle &= 4\pi \sum_{l=0}^{\infty} \sum_{m=-l}^{+l} Y_{lm}(\hat{\mathbf{q}}')\, Y^{\star}_{lm}(\hat{\mathbf{q}})\, T_l(E; \mathbf{q}', \mathbf{q}) \\ \langle\, \mathbf{q}' \,|\, V(E) \,|\, \mathbf{q} \,\rangle &= 4\pi \sum_{l=0}^{\infty} \sum_{m=-l}^{+l} Y_{lm}(\hat{\mathbf{q}}')\, Y^{\star}_{lm}(\hat{\mathbf{q}})\, V_l(E; \mathbf{q}', \mathbf{q}). \end{aligned} \tag{1.92}$$

Taking into account the orthogonality of the spherical functions, and putting $q'^2 = q_0^2$, we get the LS equation for the half-shell T-matrix:

$$T_l(q', q) = V_l(q', q) + \int_0^{\infty} \frac{dk k^2}{2\pi^2} T_l(q', k) V_l(k, q) \frac{2\mu}{k^2 - q'^2 - i\epsilon}. \tag{1.93}$$

We consider further only S-wave scattering. Let us single out the on-shell T-matrix, which is responsible for main finite-volume corrections. To separate the singular part of the LS equation, we write the propagator as

$$\frac{1}{k^2 - q'^2 - i\epsilon} = \frac{\mathcal{P}}{k^2 - q'^2} + i\pi\delta(k^2 - q'^2) \tag{1.94}$$

where $\mathcal{P}$ denotes the principal value and this identity is valid only within an integral. Then, the LS equation takes the form

$$T_l(q', q) = V_l(q', q) + \mathcal{P} \int_0^{\infty} \frac{dk k^2}{2\pi^2} T_l(q', k) V_l(k, q) \frac{2\mu}{k^2 - q'^2} + i\pi \frac{q'}{4\pi} V_l(q', q) T(q', q') \tag{1.95}$$

Furthermore, it is clear that the formal solution of Eq. (1.95) can be written in terms of the K-matrix as

$$\begin{aligned} T_l(q', q) &= K_l(q', q) \left[1 + i \frac{q'}{4\pi} T(q', q') \right] \\ K_l(q', q) &= V_l(q', q) + \int_0^{\infty} \frac{dk k^2}{2\pi^2} K_l(q', k) V_l(k, q) \frac{2\mu}{k^2 - q'^2}, \end{aligned} \tag{1.96}$$

[2] For thorough treatment of potential scattering theory reader is referred to a classical book by Goldberger and Watson [65]

As is known, the partial-wave amplitudes T_l satisfy the on-shell ($q'^2 = q^2 = q_0^2$) unitarity relation

$$\mathrm{Im}\, T_l(E;q,q) = \mathrm{Im}\, T_l(E) = \frac{\mu q}{2\pi} |\, T_l(E)\,|^2, \tag{1.97}$$

and they are expressed through the scattering phase δ_l as

$$T_l(E) = \frac{2\pi}{\mu} \frac{1}{q\,\mathrm{ctg}\,\delta_l(q) - iq}. \tag{1.98}$$

Using last equation, we arrive at the on-shell K-matrix

$$K(q,q) = \frac{q}{\mu}\mathrm{tg}\,\delta(q). \tag{1.99}$$

Let us now consider the scattering in a finite-volume. Since all momenta are quantized in a box and therefore run over discrete set of values $\{\mathbf{q}, \mathbf{q}', \mathbf{k}\} = 2\pi\mathbf{n}/L, \mathbf{n} \in \mathcal{Z}^3$, the integration must be substituted by summation over the allowed momenta:

$$\int \frac{d^3k}{(2\pi)^3} \longrightarrow \frac{1}{L^3} \sum_{\mathbf{k}=\mathbf{2\pi n/L}} \tag{1.100}$$

Furthermore, the partial wave projection is non-trivial, since spherical symmetry is broken down to the cubic group and thus higher partial waves mix with lower ones. However at low energies, the effects of partial wave mixing are suppressed and we will neglect them to simplify the derivation. In addition, the potential and masses get only exponentially suppressed corrections and thus we will use their infinite-volume values. Having the above in mind, the finite-volume version of the T-matrix, T^L satisfies the following LS equation

$$T^L(q',q) = V(q',q) + \frac{1}{L^3} \sum_{\mathbf{k}=2\pi\mathbf{n}/L} T^L(q',k)V(k,q)\frac{2\mu}{k^2 - q'^2}, \tag{1.101}$$

where no $i\epsilon$ prescription is needed, since all quantities are real. Again, the sum in right-hand side of Eq. (1.101) has a singularity when the particles go on-shell and we remove it by subtracting and adding the singular contribution

$$\begin{aligned} T^L(q',q) &= V(q',q) + \frac{1}{L^3} \sum_{\mathbf{k}=2\pi\mathbf{n}/L} \{T^L(q',k)V(k,q) - T^L(q',q')V(q',q)\}\frac{2\mu}{k^2 - q'^2} \\ &+ T^L(q',q')V(q',q)\frac{1}{L^3} \sum_{\mathbf{k}=2\pi\mathbf{n}/L} \frac{1}{k^2 - q'^2} \end{aligned} \tag{1.102}$$

In order to establish the relation between T^L and T and to quantify the finite-volume effects, let us use key result of the called the regular summation theorem. The theorem states that for a function $f(\mathbf{k})$ which is non-singular, infinitely differentiable and decays fast enough for $|\mathbf{k}| \to \infty$, the sum over the discrete set coincides with the integral up to exponentially suppressed terms

$$\frac{1}{L} \sum_{\mathbf{k}} f(\mathbf{k}) = \int \frac{d^3k}{(2\pi)^3} f(\mathbf{k}) + O(e^{-M_\pi L}). \tag{1.103}$$

The result can be derived with the help of Poisson summation formula

$$\frac{1}{L^3}\sum_{\mathbf{k}} f(\mathbf{k}) = \int \frac{d^3k}{(2\pi)^3}\, f(\mathbf{k}) + \sum_{\mathbf{k}} \int \frac{d^3k}{(2\pi)^3}\, f(\mathbf{k})\, e^{iL\mathbf{kn}}. \tag{1.104}$$

In the Eq. (1.102), we apply the regular summation theorem to the first summand on the right-hand side, which is regular. After some simple transformations we arrive at the following equation for T^L

$$T^L(q',q) = \left[1 + T^L(q',q')\frac{1}{4\pi^2 L}\mathbf{S}\left(\left(\frac{Lq'}{2\pi}\right)^2\right)\right] V(q',q) + \mathcal{P}\int \frac{d^3k}{(2\pi)^3} T^L(q,k)V(q',q)\frac{2\mu}{k^2-q'^2}, \tag{1.105}$$

where the function $\mathbf{S}$ is defined through

$$\mathbf{S}\left(\left(\frac{Lq'}{2\pi}\right)^2\right) = \left(\frac{1}{L^3}\sum_{\mathbf{k}=2\pi\mathbf{n}/L} - \int \frac{d^3k}{(2\pi)^3}\right)\frac{1}{k^2-q'^2} \tag{1.106}$$

The solution of the LS equation in a finite volume has the form

$$T^L(q',q) = \left[1 + T^L(q',q')\frac{1}{4\pi^2 L}\mathbf{S}\left(\left(\frac{Lq}{2\pi}\right)^2\right)\right] K^L(q',q). \tag{1.107}$$

Here, the K^L-matrix

$$K^L(q',q) = V(q',q) + \int_0^\infty \frac{dkk^2}{2\pi^2} K^L(q',k)V(k,q)\frac{2\mu}{k^2-q'^2} + O(e^{-M_\pi L}) \tag{1.108}$$

coincides with the K-matrix in the infinite volume up to exponentially suppressed terms.

We conclude from Eq.(1.107) that the energy levels in a finite volume, given by poles of on-shell T^L matrix, are related to infinite-volume K-matrix (see Eq.1.99) through the equation

$$q\,\mathrm{ctg}\delta(q) = \frac{1}{\pi L}\mathbf{S}\left(\left(\frac{Lq}{2\pi}\right)^2\right) \tag{1.109}$$

This formula plays a central role in our analysis and goes under the name of the Lüscher formula. In the original paper, the rhs. of the above equation is written in terms of so-called *zeta function* $\mathcal{Z}_{00}(s,\hat{q}^2)$

$$q\,\mathrm{ctg}\delta(q) = \frac{1}{\pi^{3/2}L}\mathcal{Z}_{00}(1,\hat{q}^2), \tag{1.110}$$

where, generally, the zeta function is defined as

$$\mathcal{Z}_{00}(s,\hat{q}^2) = \frac{1}{\sqrt{4\Pi}}\sum_{\mathbf{n}\in Z^3}\frac{1}{(\mathbf{n}^2-\hat{q}^2)^s}, \qquad \hat{q} = \frac{qL}{2\pi} \tag{1.111}$$

for $s > 3/2$ and can be analytically continued to $s = 1$. The function $\mathbf{S}$, defined in Eq. (1.106), is divergent and thus requires regularisation. Both dimensional and cut-off regularisation may be used, the final results should not depend on particular scheme. We introduce the cut-off momentum q_{max}. After

integration, **S** becomes [66, 67]

$$\mathbf{S}\left(\left(\frac{Lq}{2\pi}\right)^2\right) = \mathcal{Z}_{00}(1,\hat{q}^2) = \lim_{\Lambda\to\infty}\left(\frac{1}{\sqrt{4\pi}}\sum_{\mathbf{n}}^{\Lambda}\frac{1}{\mathbf{n}^2-\hat{q}^2} - \sqrt{4\pi}\Lambda\right), \tag{1.112}$$

where $\Lambda = q_{max}L/2\pi$.

Let us now consider t the large-L expansion of Lüscher's equation. To this end first note that the effective range expansion of $q\mathrm{ctg}\delta(q)$ has the well-known form

$$q\mathrm{ctg}\delta(q) = \frac{1}{a} + \frac{1}{2}rq^2 + ... \tag{1.113}$$

At large L, one expects that $\hat{q}^2 = |\mathbf{n}|^2 + O(1/L)$ and we thus need to find corrections to this leading term. We isolate further the singularity of the zeta-function at $\hat{q}^2 = \mathbf{n}^2$ as follows

$$\begin{aligned} Z_{00}(1;\mathbf{n}^2) &= \frac{1}{\sqrt{4\pi}}\sum_{\mathbf{l}\neq\mathbf{n}}^{\Lambda}\frac{1}{\mathbf{l}^2-\mathbf{n}^2} - \sqrt{4\pi}\Lambda \\ &= \lim_{\hat{p}\to|\mathbf{n}|}\left[\frac{1}{\sqrt{4\pi}}\sum_{\mathbf{n}}^{\Lambda}\frac{1}{\mathbf{n}^2-\hat{q}^2} - \sqrt{4\pi}\Lambda\right] - \frac{1}{\sqrt{4\pi}}\frac{1}{|\mathbf{n}|^2-\hat{q}^2}, \end{aligned} \tag{1.114}$$

where $\mathbf{l}$ are integers and the limit $\Lambda\to\infty$ is implied on both sides. Here $Z_{00}(1;\mathbf{n}^2)$ coincides with the subtracted Lüscher zeta function [63]. The lhs. of the above equation can now be Taylor-expanded around $\hat{q}^2 = \mathbf{n}^2$. Substituting the Taylor expansion of $\mathcal{Z}_{00}(1,\hat{q}^2)$ and Eq.(1.113) into Eq. (1.110), we arrive at the expansion of ground state energy for $L \gg a, r$

$$E_0 = -\frac{4\pi a}{mL^3}\left[1 + c_1\frac{a}{L} + c_2\frac{a^2}{L^2} + ...\right] + O(L^{-6}), \tag{1.115}$$

where coefficients c_1 and c_2 are

$$\begin{aligned} c_1 &= -2.837297 = \frac{1}{\pi}Z_{00}(1,0) \\ c_2 &= 6.375183 = \frac{1}{\pi^2}\left(Z_{00}(1,0)^2 - Z_{00}(2,0)\right) \end{aligned} \tag{1.116}$$

This formula shows, how can one extract the scattering length by calculating the ground state energy level on the lattice.

It is instructive to consider a one-dimensional scattering problem. In that case one cannot expand in large L since the leading order finite-volume effect $1/L$ whereas the energy splitting is of order $1/L^2$. In other words one must resum to all orders in Lüscher equation. In fact this can be done analytically. Note that in 1D the Lüscher function is finite and we need to evaluate only the sum in Eq.(1.106). Using Poissons' summation formula after contour integration we get the following Lüscher equation

$$\delta(q) = -\pi\hat{q} + n\pi. \tag{1.117}$$

Having derived the Lüscher equation in the non-relativistic quantum mechanics we may ask whether it remains valid in quantum field theory, when all radiation effects are included. The answer was given in the original paper and formulated as a theorem which states that the method remains valid in QFT up to

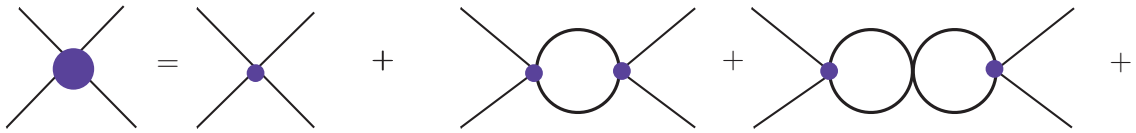

Figure 1.9: bubble sum in NREFT, s-wave, s-channel

$O(e^{-M_\pi L})$ corrections, provided the relativistic dispersion relation is used $E = 2\sqrt{m^2 + \mathbf{q}^2}$.

A very convenient way to derive Lüscher equation is to use covariant NREFT, considered in the previous section, in a finite volume. Note that the full amplitude is given by the s-channel bubble chain sum (see Fig. 1.9) and satisfies the following LS equation in the infinite volume

$$T(s) = K(s) + K(s)J(s)T(s), \tag{1.118}$$

where the loop function is given by Eq. (1.90) and the potential $V(s)$ is a low-energy polynomial, which contains only information about the short-range interactions, encoded in the low-energy constants of NREFT. Note that we consider here only s-wave scattering. In a finite volume, the potential remains the same, whereas the loop function changes as

$$J(s) \to \frac{2}{\sqrt{\pi}L}\mathcal{Z}_{00}(1;\hat{q}^2) \tag{1.119}$$

and we again arrive at the Lüscher equation for the s-wave.

1.5.2 Inclusion of higher partial waves

In the above analysis we have neglected the higher- order partial waves and the effects of the partial-wave mixing. However, for a number of interesting systems, it is necessary to include them- for example in case of $\pi\pi$ scattering which we consider below. Furthermore, the application of the Lüscher equation, which was derived above in the CM frame, requires lattice measurement with several lattice sizes and is prohibitively expensive. However, one gets more data for fixed lattice size by considering scattering with non-zero total momentum i.e., using *Lorentz boosts* [68]. In fact, the boosts are widely used in current lattice simulations and thus we give a form of Lüscher equation for this case without detailed derivation. Performing partial-wave expansion of the T^L and V, one can get the LS equation for the partial-wave components. Note that, whereas the partial- wave expansion of the potential is the same in finite and infinite volumes, the expansion of T^L differs, since the rotational symmetry is broken down to the cubic group. The final result for the boosted system looks like

$$\det\left[e^{2i\delta} - \frac{M+i}{M-i}\right] = 0, \tag{1.120}$$

where the matrix M depends on the boost direction $\mathbf{d}$ and is given by

$$M^{\mathbf{d}}_{lm,l'm'}(q) = \frac{(-1)^l}{\gamma\pi^{3/2}} \sum_{j=|l-l'|}^{l+l'} \sum_{s=-j}^{j} \frac{i^j}{\hat{q}^{j+1}} (\mathcal{Z}^{\mathbf{d}}_{js}(1;q^2))^* C_{lm,js,l'm'}, \tag{1.121}$$

where the tensor $C_{lm,js,l'm'}$ is expressed through the Wigner $3j$- symbols

$$C_{lm,js,l'm'} = (-1)^{m'} i^{l-j+l'} \sqrt{(2l+1)(2j+1)(2l'+1)} \begin{pmatrix} l & j & l' \\ m & s & -m' \end{pmatrix} \begin{pmatrix} l & j & l' \\ 0 & 0 & 0 \end{pmatrix}. \tag{1.122}$$

The function $\mathcal{Z}^{\mathbf{d}}_{js}(1;q^2)$ is the *generalised zeta function*, given by

$$\mathcal{Z}^{\mathbf{d}}_{js}(1;q^2) = \sum_{\mathbf{r}\in P_{\mathbf{d}}} \frac{r^l Y_{lm}(\theta,\phi)}{(\mathbf{r}-q^2)^s} \tag{1.123}$$

and corresponding summation set

$$P_{\mathbf{d}} = \{\mathbf{r}\in\mathcal{R}^3 | \mathbf{r} = \vec{\gamma}^{-1}(\mathbf{n}+\frac{1}{2}\mathbf{d}),\ \ \mathbf{n},\mathbf{d}\in\mathcal{Z}^3\}, \gamma = \frac{1}{\sqrt{1-\mathbf{v}^2}} \tag{1.124}$$

We now discuss implications of rotational symmetry breaking on the extraction of scattering phases. In the absence of a boost, our system exhibits cubic symmetry $O(3,Z)$, whose irreducible representations are those of special cubic group $SO(3,Z)$ fixed by parity transformations $P=\pm1$ [48]. One can simplify the form of M by taking into account the transformation properties of the zeta functions under the cubic group. From Eq.(1.123), it follows that one needs to know the transformation laws of harmonic polynomials $\mathcal{Y}_{lm}(\mathbf{r}) = r^l Y_{lm}(\theta,\phi)$ under the cubic group. For any $R\in O(3,Z)$ we can write

$$\mathcal{Y}_{lm}(R\mathbf{r}) = \sum_{m'=-l}^{l} D^{(l)}_{mm'}(R)\mathcal{Y}_{lm}(\mathbf{r}), \tag{1.125}$$

where $D^{(l)}_{mm'}(R)$ are representation matrices. Generally these representations can be expressed through the irreducible ones Γ. For example for $l=0$ we have $\mathbf{0}=A_1^+$ for $l=1-$ $\mathbf{1}=T_1^-$, for $l=2-$ $\mathbf{3}=E^+\oplus T_2^+$ and so on with corresponding basis vectors, given in Ref [48]. Then, from transformation properties of harmonic polynomials one can deduce the symmetry relation between elements of M. It is clear that in practice, one must truncate the number of partial waves in Eq.(1.122) at some $l_{max}=\Lambda$. In particular, for only S-wave, we can set $\Lambda=0$ and we are restricted to the A_1^+- sector. Then, it is straightforward to show that Eq.(1.122) reduces to the previously obtained Eq. (1.110).

In case of a non-zero boost $d\neq0$, due to deformations of the cubic lattice, the cubic symmetry $O(3,Z)$ is further reduced to point symmetry, which contains rotations and rotation-inversions. The form of the point group depends on the direction of the boost. Consider, for example, a particular case in $d=(0,0,1)$. The corresponding point group is tetragonal group D_{4h}, which has 10 irreducible representations: 8 1-dimensional $A_1^\pm, A_2^\pm, B_1^\pm, B_2^\pm$ and 2 2-dimensional $E^\pm$. From the definition of the zeta function and the symmetry properties of $3j$-symbols, in case of equal masses, one can deduce the selection rules for the elements of M-matrix [68], in case of equal masses

$$\begin{aligned} M^{\mathbf{d}}_{lm,l'm'} &= 0 \ \ l' \neq \ l(\mathrm{mod}2) \\ , M^{\mathbf{d}}_{lm,l'm'} &= 0 \ \ m' \neq m \ (\mathrm{mod}4) \\ , M^{\mathbf{d}}_{lm,l'm'} &= M^{\mathbf{d}}_{l'm',lm} = M^{\mathbf{d}}_{l(-m),l'(m')}. \end{aligned} \tag{1.126}$$

As an example, consider the ρ which is observed in p-wave $\pi\pi$ scattering. In this case, the F-wave and higher contributions can be safely neglected and thus one can choose $\Lambda=3$ [69]. For $l=1$, the

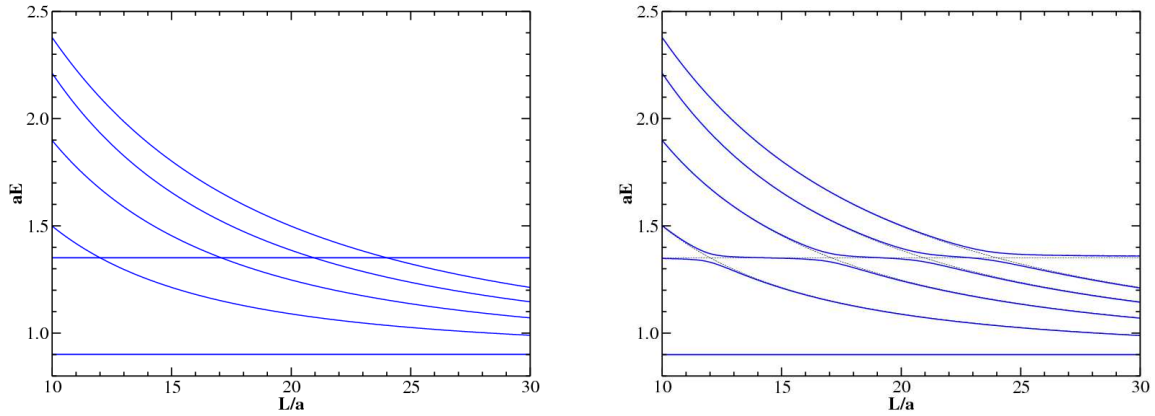

Figure 1.10: The left panel: the free spectrum and a separate resonance. The right panel: the resonance spectrum (avoided level crossing) [70]

irreducible representations of D_{4h} are

$$D^{(0)} = A_1^+ \tag{1.127}$$
$$D^{(1)} = A_2^- \oplus E^-$$

For $D^{(1)}$, we see that unlike unbroken $O(3,Z)$, when the eigenstate belongs to irreducible representation T_1^-, there is splitting into two non-degenerate eigenstates. By decomposing the determinant in Eq.(1.122) into product of several determinants, it can be shown that the phase-shift δ_1 satisfies the following equations

$$\mathrm{ctg}\delta_1(A_2^-) = \frac{\gamma^{-1}}{q\pi^{3/2}}((Z_{00}^{\mathbf{d}}(1;q^2))^* + \frac{2}{\sqrt{5}q^2}(Z_{20}^{\mathbf{d}}(1;q^2))^*), \tag{1.128}$$
$$\mathrm{ctg}\delta_1(E^-) = \frac{\gamma^{-1}}{q\pi^{3/2}}((Z_{00}^{\mathbf{d}}(1;q^2))^* - \frac{1}{\sqrt{5}q^2}(Z_{20}^{\mathbf{d}}(1;q^2))^*).$$

We now come back to the main question of the lattice study of resonances. Since any resonance is by definition a complex pole of T-matrix, it is impossible to identify it from the finite volume spectrum directly. In other words, in a finite volume, due to the discretization of states, no elastic cut is present, through which one could arrive at the second Riemann sheet on which the resonance is present. The resonance manifests itself in a peculiar behaviour of the lattice energy levels as a function of the lattice size. Such a behaviour is called *avoided level crossing*. In Fig. 1.10 we show two cases: in the left figure the resonant state does not couple with two-particle states, whereas in the right one we have a mixture of resonant and 2-particle states. The fact that the resonant state does not correspond to any level in the 2-particle spectrum can be directly observed from Eq.(1.117).

1.5.3 Inelastic scattering

Having considered elastic scattering on the lattice, we now turn our attention to the inelastic one. A lot of interesting hadronic resonances are observed in multichannel scattering processes. Therefore, to study them on the lattice one must generalize the Lüscher formalism to this case. The Lippmann-Schwinger

formalism, we used in previous section together with the covariant NREFT, is ideally suited for this purpose [66, 71, 72]. The main assumption here is that the potential in NREFT, which is a polynomial in small 3-momenta, is finite for the energies of interest. Furthermore, the statement that the Bethe-Salpeter kernel remains the same in a finite box, along with the arguments of the original paper by Lüscher is also true for coupled-channel case as long the coupling to the inelastic channels is small. Having this in mind, consider the simplest case of 2-channel S-wave $\pi\pi - K\bar{K}$ scattering. We can generalize the Eq. (1.107) as follows

$$T^L_{ij}(s) = K_{ij}(s) + \frac{2}{\sqrt{\pi}L}\sum_n K_{in}(s)\mathcal{Z}_{00}(1;\hat{q}^2_n)T^L_{nj}(s), \quad i,j,n = 1,2\,, \tag{1.129}$$

where channel indices 1 and 2 denote the $\pi\pi$ and $K\bar{K}$ channels, respectively. From the above equation we obtain the generalised version of the Lüscher equation for the K-matrix

$$\begin{aligned} &1 - \frac{2}{\sqrt{\pi}L}\mathcal{Z}_{00}(1;\hat{q}^2_1)K_{11}(s) - \frac{2}{\sqrt{\pi}L}\mathcal{Z}_{00}(1;\hat{q}^2_2)K_{22} \\ &+\frac{2}{\sqrt{\pi}L}\mathcal{Z}_{00}(1;\hat{q}^2_1)\frac{2}{\sqrt{\pi}L}\mathcal{Z}_{00}(1;\hat{q}^2_2)(K_{11}(s)K_{22}(s) - K_{12}(s)^2) = 0. \end{aligned} \tag{1.130}$$

From the last equation, we immediately observe that the crucial difference to the one-channel case is that the problem of the determination of K-matrix elements is unconstrained. In other words, for single measurement there are three unknowns K_{11}, K_{12}, K_{12}. One way to solve this issue is to parametrize T-matrix and then tune the parameters for the whole spectrum $E_n(L)$. One convenient choice for the parametrization of T-matrix is following [73]

$$T^{(l)}_{ij} = \frac{1}{(2k_i)^l}K^{-1}_{ij}\frac{1}{(2k_j)^l} + I_{ij}(s), \tag{1.131}$$

where $K_{ij}(s)$ is real function and $I_{ij}(s)$ is the Chew-Mandelstam function.

As in the one-channel case, one has to calculate both ground state and exited energy levels for various box sizes, which again increases computational costs. We introduced already the boost that help to solve this issue. Another promising approach, which plays the central role in the presented thesis is to use the *twisted boundary conditions*. Quark fields $q(x)$, which enter lattice simulations, usually obey periodic boundary conditions. However, nothing prevents us to impose a more general type of boundary condition:

$$q(x_i + L) = e^{i\theta}q(x_i) \tag{1.132}$$

They were first introduced in Refs. [74, 75]. From the last equation, the unperturbed momentum spectrum is given by

$$p_i = n_i\frac{2\pi}{L} + \frac{\theta_i}{L} \tag{1.133}$$

For a fixed L, one can smoothly vary the lattice momenta by changing the *twisting angles* θ_i, which is effectively equivalent to simulations at different volumes. From the computational point of view, it is more feasible to impose periodic boundary conditions on sea quarks whereas valence quarks are subject to twisted boundary conditions. In such case of *partially twisted boundary conditions*, there is no need to generate a set of new gauge configurations for each value of twisting angle [76]. Twisting the quarks effectively results in twisting the hadrons, making the lattice hadron momentum dependent on the twisting angle. The Lüscher formalism is therefore modified, since the loop momenta depend now on the twisting angle. In fact, what needs to be modified is the Lüscher zeta function. If we impose twisted boundary conditions on the s-quark in the $\pi\pi - K\bar{K}$ scattering, the $K\bar{K}$ pair will have a non-vanishing relative

momentum $\pm\theta/L$, whereas the $\pi\pi$ pair is not affected by twisting. Therefore, only the zeta function $\mathcal{Z}_{00}(1;\hat{q}_2^2)$ become now θ-dependent

$$\mathcal{Z}_{00}^{\theta}(1;\hat{q}_2^2) = \frac{1}{\sqrt{4\pi}} \sum_{\mathbf{n}\in Z^3} \frac{1}{(\sum_{i=1}^{3}(n_i + \frac{\theta}{2\pi})^2) - \hat{q}_2^2} \tag{1.134}$$

The generalization to an arbitrary number of channels and various twisting scenarios is straightforward and we do not consider it here.

The generalization of the Lüscher method in case of partially twisted boundary conditions is less trivial and depends on the system in question. As it was shown in Refs. [77, 78] both the partial twisting and full twisting lead to the same result as long as there are no *quark annihilation diagrams*, which is the case for many exotic states. Physically, the presence of channels, where the *valence* quark-antiquark can annihilate into a pair of *sea* quark-antiquark, obeying different boundary conditions, leads to the violation of unitarity. Therefore, on the first sight, no information about scattering can be extracted in that case. However, as it will be demonstrated in the next Chapter, using the framework of PQChPT, it is possible to *modify* the Lüscher method in a way such that the use of partial twisting is fully justified.

References

[1] G. Aad et al., *Observation of a new particle in the search for the Standard Model Higgs boson with the ATLAS detector at the LHC*, Phys. Lett. **B716** (2012) 1, arXiv: 1207.7214 [hep-ex].

[2] K. A. Olive et al., *Review of Particle Physics*, Chin. Phys. **C38** (2014) 090001.

[3] H. D. Politzer, *Reliable Perturbative Results for Strong Interactions?*, Phys. Rev. Lett. **30** (1973) 1346.

[4] D. J. Gross and F. Wilczek, *Ultraviolet Behavior of Nonabelian Gauge Theories*, Phys. Rev. Lett. **30** (1973) 1343.

[5] S. Weinberg, *Phenomenological Lagrangians*, Physica **A96** (1979) 327.

[6] S. L. Adler, *Axial vector vertex in spinor electrodynamics*, Phys. Rev. **177** (1969) 2426.

[7] J. S. Bell and R. Jackiw, *A PCAC puzzle: pi0 –> gamma gamma in the sigma model*, Nuovo Cim. **A60** (1969) 47.

[8] E. Witten, *Current Algebra Theorems for the U(1) Goldstone Boson*, Nucl. Phys. **B156** (1979) 269.

[9] C. Vafa and E. Witten, *Parity Conservation in QCD*, Phys. Rev. Lett. **53** (1984) 535.

[10] Y. Nambu, *Axial vector current conservation in weak interactions*, Phys. Rev. Lett. **4** (1960) 380.

[11] J. Goldstone, *Field Theories with Superconductor Solutions*, Nuovo Cim. **19** (1961) 154.

[12] J. Goldstone, A. Salam and S. Weinberg, *Broken Symmetries*, Phys. Rev. **127** (1962) 965.

[13] H. Leutwyler, *On the foundations of chiral perturbation theory*, Annals Phys. **235** (1994) 165, arXiv: hep-ph/9311274 [hep-ph].

[14] J. Gasser and H. Leutwyler, *Chiral Perturbation Theory: Expansions in the Mass of the Strange Quark*, Nucl. Phys. **B250** (1985) 465.

[15] J. Gasser and H. Leutwyler, *Chiral Perturbation Theory to One Loop*, Annals Phys. **158** (1984) 142.

[16] S. R. Coleman, J. Wess and B. Zumino, *Structure of phenomenological Lagrangians. 1.*, Phys. Rev. **177** (1969) 2239.

[17] C. G. Callan Jr. et al., *Structure of phenomenological Lagrangians. 2.*, Phys. Rev. **177** (1969) 2247.

[18] M. Gell-Mann, R. J. Oakes and B. Renner, *Behavior of current divergences under SU(3) x SU(3)*, Phys. Rev. **175** (1968) 2195.

[19] M. Gell-Mann, *Symmetries of baryons and mesons*, Phys. Rev. **125** (1962) 1067.

[20] A. Manohar and H. Georgi, *Chiral Quarks and the Nonrelativistic Quark Model*, Nucl. Phys. **B234** (1984) 189.

[21] K. G. Wilson, *Confinement of Quarks*, Phys. Rev. **D10** (1974) 2445, [,45(1974)].

[22] K. Osterwalder and R. Schrader, *AXIOMS FOR EUCLIDEAN GREEN'S FUNCTIONS*, Commun. Math. Phys. **31** (1973) 83.

[23] K. Osterwalder and R. Schrader, *Axioms for Euclidean Green's Functions. 2.*, Commun. Math. Phys. **42** (1975) 281.

[24] L. H. Karsten and J. Smit,
Lattice Fermions: Species Doubling, Chiral Invariance, and the Triangle Anomaly,
Nucl. Phys. **B183** (1981) 103, [,495(1980)].

[25] H. B. Nielsen and M. Ninomiya, *Absence of Neutrinos on a Lattice. 1. Proof by Homotopy Theory*,
Nucl. Phys. **B185** (1981) 20, [,533(1980)].

[26] P. H. Ginsparg and K. G. Wilson, *A Remnant of Chiral Symmetry on the Lattice*,
Phys. Rev. **D25** (1982) 2649.

[27] M. Luscher, *Exact chiral symmetry on the lattice and the Ginsparg-Wilson relation*,
Phys. Lett. **B428** (1998) 342, arXiv: hep-lat/9802011 [hep-lat].

[28] P. Hasenfratz, V. Laliena and F. Niedermayer, *The Index theorem in QCD with a finite cutoff*,
Phys. Lett. **B427** (1998) 125, arXiv: hep-lat/9801021 [hep-lat].

[29] R. Narayanan and H. Neuberger, *Chiral fermions on the lattice*,
Phys. Rev. Lett. **71**.20 (1993) 3251, arXiv: hep-lat/9308011 [hep-lat].

[30] R. Narayanan and H. Neuberger, *A Construction of lattice chiral gauge theories*,
Nucl. Phys. **B443** (1995) 305, arXiv: hep-th/9411108 [hep-th].

[31] I. Horvath, *Ginsparg-Wilson relation and ultralocality*, Phys. Rev. Lett. **81** (1998) 4063,
arXiv: hep-lat/9808002 [hep-lat].

[32] W. Bietenholz, *On the absence of ultralocal Ginsparg-Wilson fermions*, (1999),
arXiv: hep-lat/9901005 [hep-lat].

[33] P. Hernandez, K. Jansen and M. Luscher,
Locality properties of Neuberger's lattice Dirac operator, Nucl. Phys. **B552** (1999) 363,
arXiv: hep-lat/9808010 [hep-lat].

[34] D. B. Kaplan, *A Method for simulating chiral fermions on the lattice*,
Phys. Lett. **B288** (1992) 342, arXiv: hep-lat/9206013 [hep-lat].

[35] D. B. Kaplan, *Chiral fermions on the lattice*, Nucl. Phys. Proc. Suppl. **30** (1993) 597.

[36] Y. Shamir, *Chiral fermions from lattice boundaries*, Nucl. Phys. **B406** (1993) 90,
arXiv: hep-lat/9303005 [hep-lat].

[37] V. Furman and Y. Shamir, *Axial symmetries in lattice QCD with Kaplan fermions*,
Nucl. Phys. **B439** (1995) 54, arXiv: hep-lat/9405004 [hep-lat].

[38] A. G. Cohen, D. B. Kaplan and A. E. Nelson, *Testing m(u)=0 on the lattice*, JHEP **11** (1999) 027,
arXiv: hep-lat/9909091 [hep-lat].

[39] S. R. Sharpe and N. Shoresh, *Physical results from unphysical simulations*,
Phys. Rev. **D62** (2000) 094503, arXiv: hep-lat/0006017 [hep-lat].

[40] S. R. Sharpe and N. Shoresh, *Partially quenched chiral perturbation theory without Phi0*,
Phys. Rev. **D64** (2001) 114510, arXiv: hep-lat/0108003 [hep-lat].

[41] C. Bernard and M. Golterman,
On the foundations of partially quenched chiral perturbation theory,
Phys. Rev. **D88**.1 (2013) 014004, arXiv: 1304.1948 [hep-lat].

[42] Morel, A., *Chiral logarithms in quenched QCD*, J. Phys. France **48**.7 (1987) 1111,
URL: http://dx.doi.org/10.1051/jphys:01987004807011100.

[43] M. Golterman, "Applications of chiral perturbation theory to lattice QCD",
Modern perspectives in lattice QCD: Quantum field theory and high performance computing. Proceedings, International School, 93rd Session, Les Houches, France, August 3-28, 2009, 2009 423, arXiv: 0912.4042 [hep-lat],
URL: http://inspirehep.net/record/840837/files/arXiv:0912.4042.pdf.

[44] M. Peardon et al.,
A Novel quark-field creation operator construction for hadronic physics in lattice QCD,
Phys. Rev. **D80** (2009) 054506, arXiv: 0905.2160 [hep-lat].

[45] A. S. Gambhir et al., *Algorithms for Disconnected Diagrams in Lattice QCD*,
PoS **LATTICE2016** (2016) 265, arXiv: 1611.01193 [hep-lat].

[46] A. Abdel-Rehim et al., *Disconnected quark loop contributions to nucleon observables using $N_f = 2$ twisted clover fermions at the physical value of the light quark mass*,
PoS **LATTICE2015** (2016) 136, arXiv: 1511.00433 [hep-lat].

[47] J. J. Dudek et al., *Toward the excited isoscalar meson spectrum from lattice QCD*,
Phys. Rev. **D88**.9 (2013) 094505, arXiv: 1309.2608 [hep-lat].

[48] M. Luscher and U. Wolff, *How to Calculate the Elastic Scattering Matrix in Two-dimensional Quantum Field Theories by Numerical Simulation*, Nucl. Phys. **B339** (1990) 222.

[49] M. S. Mahbub et al., *Positive-parity excited states of the nucleon in quenched lattice QCD*,
Phys. Rev. D **82** (9 2010) 094504,
URL: https://link.aps.org/doi/10.1103/PhysRevD.82.094504.

[50] S. Durr et al., *Ab-Initio Determination of Light Hadron Masses*, Science **322** (2008) 1224,
arXiv: 0906.3599 [hep-lat].

[51] C. Alexandrou et al., *Low-lying baryon spectrum with two dynamical twisted mass fermions*,
Phys. Rev. D **80** (11 2009) 114503,
URL: https://link.aps.org/doi/10.1103/PhysRevD.80.114503.

[52] C. Patrignani et al., *Review of Particle Physics*, Chin. Phys. **C40**.10 (2016) 100001.

[53] W. Caswell and G. Lepage,
Effective lagrangians for bound state problems in QED, QCD, and other field theories,
Physics Letters B **167**.4 (1986) 437, ISSN: 0370-2693,
URL: http://www.sciencedirect.com/science/article/pii/0370269386912979.

[54] M. A. B. Bég and R. C. Furlong, *$\lambda\varphi^4$ theory in the nonrelativistic limit*,
Phys. Rev. D **31** (6 1985) 1370,
URL: http://link.aps.org/doi/10.1103/PhysRevD.31.1370.

[55] J. Gasser, V. E. Lyubovitskij and A. Rusetsky, *Hadronic atoms in QCD + QED*,
Phys. Rept. **456** (2008) 167, arXiv: 0711.3522 [hep-ph].

[56] J. Gasser, B. Kubis and A. Rusetsky, *Cusps in K –> 3pi decays: a theoretical framework*,
Nucl. Phys. **B850** (2011) 96, arXiv: 1103.4273 [hep-ph].

[57] M. Beneke and V. A. Smirnov, *Asymptotic expansion of Feynman integrals near threshold*,
Nucl. Phys. **B522** (1998) 321, arXiv: hep-ph/9711391 [hep-ph].

[58] V. Antonelli et al., *Effective Lagrangians in bound state calculations*,
Annals Phys. **286** (2001) 108, arXiv: hep-ph/0003118 [hep-ph].

[59] L. Maiani and M. Testa, *Final state interactions from Euclidean correlation functions*, Phys. Lett. **B245** (1990) 585.

[60] K. Huang and C. N. Yang, *Quantum-Mechanical Many-Body Problem with Hard-Sphere Interaction*, Phys. Rev. **105** (3 1957) 767, URL: https://link.aps.org/doi/10.1103/PhysRev.105.767.

[61] B. S. DeWitt, *Transition from Discrete to Continuous Spectra*, Phys. Rev. **103** (5 1956) 1565, URL: https://link.aps.org/doi/10.1103/PhysRev.103.1565.

[62] M. Guagnelli, E. Marinari and G. Parisi, *Scattering lengths from fluctuations*, Physics Letters B **240**.1 (1990) 188, ISSN: 0370-2693, URL: http://www.sciencedirect.com/science/article/pii/0370269390904315.

[63] M. Luscher, *Volume Dependence of the Energy Spectrum in Massive Quantum Field Theories. 2. Scattering States*, Commun. Math. Phys. **105** (1986) 153.

[64] M. Luscher, *Two particle states on a torus and their relation to the scattering matrix*, Nucl. Phys. **B354** (1991) 531.

[65] M. L. Goldberger and K. M. Watson, *Collision Theory*, New York: Wiley, 1964.

[66] S. R. Beane et al., *Two nucleons on a lattice*, Phys. Lett. **B585** (2004) 106, arXiv: hep-lat/0312004 [hep-lat].

[67] S. R. Beane et al., *Exploring hyperons and hypernuclei with lattice QCD*, Nucl. Phys. **A747** (2005) 55, arXiv: nucl-th/0311027 [nucl-th].

[68] K. Rummukainen and S. A. Gottlieb, *Resonance scattering phase shifts on a nonrest frame lattice*, Nucl. Phys. **B450** (1995) 397, arXiv: hep-lat/9503028 [hep-lat].

[69] P. Estabrooks and A. D. Martin, *pi pi Partial Waves from 0.6-GeV to 1.8-GeV*, Nucl. Phys. **B95** (1975) 322.

[70] P. Giudice, D. McManus and M. Peardon, *A comparison of analysis techniques for extracting resonance parameters from lattice Monte Carlo data*, Phys. Rev. **D86** (2012) 074516, arXiv: 1204.2745 [hep-lat].

[71] M. Lage, U.-G. Meissner and A. Rusetsky, *A Method to measure the antikaon-nucleon scattering length in lattice QCD*, Phys. Lett. **B681** (2009) 439, arXiv: 0905.0069 [hep-lat].

[72] V. Bernard et al., *Scalar mesons in a finite volume*, JHEP **01** (2011) 019, arXiv: 1010.6018 [hep-lat].

[73] D. J. Wilson et al., *Coupled $\pi\pi$, $K\bar{K}$ scattering in P-wave and the ρ resonance from lattice QCD*, Phys. Rev. **D92**.9 (2015) 094502, arXiv: 1507.02599 [hep-ph].

[74] P. F. Bedaque, *Aharonov-Bohm effect and nucleon nucleon phase shifts on the lattice*, Phys. Lett. **B593** (2004) 82, arXiv: nucl-th/0402051 [nucl-th].

[75] G. M. de Divitiis, R. Petronzio and N. Tantalo, *On the discretization of physical momenta in lattice QCD*, Phys. Lett. **B595** (2004) 408, arXiv: hep-lat/0405002 [hep-lat].

[76] J. Flynn et al., *Partially twisted boundary conditions in lattice simulations*, PoS **LAT2005** (2006) 352, arXiv: hep-lat/0509093 [hep-lat].

[77] P. F. Bedaque and J.-W. Chen, *Twisted valence quarks and hadron interactions on the lattice*, Phys. Lett. **B616** (2005) 208, arXiv: hep-lat/0412023 [hep-lat].

[78] C. T. Sachrajda and G. Villadoro, *Twisted boundary conditions in lattice simulations*, Phys. Lett. **B609** (2005) 73, arXiv: hep-lat/0411033 [hep-lat].

CHAPTER 2

Partial twisting for scalar mesons

2.1 Summary of the project

The aim of the project was to study the possibility of imposing partially twisted boundary conditions in the scalar sector of lattice QCD. According to previous studies, the existence of quark annihilation diagrams makes it impossible to determine the scattering parameters using the conventional Lüscher formalism with partial twisting. However, we demonstrate that this conclusion is too restrictive. Using the framework of partially quenched chiral perturbation theory, we derive the *modified* version of the Lüscher equation, valid for the case of partial twisting. The derivation was done for coupled channel channel S-wave $\pi\eta - K\bar{K}$ scattering with isopin $I = 1$. The channel space is extended, due to the presence of not only valence, but also sea and ghost quarks, to 11 channels. The graded symmetry, intrinsic to partially quenched effective theory, leads to symmetry relations between the elements of the potential and, further, to the non-trivial cancellations in the Lüscher equation, written for those 11 channels. As a result, the final Lüscher equation contains only physical channels (i.e. the one with mesons composed of valence quarks only) and its form depends on the twisting scenario. More precisely, twisting only the s-quark, one gets the Lüscher equation *with no twisting*, which does not provide new information and thus has no practical relevance. On the other hand, twisting only the u-quark, the spectrum is described by the Lüscher equation in a moving frame and it coincides with the one with full twisting. Although the derivation was performed for a particular system, qualitatively the final result remains the same in general case: if a twisted valence quark may annihilate, than the corresponding partial twisting is equivalent to no twisting; if the twisted quark propagates through all quark diagrams without annihilating, then the partially twisted Lüscher equation is identical to the fully twisted one.

Published for SISSA by Springer

Received: November 4, 2013
Revised: December 12, 2013
Accepted: December 18, 2013
Published: January 20, 2014

Partial twisting for scalar mesons

Dimitri Agadjanov,[a,b] **Ulf-G. Meißner**[a,c] **and Akaki Rusetsky**[a]

[a] *Helmholtz-Institut für Strahlen- und Kernphysik (Theorie) and Bethe Center for Theoretical Physics, Universität Bonn, Nussallee 12, D-53115 Bonn, Germany*

[b] *St. Andrew the First-Called Georgian University of the Patriarchate of Georgia, Chavchavadze Ave. 53a, 0162, Tbilisi, Georgia*

[c] *Institute for Advanced Simulation (IAS-4), Institut für Kernphysik (IKP-3) and Jülich Center for Hadron Physics, Forschungszentrum Jülich, D-52425 Jülich, Germany*

E-mail: dagadjanov@hiskp.uni-bonn.de, meissner@hiskp.uni-bonn.de, rusetsky@hiskp.uni-bonn.de

Abstract: The possibility of imposing partially twisted boundary conditions is investigated for the scalar sector of lattice QCD. According to the commonly shared belief, the presence of quark-antiquark annihilation diagrams in the intermediate state generally hinders the use of the partial twisting. Using effective field theory techniques in a finite volume, and studying the scalar sector of QCD with total isospin $I = 1$, we however demonstrate that partial twisting can still be performed, despite the fact that annihilation diagrams are present. The reason for this are delicate cancellations, which emerge due to the graded symmetry in partially quenched QCD with valence, sea and ghost quarks. The modified Lüscher equation in case of partial twisting is given.

Keywords: Lattice QCD, Chiral Lagrangians

ArXiv ePrint: 1310.7183

doi:10.1007/JHEP01(2014)103

Contents

JHEP01(2014)103

1 Introduction

Investigating the scalar sector of QCD in the region below and around 1 GeV on the lattice enables one to gain important information about the low-energy behavior of strong interactions. A few groups have addressed this problem in the recent years (see, e.g., [1–7]). Note that carrying out simulations in the scalar sector is a very challenging task by itself as many of these states share the quantum numbers of the vacuum. In addition, it is known that the particles, whose properties are investigated in these simulations, are resonances. Consequently, in order to perform the extraction of their mass and width from the data, one has to apply the Lüscher approach [8] that implies carrying out simulations at different volumes, complicating further an already difficult problem. Moreover, in case of the $f_0(980)$ and $a_0(980)$ mesons, the analysis has to be done by using a *coupled-channel* Lüscher equation [9–11], which includes $\pi\pi/K\bar{K}$ and $\pi\eta/K\bar{K}$ channels for total isospin $I = 0$ and $I = 1$, respectively. The resonances are very close to the $K\bar{K}$ (inelastic) threshold, which has the unpleasant property of "masking" the avoided level crossing that serves as a signature of the presence of a resonance in a finite volume [9–11].

Here, one should also mention that the mass and width are not the only quantities one is interested in case of scalar resonances. The nature of these states is not well established in phenomenology and is being debated at present, with the arguments given in favor of their interpretation as tetraquark states (see, e.g., [12–15]), as $K\bar{K}$ molecules [16–19], or as

a combination of a bare pole and the rescattering contribution [20, 21] (see also refs. [22–24] for more information on this issue). In view of the conflicting interpretations, it is interesting to study the signatures of a possible exotic behavior, e.g., applying Weinberg's compositeness condition or the pole counting criterion (see, e.g., [25–34]), or investigating the quark mass dependence of the resonance pole position [9]. It is possible to "translate" all these criteria into the language of lattice QCD. However, testing them in the real simulations would require much more data at different volumes and at a much higher precision than it is at our disposal at present.

Summarizing all the facts above, it is legitimate to ask, whether — given our present capabilities — the extraction of the properties of scalar resonances on the lattice can be realistically done with a sufficient rigor and yield clean and unambiguous results in the nearest future.

In refs. [9–11] it has been pointed out that using twisted boundary conditions in lattice simulations [35–39] can provide an important advantage in the scalar meson sector (for applications of this method in other systems see, e.g., [40]). First and foremost, varying the twisting angle $\boldsymbol{\theta}$ can substitute for simulations at different volumes and provide data of energy levels, which should be fitted in order to determine the resonance pole position. Note that the same effect can be achieved by carrying out simulations at a non-zero total momentum. However, whereas the components of the lattice momentum are given by integer numbers in the units of $2\pi/L$, where L is the size of the finite box, the twisting angle can be varied continuously. Another advantage is provided by the fact that twisting allows one to effectively move the threshold away from the resonance pole location. In order to illustrate this, consider an example when the s-quark is twisted in the simulations, whereas u and d quarks still obey periodic boundary conditions [9–11]. Assume, in addition, that the system is in the center-of-mass (CM) frame. In this example, the K and $\bar{K}$ mesons in the $K\bar{K}$ intermediate state acquire 3-momenta, opposite in direction and having equal magnitude, proportional to $|\boldsymbol{\theta}|$. Hence, the energy of the ground state of the $K\bar{K}$ pair goes up, whereas the resonance, which corresponds to a true pole in the S-matrix, stays, by definition, at the same position. For the volumes, which are currently used in lattice simulations, the upward displacement of the $K\bar{K}$ threshold would be a large effect. Consequently, it could be expected that, fitting twisted lattice data, one would achieve a more accurate extraction of the resonance pole position than in the case of periodic boundary conditions, when the threshold and the resonance are very close. Note that this conjecture has been fully confirmed in refs. [10, 11] by performing fits to "synthetic" data sets.

There is, however, an important caveat in the arguments above. Imposing twisted boundary conditions in lattice simulations implies the calculation of gauge configurations anew. This is a very expensive enterprise. The majority of simulations up to day are done by applying the so-called partial twisting, i.e., twisting only the valence quarks and leaving the configurations the same. It can be proven (see, e.g. [38, 39]) that in many cases the results obtained by using partial and full twisting coincide up to exponentially suppressed terms. This happens when there are no annihilation diagrams, i.e., the diagrams where the *valence* quark-antiquark pair from the initial state can annihilate and a pair of the

JHEP01(2014)103

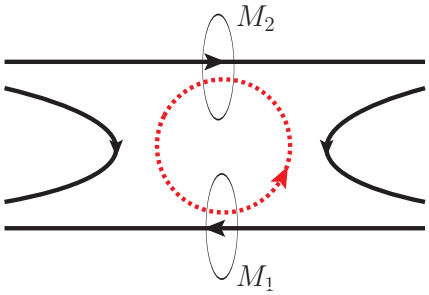

Figure 1. An example of an annihilation diagram in meson-meson scattering. The full and dashed lines denote valence and sea quarks, respectively. The intermediate state for this diagram consists of two mesons M_1 and M_2 with one valence and one sea quark.

sea quark-antiquark is produced, which obey a different boundary condition (see figure 1). However, it is easy to verify that, in case of scalar mesons, the annihilation diagrams do appear. Consequently, following the arguments of refs. [38, 39], one had to conclude that the partial twisting in this case is useless — one has either to perform a full twisting, or to give it up.

We consider this conclusion premature. One could look at the problem from a different point of view. It is definitely not possible to prove in general that in this case the partial and full twisting lead to the same result. Could one find a *modified* Lüscher equation, which corresponds to the case of partial twisting? Does this equation enable one to still extract the physically interesting information about the scattering S-matrix elements in the finite volume? If the answer to this question is yes, using partial twisting in lattice simulations can be justified.

In this paper we do not give a full-fledged solution of the problem. Rather, we have chosen to concentrate on one particular example, namely, the $a_0(980)$, which is an S-wave resonance with the isospin $I = 1$, and solve this problem to the end. Possible mixing to other partial waves is neglected. The inclusion of higher partial waves forms a subject of a separate investigation which will be carried out in the future.

A brief outline of the method is as follows. It is well known that Lüscher's equation can be most easily derived by using non-relativistic EFT framework in a finite volume [41–43]. Twisting at the quark level can be straightforwardly implemented at the hadronic level: the hadrons acquire additional momenta, proportional to the twisting angle $\boldsymbol{\theta}$. The expression for the zeta-function in the Lüscher equation also changes in a well-defined way, whereas the non-relativistic potentials, which encode the short-range dynamics, are $\boldsymbol{\theta}$-independent. All this gives the Lüscher equation in case of twisted boundary conditions.

The case of partially twisted boundary conditions can be considered analogously. The spectrum of the effective theory now contains much more hadrons, consisting of valence, sea and ghost quarks (see, e.g., [44]). Boundary conditions for each hadron are determined by the boundary conditions on its constituents, so the $\boldsymbol{\theta}$-dependence of the zeta-functions, entering the Lüscher equation, is uniquely defined also in this case. The crucial observation, which enables one to arrive at a tractable form of the Lüscher equation, is that the

JHEP01(2014)103

symmetries, which are present in the theory in the infinite volume, relate the potentials in valence, sea and ghost sectors (the masses of valence, sea and ghost quarks are taken equal). It can be shown that the Lüscher equation can be reduced to the one that contains the potentials only in the physical (valence) sector and can thus be used to analyze the lattice data.

The layout of the paper is as follows. In section 2 we describe the effective field theory (EFT) framework for partially twisted QCD — first, in the infinite volume. In section 3 we discuss in detail the constraints imposed by the symmetries on the matrix elements of the effective non-relativistic potential. In doing this, we first neglect the neutral meson mixing beyond tree level. In section 4 the Lüscher equation in case of the partially twisted boundary conditions is derived. Possible applications in the simulations in the scalar sector are discussed. In section 5 we clear the remaining loopholes by discussing the mixing to all orders in this framework and show that the results are not affected. Finally, section 6 contains our conclusions and outlook.

2 The effective field theory framework

In order to obtain the spectrum, one usually studies the behavior of certain correlators at a large Euclidean time separation t:

$$C(t) = \langle \mathcal{O}(t)\mathcal{O}^\dagger(0)\rangle = \frac{1}{Z}\int \mathcal{D}U\mathcal{D}\psi\mathcal{D}\bar{\psi}\,\mathcal{O}(t)\mathcal{O}^\dagger(0)\,\exp\left\{-S_G - \int d^4x\bar{\psi}(\not{D}+m)\psi\right\}, \quad (2.1)$$

where S_G stands for the gluon action functional, and $\mathcal{O}(t), \mathcal{O}^\dagger(t)$ are appropriate source/sink operators, which have a non-zero overlap with the physical states of interest. At this stage, we do not specify the explicit form of these operators — these can be, for example, quark-antiquark or two meson operators, etc.

In order to distinguish between valence and sea quarks, we use the standard trick (see, e.g., [44] and references therein), rewriting the above path integral in the following manner

$$\begin{aligned} C(t) = \frac{1}{Z}\int \mathcal{D}U\mathcal{D}\psi_{\mathsf{v}}\mathcal{D}\bar{\psi}_{\mathsf{v}}\mathcal{D}\psi_{\mathsf{s}}\mathcal{D}\bar{\psi}_{\mathsf{s}}\mathcal{D}\psi_{\mathsf{g}}\mathcal{D}\bar{\psi}_{\mathsf{g}}\,\mathcal{O}_{\mathsf{v}}(t)\mathcal{O}^\dagger_{\mathsf{v}}(0) \\ \times\exp\left\{-S_G - \int d^4x\left[\bar{\psi}_{\mathsf{v}}(\not{D}+m_{\mathsf{val}})\psi_{\mathsf{v}} + \bar{\psi}_{\mathsf{s}}(\not{D}+m_{\mathsf{sea}})\psi_{\mathsf{s}} + \bar{\psi}_{\mathsf{g}}(\not{D}+m_{\mathsf{gh}})\psi_{\mathsf{g}}\right]\right\}. \quad (2.2)\end{aligned}$$

Here, the subscripts "v," "s" and "g" stand for valence, sea and ghost quarks, the latter being described by *commuting* spinor fields. After performing the path integral over quarks, it is seen that the fermion determinant, coming from valence quarks, is exactly cancelled by the one from the ghost quarks, and the expression, given in eq. (2.1), is reproduced.

In order to describe the situation with partially twisted boundary conditions, one imposes twisted boundary conditions on the valence and ghost quarks and periodic boundary conditions on the sea quarks. The masses of all species of quarks are taken equal, in difference to the partially quenched case where $m = m_{\mathsf{val}} = m_{\mathsf{gh}} \neq m_{\mathsf{sea}}$. Note that $m_{\mathsf{val}}, m_{\mathsf{gh}}, m_{\mathsf{sea}}$ are matrices in flavor space. Note also that we assume isospin symmetry throughout the paper $m_u = m_d = \hat{m} \neq m_s$.

JHEP01(2014)103

In the chiral limit, the infinite-volume theory is invariant under the graded symmetry group $\mathrm{SU(2N|N)_L \times SU(2N|N)_R \times U(1)_V}$, where $N = 3$ is the number of light flavors. The low-energy effective Lagrangian,[1] corresponding to the case of partially twisted boundary conditions, contains the matrix $U = \exp\{i\sqrt{2}\Phi/F\}$ of the pseudo-Goldstone fields Φ, which transforms under this group as

$$U \to LUR^\dagger\,, \qquad L, R \in \mathrm{SU(2N|N)}\,. \tag{2.3}$$

The Hermitian matrix Φ has the following representation

$$\Phi = \begin{pmatrix} M_{\mathsf{vv}} & M_{\mathsf{sv}}^\dagger & M_{\mathsf{gv}}^\dagger \\ M_{\mathsf{sv}} & M_{\mathsf{ss}} & M_{\mathsf{gs}}^\dagger \\ M_{\mathsf{gv}} & M_{\mathsf{gs}} & M_{\mathsf{gg}} \end{pmatrix}\,. \tag{2.4}$$

Here, each of the entries is itself a $N \times N$ matrix in flavor space, containing meson fields built up from certain quark species (e.g., from valence quark and valence antiquark, from sea quark and ghost antiquark, and so on). The fields M_{gv} and M_{gs} are anti-commuting pseudoscalar fields (ghost mesons). Further, the matrix Φ obeys the condition [44]

$$\mathrm{str}\,\Phi = \mathrm{tr}\,(M_{\mathsf{vv}} + M_{\mathsf{ss}} - M_{\mathsf{gg}}) = 0\,, \tag{2.5}$$

where "str" stands for the supertrace.

The effective chiral Lagrangian takes the form

$$\mathcal{L} = \frac{F_0^2}{4}\mathrm{str}\,(\partial_\mu U \partial^\mu U^\dagger) - \frac{F_0^2}{4}\,\mathrm{str}(\chi U + U\chi^\dagger) + \text{higher-order terms}, \tag{2.6}$$

where $\chi = 2mB_0$ is proportional to the quark mass matrix.

In the infinite volume, the above theory is completely equivalent to ordinary Chiral Perturbation Theory (ChPT), since the masses of the quarks of all species are set equal. In a finite volume, the difference arises due to the different boundary conditions, set on the different meson fields. These boundary conditions are uniquely determined by the boundary conditions imposed on the constituents.

We do not intend to use the framework of the partially twisted ChPT to carry out explicit calculations. We need this framework only to facilitate the derivation of the Lüscher equation. To this end, let us consider large boxes with $L \gg M_\pi^{-1}$, where M_π is the lightest mass in the system (the pion mass). The characteristic 3-momenta in such a box are much smaller than all masses — consequently, the system can be described by a non-relativistic EFT, whose low-energy couplings are consistently matched to the relativistic theory with the Lagrangian given in eq. (2.6) (for a detailed review of the non-relativistic theory in the infinite volume, we refer the reader, e.g., to the refs. [46, 47]; non-relativistic effective field theories in a finite volume are considered in refs. [41–43].). The two-body scattering

[1] We assume throughout this paper that the partially quenched theory is a theory with a well-defined Hamiltonian and spectrum, the presence of the negative-norm states being a sole artefact of the partial quenching. Recent investigations that can be found in the literature [45], support the above conjecture.

JHEP01(2014)103

T-matrix in the non-relativistic theory obeys the multi-channel Lippmann-Schwinger (LS) equation (for simplicity, we write down this equation in the CM frame)

$$T_{\alpha\beta}(\mathbf{p},\mathbf{q};P_0) = V_{\alpha\beta}(\mathbf{p},\mathbf{q}) + \sum_\gamma \int \frac{d^d\mathbf{k}}{(2\pi)^d} \frac{V_{\alpha\gamma}(\mathbf{p},\mathbf{q})T_{\gamma\beta}(\mathbf{p},\mathbf{q};P_0)}{2w_1^{(\gamma)}(\mathbf{k})2w_2^{(\gamma)}(\mathbf{k})(w_1^{(\gamma)}(\mathbf{k})+w_2^{(\gamma)}(\mathbf{k})-P_0-i0)}\,, \tag{2.7}$$

where the sum runs over all two-body channels labeled by the index γ, and $w_1^{(\gamma)}(\mathbf{k})$, $w_2^{(\gamma)}(\mathbf{k})$ stand for the (relativistic) energies of the first and the second particle in this channel. The potentials $V_{\alpha\beta}(\mathbf{p},\mathbf{q})$ encode the short-range dynamics, including inelastic many-body channels, which are closed at low energies.[2] These potentials are constructed perturbatively and contain the couplings of the non-relativistic effective Lagrangian.

We use dimensional regularization throughout. In this regularization, the potentials $V_{\alpha\beta}(\mathbf{p},\mathbf{q})$ coincide with the K-matrix elements. Expanding into the partial waves gives:

$$V_{\alpha\beta}(\mathbf{p},\mathbf{q}) = 4\pi \sum_{lm} Y_{lm}(\hat{\mathbf{p}}) V^l_{\alpha\beta}(|\mathbf{p}|,|\mathbf{q}|) Y^*_{lm}(\hat{\mathbf{q}})\,, \tag{2.8}$$

where $\hat{\mathbf{k}}$ denotes a unit vector in the direction of $\mathbf{k}$. It is easy to see that in the elastic region for the channel α, on the energy shell where $|\mathbf{p}| = |\mathbf{q}| = q_0$,

$$V^l_{\alpha\alpha}(q_0,q_0) = \frac{8\pi P_0}{q_0}\,\tan\delta_l^{(\alpha)}(q_0)\,, \qquad P_0 = w_1^{(\alpha)}(q_0) + w_2^{(\alpha)}(q_0)\,, \tag{2.9}$$

where $\delta_l^{(\alpha)}$ denotes the elastic scattering phase shift with angular momentum l. In the following, we shall neglect all partial waves except $l = 0$. The inclusion of partial-wave mixing will be considered in the future.

When the relativistic theory, described by the Lagrangian given in eq. (2.6), is matched to the non-relativistic EFT, a complication arises, which stems from the mixing of the states containing neutral mesons. Namely, in the equation (2.7), the states α, β, γ correspond to the *physical* two-particle states. These are not always described by the meson fields which are present in the matrix Φ. The reason for this is that not all the components of Φ are independent due to the condition $\mathrm{str}\,\Phi = 0$.

In order to study the issue of mixing, let us again start with the relativistic theory described by the Lagrangian in eq. (2.6). We restrict ourselves first to order p^2, and retain only diagonal terms in the matrix $\Phi = \mathrm{diag}\,(\phi_1,\ldots,\phi_9)$ (the non-diagonal terms do not mix). The quadratic piece in the $O(p^2)$ Lagrangian takes the form

$$\begin{aligned}
\mathcal{L}_0^{(2)} &= \frac{1}{2}\sum_{i=1}^{6}(\partial_\mu\phi_i)^2 - \frac{1}{2}\sum_{i=7}^{9}(\partial_\mu\phi_i)^2 \\
&\quad -\frac{M^2}{2}\,(\phi_1^2+\phi_2^2+\phi_4^2+\phi_5^2-\phi_7^2-\phi_8^2) - \frac{M_s^2}{2}\,(\phi_3^2+\phi_6^2-\phi_9^2)\,, \\
M^2 &= 2\hat{m}B_0\,, \qquad M_s^2 = 2m_sB_0\,.
\end{aligned} \tag{2.10}$$

[2] There is a caveat in this argument. For example, there are multi-pion channels below $K\bar{K}$ channel. However, since the couplings to these channels are very weak, they can be safely ignored without changing the result. For more discussion on this issue, see ref. [9].

JHEP01(2014)103

Introducing the following linear combinations

$$\begin{aligned}
\phi_1 &= \frac{1}{\sqrt{2}}\,\omega_1 - \frac{1}{\sqrt{6}}\,\omega_2 - \frac{1}{2}\,\omega_5 + \frac{1}{2}\,\omega_8\,,\\
\phi_2 &= -\frac{1}{\sqrt{2}}\,\omega_1 - \frac{1}{\sqrt{6}}\,\omega_2 - \frac{1}{2}\,\omega_5 + \frac{1}{2}\,\omega_8\,,\\
\phi_3 &= \frac{\sqrt{6}}{3}\,\omega_2 + \frac{1}{\sqrt{2}}\,\omega_3 - \frac{1}{\sqrt{2}}\,\omega_6\,,\\
\phi_4 &= -\frac{1}{\sqrt{6}}\,\omega_2 + \frac{1}{\sqrt{2}}\,\omega_4 + \frac{1}{2}\,\omega_5 + \frac{1}{2}\,\omega_8\,,\\
\phi_5 &= -\frac{1}{\sqrt{6}}\,\omega_2 - \frac{1}{\sqrt{2}}\,\omega_4 + \frac{1}{2}\,\omega_5 + \frac{1}{2}\,\omega_8\,,\\
\phi_6 &= \frac{\sqrt{6}}{3}\omega_2 + \frac{1}{\sqrt{2}}\,\omega_3 + \frac{1}{\sqrt{2}}\,\omega_6\,,\\
\phi_7 &= -\frac{1}{\sqrt{6}}\,\omega_2 + \frac{1}{\sqrt{2}}\,\omega_7 + \omega_8\\
\phi_8 &= -\frac{1}{\sqrt{6}}\,\omega_2 - \frac{1}{\sqrt{2}}\,\omega_7 + \omega_8\\
\phi_9 &= \frac{\sqrt{6}}{3}\,\omega_2 + \sqrt{2}\,\omega_3\,,
\end{aligned} \tag{2.11}$$

it is straightforward to check that the quadratic piece of the Lagrangian can be rewritten in terms of the fields $\omega_1,\ldots,\omega_8$:

$$\begin{aligned}
\mathcal{L}_0^{(2)} = \frac{1}{2}\Big\{&(\partial_\mu\omega_1)^2 + (\partial_\mu\omega_2)^2 - (\partial_\mu\omega_3)^2 + (\partial_\mu\omega_4)^2 + (\partial_\mu\omega_5)^2 + (\partial_\mu\omega_6)^2 - (\partial_\mu\omega_7)^2 - (\partial_\mu\omega_8)^2\Big\}\\
&-\frac{M^2}{2}\,(\omega_1^2+\omega_4^2+\omega_5^2-\omega_7^2-\omega_8^2) + \frac{M_s^2}{2}\,(\omega_3^2-\omega_6^2) - \frac{M_\eta^2}{2}\,\omega_2^2\,,
\end{aligned} \tag{2.12}$$

where $M_\eta^2 = \frac{2}{3}\,M_s^2 + \frac{1}{3}\,M^2$. Note that the condition $\mathrm{str}\,\Phi = 0$ is automatically fulfilled for the fields given by eq. (2.11). The eight fields $\omega_1,\ldots,\omega_8$ are unconstrained as opposed to the nine fields $\phi_1,\ldots,\phi_9$. The propagators for the physical particles can be read off from eq. (2.12). The fields $\omega_3,\omega_7,\omega_8$ are ghost fields (they enter the Lagrangian with a "wrong" sign). Note also that the transformation given in eq. (2.11) can be written in the compact form

$$\Phi_{\mathsf{diag}} = \sum_{j=1}^{8} \omega_j T_j\,, \tag{2.13}$$

where in Φ_{diag} all components except those on the diagonal are set to zero, and the explicit form of the matrices T_j is given in appendix A.

The fields ω_i describe physical particles at $O(p^2)$, and matching to the non-relativistic theory is most easily performed in this basis. The symmetry relations between various matrix elements get, however, very complicated in this basis. In order to circumvent this

JHEP01(2014)103

problem, we have chosen to work in another basis

$$\begin{aligned}
&\pi^0_{\mathsf{vv}} = \omega_1\,, \qquad \pi^0_{\mathsf{ss}} = \omega_4\,, \qquad \pi^0_{\mathsf{gg}} = \omega_7\,,\\
&\eta_{\mathsf{vv}} = -\omega_2 + \frac{1}{\sqrt{6}}\,(-\omega_5 + \omega_8 - \sqrt{2}\omega_3 + \sqrt{2}\omega_6)\,, \qquad \eta'_{\mathsf{vv}} = \frac{1}{\sqrt{6}}\,(-\sqrt{2}\omega_5 + \sqrt{2}\omega_8 + \omega_3 - \omega_6)\,,\\
&\eta_{\mathsf{ss}} = -\omega_2 + \frac{1}{\sqrt{6}}\,(\omega_5 + \omega_8 - \sqrt{2}\omega_3 - \sqrt{2}\omega_6)\,, \qquad \eta'_{\mathsf{ss}} = \frac{1}{\sqrt{6}}\,(\sqrt{2}\omega_5 + \sqrt{2}\omega_8 + \omega_3 + \omega_6)\,,\\
&\eta_{\mathsf{gg}} = -\omega_2 + \frac{1}{\sqrt{6}}\,(2\omega_8 - 2\sqrt{2}\omega_3)\,, \qquad \eta'_{\mathsf{gg}} = \frac{1}{\sqrt{3}}\,(2\omega_8 + \sqrt{2}\omega_3)\,.
\end{aligned} \tag{2.14}$$

Note also that the fields ϕ_i and π^0, η, η' are related by usual SU(3) relations:

$$\begin{aligned}
\phi_1 &= \frac{1}{\sqrt{2}}\,\pi^0_{\mathsf{vv}} + \frac{1}{\sqrt{6}}\,\eta_{\mathsf{vv}} + \frac{1}{\sqrt{3}}\,\eta'_{\mathsf{vv}},\\
\phi_2 &= -\frac{1}{\sqrt{2}}\,\pi^0_{\mathsf{vv}} + \frac{1}{\sqrt{6}}\,\eta_{\mathsf{vv}} + \frac{1}{\sqrt{3}}\,\eta'_{\mathsf{vv}},\\
\phi_3 &= -\frac{2}{\sqrt{6}}\,\eta_{\mathsf{vv}} + \frac{1}{\sqrt{3}}\,\eta'_{\mathsf{vv}},\\
\phi_4 &= \frac{1}{\sqrt{2}}\,\pi^0_{\mathsf{ss}} + \frac{1}{\sqrt{6}}\,\eta_{\mathsf{ss}} + \frac{1}{\sqrt{3}}\,\eta'_{\mathsf{ss}},\\
\phi_5 &= -\frac{1}{\sqrt{2}}\,\pi^0_{\mathsf{ss}} + \frac{1}{\sqrt{6}}\,\eta_{\mathsf{ss}} + \frac{1}{\sqrt{3}}\,\eta'_{\mathsf{ss}},\\
\phi_6 &= -\frac{2}{\sqrt{6}}\,\eta_{\mathsf{ss}} + \frac{1}{\sqrt{3}}\,\eta'_{\mathsf{ss}},\\
\phi_7 &= \frac{1}{\sqrt{2}}\,\pi^0_{\mathsf{gg}} + \frac{1}{\sqrt{6}}\,\eta_{\mathsf{gg}} + \frac{1}{\sqrt{3}}\,\eta'_{\mathsf{gg}},\\
\phi_8 &= -\frac{1}{\sqrt{2}}\,\pi^0_{\mathsf{gg}} + \frac{1}{\sqrt{6}}\,\eta_{\mathsf{gg}} + \frac{1}{\sqrt{3}}\,\eta'_{\mathsf{gg}},\\
\phi_9 &= -\frac{2}{\sqrt{6}}\,\eta_{\mathsf{gg}} + \frac{1}{\sqrt{3}}\,\eta'_{\mathsf{gg}},
\end{aligned} \tag{2.15}$$

The propagator matrix is defined as

$$i\langle 0|T\varphi_A(x)\varphi_B(0)|0\rangle = \int \frac{d^4p}{(2\pi)^4}\,e^{-ipx}\,D_{\varphi_A\varphi_B}(p)\,, \qquad A, B = \mathsf{vv}, \mathsf{ss}, \mathsf{gg}\,, \tag{2.16}$$

and φ stands for π^0, η or η'. Further, due to isospin symmetry this matrix is diagonal in the subspace with different species of π^0:

$$D_{\pi^0_{\mathsf{vv}}\pi^0_{\mathsf{vv}}}(p) = D_{\pi^0_{\mathsf{ss}}\pi^0_{\mathsf{ss}}}(p) = -D_{\pi^0_{\mathsf{gg}}\pi^0_{\mathsf{gg}}}(p) = D_\pi\,, \tag{2.17}$$

However, different species of the η and η' mix. Defining the 2×2 matrix

$$\Omega_{AB}(p) = \begin{pmatrix} D_{\eta_A\eta_B}(p) & D_{\eta_A\eta'_B}(p) \\ D_{\eta'_A\eta_B}(p) & D_{\eta'_A\eta'_B}(p) \end{pmatrix}\,, \tag{2.18}$$

we get

$$\begin{aligned}
&\Omega_{\mathsf{vv},\mathsf{vv}} = \Omega_{\mathsf{ss},\mathsf{ss}} = A\,, \qquad \Omega_{\mathsf{gg},\mathsf{gg}} = A + 2X\,,\\
&\Omega_{\mathsf{vv},\mathsf{ss}} = \Omega_{\mathsf{vv},\mathsf{gg}} = \Omega_{\mathsf{ss},\mathsf{vv}} = \Omega_{\mathsf{ss},\mathsf{gg}} = \Omega_{\mathsf{gg},\mathsf{vv}} = \Omega_{\mathsf{gg},\mathsf{ss}} = A + X\,,
\end{aligned} \tag{2.19}$$

JHEP01(2014)103

where

$$A = \begin{pmatrix} D_\eta & 0 \\ 0 & 0 \end{pmatrix}, \qquad X = \begin{pmatrix} -\frac{1}{3} D_\pi - \frac{2}{3} D_s & -\frac{\sqrt{2}}{3} (D_\pi - D_s) \\ -\frac{\sqrt{2}}{3} (D_\pi - D_s) & -\frac{2}{3} D_\pi - \frac{1}{3} D_s \end{pmatrix}. \tag{2.20}$$

In the above equations, the following notations were used:

$$D_\pi = \frac{1}{M^2 - p^2}, \qquad D_\eta = \frac{1}{M_\eta^2 - p^2}, \qquad D_s = \frac{1}{M_s^2 - p^2}. \tag{2.21}$$

If matching to the non-relativistic theory is performed in this basis, the free two-particle Green function is no more diagonal in the channel basis and the equation (2.7) is replaced by[3]

$$T_{ij}(\mathbf{p}, \mathbf{q}; P_0) = V_{ij}(\mathbf{p}, \mathbf{q}) + \sum_{nm} \int \frac{d^d \mathbf{k}}{(2\pi)^d} V_{in}(\mathbf{p}, \mathbf{q}) \tilde{G}_{nm}(\mathbf{k}; P_0) T_{mj}(\mathbf{p}, \mathbf{q}; P_0). \tag{2.22}$$

The entries of the matrix $\tilde{G}_{nm}$ can be easily determined by using eqs. (2.17), (2.18), (2.19) and (2.20), see below. As already mentioned, the advantage of such a choice of the basis is that the symmetry relations for the matrix elements V_{ij}, T_{ij} are less complicated in this basis.

An important remark is in order. Up to now, we have considered the mixing of the neutral states only at $O(p^2)$ in ChPT. The coefficients, e.g., in eq. (2.11) will change, if higher-order terms are included. How will this affect our expressions? In order not to obscure the crucial physical arguments, we shall neglect higher-order corrections for now. At the end, we return to this question and show that the final result remains unaffected by these corrections.

3 Symmetries of the potential

As already mentioned in the introduction, we concentrate on S-wave scattering in the sector with total isospin $I = 1$. It is convenient to choose $I_3 = 1$. Tracking the quarks of different species, flowing through the diagrams describing meson-meson scattering, and starting from the state that contains only valence quarks, it is easy to see that the LS equation couples 11 different channels, as given in table 1.

As immediately seen from this table, the valence sector couples to the sea and ghost sectors through the annihilation diagrams of the type shown in figure 1. In addition, $\pi^+\pi^0$ states with quarks of different species are no more forbidden in the S-wave.[4] Hence, in general, the partially twisted Lüscher equation will differ from the fully twisted one.

[3] We shall use Greek indices $\alpha, \beta, \gamma, \ldots$, to label channels in the basis where the matrix of the two-point functions of the meson fields is diagonal. This corresponds to working with the fields $\omega_1, \cdots, \omega_8$. On the other hand, in the transformed basis (see eq. (2.14)), we label the channels by Latin letters $i, j, n, m, \ldots$.

[4] As it is easily seen, the components $|(u_v \bar{d}_s)(u_s \bar{u}_v)\rangle$ and $|(d_v \bar{d}_s)(u_s \bar{d}_v)\rangle$ (similarly, with $s \to g$) in the entries 10 and 11 of the table 1 do not indeed contribute to the matrix elements under consideration. We have nevertheless retained them in order to preserve a (formal) analogy with the wave function of the π^0 in the diagonal sectors. Nothing changes in the results, if these components are omitted from the beginning.

JHEP01(2014)103

Index	Channel	Quark content
1	$\lvert\pi^+_{\mathsf{vv}}\eta_{\mathsf{vv}}\rangle$	$-\frac{1}{\sqrt{6}}\lvert(u_{\mathsf{v}}\bar{d}_{\mathsf{v}})(u_{\mathsf{v}}\bar{u}_{\mathsf{v}}+d_{\mathsf{v}}\bar{d}_{\mathsf{v}}-2s_{\mathsf{v}}\bar{s}_{\mathsf{v}})\rangle$
2	$\lvert\pi^+_{\mathsf{vv}}\eta'_{\mathsf{vv}}\rangle$	$-\frac{1}{\sqrt{3}}\lvert(u_{\mathsf{v}}\bar{d}_{\mathsf{v}})(u_{\mathsf{v}}\bar{u}_{\mathsf{v}}+d_{\mathsf{v}}\bar{d}_{\mathsf{v}}+s_{\mathsf{v}}\bar{s}_{\mathsf{v}})\rangle$
3	$\lvert\pi^+_{\mathsf{vv}}\eta_{\mathsf{ss}}\rangle$	$-\frac{1}{\sqrt{6}}\lvert(u_{\mathsf{v}}\bar{d}_{\mathsf{v}})(u_{\mathsf{s}}\bar{u}_{\mathsf{s}}+d_{\mathsf{s}}\bar{d}_{\mathsf{s}}-2s_{\mathsf{s}}\bar{s}_{\mathsf{s}})\rangle$
4	$\lvert\pi^+_{\mathsf{vv}}\eta'_{\mathsf{ss}}\rangle$	$-\frac{1}{\sqrt{3}}\lvert(u_{\mathsf{v}}\bar{d}_{\mathsf{v}})(u_{\mathsf{s}}\bar{u}_{\mathsf{s}}+d_{\mathsf{s}}\bar{d}_{\mathsf{s}}+s_{\mathsf{s}}\bar{s}_{\mathsf{s}})\rangle$
5	$\lvert\pi^+_{\mathsf{vv}}\eta_{\mathsf{gg}}\rangle$	$-\frac{1}{\sqrt{6}}\lvert(u_{\mathsf{v}}\bar{d}_{\mathsf{v}})(u_{\mathsf{g}}\bar{u}_{\mathsf{g}}+d_{\mathsf{g}}\bar{d}_{\mathsf{g}}-2s_{\mathsf{g}}\bar{s}_{\mathsf{g}})\rangle$
6	$\lvert\pi^+_{\mathsf{vv}}\eta'_{\mathsf{gg}}\rangle$	$-\frac{1}{\sqrt{3}}\lvert(u_{\mathsf{v}}\bar{d}_{\mathsf{v}})(u_{\mathsf{g}}\bar{u}_{\mathsf{g}}+d_{\mathsf{g}}\bar{d}_{\mathsf{g}}+s_{\mathsf{g}}\bar{s}_{\mathsf{g}})\rangle$
7	$\lvert K^+_{\mathsf{vv}}\bar{K}^0_{\mathsf{vv}}\rangle$	$\lvert(u_{\mathsf{v}}\bar{s}_{\mathsf{v}})(s_{\mathsf{v}}\bar{d}_{\mathsf{v}})\rangle$
8	$\lvert K^+_{\mathsf{vs}}\bar{K}^0_{\mathsf{sv}}\rangle$	$\lvert(u_{\mathsf{v}}\bar{s}_{\mathsf{s}})(s_{\mathsf{s}}\bar{d}_{\mathsf{v}})\rangle$
9	$\lvert K^+_{\mathsf{vg}}\bar{K}^0_{\mathsf{gv}}\rangle$	$\lvert(u_{\mathsf{v}}\bar{s}_{\mathsf{g}})(s_{\mathsf{g}}\bar{d}_{\mathsf{v}})\rangle$
10	$\lvert\pi^+_{\mathsf{vs}}\pi^0_{\mathsf{sv}}\rangle$	$\frac{1}{2}(-(u_{\mathsf{v}}\bar{d}_{\mathsf{s}})(u_{\mathsf{s}}\bar{u}_{\mathsf{v}}-d_{\mathsf{s}}\bar{d}_{\mathsf{v}})+(u_{\mathsf{v}}\bar{u}_{\mathsf{s}}-d_{\mathsf{v}}\bar{d}_{\mathsf{s}})(u_{\mathsf{s}}\bar{d}_{\mathsf{v}})\rangle$
11	$\lvert\pi^+_{\mathsf{vg}}\pi^0_{\mathsf{gv}}\rangle$	$\frac{1}{2}(-(u_{\mathsf{v}}\bar{d}_{\mathsf{g}})(u_{\mathsf{g}}\bar{u}_{\mathsf{v}}-d_{\mathsf{g}}\bar{d}_{\mathsf{v}})+(u_{\mathsf{v}}\bar{u}_{\mathsf{g}}-d_{\mathsf{v}}\bar{d}_{\mathsf{g}})(u_{\mathsf{g}}\bar{d}_{\mathsf{v}})\rangle$

Table 1. Scattering channels for the case of $I = I_3 = 1$.

For comparison, let us consider a (trivial) example of meson scattering in the channel with $I = 2$, where the answer is already known. Take, for simplicity, $I_3 = 2$. In this case, starting in the valence quark sector, one gets only one state $|\pi_{\mathsf{vv}}\pi^+_{\mathsf{vv}}\rangle = |(u_{\mathsf{v}}\bar{d}_{\mathsf{v}})(u_{\mathsf{v}}\bar{d}_{\mathsf{v}})\rangle$. Annihilation diagrams are absent and, consequently, partial and full twisting are equivalent up to exponentially suppressed contributions.

Using dimensional regularization, it is easy to see that the LS equation reduces to an *algebraic* matrix equation (see, e.g., refs. [42, 43])

$$T_{ij} = V_{ij} + \sum_{nm} V_{im} G_{nm} T_{mj} \,. \tag{3.1}$$

This equation relates the *on-shell* matrix elements of T and V.

JHEP01(2014)103

The free Green function G_{nm} in the channel with $I = 1$ is given by the 11×11 matrix

$$G = \begin{pmatrix} B & B+Y & B+Y & O_1 & O_1 & O_1 & O_1 & O_1 \\ B+Y & B & B+Y & O_1 & O_1 & O_1 & O_1 & O_1 \\ B+Y & B+Y & B+2Y & O_1 & O_1 & O_1 & O_1 & O_1 \\ O_1^T & O_1^T & O_1^T & K & 0 & 0 & 0 & 0 \\ O_1^T & O_1^T & O_1^T & 0 & K & 0 & 0 & 0 \\ O_1^T & O_1^T & O_1^T & 0 & 0 & -K & 0 & 0 \\ O_1^T & O_1^T & O_1^T & 0 & 0 & 0 & P & 0 \\ O_1^T & O_1^T & O_1^T & 0 & 0 & 0 & 0 & -P \end{pmatrix}, \tag{3.2}$$

where B and Y are 2×2 matrices (cf. with eq. (2.20)), and O_1 is a 2×1 matrix:

$$O_1 = \begin{pmatrix} 0 \\ 0 \end{pmatrix}, \qquad B = \begin{pmatrix} E & 0 \\ 0 & 0 \end{pmatrix}, \qquad Y = \begin{pmatrix} -\frac{1}{3}P - \frac{2}{3}S & -\frac{\sqrt{2}}{3}(P-S) \\ -\frac{\sqrt{2}}{3}(P-S) & -\frac{2}{3}P - \frac{1}{3}S \end{pmatrix}, \tag{3.3}$$

and the quantities K, E, P, S are loops with free Green functions in the non-relativistic EFT, corresponding to the different two-particle channels:

$$\begin{aligned} K\bar{K}: \quad & K = \int \frac{d^dk}{(2\pi)^d} \frac{1}{(2w_K(\mathbf{k}))^2} \frac{1}{2w_K(\mathbf{k}) - P_0}, \\ \pi\eta: \quad & E = \int \frac{d^dk}{(2\pi)^d} \frac{1}{2w_\pi(\mathbf{k})2w_\eta(\mathbf{k})} \frac{1}{w_\pi(\mathbf{k}) + w_\eta(\mathbf{k}) - P_0}, \\ \pi\pi: \quad & P = \int \frac{d^dk}{(2\pi)^d} \frac{1}{(2w_\pi(\mathbf{k}))^2} \frac{1}{2w_\pi(\mathbf{k}) - P_0}, \\ \pi\eta^s: \quad & S = \int \frac{d^dk}{(2\pi)^d} \frac{1}{2w_\pi(\mathbf{k})2w_s(\mathbf{k})} \frac{1}{w_\pi(\mathbf{k}) + w_s(\mathbf{k}) - P_0}. \end{aligned} \tag{3.4}$$

Here, $w_s(\mathbf{k}) = (M_s^2 + \mathbf{k}^2)^{1/2}$, where M_s denotes the physical mass of the $\eta^s \doteq \bar{s}s$ meson, which emerges in the partially twisted ChPT (to the lowest order, $M_s^2 = 2m_sB_0$, see eq. (2.10)).

Calculating the above integrals by using the technique, described in ref. [47], we finally get

$$K, E, P, S = \frac{ip}{8\pi P_0}, \qquad p = \frac{\lambda^{1/2}(P_0^2, m_1^2, m_2^2)}{2P_0}. \tag{3.5}$$

Here, p stands for the relative momentum of the pair of particles in the intermediate state, m_1, m_2 are masses of these particles, and $\lambda(x, y, z) = x^2 + y^2 + z^2 - 2xy - 2yz - 2zx$ denotes the triangle function.

JHEP01(2014)103

The potential V and the T-matrix are also 11×11 matrices. The T-matrix can be written in the following form

$$T = \begin{pmatrix}
c & d & \omega & \omega' & -\omega & -\omega' & b & y' & y' & y'' & y'' \\
d & c' & \nu & \nu' & -\nu & -\nu' & b' & z' & z' & z'' & z'' \\
\omega & \nu & f & f' & f'' & -\hat{f} & -\lambda & t & t' & u & u' \\
\omega' & \nu' & f' & f_0 & -\hat{f} & f''' & -\lambda' & h & h' & r & r' \\
-\omega & -\nu & f'' & -\hat{f} & \tilde{f} & \tilde{f}' & \lambda & -t' & -\tilde{t} & -u' & -\tilde{u} \\
-\omega' & -\nu' & -\hat{f} & f''' & \tilde{f}' & \tilde{f}_0 & \lambda' & -h' & -\tilde{h} & -r' & -\tilde{r} \\
b & b' & -\lambda & -\lambda' & \lambda & \lambda' & a & y & y & z & z \\
y' & z' & t & h & -t' & -h' & y & a & y & z & z \\
y' & z' & t' & h' & -\tilde{t} & -\tilde{h} & y & y & \tilde{a} & z & z \\
y'' & z'' & u & r & -u' & -r' & z & z & z & q & q' \\
y'' & z'' & u' & r' & -\tilde{u} & -\tilde{r} & z & z & z & q' & \tilde{q}
\end{pmatrix} . \tag{3.6}$$

Here, $c, d, \omega, \ldots$ denote the entries of the matrix T_{ij}. Some (trivial) symmetry relations are already taken into account, for example, $T_{36} = T_{45} = -\hat{f}$. Note also that the matrix T_{ij} is symmetric. On the mass shell, the entries of the above matrix are the functions of a single Mandelstam variable s (we remind the reader that all partial waves except the S-wave are neglected). We use the name *physical* for the amplitudes that describe the scattering in the sector of only valence quarks: $T_{77} = a$ corresponds to the $K\bar{K}$ elastic scattering, $T_{11} = c$ to the $\pi\eta$ elastic scattering and $T_{17} = T_{71} = b$ to the $K\bar{K} \to \pi\eta$ transition amplitude. Other entries in this matrix are "unphysical." For example, y corresponds to the transition between the valence and sea quark sectors. Considering the quark diagrams for this process (see figure 2 and eq. (3.7) below), one straightforwardly ensures that y corresponds to the contribution of the *disconnected* diagrams to the $K\bar{K}$ elastic amplitude.

There exist more symmetry relations, which relate various entries in the above matrix. A straightforward way to derive these relations in general is to express these amplitudes in terms of the quark propagators and take into account the fact that the valence, sea and ghost quark masses all coincide. Below, we give few examples of such calculations.[5]

[5] A crucial property of the Lippmann-Schwinger equation with the Green function given in eq. (3.2) is that the symmetries of the matrix T are the same as the symmetries of the potential matrix V. Later, we shall check this property explicitly.

JHEP01(2014)103

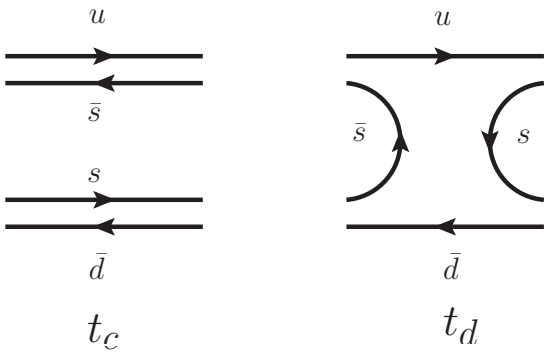

Figure 2. Connected (t_c) and disconnected (t_d) diagrams, emerging in $K\bar{K} \to K\bar{K}$ scattering amplitudes with various quark species, see eq. (3.7).

Example 1. Consider the quark diagrams for the transition between various $K\bar{K}$ states. The full 4-point Green functions of the bilinear quark operators are given by

$$\begin{aligned}
\Gamma_{77} &= t_c - t_d\,, \\
\Gamma_{88} &= t_c - t_d\,, \\
\Gamma_{99} &= -t_c - t_d\,, \\
\Gamma_{78} &= \Gamma_{79} = \Gamma_{89} = \Gamma_{87} = \Gamma_{97} = \Gamma_{98} = -t_d\,,
\end{aligned} \tag{3.7}$$

where t_c and t_d denote connected and disconnected diagrams, respectively, as shown in figure 2. Different signs in different matrix elements emerge from calculations with anti-commuting (valence, sea) and commuting (ghost) fields. The connected diagrams are, of course, absent in the non-diagonal matrix elements. Note that the quark propagators, used in the diagrams, are the same for all quark species, since that masses of valence, sea and ghost quarks are the same.

The scattering matrix elements are given by the residues of the 4-point Green functions at the poles, corresponding to the external mesonic legs. It is seen that all Green functions in eq. (3.7) are expressed only through two quantities and, hence, there are some linear relations between them. It can be shown (see section 5 for the details) that the scattering matrix elements obey exactly the same linear relations even if $\hat{m} \neq m_s$. Introducing the notations $T_{77} = a$, and $T_{78} = y$, we finally arrive at the relations

$$T_{88} = a, \quad T_{99} = \tilde{a} = -a + 2y\,, \quad T_{78} = T_{79} = T_{89} = T_{87} = T_{97} = T_{98} = y\,. \tag{3.8}$$

Example 2. Consider

$$\Gamma_{33} = \frac{1}{6}\Big\{[4W_{ll} - 8W_{ls} + 4W_{ss}] + 2x_l + 4x_s\Big\}\,, \tag{3.9}$$

where the terms in square brackets stem from the tadpole diagrams, see figure 3, and the subscripts "l" and "s" stand for "light" and "strange."

JHEP01(2014)103

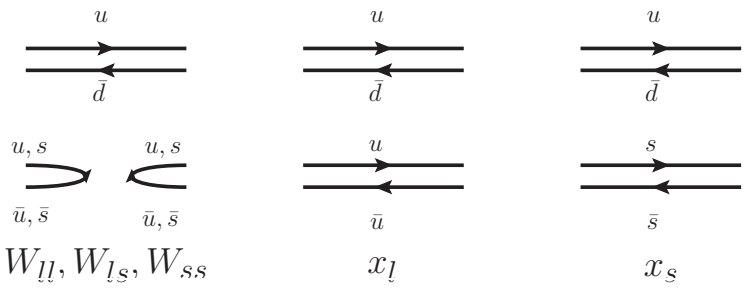

Figure 3. Diagrams contributing to $\pi\eta$ scattering in the valence quark sector, see eq. (3.9). W_{ll}, W_{ls}, W_{ss} correspond to the diagrams with zero, one, two strange quarks in the tadpoles. x_l and x_s are connected diagrams without and with strange quarks.

Carrying out similar calculations, we get

$$\begin{aligned}
\Gamma_{34} &= \frac{1}{3\sqrt{2}}\Big\{[4W_{ll} - 2W_{ls} + 2W_{ss}] + 2x_l - 2x_s\Big\}\,,\\
\Gamma_{35} &= -\frac{1}{6}\Big\{[4W_{ll} - 8W_{ls} + 4W_{ss}]\Big\}\,,\\
\Gamma_{45} &= -\frac{1}{3\sqrt{2}}\Big\{[4W_{ll} - 2W_{ls} + 2W_{ss}]\Big\}\,,\\
\Gamma_{44} &= \frac{1}{3}\Big\{[4W_{ll} + 4W_{ls} + W_{ss}] + 2x_l + x_s\Big\}\,,\\
\Gamma_{46} &= -\frac{1}{3}\Big\{[4W_{ll} + 4W_{ls} + W_{ss}]\}\,,\\
\Gamma_{55} &= \frac{1}{6}\Big\{[4W_{ll} - 8W_{ls} + 4W_{ss}] - 2x_l - 4x_s\Big\}\,,\\
\Gamma_{56} &= \frac{1}{3\sqrt{2}}\Big\{[4W_{ll} - 2W_{ls} + 2W_{ss}] - 2x_l + 2x_s\Big\}\,,\\
\Gamma_{66} &= \frac{1}{3}\Big\{[4W_{ll} + 4W_{ls} + W_{ss}] - 2x_l - x_s\Big\}\,.
\end{aligned} \tag{3.10}$$

From these relations one easily gets

$$\begin{aligned}
f + \tilde{f} &= -2f''\,,\\
f' + \tilde{f}' &= 2\hat{f}\,,\\
f_0 + \tilde{f}_0 &= -2f'''\,,\\
f' - \tilde{f}' &= -\sqrt{2}(f - \tilde{f} - f_0 + \tilde{f}_0)\,.
\end{aligned} \tag{3.11}$$

Acting in the same manner as described in the examples, we get more relations. The

JHEP01(2014)103

ones listed below will be used further:

$$
\begin{aligned}
t+\tilde{t} &= 2t'\,,\\
y'+t-t' &= y'+t'-\tilde{t} \;=\; b\\
h+\tilde{h} &= 2h'\,,\\
z'+h-h' &= z'+h'-\tilde{h}=b'\\
u+\tilde{u} &= 2u'\,,\\
r+\tilde{r} &= 2r'\,,\\
\sqrt{2}(\tilde{u}-u) &= \tilde{r}-r\,,\\
-\sqrt{2}(\tilde{h}-h) &= \tilde{t}-t\,,\\
\lambda &= -t'\,,\\
\lambda' &= -h'\,,\\
z'-\sqrt{2}y' &= h'-\sqrt{2}t'\,,\\
\sqrt{2}d &= 2c-2\omega+\sqrt{2}\omega'+\sqrt{2}\,(f'-\tilde{f}')-(f_0-\tilde{f}_0)\,,\\
q+\tilde{q} &= 2q'\,,\\
\nu &= \sqrt{2}\omega+\hat{f}+\sqrt{2}f''\,,\\
\nu' &= \sqrt{2}\omega'-\sqrt{2}\hat{f}-f'''\,,\\
c' &= c+\frac{d}{\sqrt{2}}-f'''-2f''-2\sqrt{2}\hat{f}-3\omega+\frac{3}{\sqrt{2}}\,\omega'\\
\sqrt{2}b' &= \sqrt{2}z'+y'-b\,,\\
\sqrt{2}y''-z'' &= \sqrt{2}u-r\,.
\end{aligned}
\tag{3.12}
$$

As the next step, we would like to establish, what are the implications of the above symmetry relations for the potential matrix V_{ij}. Recalling that in dimensional regularization the T-matrix obeys the *algebraic* LS equation (3.1), where T and G are given by 11×11 matrices in eqs. (3.6) and (3.2), respectively, it is a straightforward task to solve the above matrix equation with respect to V. In doing so, we find it useful to first perform the linear

JHEP01(2014)103

transformation of the LS equation with the matrix

$$O = \begin{pmatrix} 1/2 & 0 & 1/2 & 0 & 0 & 0 & 0\,0\,0\,0\,0 \\ 0 & 1/2 & 0 & 1/2 & 0 & 0 & 0\,0\,0\,0\,0 \\ 1/4 & 0 & -1/4 & 0 & 1/2 & 0 & 0\,0\,0\,0\,0 \\ 0 & 1/4 & 0 & -1/4 & 0 & 1/2 & 0\,0\,0\,0\,0 \\ 1/4 & 0 & -1/4 & 0 & -1/2 & 0 & 0\,0\,0\,0\,0 \\ 0 & 1/4 & 0 & -1/4 & 0 & -1/2 & 0\,0\,0\,0\,0 \\ 0 & 0 & 0 & 0 & 0 & 0 & 1\,0\,0\,0\,0 \\ 0 & 0 & 0 & 0 & 0 & 0 & 0\,1\,0\,0\,0 \\ 0 & 0 & 0 & 0 & 0 & 0 & 0\,0\,1\,0\,0 \\ 0 & 0 & 0 & 0 & 0 & 0 & 0\,0\,0\,1\,0 \\ 0 & 0 & 0 & 0 & 0 & 0 & 0\,0\,0\,0\,1 \end{pmatrix} . \tag{3.13}$$

The transformed Green function is given by the matrix

$$\hat{G} = O^T G O = \begin{pmatrix} B + \frac{3}{4}Y & -\frac{1}{4}Y & -\frac{1}{4}Y & O_1 & O_1 & O_1 & O_1 & O_1 \\ -\frac{1}{4}Y & -\frac{1}{4}Y & \frac{1}{4}Y & O_1 & O_1 & O_1 & O_1 & O_1 \\ -\frac{1}{4}Y & \frac{1}{4}Y & O_2 & O_1 & O_1 & O_1 & O_1 & O_1 \\ O_1^T & O_1^T & O_1^T & K & 0 & 0 & 0 & 0 \\ O_1^T & O_1^T & O_1^T & 0 & K & 0 & 0 & 0 \\ O_1^T & O_1^T & O_1^T & 0 & 0 & -K & 0 & 0 \\ O_1^T & O_1^T & O_1^T & 0 & 0 & 0 & P & 0 \\ O_1^T & O_1^T & O_1^T & 0 & 0 & 0 & 0 & -P \end{pmatrix} , \tag{3.14}$$

where

$$O_2 = \begin{pmatrix} 0 & 0 \\ & \\ 0 & 0 \end{pmatrix} . \tag{3.15}$$

JHEP01(2014)103

Note that this linear transformation minimizes the number of the entries in the free Green function, corresponding to the physical $\pi\eta$ state. Namely, as seen from eq. (3.14), the $\pi\eta$ state appears only once, on the main diagonal of the matrix $\hat{G}$. The physical $K\bar{K}$ intermediate states also appear only on the diagonal. Consequently, after using Feshbach's method [48, 49] to define the effective potential that includes all unphysical intermediate states, the resulting LS equation with this effective potential is expected to have a particularly simple form. We shall explicitly see this below.

The transformed LS equation (3.1) takes the form

$$\hat{T} = \hat{V} + \hat{V}\hat{G}\hat{T}\,, \qquad \hat{T} = O^{-1}T(O^T)^{-1}\,, \qquad \hat{V} = O^{-1}V(O^T)^{-1}\,. \tag{3.16}$$

For the analysis of the symmetries of the potential V, it is convenient to further split the Green function

$$\hat{G} = \hat{G}_0 + \hat{G}_1\,, \qquad \hat{G}_0 = \mathrm{diag}\,(E, 0, 0, 0, 0, 0, K, K, -K, 0, 0)\,. \tag{3.17}$$

The split LS equation is:

$$\hat{T} = \hat{W} + \hat{W}\hat{G}_0\hat{T}\,, \qquad \hat{W} = \hat{V} + \hat{V}\hat{G}_1\hat{W}\,. \tag{3.18}$$

A crucial point is that the certain matrix elements of the matrix W do not contain $\pi\pi$ and $\pi\eta^s$ loops.

$$\hat{V}_{11} = \hat{W}_{11}\,, \quad \hat{V}_{17} = \hat{W}_{17}\,, \quad \hat{V}_{18} = \hat{W}_{18}\,, \quad \hat{V}_{19} = \hat{W}_{19}\,, \quad \hat{V}_{77} = \hat{W}_{77}\,, \quad \hat{V}_{88} = \hat{W}_{88}\,. \tag{3.19}$$

This property does not hold in general. For example,

$$\hat{W}_{78} = \hat{W}_{79} = \hat{W}_{89} = \frac{1}{2}\,(\hat{W}_{99} + \hat{V}_{77}) \neq \hat{V}_{78}\,. \tag{3.20}$$

The above property has direct implications for the matrix elements of T as well. Namely, iterating the matrix W, it can be shown that in the physical matrix elements a, b, c no $\pi\pi$ and $\pi\eta^s$ loops are present, whereas the unphysical matrix elements (e.g., y), in general, contain such loops. The above statements can be verified explicitly by direct calculations, in which the use of eqs. (3.8), (3.11) and (3.12) is crucial.[6]

Taking into account the above relations, it is now straightforwardly seen that the physical matrix elements a, b, c are determined from a much simpler LS equation

$$\tau = \sigma + \sigma g \tau\,, \tag{3.21}$$

where τ, g, σ are 4×4 matrices that are obtained from the matrices $\hat{T}, \hat{G}_0, \hat{W}$, respectively, by deleting all rows/columns with the indices $i, j = 2, 3, 4, 5, 6, 10, 11$ (for these values of

[6]Inverting 11×11 matrices analytically have turned to be a very demanding task, leading to extremely lengthy expressions. What we have explicitly checked in analytic calculations is that the above statements are valid for first few terms in the Born expansion of the LS equation. In addition, taking random numerical input for the T-matrix elements, we have checked that all symmetry relations hold *numerically* for the matrix elements of the potential as well.

JHEP01(2014)103

the indices the matrix $\hat{G}_0$ has vanishing entries on the diagonal). Namely, these matrices are given by

$$\tau = \begin{pmatrix} c & b & b & b \\ b & a & y & y \\ b & y & a & y \\ b & y & y & -a+2y \end{pmatrix}, \quad g = \begin{pmatrix} E & 0 & 0 & 0 \\ 0 & K & 0 & 0 \\ 0 & 0 & K & 0 \\ 0 & 0 & 0 & -K \end{pmatrix}, \quad \sigma = \begin{pmatrix} \gamma & \beta & \beta & \beta \\ \beta & \alpha & \delta & \delta \\ \beta & \delta & \alpha & \delta \\ \beta & \delta & \delta & -\alpha+2\delta \end{pmatrix}, \tag{3.22}$$

where

$$\alpha = \hat{V}_{77}\,, \quad \beta = \hat{V}_{17}\,, \quad \gamma = \hat{V}_{11}\,, \quad \delta = \hat{W}_{78}\,. \tag{3.23}$$

The solution of the LS equation for the physical matrix elements gives:

$$\begin{aligned} a&=\frac{\alpha - E(\alpha\gamma-\beta^2)}{D}\,, \quad b = \frac{\beta}{D}\,, \quad c = \frac{\gamma - K(\alpha\gamma-\beta^2)}{D}\,, \\ D&=(1-K\alpha)(1-E\gamma) - KE\beta^2\,. \end{aligned} \tag{3.24}$$

This solution is exactly the same as in the "ordinary" non-relativistic EFT (without sea and ghost sectors), with α, β, γ being the physical K-matrix elements, which we are aiming to extract from the lattice data. Note that the physical matrix elements do not depend on the unphysical entry δ.

To summarize, in the infinite volume the solutions of the LS equation of the non-relativistic EFT with valence, sea and ghost sectors coincide with those in the theory with the valence quarks only. In order to prove this statement, it was crucial to use the symmetry relations between various physical and non-physical T-matrix matrix elements, which are given eqs. (3.8), (3.11) and (3.12). This result, of course, was expected from the beginning, since these two theories are equivalent in the infinite volume.

4 Derivation of the partially twisted Lüscher equation

Establishing the symmetries of the potential V was the most difficult part of the problem. After this, the derivation of the partially twisted Lüscher equation is straightforward. The prescription, which allows one to get the finite-volume spectrum from the Lüscher equation is to replace the free Green function G by its finite-volume counterpart. Different boundary conditions will lead to the different modifications of G. On the contrary, the potential V, which encodes the short-range physics, stays unaffected (up to exponentially suppressed contributions).

Let us consider various scenarios and see in detail, how this prescription works.

JHEP01(2014)103

Scenario 1. We impose periodic boundary conditions on the u-,d-quarks and twisted boundary conditions on the s-quark:

$$u(\mathbf{x}+\mathbf{n}L)=u(\mathbf{x})\,,\quad d(\mathbf{x}+\mathbf{n}L)=d(\mathbf{x})\,,\quad s(\mathbf{x}+\mathbf{n}L)=e^{i\boldsymbol{\theta}_{\mathbf{n}}}s(\mathbf{x})\,. \tag{4.1}$$

These boundary conditions translate into the boundary conditions for the meson states: the pions, etas and η^s fields obey periodic boundary conditions, whereas the boundary conditions for the kaons change:

$$K^{\pm}(\mathbf{x}+\mathbf{n}L)=e^{\mp i\boldsymbol{\theta}_{\mathbf{n}}}K^{\pm}(\mathbf{x})\,,\ K^{0}(\mathbf{x}+\mathbf{n}L)=e^{-i\boldsymbol{\theta}_{\mathbf{n}}}K^{0}(\mathbf{x})\,,\ \bar{K}^{0}(\mathbf{x}+\mathbf{n}L)=e^{i\boldsymbol{\theta}_{\mathbf{n}}}\bar{K}^{0}(\mathbf{x})\,. \tag{4.2}$$

This means that K and $\bar{K}$ mesons *containing valence and ghost s-quarks* get additional 3-momenta $\mp\boldsymbol{\theta}/L$. The system stays in the CM frame.

The modified Green function takes the form (cf. with eq. (3.14))

$$\hat{G}^{L}=\begin{pmatrix}
B_L+\frac{3}{4}Y_L & -\frac{1}{4}Y_L & -\frac{1}{4}Y_L & O_1 & O_1 & O_1 & O_1 & O_1\\
-\frac{1}{4}Y_L & -\frac{1}{4}Y_L & \frac{1}{4}Y_L & O_1 & O_1 & O_1 & O_1 & O_1\\
-\frac{1}{4}Y_L & \frac{1}{4}Y_L & O_2 & O_1 & O_1 & O_1 & O_1 & O_1\\
O_1^T & O_1^T & O_1^T & K_L^{\theta} & 0 & 0 & 0 & 0\\
O_1^T & O_1^T & O_1^T & 0 & K_L & 0 & 0 & 0\\
O_1^T & O_1^T & O_1^T & 0 & 0 & -K_L^{\theta} & 0 & 0\\
O_1^T & O_1^T & O_1^T & 0 & 0 & 0 & P_L & 0\\
O_1^T & O_1^T & O_1^T & 0 & 0 & 0 & 0 & -P_L
\end{pmatrix}, \tag{4.3}$$

where the substitution rule is (cf. with ref. [9])

$$\begin{aligned}
K_L,E_L,P_L,S_L &= \frac{1}{4\pi^{3/2}P_0L}\,Z_{00}(1;q^2)\,,\\
K_L^{\theta} &= \frac{1}{4\pi^{3/2}P_0L}\,Z_{00}^{\theta}(1;q^2)\,,\qquad q=\frac{pL}{2\pi}\,.
\end{aligned} \tag{4.4}$$

Here, Z_{00} (Z_{00}^{θ}) denotes the (twisted) Lüscher zeta-function

$$\begin{aligned}
Z_{00}(1;q^2) &= \frac{1}{\sqrt{4\pi}}\sum_{\mathbf{n}\in\mathbb{Z}^3}\frac{1}{\mathbf{n}^2-q^2}\,,\\
Z_{00}^{\theta}(1;q^2) &= \frac{1}{\sqrt{4\pi}}\sum_{\mathbf{n}\in\mathbb{Z}^3}\frac{1}{\left(\mathbf{n}+\boldsymbol{\theta}/2\pi\right)^2-q^2}\,.
\end{aligned} \tag{4.5}$$

In the above equation, an ultraviolet regularization (e.g., the analytic regularization) is implicit. The free Green function in a finite volume, $\hat{G}_L$, can be again split in analogy with

JHEP01(2014)103

eq. (3.17). The crucial point here is that the symmetry of the $\hat{G}_{1L}$, which is the finite-volume counterpart of $\hat{G}_1$, remains the same. Consequently, the relations in eq. (3.19) still hold in a finite volume. Taking into account this fact, we can rewrite the LS equation (3.21) in a finite volume:

$$\tau_L = \sigma_L + \sigma_L g_L \tau_L \,, \tag{4.6}$$

where

$$g_L = \mathrm{diag}\,(E_L, K_L^\theta, K_L, -K_L^\theta) \,, \tag{4.7}$$

and σ_L is obtained from σ through the replacement $\delta \to \delta_L$. Other entries in the matrix σ, which do not contain contributions from the $\pi\pi$ and $\pi\eta^s$ loops, stay volume-independent.

The Lüscher equation takes the form

$$d_L = \det\,(1 - \sigma_L g_L) = (1 - \alpha K_L - \gamma E_L + (\alpha\gamma - \beta^2) K_L E_L)(1 - (\alpha - \delta_L) K_L^\theta)^2 = 0 \,. \tag{4.8}$$

It is immediately seen that the determinant vanishes for those energies which obey one of the equations

$$\begin{aligned} 0 &= 1 - \alpha K_L - \gamma E_L + (\alpha\gamma - \beta^2) K_L E_L \,, \\ 0 &= 1 - (\alpha - \delta_L) K_L^\theta \,. \end{aligned} \tag{4.9}$$

The first equation is identical to the Lüscher equation with *no twisting*. It does not depend on the non-physical entry δ_L. The second equation depends on the twisting angle and contains δ_L. Since unphysical quantities appear, this equation is not very useful for the analysis of the data.

As seen, the spectrum of the partially twisted equation contains more states than the fully twisted one. Choosing particular source/sink operators, which do not have an overlap with some of the states, one may project out a part of the spectrum. For example, in our case we may consider the quark-antiquark scalar operator $\mathcal{O}_s = \bar{u}d$, or the 4-quark operator producing $\pi\eta$ scattering state $\mathcal{O}_{\pi\eta} = (\bar{u}\gamma_5 d)(\bar{u}\gamma_5 u + \bar{d}\gamma_5 d - 2\bar{s}\gamma_5 s)/\sqrt{6}$. It is clear that the spectrum, "seen" by these operators, does not depend on the twisting angle $\boldsymbol{\theta}$. Consequently, these operators do not overlap with the part of the spectrum, described by the second equation in eq. (4.9). At the level of the EFT, this is verified, e.g, from the fact that the $\pi\eta$ scattering amplitude

$$(\tau_L)_{11} = \frac{\gamma - (\alpha\gamma - \beta^2) K_L}{1 - \alpha K_L - \gamma E_L + (\alpha\gamma - \beta^2) K_L E_L} \,, \tag{4.10}$$

has poles, emerging only from the first equation in eq. (4.9) (note that, say, the $K\bar{K}$ amplitude, which is the solution of the same LS equation in a finite volume, contains all poles from eq. (4.9)).

To summarize, it is possible to derive the Lüscher equation with a partially twisted s-quark. The spectrum is dependent on the choice of the source/sink operators. Choosing the operators that do not have overlap on the unphysical part of the spectrum, it is seen that the remaining energy levels can be analyzed by using the Lüscher equation *with no twisting at all*. This is not interesting, because imposing partially twisted boundary condition does not yield new information in this case.

JHEP01(2014)103

Scenario 2. Here we consider twisting of the u-quark, leaving the d- and s-quarks to obey periodic boundary conditions. What changes here is the free Green function in a finite volume.

$$K, E, P, S \to K_L^\theta, E_L^\theta, P_L^\theta, S_L^\theta = \frac{1}{4\pi^{3/2}\sqrt{s}\gamma L}\, Z_{00}^{\mathbf{d}}(1;(q^*)^2)\,, \tag{4.11}$$

where $\mathbf{d} = \mathbf{P}L/2\pi = \boldsymbol{\theta}/2\pi$, $s = P_0^2 - \mathbf{P}^2$, $\gamma = P_0/\sqrt{s}$, and

$$q^* = \frac{p^* L}{2\pi}\,, \qquad p^* = \frac{\lambda^{1/2}(s, m_1^2, m_2^2)}{2\sqrt{s}}\,. \tag{4.12}$$

The quantity $Z_{00}^{\mathbf{d}}(1;(q^*)^2)$ denotes the Lüscher zeta-function in the moving frame [50], see also refs. [43, 51]:

$$\begin{aligned} Z_{00}^{\mathbf{d}}(1;(q^*)^2) &= \frac{1}{\sqrt{4\pi}} \sum_{\mathbf{r}\in P_d} \frac{1}{\mathbf{r}^2 - (q^*)^2}\,, \\ P_d &= \{\mathbf{r} = \mathbb{R}^3 \mid r_\parallel = \gamma^{-1}(n_\parallel - \mu_1|\mathbf{d}|),\ \mathbf{r}_\perp = \mathbf{n}_\perp,\ \mathbf{n}\in\mathbb{Z}^3\}\,, \end{aligned} \tag{4.13}$$

where $\mu_1 = \big(1 - (m_1 2 - m_2 2)/s\big)/2$. Here, we would like to mention that, in this scenario, π^+ (particle 2 in our nomenclature) is twisted in the propagators E_L^θ, S_L^θ, whereas η, η^s (particle 1) are subject to the periodic boundary conditions. This can be easily understood, analyzing the quark diagrams for the different intermediate states given in table 1. For K_L^θ, P_L^θ, either particle can be twisted since both particles in the intermediate state have the same mass.

The solution of the Lippmann-Schwinger equation in a finite volume takes the following form (cf. with eq. (3.24))

$$\begin{aligned} a_L &= \frac{\alpha - E_L^\theta(\alpha\gamma - \beta^2)}{D_L^\theta}\,, \quad b_L = \frac{\beta}{D_L^\theta}\,, \quad c_L = \frac{\gamma - K_L^\theta(\alpha\gamma - \beta^2)}{D_L^\theta}\,, \\ D_L^\theta &= (1 - K_L^\theta\alpha)(1 - E_L^\theta\gamma) - K_L^\theta E_L^\theta \beta^2\,. \end{aligned} \tag{4.14}$$

It is seen that the spectra in case of the partial and full twisting coincide. Both 4-quark and quark-antiquark operators couple to those eigenstates, whose energies are described by the Lüscher equation in the moving frame

$$D_L^\theta = 0\,. \tag{4.15}$$

Summary. Other scenarios are possible. For example, one may consider twisting u- and d-quarks with the same angle, in order to bring two particles again in the CM frame. We do not consider more scenarios in detail, since the pattern is already clear from the above examples.

One observes that there exists the rule of thumb for the scenarios considered above. Namely, if in a given scenario the twisted valence quarks may annihilate (as in the scenario 1), then the corresponding partial twisting will effectively yield no twisting. On the other hand, if the twisted valence quarks "go through" all diagrams without annihilating (as in

JHEP01(2014)103

the scenario 2), then the partially twisted Lüscher equation is equivalent to the fully twisted one up to exponentially suppressed terms. The first case is indeed easy to understand without doing any calculations: for studying the spectrum, one could use, for example, the quark-antiquark source and sink operators $\bar{u}d$, $\bar{d}u$, which do not change at all, when the valence s-quarks are twisted. The result in the second case looks also plausible, when one considers quark diagrams, corresponding to the two-particle scattering processes. However, due to technical complications, arising mainly from the neutral meson mixing, certain effort is needed to elevate a plausible statement to a proof.

5 Meson mixing in the neutral sector

In the preceding sections we have derived symmetry relations for the elements of the scattering T-matrix, assuming the exact SU(3)-symmetric quark content of the states corresponding to the η, η' mesons: $\eta = \eta^8 \sim (u\bar{u}+d\bar{d}-2s\bar{s})/\sqrt{6}$ and $\eta' = \eta^0 \sim (u\bar{u}+d\bar{d}+s\bar{s})/\sqrt{3}$ in the valence, sea and ghost quark sectors (note that not all of these states are independent due to the condition $\mathrm{str}\,\Phi = 0$). This assumption holds only, if $m_s = \hat{m}$. At the level of the EFT, described by the Lagrangian in eq. (2.6), the above relations hold at tree level and are broken by $O(p^4)$ corrections. Do our results, which rely heavily on the symmetry relations, survive, if the mixing is taken into account to all orders?

The answer to this question is positive. The physical justification of this fact is very transparent: in the derivation of the symmetry relations itself that involved the comparison of the quark diagrams (see section 3), we have never required $m_s = \hat{m}$. Rather, it was assumed that the masses of the valence, sea and ghost quarks for each flavor coincide (this requirement is fulfilled in our case). So, one expects that the results are not affected by the breaking of the flavor SU(3).

To elevate this argument to a formal level, let us consider the two-point function of two quark bilinears in the EFT

$$D_{ij}(p^2) = i \int dx e^{ipx} \langle 0|T\chi_i(x)\chi_j(0)|0\rangle\,, \qquad i,j = 1,\cdots,6\,, \tag{5.1}$$

where $\chi_i = \bar{\psi}\Gamma_i\psi$ and the matrices Γ_i carry all information about the spin-flavor content of the mesons. For our goals, it suffices to consider η, η' mesons only (the pions and kaons do not mix). The fermions $\psi, \bar{\psi}$ belong to either valence, sea or ghost sectors.

The pole structure of $D_{ij}(p^2)$ is given by

$$D_{ij}(p^2) = \sum_{\alpha=1}^{6} \Lambda_{i\alpha} D_\alpha(p^2) \Lambda^T_{\alpha j} + D_{ij}(p^2)^{\mathsf{non-pole}}\,, \quad D_\alpha(p^2) = \frac{c_\alpha}{M_\alpha^2 - p^2}\,, \quad c_\alpha = \pm 1, 0\,, \tag{5.2}$$

where, at tree level, the elements of the matrix, up to a common normalization, $\Lambda_{i\alpha}$, can be read off from eq. (2.11). These matrix elements get modified at higher orders in ChPT, if the flavor SU(3) is broken through $\hat{m} \neq m_s$. The masses $M_\alpha^2 = M_\pi^2, M_\eta^2, M_s^2$ are all equal in the SU(3) symmetry limit. At $O(p^2)$, their values can be read off from eq. (2.12).

JHEP01(2014)103

The matrix Λ, which relates the meson fields in the SU(3) and physical bases, can be written in the following form:

$$\Lambda_{i\alpha} = \sum_{m=1}^{6} \tilde{\Lambda}_{im} \overset{0}{\Lambda}_{m\alpha}\,, \tag{5.3}$$

where $\overset{0}{\Lambda}_{m\alpha}$ denotes the matrix at $O(p^2)$ (so far, we have worked with this matrix), and $\tilde{\Lambda}_{im}$ collects all higher-order corrections.

Let us now consider the 4-point function of the quark bilinears, corresponding to the $\pi^+\eta(\eta') \to \pi^+\eta(\eta')$ scattering, see the table 1,

$$\begin{aligned}
&(2\pi)^4\delta^4(p_1+p_2-q_1-q_2)\,\Gamma_{ij}(p_1,p_2;q_1,q_2)\\
&= \int dx_1dx_2dy_1dy_2\, e^{ip_1x_1+ip_2x_2-iq_1y_1-iq_2y_2}\,\langle 0|T\chi_i(x_1)\chi_{\pi^+}(x_2)\chi_j(y_1)\chi_{\pi^-}(y_2)|0\rangle.
\end{aligned} \tag{5.4}$$

The connected piece of the 4-point function can be written as

$$\begin{aligned}
&\Gamma_{ij}(p_1,p_2;q_1,q_2)^{\mathsf{conn}}\\
&= \sum_{kl} D_{ik}(p_1^2)D_{\pi^+}(p_2^2)T_{kl}(p_1,p_2;q_1,q_2)D_{\pi^+}(q_2^2)D_{lj}(q_1^2)\\
&= \sum_{kl}\sum_{\alpha\beta} \Lambda_{i\alpha}D_\alpha(p_1^2)\Lambda^T_{\alpha k}D_{\pi^+}(p_2^2)T_{kl}(p_1,p_2;q_1,q_2)D_{\pi^+}(q_2^2)\Lambda_{l\beta}D_\beta(q_1^2)\Lambda^T_{\beta j} + \cdots .
\end{aligned} \tag{5.5}$$

From the above expression it is clear that the scattering amplitude in the "physical" basis (i.e., the basis which diagonalizes the matrix of the two-point functions), *on the mass shell* is given by

$$\begin{aligned}
T^{\mathsf{on-shell}}_{\alpha\beta}(s,t) &= \lim_{p_1^2\to M_\alpha^2,\ q_1^2\to M_\beta^2,\ p_2^2,q_2^2\to M_\pi^2} T_{\alpha\beta}(p_1,p_2;q_1,q_2)\\
&= \lim_{p_1^2\to M_\alpha^2,\ q_1^2\to M_\beta^2,\ p_2^2,q_2^2\to M_\pi^2} \Lambda^T_{\alpha k}T_{kl}(p_1,p_2;q_1,q_2)\Lambda_{l\beta}\,,
\end{aligned} \tag{5.6}$$

where s,t are the usual Mandelstam variables.

Now, let us consider the situation that the 4-point function of the quark-antiquark bilinears obeys some symmetry relations (an analogy of the relations considered in the section 3)

$$\sum_{ij} d_{ji}\Gamma_{ij}(p_1,p_2;q_1,q_2) = 0\,, \tag{5.7}$$

where d_{ij} are some numerical coefficients related to the structure of the symmetry group (but not to the dynamics). Note that these are relations that hold for *off-shell* momenta p_1,p_2,q_1,q_2.

One has to further distinguish between the case of the exact SU(3) flavor symmetry and broken SU(3) flavor symmetry.

JHEP01(2014)103

Exact SU(3) symmetry. In this case $\Lambda = \overset{0}{\Lambda}$ exactly, to all orders in ChPT. Further, substituting eq. (5.5) into eq. (5.7) and performing the mass-shell limit, we get

$$\sum_{\alpha\beta} k_{\beta\alpha} T^{\text{on-shell}}_{\alpha\beta}(s,t) = 0\,, \qquad k_{\beta\alpha} = \sum_{ij} \Lambda^T_{\beta j} d_{ji} \Lambda_{i\alpha} \tag{5.8}$$

We remind the reader that the disconnected piece does not have four poles in the external momenta squared.

Next we define the on-shell amplitudes in the SU(3) basis

$$T^{\text{on-shell}}_{ij}(s,t) = \sum_{\alpha\beta} \Lambda_{i\alpha} T^{\text{on-shell}}_{\alpha\beta}(s,t) \Lambda^T_{\beta j}\,, \qquad \sum_{ij} d_{ji} T^{\text{on-shell}}_{ij}(s,t) = 0\,. \tag{5.9}$$

In other words, in case of exact SU(3) symmetry, the symmetry relations on the 4-point functions directly translate in the relations for the on-shell amplitudes.

The LS equation in the non-relativistic EFT is derived in the basis where the two-point function is diagonal (see section 2). This (matrix) equation can be written in the form

$$T^{\text{on-shell}}_{\alpha\beta} = V_{\alpha\beta} + \sum_{\gamma} V_{\alpha\gamma} G_\gamma T^{\text{on-shell}}_{\gamma\beta}\,, \tag{5.10}$$

where the G_γ are loops[7] with the π^+ and the "particle" γ. Changing now to the SU(3) basis, we arrive at the equation

$$T^{\text{on-shell}}_{ij} = V_{ij} + \sum_{nm} V_{in} G_{nm} T^{\text{on-shell}}_{mj}\,, \tag{5.11}$$

where the relation between V_{ij} and $V_{\alpha\beta}$ is the same as between $T^{\text{on-shell}}_{ij}$ and $T^{\text{on-shell}}_{\alpha\beta}$, and the free Green function in the new basis is given by

$$G_{ij} = \sum_{\gamma} (\Lambda^T)^{-1}_{i\gamma} G_\gamma \Lambda^{-1}_{\gamma j}\,. \tag{5.12}$$

Our equations given in section 3 are exactly reproduced. The derivation of the Lüscher equation is straightforward. All results remain valid.

Broken SU(3) symmetry. In Nature, $\hat{m} \neq m_s$. One may still have some exact relations of the type given in eq. (5.7) — those, which do not require $\hat{m} = m_s$. Examples of such relations are given in section 3.

There are five neutral one-particle states with isospin $I = 0$ in the physical basis (cf. with eq. (2.14)). These states belong to the three different classes. Namely, there is one state with $M^2_\alpha = M^2_\eta$, two states (one with the wrong sign in the kinetic term) with $M^2_\alpha = M^2_s$ and two states (one with the wrong sign in the kinetic term) with $M^2_\alpha = M^2_\pi$. In eq. (2.14), these states are described by the fields ω_2 and ω_3, ω_6 and ω_5, ω_8, respectively (of course, the numerical values of the coefficients in this equation are different from the

[7] For simplicity, we neglect here the part of the free Green function, which is already diagonal, e.g., the $K\bar{K}$ loops. Taking them into account does not change anything in our argumentation.

JHEP01(2014)103

$O(p^2)$ values given in eq. (2.14)). We introduce a special notation for the above classes $M = \eta, \eta^s, \pi$.

Let us now consider eq. (5.7) in the vicinity of the poles in the momenta of the external particles. Since the masses of the particles, belonging to the different classes, differ, if $\hat{m} \neq m_s$, the residues should vanish independently for each class. Consequently,

$$\sum_{\text{state } \alpha \text{ in } M_1,\ \text{state } \beta \text{ in } M_2} k_{\beta\alpha} T^{\mathsf{on-shell}}_{\alpha\beta}(s,t) = 0\,, \tag{5.13}$$

where the sum runs only over those states which belong to the classes M_1 and M_2, respectively. For example, if $M_1 = M_2 = \eta$, from the above equation we get: $k_{22} T^{\mathsf{on-shell}}_{22} = 0$. If $M_1 = \eta$ and $M_2 = \eta^s$, we get $k_{32}(T^{\mathsf{on-shell}}_{23} + T^{\mathsf{on-shell}}_{32}) + k_{62}(T^{\mathsf{on-shell}}_{26} + T^{\mathsf{on-shell}}_{62}) = 0$, and so on (here, we have used the fact that the matrix $T^{\mathsf{on-shell}}_{\alpha\beta}$ is symmetric, as well as the matrix $k_{\alpha\beta}$).

Now, let us define

$$\overset{0}{k}_{\beta\alpha} = \sum_{ij} \overset{0}{\Lambda}{}^{T}_{\beta j}\, d_{ji}\, \overset{0}{\Lambda}_{i\alpha}\ . \tag{5.14}$$

The following crucial statement is proven in the appendix B:

> There is certain freedom in choosing the quantities d_{ij}. For example, if we have two independent linear relations between Γ_{ij}, adding these relations with arbitrary coefficients will yield a relation as well. Using this freedom, one may choose the quantities d_{ij} so that the following relation holds separately for each M_1, M_2
>
> $$k_{\beta\alpha} = h(M_1, M_2)\ \overset{0}{k}_{\beta\alpha}\ . \tag{5.15}$$
>
> Here, α, β label the states in the classes M_1, M_2, respectively, and the number $h(M_1, M_2)$ does not depend on α and β.

The rest of the proof is straightforward. We define the T-matrix in the SU(3) basis through

$$T^{\mathsf{on-shell}}_{ij}(s,t) = \sum_{\alpha\beta} \overset{0}{\Lambda}_{i\alpha}\, T^{\mathsf{on-shell}}_{\alpha\beta}(s,t)\, \overset{0}{\Lambda}{}^{T}_{\beta j}\ . \tag{5.16}$$

We would like to stress that this is merely a *definition,* which is made for mathematical convenience only. Physically, it does not make sense to consider a superposition of the states with different masses in case of broken SU(3) symmetry.

Using eqs. (5.13) and (5.15), we easily derive a counterpart of eq. (5.8)

$$\sum_{\alpha\beta} \overset{0}{k}_{\beta\alpha}\, T^{\mathsf{on-shell}}_{\alpha\beta}(s,t) = 0\,, \tag{5.17}$$

where the sum now runs over all α, β from different classes M_1, M_2.

JHEP01(2014)103

Finally, for the above definition of the T-matrix, one gets

$$\sum_{ij} d_{ji} T_{ij}^{\text{on-shell}}(s,t) = 0\,. \tag{5.18}$$

The free Green function in the LS equation is given by

$$G_{ij} = \sum_{\gamma} (\overset{0}{\Lambda}{}^{T})^{-1}_{i\gamma} G_{\gamma} (\overset{0}{\Lambda})^{-1}_{\gamma j}\,, \tag{5.19}$$

and we arrive exactly at the same expressions as before. The derivation of the Lüscher equation is again straightforward, since only neutral mesons with the isospin $I = 0$ are affected by the mixing. The crucial point is that there is no effect of twisting for these mesons because they are neutral. Consequently, no ambiguity arises in the construction of the free Green function in the partially twisted case.

To summarize, the SU(3) breaking affects both the free Green function and the scattering amplitude. The matrix $\Lambda_{i\alpha}$ differs from its $O(p^2)$ value $\overset{0}{\Lambda}_{i\alpha}$. It is, however, possible to define the free Green function and the T-matrix in the SU(3) basis, still using the matrix $\overset{0}{\Lambda}_{i\alpha}$, even if $\hat{m} \neq m_s$. It can be now checked explicitly that the symmetry relations from section 3 hold for the elements of the T-matrix in the SU(3) basis. Consequently, our final results are unaffected by SU(3) breaking. This was, of course, expected from the beginning, since the LS equation — with the use of the above-mentioned symmetry relations — should reduce to the one in the valence sector only in the infinite volume even in case of $\hat{m} \neq m_s$.

6 Conclusions and outlook

i) Using the non-relativistic EFT technique in a finite volume, we have derived the Lüscher equation for the partially twisted boundary conditions for coupled-channel $\pi\eta - K\bar{K}$ scattering. At an intermediate step, the matching of the non-relativistic Lagrangian to partially quenched ChPT has been considered.

ii) Our final result is remarkably simple. If in the channel with $I = I_3 = 1$ the light quarks are subject to twisting, the partially twisted Lüscher equation is equivalent to the fully twisted one, despite the presence of annihilation diagrams. If, on the contrary, partial twisting of the strange quark is performed, the physically interesting part of the spectrum is not affected. Other scenarios are also possible and can be investigated by using the same methods. We think that this result is interesting for the lattice practitioners studying the properties of scalar mesons. We have shown that, instead of carrying out simulations at different volumes, as required in the Lüscher approach, one may perform relatively cheaper partially twisted simulations.

iii) In order to demonstrate the above result, one relies heavily on the relations that emerge between the various T-matrix elements from the valence, sea and ghost sectors of the theory, and stem from the fact that the masses of the valence, sea and

JHEP01(2014)103

ghost quarks are taken equal. These relations lead to numerous cancellations in the LS equation, so that in the final equation only the physical amplitudes, i.e., the amplitudes from the valence quark sector, are present. There are strong intuitive arguments, which support the above statement. However, due to the techical complications, owing mainly to the neutral meson mixing, a certain effort was still needed to transform these arguments into a valid proof.

iv) We have carried out the derivation within certain approximations. For example, we consider only the channel with total isospin $I = 1$. Moreover, all partial waves except $l = 0$ are neglected from the beginning. The partial-wave mixing can be included later by using standard techniques (see, e.g., refs. [51–53]). Here, our aim was to describe the method in the most transparent manner for one particular example, without overloading the arguments with inessential details. Further, the method described above can be used in other systems as well, for example, in the study of the DK molecules in lattice QCD (the work on this problem is in progress, and the results will be reported elsewhere).

Acknowledgments

The authors thank S. Beane, J. Bijnens, J. Gasser, T. Lähde, Ch. Liu, M. Savage, S. Sharpe and C. Urbach for interesting discussions. One of us (AR) thanks the Institute for Nuclear Theory at the University of Washington for its hospitality and the Department of Energy for partial support during the completion of this work. This work is partly supported by the EU Integrated Infrastructure Initiative HadronPhysics3 Project under Grant Agreement no. 283286. We also acknowledge the support by the DFG (CRC 16, "Subnuclear Structure of Matter"), by the DFG and NSFC (CRC 110, "Symmetries and the Emergence of Structure in QCD"), by the Shota Rustaveli National Science Foundation (Project DI/13/02) and by the Bonn-Cologne Graduate School of Physics and Astronomy. This research is supported in part by Volkswagenstiftung under contract no. 86260.

A Explicit form of the matrices T_j in eq. (2.13)

In this appendix we give an explicit form of the matrices T_j which appear in eq. (2.13)

$$
\begin{aligned}
T_1 &= \frac{1}{\sqrt{2}}\,\mathrm{diag}(1,-1,0,0,0,0,0,0,0)\,,\\
T_2 &= \frac{1}{\sqrt{6}}\,\mathrm{diag}(-1,-1,2,-1,-1,2,-1,-1,2)\,,\\
T_3 &= \frac{1}{\sqrt{2}}\,\mathrm{diag}(0,0,1,0,0,1,0,0,2)\,,\\
T_4 &= \frac{1}{\sqrt{2}}\,\mathrm{diag}(0,0,0,1,-1,0,0,0,0)\,,\\
T_5 &= \frac{1}{2}\,\mathrm{diag}(-1,-1,0,1,1,0,0,0,0)\,,
\end{aligned}
$$

JHEP01(2014)103

$$
\begin{aligned}
T_6 &= \frac{1}{\sqrt{2}}\,\mathrm{diag}(0,0,-1,0,0,1,0,0,0)\,,\\
T_7 &= \frac{1}{\sqrt{2}}\,\mathrm{diag}(0,0,0,0,0,0,1,-1,0)\,,\\
T_8 &= \frac{1}{2}\,\mathrm{diag}(1,1,0,1,1,0,2,2,0)\,.
\end{aligned}
\tag{A.1}
$$

B Proof of eq. (5.15)

B.1 The structure of the matrix $\Lambda_{i\alpha}$

The quantity D_{ij} in eq. (5.1) is a 6×6 matrix. containing correlators of the quark bilinears $\eta^8_{\mathsf{vv}}, \eta^0_{\mathsf{vv}}, \eta^8_{\mathsf{ss}}, \eta^0_{\mathsf{ss}}, \eta^8_{\mathsf{gg}}, \eta^0_{\mathsf{gg}}$ where, for example, $\eta^8_{\mathsf{vv}} = (\bar{u}_{\mathsf{v}}u_{\mathsf{v}} + \bar{d}_{\mathsf{v}}d_{\mathsf{v}} - 2\bar{s}_{\mathsf{v}}s_{\mathsf{v}})/\sqrt{6}$ and so on. Consider now the quark diagrams describing the two-point function of the quark bilinears, see figure B.4. The diagonal matrix elements contain both connected and disconnected pieces. Keeping track of the signs emerging in the result of (anti)commuting the fields, we get

$$
D_{\mathsf{vv}} = D_{\mathsf{ss}} = -z_c + z_d\,, \qquad D_{\mathsf{gg}} = z_c + z_d\,. \tag{B.1}
$$

Here, all quantities are 2×2 matrices.

The non-diagonal matrix elements contain only the disconnected piece:

$$
D_{\mathsf{vs}} = D_{\mathsf{sg}} = D_{\mathsf{gv}} = z_d\,. \tag{B.2}
$$

Taking into account the above formulae, one may conclude that the matrix D_{ij} has, in general, the following structure (cf. with eq. (2.19))[8]

$$
D_{ij} = \begin{pmatrix} \hat{A} & \hat{A}+\hat{X} & \hat{A}+\hat{X} \\ \hat{A}+\hat{X} & \hat{A} & \hat{A}+\hat{X} \\ \hat{A}+\hat{X} & \hat{A}+\hat{X} & \hat{A}+2\hat{X} \end{pmatrix}, \qquad \hat{A} = -z_c + z_d\,, \quad \hat{X} = z_c\,. \tag{B.3}
$$

Here, $\hat{A}, \hat{X}$ are 2×2 matrices.

The quantity $\hat{A}$ in the upper left corner of the matrix D is the physical propagator (it contains only valence quarks). Consequently, it has only a pole at $p^2 \to M_\eta^2$. In the vicinity of the pole,

$$
\hat{A}_{ij}(p^2) \to \frac{\Lambda_{i\alpha}\Lambda^T_{\alpha j}}{M_\eta^2 - p^2} + \text{regular terms}, \qquad i,j = 1,2\,, \qquad \text{state } \alpha \text{ in } \eta. \tag{B.4}
$$

[8] The general structure of the two-point function in the partially quenched ChPT has been discussed, e.g., in ref. [54]

JHEP01(2014)103

Figure B.4. Quark diagrams for the two-point function of two quark bilinears. There are connected, z_c and disconnected, z_d contributions in the diagonal matrix elements. Non-diagonal matrix elements contain only disconnected contribution.

Following the nomenclature of eq. (2.14), the state in the class η corresponds to $\alpha = 2$. Further, choosing the proper normalization, we may write

$$\Lambda_{1\alpha} = \cos\tilde{\theta} \doteq c\,, \qquad \Lambda_{2\alpha} = \sin\tilde{\theta} \doteq s\,, \qquad \text{state } \alpha \text{ in } \eta. \tag{B.5}$$

We shall call $\tilde{\theta}$ the mixing angle. The equation (2.20) corresponds to $\tilde{\theta} = 0$.

Now, let us prove that the quantity $\hat{X}$ does not have a pole at $p^2 \to M_\eta^2$. To this end, note that the residue at the pole should be separable. Consequently, the 2×2 matrices $\hat{A}$, $\hat{A} + \hat{X}$, $\hat{A} + 2\hat{X}$ are all separable in the vicinity of $p^2 = M_\eta^2$. Since a separable matrix has one vanishing eigenvalue, with a orthogonal transformation O the matrix $\hat{A}$ can be brought to the diagonal form $O\hat{A}O^T = \mathrm{diag}\,(\lambda, 0)$. Further, since the determinant of a separable matrix vanishes, we have: $\det(\hat{A} + \hat{X}) = \det(\hat{A} + 2\hat{X}) = 0$ in the vicinity of the pole. Recalling that the matrix $\hat{X}$ is symmetric, it can be explicitly checked that this condition can be fulfilled, if and only if $O\hat{X}O^T = \mathrm{diag}\,(\lambda', 0)$, i.e., $\hat{X} = \mathcal{N}\,\hat{A}$ in the vicinity of the pole.

The value of the constant $\mathcal{N}$ can be fixed through the following argument. One may change the basis η^8, η^0 to $\eta^l = (\bar{u}u + \bar{d}d)/\sqrt{2}$ and $\eta^s = \bar{s}s$, in valence, sea and ghost sectors. The matrix D_{ij} in the new basis has the same general structure as before. Further, it is immediately seen that certain diagonal and non-diagonal matrix elements are equal (both contain only disconnected contributions). For example,

$$\langle 0|T\eta^l_{\mathsf{vv}}(x)\eta^s_{\mathsf{vv}}(y)|0\rangle = \langle 0|T\eta^l_{\mathsf{vv}}(x)\eta^s_{\mathsf{ss}}(y)|0\rangle\,. \tag{B.6}$$

Considering the limit $p^2 \to M_\eta^2$, one may check that the above condition is fulfilled, if and only if $\mathcal{N} = 0$. In other words, the matrix $\hat{X}$ does not have a pole at $p^2 \to M_\eta^2$.

Next, we wish to demonstrate that there is no mixing, when $p^2 \to M_s^2$ or $p^2 \to M_\pi^2$. To this end, it is again convenient to use the basis η^l, η^s instead of η^8, η^0. Consider, for example, the case $p^2 \to M_s^2$. Near the pole,

$$D'_{ij}(p^2) \to \sum_{\text{state } \alpha \text{ in } \eta^s} \frac{c_\alpha \Lambda'_{i\alpha}\Lambda'^T_{\alpha j}}{M_s^2 - p^2} + \text{regular terms}\,, \qquad i,j = 1,6\,, \quad c_\alpha = \pm 1\,. \tag{B.7}$$

Here, D'_{ij} is obtained from D_{ij} via the orthogonal transformation that corresponds to the change of the basis from η^8, η^0 to η^l, η^s. Again following the nomenclature of eq. (2.14), two states in the class η^s are $\alpha = 3$ with $c_\alpha = -1$ and $\alpha = 6$ with $c_\alpha = 1$.

It is immediately seen that $\hat{X}'_{12} = \hat{X}'_{21} = 0$ (there are no connected diagrams for the $\eta^l - \eta^s$ transition). Also, as we shall see below, the pole can be contained either in $\hat{X}'_{11}$

JHEP01(2014)103

or in $\hat{X}'_{22}$, but not in both. In accordance with eq. (2.20), we assume that the pole is contained in $\hat{X}'_{22}$. Taking into account eq. (B.3) and the fact that $\hat{A}'$ does not have a pole when $p^2 \to M_s^2$, the following relations hold (up to an overall normalization):

$$\begin{aligned} \Lambda'^2_{23} - \Lambda'^2_{26} &= \Lambda'^2_{43} - \Lambda'^2_{46} = 0\,, \qquad \Lambda'^2_{63} - \Lambda'^2_{66} = 2\,, \\ \Lambda'_{23}\Lambda'_{43} - \Lambda'_{26}\Lambda'_{46} &= \Lambda'_{23}\Lambda'_{63} - \Lambda'_{26}\Lambda'_{66} = \Lambda'_{43}\Lambda'_{63} - \Lambda'_{46}\Lambda'_{66} = 1\,. \end{aligned} \tag{B.8}$$

These equations still do not suffice to determine all quantities unambiguously. To proceed further, note that $\Lambda'_{2\alpha}$ and $\Lambda'_{4\alpha}$ describe the coupling of the η^s_{vv} and η^s_{ss} fields to the state $|\alpha\rangle$:

$$\langle 0|\bar{s}_{\mathsf{v}} s_{\mathsf{v}}|\alpha\rangle = \Lambda'_{2\alpha}\,, \qquad \langle 0|\bar{s}_{\mathsf{s}} s_{\mathsf{s}}|\alpha\rangle = \Lambda'_{4\alpha}\,. \tag{B.9}$$

Consequently,

$$\frac{1}{\sqrt{2}}\,\langle 0|(\bar{s}_{\mathsf{v}} s_{\mathsf{v}} \pm \bar{s}_{\mathsf{s}} s_{\mathsf{s}})|\alpha\rangle = \frac{1}{\sqrt{2}}\,(\Lambda'_{2\alpha} \pm \Lambda'_{4\alpha})\,. \tag{B.10}$$

Recall now that the operators $(\bar{s}_{\mathsf{v}} s_{\mathsf{v}} \pm \bar{s}_{\mathsf{s}} s_{\mathsf{s}})/\sqrt{2}$ transform differently with respect to the *horizontal isospin*, corresponding to the SU(2) rotation of the valence quarks into the sea quarks of the same flavor and *vice versa.* Horizontal isospin is a good quantum number, since the masses of the quarks of different species coincide. The physical states $|\alpha\rangle$ should be characterized by a definite horizontal isospin. This means that both $(\bar{s}_{\mathsf{v}} s_{\mathsf{v}} + \bar{s}_{\mathsf{s}} s_{\mathsf{s}})/\sqrt{2}$ and $(\bar{s}_{\mathsf{v}} s_{\mathsf{v}} - \bar{s}_{\mathsf{s}} s_{\mathsf{s}})/\sqrt{2}$ can not couple to the same state $|\alpha\rangle$ and, consequently,

$$|\Lambda'_{2\alpha}| = |\Lambda'_{4\alpha}|\,, \qquad \alpha = 3, 6\,. \tag{B.11}$$

With this additional constraint, the above equations have the following solution:

$$-\Lambda'_{23} = \Lambda'_{26} = -\Lambda'_{43} = -\Lambda'_{46} = \frac{1}{\sqrt{2}}\,, \quad \Lambda'_{63} = -\sqrt{2}\,, \quad \Lambda'_{66} = 0\,. \tag{B.12}$$

Further, since in this basis the non-diagonal matrix elements, corresponding to the $\eta^l - \eta^s$ transition, do not have a pole, we get

$$\Lambda'_{13} = \Lambda'_{16} = \Lambda'_{33} = \Lambda'_{36} = \Lambda'_{53} = \Lambda'_{56} = 0\,. \tag{B.13}$$

We see that the pole can not be contained both in $\hat{X}'_{11}$ and $\hat{X}'_{22}$. The case of $p^2 \to M_\pi^2$ is treated analogously, only the pole appears now in $\hat{X}'_{11}$. Transforming the propagator back to the basis η^8, η^0, we finally conclude that, up to a normalization of the quantities D_s and D_π, the structure of the matrix $\hat{X}$ in the vicinity of the pole is the same as of the matrix X given by eq. (2.20). Consequently, no mixing occurs in the matrix $\hat{X}$.

To summarize, the matrix $\Lambda_{i\alpha}$ has the following structure (the index i runs from 1 to 6):

- The class $M = \eta$, one state

JHEP01(2014)103

$$\Lambda_{i,\alpha=2} \doteq n_i = \begin{pmatrix} c \\ s \\ c \\ s \\ c \\ s \end{pmatrix} . \tag{B.14}$$

- The class $M = \eta^s$, two states

$$\Lambda_{i,\alpha=3} \doteq w_i^{(1)} = \begin{pmatrix} -\frac{1}{\sqrt{3}} \\ \frac{1}{\sqrt{6}} \\ -\frac{1}{\sqrt{3}} \\ \frac{1}{\sqrt{6}} \\ -\frac{2}{\sqrt{3}} \\ \frac{2}{\sqrt{6}} \end{pmatrix} , \qquad \Lambda_{i,\alpha=6} \doteq w_i^{(2)} = \begin{pmatrix} \frac{1}{\sqrt{3}} \\ -\frac{1}{\sqrt{6}} \\ -\frac{1}{\sqrt{3}} \\ \frac{1}{\sqrt{6}} \\ 0 \\ 0 \end{pmatrix} . \tag{B.15}$$

- The class $M = \pi$, two states

$$\Lambda_{i,\alpha=5} \doteq \nu_i^{(1)} = \begin{pmatrix} -\frac{1}{\sqrt{6}} \\ -\frac{1}{\sqrt{3}} \\ \frac{1}{\sqrt{6}} \\ \frac{1}{\sqrt{3}} \\ 0 \\ 0 \end{pmatrix} , \qquad \Lambda_{i,\alpha=8} \doteq \nu_i^{(2)} = \begin{pmatrix} \frac{1}{\sqrt{6}} \\ \frac{1}{\sqrt{3}} \\ \frac{1}{\sqrt{6}} \\ \frac{1}{\sqrt{3}} \\ \frac{2}{\sqrt{6}} \\ \frac{2}{\sqrt{3}} \end{pmatrix} . \tag{B.16}$$

The formulae for $M = \eta^s, \pi$ were read off eq. (2.14). The common normalization in each class is unimportant and is omitted. The quantity $\overset{0}{\Lambda}_{i\alpha}$ is obtained from $\Lambda_{i\alpha}$ by putting the mixing angle $\tilde{\theta} = 0$, i.e., $c = 1, s = 0$.

JHEP01(2014)103

B.2 The linear relations between the four-point functions

The relation given in eq. (5.15) holds trivially, if $M_1 = M_2 = \eta$, since in this case, there is only one state. Moreover, since, as we have found, the structure of $\Lambda_{i\alpha}$ is the same as of $\overset{0}{\Lambda}_{i\alpha}$, when $M = \eta^s$ or π, eq. (5.15) also holds, if both M_1 and M_2 are either η^s or π. What remains to be checked is the case when $M_1 = \eta$ and $M_2 = \eta^s$ or π.

Our strategy will be explained in few examples below. Let us start from the identity $f + \tilde{f} = -2f''$, see eq. (3.11). The corresponding (symmetrized) relation for the four-point functions is:

$$\Gamma_{33} + \Gamma_{55} + \Gamma_{53} + \Gamma_{35} = 0\,. \tag{B.17}$$

From this, one may read off the coefficients d_{ij}

$$d_{33} = d_{55} = d_{35} = d_{53} = 1\,, \qquad d_{ij} = 0 \text{ otherwise.} \tag{B.18}$$

Now, define,

$$k_\alpha^{(s)} = \sum_{i,j=1}^{6} n_i w_j^{(\alpha)} d_{ji}\,, \qquad k_\alpha^{(\pi)} = \sum_{i,j=1}^{6} n_i \nu_j^{(\alpha)} d_{ji}\,. \tag{B.19}$$

Using the explicit expressions, given in eqs. (B.14), (B.15) and (B.16), we get

$$k_1^{(s)} = -2c\sqrt{3}\,, \qquad k_2^{(s)} = -\frac{2c}{\sqrt{3}}\,, \qquad k_1^{(\pi)} = \frac{2c}{\sqrt{6}}\,, \qquad k_2^{(\pi)} = c\sqrt{6}\,. \tag{B.20}$$

It is clear that eq. (5.15) is fulfilled. The factor $h(M_1, M_2) = c$, if $M_1 = \eta$ and $M_2 = \eta^s$ or π.

Using the same strategy, one may verify that the eq. (5.15) holds also for the following linear relations (cf. with section 3):

$$\begin{aligned} f_0 + \tilde{f}_0 &= -2f'''\,, \\ f' + \tilde{f}' &= 2\hat{f}\,, \\ f' - \tilde{f}' &= -\sqrt{2}(f - \tilde{f} - f_0 + \tilde{f}_0)\,. \end{aligned} \tag{B.21}$$

The relation

$$\sqrt{2}d = 2c - 2\omega + \sqrt{2}\omega' + \sqrt{2}(f' - \tilde{f}') - (f_0 - \tilde{f}_0) \tag{B.22}$$

is more complicated. Using the identity $\Gamma_{36} - \Gamma_{45} + \Gamma_{63} - \Gamma_{54} = 0$, we may rewrite eq. (B.22) in the following form:

$$\begin{aligned} &\frac{1}{\sqrt{2}}(\Gamma_{12} + \Gamma_{21}) - 2\Gamma_{11} + (\Gamma_{13} + \Gamma_{31}) - \frac{1}{\sqrt{2}}(\Gamma_{14} + \Gamma_{41}) \\ &-\frac{1}{\sqrt{2}}(\Gamma_{34} + \Gamma_{43} - \Gamma_{56} + \Gamma_{65}) + a(\Gamma_{36} - \Gamma_{45} + \Gamma_{63} - \Gamma_{54}) = 0\,, \end{aligned} \tag{B.23}$$

where a is arbitrary. Reading off the coefficients d_{ij} from the above equation, one may verify by direct calculations that eq. (5.15) holds, if the choice $a = \sqrt{2}$ is made.

JHEP01(2014)103

We have further checked that the remaining identities

$$
\begin{aligned}
c' &= c + \frac{d}{\sqrt{2}} - f''' - 2f'' - 2\sqrt{2}\hat{f} - 3\omega + \frac{3}{\sqrt{2}}\omega' \,, \\
\nu &= \sqrt{2}\omega + \hat{f} + \sqrt{2}f'' \,, \\
\nu' &= \sqrt{2}\omega' - \sqrt{2}\hat{f} - f''' \,,
\end{aligned}
\tag{B.24}
$$

can be treated in a similar fashion. Adding the term $a(\Gamma_{36} - \Gamma_{45} + \Gamma_{63} - \Gamma_{54})$ to the pertinent linear relations for the four-point functions, it is shown that the constant a can be always adjusted so that the eq. (5.15) is fulfilled.

In section 3 more linear relations are displayed, which correspond to the transitions involving the states not affected by mixing. It is a straightforward task to verify that the same arguments can be applied in this case as well.

References

[1] SCALAR collaboration, T. Kunihiro et al., *Scalar mesons in lattice QCD*, *Phys. Rev.* **D 70** (2004) 034504 [hep-ph/0310312] [INSPIRE].

[2] UKQCD collaboration, C. McNeile and C. Michael, *Properties of light scalar mesons from lattice QCD*, *Phys. Rev.* **D 74** (2006) 014508 [hep-lat/0604009] [INSPIRE].

[3] UKQCD collaboration, A. Hart, C. McNeile, C. Michael and J. Pickavance, *A Lattice study of the masses of singlet 0++ mesons*, *Phys. Rev.* **D 74** (2006) 114504 [hep-lat/0608026] [INSPIRE].

[4] S. Prelovsek and D. Mohler, *A Lattice study of light scalar tetraquarks*, *Phys. Rev.* **D 79** (2009) 014503 [arXiv:0810.1759] [INSPIRE].

[5] S. Prelovsek, T. Draper, C.B. Lang, M. Limmer, K.-F. Liu et al., *Lattice study of light scalar tetraquarks with I=0,2,1/2,3/2: Are σ and κ tetraquarks?*, *Phys. Rev.* **D 82** (2010) 094507 [arXiv:1005.0948] [INSPIRE].

[6] C. Alexandrou, J.O. Daldrop, M. Dalla Brida, M. Gravina, L. Scorzato et al., *Lattice investigation of the scalar mesons $a_0(980)$ and κ using four-quark operators*, *JHEP* **04** (2013) 137 [arXiv:1212.1418] [INSPIRE].

[7] European Twisted Mass collaboration, M. Wagner et al., *Scalar mesons and tetraquarks from twisted mass lattice QCD*, *Acta Phys. Polon. Supp.* **6** (2013) 847 [arXiv:1302.3389] [INSPIRE].

[8] M. Lüscher, *Two particle states on a torus and their relation to the scattering matrix*, *Nucl. Phys.* **B 354** (1991) 531 [INSPIRE].

[9] V. Bernard, M. Lage, U.-G. Meißner and A. Rusetsky, *Scalar mesons in a finite volume*, *JHEP* **01** (2011) 019 [arXiv:1010.6018] [INSPIRE].

[10] M. Döring, U.-G. Meißner, E. Oset and A. Rusetsky, *Unitarized Chiral Perturbation Theory in a finite volume: Scalar meson sector*, *Eur. Phys. J.* **A 47** (2011) 139 [arXiv:1107.3988] [INSPIRE].

JHEP01(2014)103

[11] M. Döring, U. Meißner, E. Oset and A. Rusetsky, *Scalar mesons moving in a finite volume and the role of partial wave mixing*, *Eur. Phys. J.* **A 48** (2012) 114 [arXiv:1205.4838] [INSPIRE].

[12] R.L. Jaffe, *Multi-Quark Hadrons. 1. The Phenomenology of (2 Quark 2 anti-Quark) Mesons*, *Phys. Rev.* **D 15** (1977) 267 [INSPIRE].

[13] D. Black, A.H. Fariborz, F. Sannino and J. Schechter, *Putative light scalar nonet*, *Phys. Rev.* **D 59** (1999) 074026 [hep-ph/9808415] [INSPIRE].

[14] N. Achasov and A. Kiselev, *The New analysis of the KLOE data on the $\phi \to \eta\pi^0\gamma$ decay*, *Phys. Rev.* **D 68** (2003) 014006 [hep-ph/0212153] [INSPIRE].

[15] J. Pelaez, *Light scalars as tetraquarks or two-meson states from large-N_c and unitarized chiral perturbation theory*, *Mod. Phys. Lett.* **A 19** (2004) 2879 [hep-ph/0411107] [INSPIRE].

[16] J.D. Weinstein and N. Isgur, *Do Multi-Quark Hadrons Exist?*, *Phys. Rev. Lett.* **48** (1982) 659 [INSPIRE].

[17] J. Oller and E. Oset, *Chiral symmetry amplitudes in the S wave isoscalar and isovector channels and the sigma, f0(980), a0(980) scalar mesons*, *Nucl. Phys.* **A 620** (1997) 438 [*Erratum ibid.* **A 652** (1999) 407] [hep-ph/9702314] [INSPIRE].

[18] J. Oller, E. Oset and J. Pelaez, *Nonperturbative approach to effective chiral Lagrangians and meson interactions*, *Phys. Rev. Lett.* **80** (1998) 3452 [hep-ph/9803242] [INSPIRE].

[19] J. Oller, E. Oset and J. Pelaez, *Meson meson interaction in a nonperturbative chiral approach*, *Phys. Rev.* **D 59** (1999) 074001 [*Erratum ibid.* **D 60** (1999) 099906] [hep-ph/9804209] [INSPIRE].

[20] J. Oller and E. Oset, *N/D description of two meson amplitudes and chiral symmetry*, *Phys. Rev.* **D 60** (1999) 074023 [hep-ph/9809337] [INSPIRE].

[21] J. Oller, E. Oset and J. Pelaez, *Meson meson interaction in a nonperturbative chiral approach*, *Phys. Rev.* **D 59** (1999) 074001 [*Erratum ibid.* **D 60** (1999) 099906] [hep-ph/9804209] [INSPIRE].

[22] S. Peris, M. Perrottet and E. de Rafael, *Matching long and short distances in large-N_c QCD*, *JHEP* **05** (1998) 011 [hep-ph/9805442] [INSPIRE].

[23] V. Elias, A. Fariborz, F. Shi and T.G. Steele, *QCD sum rule consistency of lowest lying $q\bar{q}$ scalar resonances*, *Nucl. Phys.* **A 633** (1998) 279 [hep-ph/9801415] [INSPIRE].

[24] G. Janssen, B. Pearce, K. Holinde and J. Speth, *On the structure of the scalar mesons f0 (975) and a0 (980)*, *Phys. Rev.* **D 52** (1995) 2690 [nucl-th/9411021] [INSPIRE].

[25] S. Weinberg, *Elementary particle theory of composite particles*, *Phys. Rev.* **130** (1963) 776 [INSPIRE].

[26] S. Weinberg, *Quasiparticles and the Born Series*, *Phys. Rev.* **131** (1963) 440 [INSPIRE].

[27] S. Weinberg, *Evidence That the Deuteron Is Not an Elementary Particle*, *Phys. Rev.* **B 137** (1965) 672.

[28] D. Morgan, *Pole counting and resonance classification*, *Nucl. Phys.* **A 543** (1992) 632 [INSPIRE].

[29] N.A. Tornqvist, *How to parametrize an S wave resonance and how to identify two hadron composites*, *Phys. Rev.* **D 51** (1995) 5312 [hep-ph/9403234] [INSPIRE].

JHEP01(2014)103

[30] D. Morgan and M. Pennington, *f0 (S*): Molecule or quark state?*, *Phys. Lett.* **B 258** (1991) 444 [*Erratum ibid.* **B 269** (1991) 477] [INSPIRE].

[31] D. Morgan and M. Pennington, *New data on the $K\bar{K}$ threshold region and the nature of the f0 (S*)*, *Phys. Rev.* **D 48** (1993) 1185 [INSPIRE].

[32] V. Baru, J. Haidenbauer, C. Hanhart, Y. Kalashnikova and A.E. Kudryavtsev, *Evidence that the a(0)(980) and f(0)(980) are not elementary particles*, *Phys. Lett.* **B 586** (2004) 53 [hep-ph/0308129] [INSPIRE].

[33] V. Baru, J. Haidenbauer, C. Hanhart, A.E. Kudryavtsev and U.-G. Meißner, *Flatte-like distributions and the a(0)(980)/f(0)(980) mesons*, *Eur. Phys. J.* **A 23** (2005) 523 [nucl-th/0410099] [INSPIRE].

[34] C. Hanhart, *Towards an understanding of the light scalar mesons*, *Eur. Phys. J.* **A 31** (2007) 543 [hep-ph/0609136] [INSPIRE].

[35] P.F. Bedaque, *Aharonov-Bohm effect and nucleon nucleon phase shifts on the lattice*, *Phys. Lett.* **B 593** (2004) 82 [nucl-th/0402051] [INSPIRE].

[36] G. de Divitiis, R. Petronzio and N. Tantalo, *On the discretization of physical momenta in lattice QCD*, *Phys. Lett.* **B 595** (2004) 408 [hep-lat/0405002] [INSPIRE].

[37] G.M. de Divitiis and N. Tantalo, *Non leptonic two-body decay amplitudes from finite volume calculations*, hep-lat/0409154 [INSPIRE].

[38] C. Sachrajda and G. Villadoro, *Twisted boundary conditions in lattice simulations*, *Phys. Lett.* **B 609** (2005) 73 [hep-lat/0411033] [INSPIRE].

[39] P.F. Bedaque and J.-W. Chen, *Twisted valence quarks and hadron interactions on the lattice*, *Phys. Lett.* **B 616** (2005) 208 [hep-lat/0412023] [INSPIRE].

[40] S. Ozaki and S. Sasaki, *Lüscher's finite size method with twisted boundary conditions: an application to J/ψ-ϕ system to search for narrow resonance*, *Phys. Rev.* **D 87** (2013) 014506 [arXiv:1211.5512] [INSPIRE].

[41] S. Beane, P. Bedaque, A. Parreno and M. Savage, *Exploring hyperons and hypernuclei with lattice QCD*, *Nucl. Phys.* **A 747** (2005) 55 [nucl-th/0311027] [INSPIRE].

[42] V. Bernard, M. Lage, U.-G. Meißner and A. Rusetsky, *Resonance properties from the finite-volume energy spectrum*, *JHEP* **08** (2008) 024 [arXiv:0806.4495] [INSPIRE].

[43] V. Bernard, D. Hoja, U. Meißner and A. Rusetsky, *Matrix elements of unstable states*, *JHEP* **09** (2012) 023 [arXiv:1205.4642] [INSPIRE].

[44] S.R. Sharpe and N. Shoresh, *Partially quenched chiral perturbation theory without Phi0*, *Phys. Rev.* **D 64** (2001) 114510 [hep-lat/0108003] [INSPIRE].

[45] C. Bernard and M. Golterman, *On the foundations of partially quenched chiral perturbation theory*, *Phys. Rev.* **D 88** (2013) 014004 [arXiv:1304.1948] [INSPIRE].

[46] J. Gasser, V. Lyubovitskij and A. Rusetsky, *Hadronic atoms in QCD + QED*, *Phys. Rept.* **456** (2008) 167 [arXiv:0711.3522] [INSPIRE].

[47] J. Gasser, B. Kubis and A. Rusetsky, *Cusps in $K \to 3\pi$ decays: a theoretical framework*, *Nucl. Phys.* **B 850** (2011) 96 [arXiv:1103.4273] [INSPIRE].

[48] H. Feshbach, *Unified theory of nuclear reactions*, *Annals Phys.* **5** (1958) 357 [INSPIRE].

[49] H. Feshbach, *A Unified theory of nuclear reactions. 2.*, *Annals Phys.* **19** (1962) 287 [INSPIRE].

JHEP01(2014)103

[50] K. Rummukainen and S.A. Gottlieb, *Resonance scattering phase shifts on a nonrest frame lattice*, *Nucl. Phys.* **B 450** (1995) 397 [hep-lat/9503028] [INSPIRE].

[51] M. Göckeler, R. Horsley, M. Lage, U.-G. Meißner, P. Rakow et al., *Scattering phases for meson and baryon resonances on general moving-frame lattices*, *Phys. Rev.* **D 86** (2012) 094513 [arXiv:1206.4141] [INSPIRE].

[52] L. Leskovec and S. Prelovsek, *Scattering phase shifts for two particles of different mass and non-zero total momentum in lattice QCD*, *Phys. Rev.* **D 85** (2012) 114507 [arXiv:1202.2145] [INSPIRE].

[53] N. Li and C. Liu, *Generalized Lüscher Formula in Multi-channel Baryon-Meson Scattering*, *Phys. Rev.* **D 87** (2013) 014502 [arXiv:1209.2201] [INSPIRE].

[54] J. Bijnens and N. Danielsson, *The Eta mass and NNLO three-flavor partially quenched chiral perturbation theory*, *Phys. Rev.* **D 74** (2006) 054503 [hep-lat/0606017] [INSPIRE].

JHEP01(2014)103

CHAPTER 3

Bound States on the Lattice with partial twisting

3.1 Summary of the project

The aim of the project was to develop a method, which allows to determine the compositeness content of exotic states from lattice simulations. The original idea, which goes under the name of Weinberg's compositeness criterion, allows, knowing the value of wave-function renormalization constant $0 \leq Z \leq 1$, to distinguish the loosely bound states and tight QCD composites. Here, the value $Z = 0$ corresponds to a predominantly molecular state, whereas the value $Z = 1$ to a loosely bound state. Our key idea is to extract Z from lattice simulations, using twisted boundary conditions. Although the framework we have formulated is general, we have considered the particular case of the $D^*_{s0}(2317)$ meson, which does not fit well into the quark model, and favours the molecular pictures due to closeness to the DK threshold. We have formulated the lattice version of compositeness criterion, suited for the extraction of Z with partial twisting. We tested the method with synthetic data, generated from the leading-order heavy flavour chiral Lagrangian. Measuring the spectrum for different twisting scenarios, we observed that the finite-volume effect on the bound state mass shift is almost twice as large in magnitude than without twisting and, further, less computational resources are required. We also performed an error analysis to estimate the accuracy of the extraction of Z for different lattice volume, also input lattice errors and number of data points.

JHEP

Published for SISSA by Springer

Received: November 21, 2014
Accepted: January 5, 2015
Published: January 21, 2015

Bound states on the lattice with partially twisted boundary conditions

D. Agadjanov,[a,b] **F.-K. Guo,**[a] **G. Ríos**[a] **and A. Rusetsky**[a]

[a] *Helmholtz-Institut für Strahlen- und Kernphysik (Theorie) and Bethe Center for Theoretical Physics, Universität Bonn, Nussallee 14-16, D-53115 Bonn, Germany*

[b] *St. Andrew the First-Called Georgian University of the Patriarchate of Georgia, Chavchavadze Ave. 53a, 0162, Tbilisi, Georgia*

E-mail: dagadjanov@hiskp.uni-bonn.de, fkguo@hiskp.uni-bonn.de, marquez@hiskp.uni-bonn.de, rusetsky@hiskp.uni-bonn.de

Abstract: We propose a method to study the nature of exotic hadrons by determining the wave function renormalization constant Z from lattice simulations. It is shown that, instead of studying the volume-dependence of the spectrum, one may investigate the dependence of the spectrum on the twisting angle, imposing twisted boundary conditions on the fermion fields on the lattice. In certain cases, e.g., the case of the DK bound state which is addressed in detail, it is demonstrated that the partial twisting is equivalent to the full twisting up to exponentially small corrections.

Keywords: Lattice QCD, Phenomenological Models

ArXiv ePrint: 1411.1859

doi:10.1007/JHEP01(2015)118

JHEP01(2015)118

Contents

JHEP01(2015)118

1 Introduction

The search for the exotic states (tetraquarks, hybrids, hadronic molecules, etc) in the observed hadron spectrum has been a subject of both theoretical and experimental investigations for decades. The exact pattern, how these states emerge, should be strictly determined by the underlying theory and should therefore contain important information about the behavior of QCD at low energies. In practice, however, extracting such information from the data encounters certain challenges, which are in part of a conceptual nature. In the present paper we wish to focus exactly on this issue.

In general, a state is called "exotic" if its quark content does not correspond to the "standard" constellation given by the non-relativistic quark model ($q\bar{q}$ for mesons and qqq for baryons). Consequently, one needs to use a particular model as a reference point to define how the exotic states are meant (note that the very notion of constituent quarks is, strictly speaking, model-dependent). Putting it differently, one has to *agree* on certain *criteria* formulated in terms of certain hadronic *observables*: if these observables are measured, or calculated on the lattice, and the results do not follow the pattern predicted by the quark model, this then should be interpreted as a signature for exotica.

A standard example for the exotic state candidates is given by the scalar nonet with the masses around 1 GeV. As it is well known, the observed mass hierarchy in this nonet is reversed as compared to, e.g., the pseudoscalar or vector multiplets. Such a mass ordering is counter-intuitive from the point of view of the naive quark model, but can be easily understood, if the scalar mesons were interpreted as tetraquark states (see, e.g., [1–4]). This is, however, not the only possible interpretation. In refs. [5–7], the $a_0(980)$ and $f_0(980)$ were considered as hadronic molecules, whereas in refs. [8] these states were described as a combination of a bare pole and the rescattering contribution. In the Jülich meson-exchange model, the $f_0(980)$ appears to be a bound $K\bar{K}$ state, whereas the $a_0(980)$ is a dynamically generated threshold effect [9]. Similar conclusions were inferred in ref. [10] from the calculations in the unitarized ChPT with explicit resonance states. Finally, the investigations carried out within the framework of QCD sum rules are also indicative of the non-$q\bar{q}$ nature of $a_0(980)$ [11, 12]. Given these multiple interpretations, it is natural to look for the clear-cut criteria based on the *observables* in order to minimize the *model-dependence* of the statements about the nature of the hadronic states in question.

In fact, such criteria are known for quite some time already. The "pole counting" method, considered in refs. [13, 14], relates the number of the S-matrix poles near threshold to the molecular nature of the states corresponding to these poles. Namely, it has been argued that the loosely bound states of hadrons (hadronic molecules) correspond to a single pole, whereas the poles corresponding to the tightly bound quark states (of standard or exotic nature) always come in pairs. A closely related criterion goes under the name of Weinberg's compositeness condition [15], which uses the quantity called the wave function renormalization constant Z, where $0 \leq Z \leq 1$, to differentiate between the loosely bound states and tight QCD composites, the values $Z \simeq 0$ corresponding to the molecular states and *vice versa.* The application of these methods for the analysis of the data on scalar mesons are considered in refs. [16–22], and the recent review on the subject may be found in ref. [23]. Moreover, *theoretically,* one may study the dependence of the pole positions on the number of the colors N_c (see refs. [10, 24, 25]) or the quark masses (refs. [26–29]). From the above studies, one can judge about the precise structure of these states beyond the simple alternative between a molecule and a tight quark composite.

Recent years have seen a renewed interest in the field, which is partly related to the progress in the lattice calculations of the QCD spectrum at the quark masses close to the physical values. It should be realized that the lattice studies have powerful tools at their disposal to analyze the nature of the states that emerge in QCD. Apart from the information about the dependence of the spectrum on quark masses, a valuable information comes from the volume dependence of the calculated spectrum as well as its dependence on the twisting angle in case of twisted boundary conditions, see refs. [30–37]. Note that all this information is obtained from the first-principle calculations on the lattice and is thus in principle devoid of any model-dependent input.

In this paper we investigate the nature of the scalar states in the sector with one charm quark that is a natural generalization of our treatment of the light scalar mesons. We mainly focus on the case of the $D_{s0}^*(2317)$ meson [38, 39], albeit the formalism, which we develop here, can be straightforwardly applied to the other cases where a bound state

JHEP01(2015)118

close to the elastic threshold emerges (note that, in this paper, we do not consider the generalization of the approach to the inelastic case. This forms a subject of a separate investigation.). The $D^*_{s0}(2317)$ does not fit very nicely to the quark-model picture, and its structure is still debated, see, e.g., ref. [40] for a recent review. The molecular picture, due to the closeness of the DK threshold and a large coupling to the DK channel looks most promising among other alternatives. It would be highly desirable to verify this conjecture in a model-independent manner, on the basis of the lattice calculations. To this end, one may use the fact that the dependence of the bound-state energy on the kaon mass is very different for a molecule and a standard quark-model state, see ref. [41]. Another possible method to address this issue has been described, e.g., in refs. [33, 34], where the authors propose to study the volume-dependence of the spectrum in order to apply the Weinberg's compositeness criterion on the lattice.

The exploratory study of light pseudoscalar mesons (π, K) of (D, D_s) in full lattice QCD has been carried out in refs. [42–45]. In some isospin channels the study is plagued by the presence of disconnected contributions. The implementation of the method from refs. [33, 34], which implies carrying out calculations at different volumes, could be therefore quite expensive. In this paper we propose an alternative, which requires calculations at one volume, albeit with twisted boundary conditions. Moreover, we show that, in the study of $D^*_{s0}(2317)$, one may use *partially twisted* boundary conditions, despite the fact that the quark annihilation diagrams are present. The method used in the proof is the same as in ref. [46]. Generally, one may expect that the simulations with partially twisted boundary conditions could be less expensive than working at different volumes, while they provide us the same information about the nature of the bound states in question.

This article is organized as follows. In section 2, we briefly review Weinberg's argument for the compositeness of particles. In section 3 we describe the procedure of extraction of the parameter Z from the data with twisted boundary condition. Further, in section 4 we use some models and produce synthetic lattice data in order to check the procedure of the extraction in practice. The error analysis has also been carried out. Separately, in section 5, we discuss the use of the partially twisted boundary conditions and show that they are equivalent to the full twisting in our case. Section 6 contains our conclusions.

2 Compositeness of bound states

As mentioned before, in view of the plethora of candidates of exotic hadrons, it is very important to make model-independent statements on the nature of these states. Model-independence requires that we can only study the physical observables which can be defined in terms of the matrix elements between asymptotic states. In particular, we would like to ask a question, whether a given particle, corresponding to the S-matrix pole, can be regarded as "elementary" or rather as a bound state (molecule) of other hadrons. The central place in this identification belongs to the so-called wave function renormalization constant Z, which has been used to distinguish composite particles from elementary ones since the early 1960's [15, 47–51]. To see its role, we will first discuss a non-relativistic quantum mechanical system, following the discussion of ref. [15].

JHEP01(2015)118

In this section, we will restrict our discussion to the infinite volume. Let us consider a two-body system with a Hamiltonian $\mathcal{H} = \mathcal{H}_0 + V$, where $\mathcal{H}_0$ is the free Hamiltonian, and V specifies the interaction. Both $\mathcal{H}$ and $\mathcal{H}_0$ have a continuum spectrum. Let us assume that there is a bound state solution of the Schrödinger equation with a binding energy E_B,

$$\mathcal{H}|B\rangle = -E_B|B\rangle, \tag{2.1}$$

and $\mathcal{H}_0$ also has a discrete spectrum which are the bare elementary particles. For simplicity, we will assume that there is only one such state, denoted by $|B_0\rangle$. In the Hilbert space spanned by the eigenstates of the free Hamiltonian, the completeness relation is thus given by

$$1 = |B_0\rangle\langle B_0| + \int \frac{d^3\vec{q}}{(2\pi)^3}\,|\vec{q}\rangle\langle\vec{q}| \quad \text{with} \quad \mathcal{H}_0|\vec{q}\rangle = \frac{\vec{q}^{\,2}}{2\mu}|\vec{q}\rangle, \tag{2.2}$$

where $\mu = m_1 m_2/(m_1+m_2)$ is the reduced mass. Thus, the probability for the physical state $|B\rangle$ overlapping with the elementary state $|B_0\rangle$ which, by definition, equals to Z, is given by

$$Z = \left|\langle B_0|B\rangle\right|^2 = 1 - \int \frac{d^3\vec{q}}{(2\pi)^3}\left|\langle\vec{q}|B\rangle\right|^2 = 1 - \int \frac{d^3\vec{q}}{(2\pi)^3}\,\frac{\left|\langle\vec{q}|V|B\rangle\right|^2}{\left[E_B + \vec{q}^{\,2}/(2\mu)\right]^2}, \tag{2.3}$$

where eq. (2.1) is used. The quantity $1 - \left|\langle B_0|B\rangle\right|^2$ then describes the probability of the physical state not being the elementary state or finding the physical state in the two-particle state. In other words, $Z \simeq 1$ corresponds to a mostly elementary state whereas a state with $Z \simeq 0$ can be interpreted as a predominately molecular one.

In general, the above integral depends on the matrix element $\langle\vec{q}|V|B\rangle$, which is not directly measurable. However, for loosely bound states, the quantity Z can be related to the observables. Consider, for instance, an S-wave bound state with a small binding energy. The binding energy should be much smaller than the inverse of the range of forces so that the matrix element $\langle\vec{q}|V|B\rangle$ can be approximated by a constant $g_{\rm NR}$. We get from eq. (2.3)

$$g_{\rm NR}^2 = (1-Z)\frac{2\pi}{\mu^2}\sqrt{2\mu E_B}. \tag{2.4}$$

Note that, in the past, this equation has been often applied to distinguish composite particles from elementary ones, see e.g. [15, 18, 23, 52]. The non-relativistic coupling constant $g_{\rm NR}^2$ coincides with the residue of the non-relativistic scattering matrix at the bound state pole. This can be immediately seen, considering the Low equation

$$t(E) = \frac{g_{\rm NR}^2}{E + E_B + i\epsilon} + \int \frac{d^3\vec{q}}{(2\pi)^3}\,\frac{|t(E_q)|^2}{E - E_q + i\epsilon} \tag{2.5}$$

in the vicinity of the pole [15, 51]. Here, $E_q = \vec{q}^{\,2}/(2\mu)$.

Finally, we would like to relate the quantity Z to the physical observables, namely, to the scattering length a and effective range r. Here, we are closely following the path of ref. [15]. It is important to note that these relations can be derived when the binding energy

JHEP01(2015)118

is much smaller than the inverse of the range of forces. We start with the twice-subtracted dispersion relation for the inverse of $t(E)$

$$t^{-1}(E) = \frac{E+E_B}{g_{\rm NR}^2} + \frac{(E+E_B)^2}{\pi}\int_0^\infty dw \frac{{\rm Im}\, t^{-1}(w)}{(w-E-i\epsilon)(w+E_B)^2}, \tag{2.6}$$

where the two subtraction constants have been determined from eq. (2.5). The S-wave transition matrix element is related to the non-relativistic S-wave scattering amplitude $f(k) = 1/[k\cot\delta(k) - i\,k]$ as $f(k) = -\mu\, t(E)/(2\pi)$ with $k = \sqrt{2\mu E}$ and $\delta(k)$ being the S-wave phase shift. Thus, one gets ${\rm Im}\, t^{-1}(w) = \mu\sqrt{2\mu w}/(2\pi)$. Inserting this into eq. (2.6), we obtain

$$t^{-1}(E) = \frac{E+E_B}{g_{\rm NR}^2} + \frac{\mu}{4\pi} R\left(\frac{1}{R} + i\,k\right)^2, \tag{2.7}$$

where $R = 1/\sqrt{2\mu E_B}$ denotes the characteristic distance between the constituents in the two-body bound system. Comparing the above expression with the effective range expansion $t^{-1}(E) = -\mu/2\pi\left(-1/a + r\,k^2/2 - i\,k\right)$, and using eq. (2.4), one can express the scattering length and effective range in terms of the binding energy and compositeness [15]

$$a = \frac{2\,R\,(1-Z)}{2-Z}, \qquad r = -\frac{R\,Z}{1-Z}. \tag{2.8}$$

Therefore, for an S-wave shallow two-body bound state, the compositeness can be measured by measuring the low-energy scattering parameters.

Next, we turn to the compositeness condition within the framework of the quantum field theory. For simplicity, let us first consider the situation when a scalar particle described by a field $\Phi(x)$ with the bare mass M_0 couples with two scalars $\phi_{1,2}(x)$ with the masses $m_{1,2}$. The interaction Lagrangian takes the form $\mathcal{L}_{\rm int} = g_0\,\Phi\phi_1\phi_2$.

Consider now the two-point function of the field $\Phi(x)$

$$\mathcal{G}_\Phi(s) = \int d^4x\, e^{i\,Px}\,\langle 0\,|T\Phi(x)\,\Phi(0)|\,0\rangle\ , \quad \text{with} \quad s = P^2\,. \tag{2.9}$$

Summing up one-loop bubble diagrams to the two-point function, one arrives at the expression (see figure 1)

$$\mathcal{G}_\Phi(s) = \frac{i}{s - M_0^2 - g_0^2\,G(s)}\,, \tag{2.10}$$

where the one-loop self-energy is given by

$$G(s) = i\int \frac{d^4q}{(2\pi)^4}\frac{1}{(P-q)^2 - m_1^2 + i\epsilon}\frac{1}{q^2 - m_2^2 + i\epsilon}. \tag{2.11}$$

The relativistic scattering amplitude for the process $\phi_1\phi_2 \to \phi_1\phi_2$ in the same approximation is given by (see figure 1)[1]

$$T(s) = \frac{g_0^2}{s - M_0^2 - g_0^2\,G(s)}\,. \tag{2.12}$$

[1]Here, in order to be consistent with the non-relativistic formalism, the sign convention $S = 1 - iT$ is used in the definition of the T-matrix.

JHEP01(2015)118

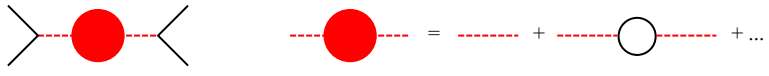

(a) (b)

Figure 1. The scattering matrix for the process $\phi_1\phi_2 \to \phi_1\phi_2$ (a) and the two-point function of the field Φ (b). Only one-loop bubbles are summed up. Solid (dashed) lines denote $\phi_{1,2}$ (Φ) fields, respectively.

The relativistic and the non-relativistic scattering matrices are the same up to an overall normalization. In the rest frame of the bound system, the relation takes the form

$$T(s) = 4w_1(k)w_2(k)\,t(E)\,, \qquad E = \sqrt{s} - (m_1 + m_2)\,, \tag{2.13}$$

where $w_i(k) = \sqrt{m_i^2 + k^2}$. Now, let us consider the behavior of the scattering amplitude in the vicinity of the bound-state pole. The two-point function has the following behavior

$$\mathcal{G}_\Phi(s) \to= \frac{i\,Z}{s - M^2 + i\epsilon} + \text{less singular terms}\,, \quad M^2 = M_0^2 + g_0^2 G(M^2)\,, \tag{2.14}$$

where M is the physical mass.

The residue of the propagator determines the wave function renormalization constant for the particle Φ:

$$Z = \frac{1}{1 - g_0^2\,G'(M^2)} = 1 + g^2\,G'(M^2), \tag{2.15}$$

where $g^2 = Z\,g_0^2$ is the renormalized coupling constant, and $G'(M^2) = \frac{d}{ds}G(s)\big|_{s=M^2}$. In order to establish the relation of the quantity Z, defined by eq. (2.15), with its non-relativistic counterpart, we perform the contour integration over q^0 of the loop integral in eq. (2.11):

$$G(s) = \int \frac{d^3\vec{q}}{(2\pi)^3}\frac{1}{2\omega_1\omega_2}\frac{\omega_1 + \omega_2}{s + \vec{P}^2 - (\omega_1 + \omega_2)^2 + i\epsilon}, \tag{2.16}$$

where $\omega_1^2 = (\vec{P} - \vec{q})^2 + m_1^2$ and $\omega_2^2 = \vec{q}^{\,2} + m_2^2$. In the rest frame of the bound state, one has $\vec{P} = 0$. Taking derivative with respect to s, and then taking the non-relativistic approximation which amounts to $\omega_1 \simeq m_1 + \vec{q}^{\,2}/(2m_1)$ and $\omega_2 \simeq m_2 + \vec{q}^{\,2}/(2m_2)$, we get

$$g^2\,G'(M^2) \simeq -\frac{g^2}{8m_1m_2M}\int \frac{d^3\vec{q}}{(2\pi)^3}\frac{1}{\left[E_B + \vec{q}^{\,2}/(2\mu)\right]^2}, \tag{2.17}$$

where we have used $E_B = m_1 + m_2 - M$. Taking into account the difference between relativistic and non-relativistic normalizations, we finally arrive at the relation $g = \sqrt{2m_1}\sqrt{2m_2}\sqrt{2M}\,g_{\rm NR}$, cf. with eq. (2.5). Comparing now this relation with eq. (2.3), one immediately sees that the wave function renormalization constant Z is the same as its non-relativistic counterpart and thus the compositeness condition for an S-wave bound state can be written as

$$Z = 1 + g^2\,G'(M^2) \to 0. \tag{2.18}$$

One might treat the above argumentation with a grain of salt, since it is based on certain approximations. Namely, the amplitude is given as a sum of one-loop diagrams only. It

JHEP01(2015)118

is, however, clear that the result is valid beyond this approximation, if bound states close to an elastic threshold are considered. The justification is provided by the statement that such bound states can be consistently described within a non-relativistic effective field theory, which is perturbatively matched to the underlying relativistic theory (see, e.g., ref. [53] for a review on the subject). Such an effective theory is equivalent to the non-relativistic quantum mechanics (the number of particles is conserved) and hence the compositeness can be rigorously defined along the lines discussed above. Finally, we would like to mention that the quantity Z, which is defined in eq. (2.15), is ultraviolet finite, since the quantity g is defined through the residue of the *renormalized* scattering amplitude.

3 Compositeness from lattice data

As stated above, the wave function renormalization constant, Z, gives an overlap of the physical state with the elementary state and hence could be used as a parameter that describes the compositeness of a given state. Lattice calculations provide a model-independent way to determine Z from the volume dependence of the spectrum [34, 54–58], or — as we propose in this paper — from the dependence on the twisting angle. In this section we set up a finite-volume formalism, which describes the dependence of the bound-state mass on the volume or twisting angle.

3.1 Finite volume formalism

We consider elastic scattering of particles with the masses m_1 and m_2 in the S-wave.[2] Then, generally, a unitary partial-wave amplitude in infinite volume is given by

$$T(s) = \frac{1}{V^{-1}(s) - G(s)} = \frac{-8\pi\sqrt{s}}{k\cot\delta(k) - ik}, \tag{3.1}$$

where $k^2 = \frac{1}{4s}[s-(m_1+m_2)^2][s-(m_1-m_2)^2]$ is the relative momentum squared in the center of mass (c.m.) frame. Further, the function $V^{-1}(s)$ ("the inverse potential") is a regular function in the vicinity of the threshold. The notation used here is reminiscent of that of unitarized Chiral Perturbation Theory, but eq. (3.1) may in fact describe any elastic unitary amplitude, with the particular dynamics encoded in the function $V(s)$. The loop function $G(s)$ is given by eqs. (2.11) and (2.16). This function contains a unitarity cut. Across this cut, we have $\mathrm{Im}\, G(s) = -k/(8\pi\sqrt{s})$. Other (distant) cuts that may be also present are included in $V(s)$. The loop function $G(s)$ is divergent and has to be renormalized. Here we do the renormalization with a subtraction constant. As it will be seen below, the extension to the finite volume is independent of any regulator.

When the particles are put in a finite box of size L, their momenta become discretized due to boundary conditions. So, the continuum spectrum, which gives rise to the cut in the infinite volume, becomes a discrete set of two-particle levels. In order to obtain the spectrum in a finite volume, one should replace the momentum integrals by the sums over the discretized momenta in the expression of the scattering amplitude. Then, the "finite

[2] In order to make the presentation transparent, throughout this paper we do not consider the partial-wave mixing in a finite volume. This effect can be later included in a standard manner.

JHEP01(2015)118

volume scattering amplitude" $\tilde{T}$ contains poles on the real axis that correspond to the discrete two-particle levels. It should be noted that the finite-volume effects in $V(s)$ are exponentially suppressed (see, e.g., [59]), so the the finite volume scattering amplitude can be obtained just by changing the loop function by its finite volume counterpart $\tilde{G}_L^{\vec{\theta}}(s) = G(s) + \Delta G_L^{\vec{\theta}}(s)$ [60], where

$$\Delta G_L^{\vec{\theta}}(s) = \lim_{\Lambda\to\infty}\left[\frac{1}{L^3}\sum_{|\vec{q}_n|<\Lambda} I(\vec{q}_n) - \int_{|\vec{q}|<\Lambda}\frac{d^3\vec{q}}{(2\pi)^3} I(\vec{q})\right]. \tag{3.2}$$

Here $I(\vec{q})$ denotes the integrand in eq. (2.16), and $\vec{q}_n$ the allowed momenta in a finite volume, whose value depends on the box size L and the boundary conditions used. For the periodic boundary conditions we have $\vec{q}_n = \frac{2\pi}{L}\vec{n}$, $\vec{n}\in\mathbb{Z}^3$. In case of twisted boundary conditions, the momenta also depend on the twisting angle $\vec{\theta}$ according to $\vec{q}_n = \frac{2\pi}{L}\vec{n} + \frac{\vec{\theta}}{L}$, $0 \le \theta_i < 2\pi$. Using the methods of ref. [60], it can be shown that $\Delta G_L^{\vec{\theta}}$ can be related to the modified Lüscher function $Z_{00}^{\vec{\theta}}$, see appendix A,

$$\Delta G_L^{\vec{\theta}}(s) = \frac{1}{8\pi\sqrt{s}}\left(ik - \frac{2}{\sqrt{\pi}L} Z_{00}^{\vec{\theta}}(1,\hat{k}^2)\right) + \cdots, \tag{3.3}$$

where $\hat{k} = kL/(2\pi)$ and the dots stand for terms that are exponentially suppressed with the volume size L [60].

In this paper, we are going to apply Lüscher formalism to study shallow bound states, where the finite-volume effects are exponentially suppressed. Since, for such states, the binding momentum κ is presumed to be much smaller than the lightest mass in the system, the exponentially suppressed corrections emerging, e.g., from the potential $V(s)$ could be consistently neglected as compared to the corrections $\sim e^{-\kappa L}$ that arise from $Z_{00}^{\vec{\theta}}(1,\hat{k}^2)$. Note however that, if masses of the constituents increase for a fixed binding energy, then the magnitude of the binding momentum also increases and, for the bound states of heavy mesons, may become comparable to the pion mass. In this case, further study of the problem is necessary. A recent example of such a study (albeit in the light quark sector) is given in ref. [61]. In the present paper this issue is not addressed.

Finally, note that the divergences arising at $\Lambda\to\infty$ in eq. (3.2) cancel between the sum and the integral, so we can safely send the cutoff to infinity. Thus, $\Delta G_L^{\vec{\theta}}$ does not depend on any regulator. In appendix A we show in detail, how $\Delta G_L^{\vec{\theta}}$ could be calculated below threshold for different types of boundary conditions.

3.2 Bound states in finite volume

Bound states show up in the scattering amplitude as poles on the real axis below threshold. Namely, if we have a bound state with the mass M in the infinite volume, the scattering amplitude should have a pole at $s = M^2$, with the corresponding binding momentum $k_B \equiv i\kappa$, $\kappa > 0$. From eq. (3.1), it is clear that M and k_B satisfy the equation

$$\psi(k_B^2) + \kappa = -8\pi M\Big[V^{-1}(M^2) - G(M^2)\Big] = 0, \tag{3.4}$$

JHEP01(2015)118

where $\psi(k^2)$ is the analytic continuation of $k\cot\delta(k)$ for arbitrary complex values of k^2, which is needed since the bound state is located below threshold, $k_B^2 < 0$. On the other hand, the discrete levels in a finite volume are obtained as the poles of the finite-volume scattering amplitude $\tilde{T}$ and, in particular, the bound state pole gets shifted to M_L, with binding momentum $k_L \equiv i\kappa_L$, given by

$$\tilde{T}^{-1}(M_L^2) = T^{-1}(M_L^2) - \Delta G_L^{\vec{\theta}}(M_L^2) = 0 \quad \Rightarrow \quad \psi(k_L^2) + \kappa_L + 8\pi M_L \Delta G_L^{\vec{\theta}}(M_L^2) = 0\,. \tag{3.5}$$

Note that, below threshold, both T^{-1} and $\Delta G_L^{\vec{\theta}}$ are real, so the pole position is real. The discrete scattering levels above threshold are real as well (as they should be), since the imaginary part of $\Delta G_L^{\vec{\theta}}$ cancels exactly with that of T^{-1}.

Next, we relate the finite-volume pole position with the infinite-volume quantities as the bound state mass, M, and the coupling, g^2 (defined as the residue of the scattering amplitude at the pole $s = M^2$). To this end, we expand $\psi(k_L^2)$ around the infinite-volume pole position, $k_B = i\kappa$,

$$\psi(k_L^2) \simeq \psi(k_B^2) - \psi'(k_B^2)(\kappa_L^2 - \kappa^2) = -\kappa - \psi'(k_B^2)(\kappa_L - \kappa)(\kappa_L + \kappa), \tag{3.6}$$

where the prime denotes a derivative respect to k^2. Then, evaluating the residue at M^2 in eq. (3.1) we obtain

$$\psi'(k_B^2) = \frac{1}{2\kappa} - \frac{8\pi M}{g^2 \frac{dk^2}{ds}}, \tag{3.7}$$

where the derivative dk^2/ds is to be evaluated at $s = M^2$. Finally, using eqs. (3.5) and (3.6), we obtain for the pole position shift

$$\kappa_L - \kappa = \frac{1}{1 - 2\kappa\psi'(k_B^2)} \left[-8\pi M_L \Delta G_L^{\vec{\theta}}(M_L^2) + \psi'(k_B^2)(\kappa_L - \kappa)^2 \right] \tag{3.8}$$

This equation gives the bound state pole position, κ_L (or, equivalently, $M_L = \sqrt{m_1^2 - \kappa_L^2} + \sqrt{m_2^2 - \kappa_L^2}$) as a function of the infinite-volume parameters g^2 and κ. It is worth noting that, within the approximation (3.6), the position of the bound state pole in a finite volume depends only on these two parameters. This approximation works remarkably well in all cases considered in this paper.

If the difference $\kappa_L - \kappa$ is small enough, eq. (3.8) can be solved iteratively. For periodic boundary conditions, with the use of eq. (A.3), it can be shown that the lowest-order iterative solution reads

$$\kappa_L = \kappa + \frac{6}{1 - 2\kappa\psi'(k_B^2)} \frac{1}{L} e^{-\kappa L}\,, \tag{3.9}$$

which coincides with the result given in refs. [34, 55, 57]. However, it will be shown below that, for shallow bound states, where κ is very small, one should take more than just the first term in the sum (A.3). Moreover, in some cases, the iterations converge very slowly, if at all. Therefore, in our opinion, it is safer to consider solving eq. (3.8) numerically, without further approximations, in order to obtain the finite volume pole position κ_L. This is the way we proceed.

JHEP01(2015)118

Using eq. (3.8), it is possible to fit the infinite-volume parameters M and g^2 from the bound state levels κ_L, obtained through lattice simulations at different L or $\vec{\theta}$. This, in turn, allows one to determine the compositeness parameter from eq. (2.18). However, in actual lattice simulations, the measured energy levels have some uncertainty, and the number of different volumes or different twisting angles might be not very large. Therefore, it is important to know in advance, at which accuracy should be the lattice measurements carried out, in order to render the extraction of the parameter Z reliable. We address this question in some exactly solvable models with a given $V(s)$, producing "synthetic lattice data," adding random errors and trying to extract back the infinite volume parameters M, g^2 and Z from data.

4 Analysis with two models

4.1 A toy model

The potential in this model is given by a "bare state pole",

$$V_{\text{toy}}(s) = \frac{g_0^2}{s - s_0}, \tag{4.1}$$

which depends on two parameters: a bare pole position s_0 and a bare coupling constant g_0. By appropriately choosing the value of the bare parameters, we can reproduce a bound state with any given mass M and coupling g.

If our model describes the interaction of two particles, where a bound state with the mass M is present, the scattering partial wave amplitude (3.1) should have a pole at $s = M^2$,

$$M^2 - s_0 - g_0^2 G(M^2) = 0. \tag{4.2}$$

The physical coupling of the bound state, g, is given by the residue of the scattering partial-wave amplitude at the bound state pole

$$g^2 = \frac{g_0^2}{1 - g_0^2 G'(M^2)} = [1 + g^2 G'(M^2)] g_0^2 = Z g_0^2 \,. \tag{4.3}$$

One can use above equations to trade the bare parameters for the physical ones in the expression of the scattering amplitude and write the latter in terms of M and Z:

$$T_{\text{toy}}(s) = \frac{Z - 1}{(s - M^2) Z G'(M^2) + (1 - Z)[G(s) - G(M^2)]}. \tag{4.4}$$

Note that the above amplitude does not depend on the subtraction constant that renders $G(s)$ finite. This model can describe a bound state with any given value of the wave function renormalization constant.

Next, we study the finite volume effects in the bound-state mass. In the actual calculations, we take $m_1 = m_D$, $m_2 = m_K$ and choose the mass of the bound state to be $M = 2340\,\text{MeV}$. This is a shallow bound state at $20\,\text{MeV}$ below threshold, which corresponds to a binding momentum $\kappa \simeq 133\,\text{MeV}$. For the mainly molecular state we take

JHEP01(2015)118

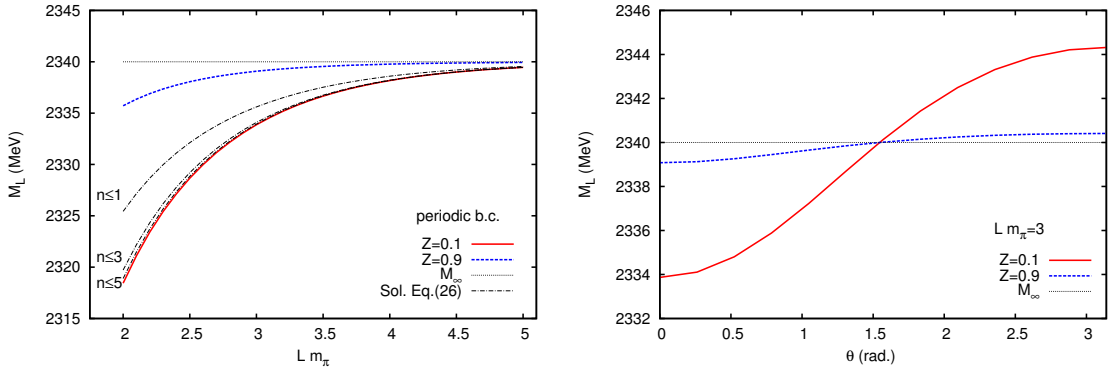

Figure 2. Bound state mass in the finite volume, M_L, as a function of L for periodic boundary conditions (left) and as a function of the twisting angle for twisted boundary conditions (right). The solid/dashed lines correspond to $Z = 0.1$ and $Z = 0.9$, respectively. The dotted line stands for the infinite-volume mass M. In order to test the accuracy of the iterative solution, for the case of $Z = 0.1$ we also plot (dot-dashed lines) the solutions of eq. (3.8) with an approximate expression of $\Delta G_L^{\vec{\theta}}$ (only the first $n \equiv |\vec{n}|$ terms are retained in the expression (A.3) for $\Delta G_L^{\vec{\theta}}$).

$Z = 0.1$, and $Z = 0.9$ is chosen for the mainly elementary one. For each of these two states, we calculate their finite-volume mass M_L as the subthreshold pole position in the finite-volume scattering amplitude.

In the left panel of figure 2, we show the mass of the two states with $Z = 0.1$ and $Z = 0.9$ as a function of L for periodic boundary conditions.[3] These are obtained from the solution of the exact equation (3.5). It is easy to see that the finite volume effects are much bigger in the case of the molecular state with $Z = 0.1$ than in the case of an elementary state with $Z = 0.9$. This was of course expected in advance, since small finite-volume effects point on a compact nature of the state in question. Here we also plot the solutions of eq. (3.8), using the known values of M and g, taken from the infinite volume model. In this way we can test the validity of the approximation in eq. (3.6), used to derive eq. (3.8) from eq. (3.5), which basically states that all relevant dynamics is encoded only in the two parameters M and g. As can be seen in figure 2, eq. (3.8) is able to reproduce the synthetic lattice results very accurately. On the other hand, note that for shallow bound states the binding momentum κ is small, so no wonder that the expansion in $\Delta G_L^{\vec{\theta}}$ converges rather slowly. Consequently, retaining only the leading-order term and constructing iterative solution, see eq. (3.9), might not be sufficient in all cases.

In the right panel of the same figure we show the dependence of the bound-state mass on the twisting angle $\vec{\theta} = (\theta, \theta, \theta)$ for the fixed value of $Lm_\pi = 3$. We see that, for such a choice of twisting, the size of the effect of twisting for a fixed L is almost the double of the maximal effect caused by the variation of L from the same value to infinity (periodic boundary conditions). Thus, using (partially) twisted boundary conditions to determine Z, besides being cheaper, could give more accurate results than a method based on the study of the volume-

[3]Note that throughout this paper we take the physical value of m_π and do not discuss the pion mass dependence.

JHEP01(2015)118

dependence of the energy level. Note also that, for the above choice of the twisting angle, the twisting effect is maximal. Other choices, e.g., $\vec{\theta} = (0, 0, \theta)$ lead to a smaller effect.

4.2 DK scattering and the $D_{s0}^*(2317)$

Now we turn our attention to the realistic case of the hadronic bound state $D_{s0}^*(2317)$ in the DK scattering channel with isospin $I = 0$ and strangeness $S = 1$. When isospin symmetry is exact, this state is stable under strong interactions, since it does not couple to the lighter hadronic channels (the observed decay $D_{s0}^*(2317) \to D_s\pi$ breaks isospin symmetry). Thus, the formalism above, tailored for stable bound states, does apply in this case. The case of quasi-bound states, which are coupled to inelastic channels, requires special treatment and is not addressed here.

A popular view on the $D_{s0}^*(2317)$ meson is that this state is dynamically generated as a pole through the S-wave interactions between the D-meson and the kaon in the isoscalar channel [42, 62–66]. We shall study this system, using the model used from ref. [63], which is based on the leading-order heavy flavor chiral Lagrangian [67–69] and unitarizes the amplitude [6, 7, 70, 71]. Namely, the infinite-volume amplitude is obtained from eq. (3.1) with the S-wave-projected potential

$$V(s) = \frac{1}{2}\int_{-1}^{1} dx\, \frac{u(s,x) - s}{2f_\pi^2} = \frac{1}{2f_\pi^2}\left[m_D^2 + m_K^2 + \frac{(m_D^2 - m_K^2)^2}{2s} - \frac{3s}{2}\right], \tag{4.5}$$

where $x = \cos\theta$ is the cosine of the scattering angle, $f_\pi \simeq 92.4\,\text{MeV}$ is the pion decay constant, and s and u are usual Mandelstam variables. We regularize the loop function with a subtraction constant $a(\mu)$, as done in refs. [63, 72]. Its value at the scale $\mu = m_D$ is taken to be $a(m_D) = -0.71$. With this value of the subtraction constant, we find a bound state pole, associated with the $D_{s0}^*(2317)$, at $M = 2316.9$ MeV, and the coupling to DK, which is given by the residue of the pole,

$$g^2 = \lim_{s \to M^2} (s - M^2) T(s), \tag{4.6}$$

takes the value $g = 10.7$ GeV. One can easily calculate the compositeness parameter of the bound state as well, using eq. (2.18). The calculation yields $Z = 0.29$. Hence, in this model, the $D_s^*(2317)$ is predominately a molecular state.

Next, we study this model in a finite volume and consider twisting of different quarks, from which the D and K mesons consist. The net effect is that these mesons get different momenta as a result of such twisting, so the expression for $G_L^{\vec{\theta}}$ changes. Note that this issue is important in view of the fact that partial twisting is allowed only for certain quarks (see section 5 for more details).

In figure 3, we display the volume dependence of the bound state mass for different twisting angles which are again chosen as $\vec{\theta} = (\theta, \theta, \theta)$. In the left panel, we plot the L-dependence for three different values of the twisting angle, when twisted boundary conditions are applied to the u-quark. In the right panel, twisted boundary conditions are applied to the s-quark. As we shall see later, in the latter case the use of partial twisting gives the same results as using fully twisted boundary conditions. The size of the finite volume effects, using twisted boundary conditions for the c-quark, is very small, so we do not discuss

JHEP01(2015)118

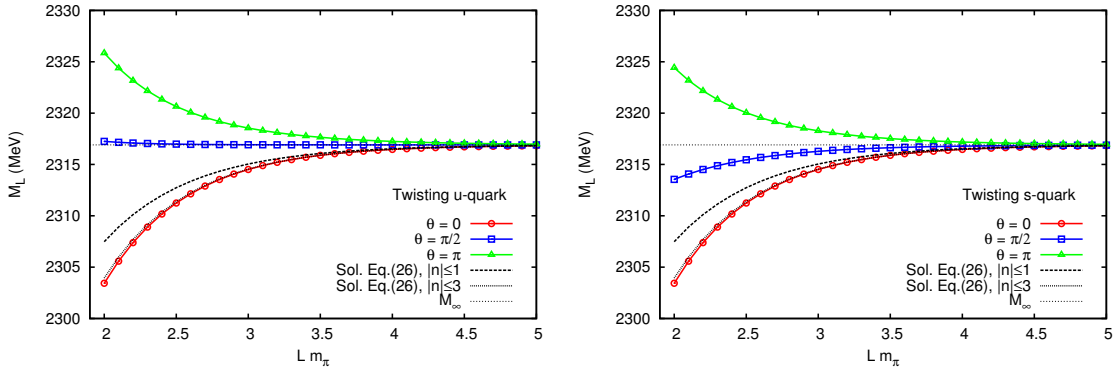

Figure 3. L-dependence of the DK bound-state mass for different twisting angles. Left: twisted boundary conditions applied to the u-quark. Right: twisted boundary conditions applied to the s-quark. The dashed lines give the solution of eq. (3.8), using the values for M and g from the infinite-volume model. In these solutions, approximate expression for $G_L^{\vec{\theta}}$ at $\vec{\theta} = 0$ was used, that amounts to summing up exponentials only up to $|\vec{n}| \leq n_{\max}$.

this case. In this model, we test again that the predictions obtained from eq. (3.8), using the values of M and g from the infinite-volume model, reproduce very well the exact solution. Consequently, all relevant dynamics of the model near threshold is encoded in just two parameters g and M. On the other hand, we see that retaining only the leading exponential in the expansion of $G_L^{\vec{\theta}}$ will have a large impact on the accuracy. Consequently, the first few terms should be retained. We see that the convergence is satisfactory: e.g., taking $n_{\max} \geq 3$, where $n_{\max}$ denotes the number of terms retained in the expansion, we see that the largest difference between the synthetic data and the prediction from eq. (3.8) is less than 0.1 MeV.

Analyzing figure 3, we again come to the conclusion that the use of (partially) twisted boundary conditions can provide a better way to extract the compositeness parameter Z from lattice results. This can already be seen by comparing the curves for $\theta = 0$ and $\theta = \pi$. One namely observes that the size of the effect due to twisting at a fixed volume is almost twice as big as due to changing the volume for periodic boundary conditions.

In figure 4, for three different volumes, we show the dependence of the bound-state mass on the twisting angle both for u- and s-quark twisting. On the other hand, taking the results of the θ-dependence (like in figure 4) at a fixed volume for granted, one could fit the value of the infinite-volume mass and coupling constant to these data, using eq. (3.8). After this, it is straightforward to obtain the value of Z. In fact, producing four synthetic lattice data points at a fixed $Lm_\pi = 2.5$ and $\theta = 0, \pi/3, 2\pi/3, \pi$ (either for u- or s- quark twisting), we were able to obtain values for M and g that differ less than 1% from those calculated from the infinite volume model by fitting the solution to eq. (3.8) (with $n_{\max} = 5$) to the synthetic data.

Real lattice simulations, however, produce results which carry uncertainties. Hence, the question arises, how big these errors could be in order to be still able to determine Z with a desired accuracy. Since, as seen from the figures, the finite volume effects (for reasonable volume sizes, say, above $Lm_\pi = 2.5$) are at most around 10 MeV, one expects

JHEP01(2015)118

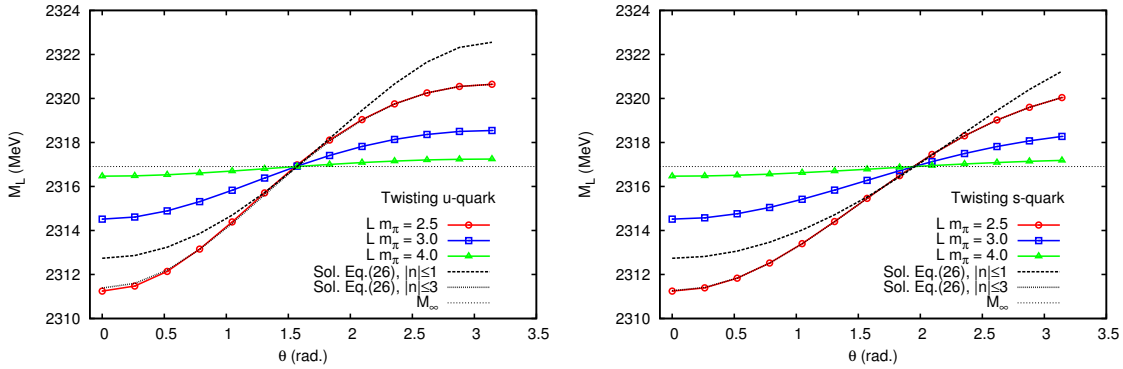

Figure 4. θ dependence of the DK bound state mass for different lattice volumes. Left: twisted boundary conditions applied to the u-quark. Right: twisted boundary conditions applied to the s-quark. The dashed lines give the solution of eq. (3.8), using the values for M and g from the infinite-volume model. In these solutions, approximate expression for $G_L^{\vec{\theta}}$ at $\vec{\theta} = 0$ was used, that amounts to summing up exponentials only up to $|\vec{n}| \leq n_{\max}$.

	4 lattice data points		8 lattice data points	
ΔM_L (MeV)	$Lm_\pi = 2.5$	$Lm_\pi = 3.0$	$Lm_\pi = 2.5$	$Lm_\pi = 3.0$
2	0.21	0.47	0.17	0.36
1	0.11	0.23	0.08	0.19
0.5	0.05	0.12	0.04	0.09

Table 1. The accuracy of the extraction of the parameter Z from the fits to the synthetic lattice data for different input error ΔM_L. Four or eight data points and two different volumes $Lm_\pi = 2.5$ and $Lm_\pi = 3.0$ were used, see main text for details.

that a relatively high accuracy will be needed in the measurement of the bound-state energy. In order to determine, how high this accuracy should actually be, we assign an uncertainty to the synthetic data that we generate from our model. In particular, using the von Neumann rejection method, from the "exact" data points we generate a new, "randomized" data set, where the central values of each data point are shifted randomly, following the Gaussian distribution centered at exact data values and with a standard deviation, given by the lattice data error. Repeating this process several times, we obtain several sets of synthetic lattice data with errors and central values shifted accordingly. We then fit each of the randomized data sets and obtain a corresponding value for M and g (and therefore, for Z), one for each set, ending up with as many values for the parameters, as many randomized data sets we have generated. We can obtain then the mean and standard deviation of the distributions for M, g and Z. Thus, for a given data error, we can estimate the accuracy of the parameter extraction.

For the case of the s-quark twisting, we construct 5000 sets of randomized data at a fixed volume, for different input errors ΔM_L and different number of data points per set. Fitting the parameters to each set, we obtain the corresponding distributions of 5000 points

JHEP01(2015)118

Index	Channel	Quark content
1	$\lvert K_{\mathsf{vv}} D_{\mathsf{vv}}\rangle$	$-\frac{1}{\sqrt{2}}\lvert u_{\mathsf{v}}\bar{s}_{\mathsf{v}}c_{\mathsf{v}}\bar{u}_{\mathsf{v}} + d_{\mathsf{v}}\bar{s}_{\mathsf{v}}c_{\mathsf{v}}\bar{d}_{\mathsf{v}}\rangle$
2	$\lvert K_{\mathsf{vs}} D_{\mathsf{vs}}\rangle$	$-\frac{1}{\sqrt{2}}\lvert u_{\mathsf{s}}\bar{s}_{\mathsf{v}}c_{\mathsf{v}}\bar{u}_{\mathsf{s}} + d_{\mathsf{s}}\bar{s}_{\mathsf{v}}c_{\mathsf{v}}\bar{d}_{\mathsf{s}}\rangle$
3	$\lvert K_{\mathsf{vg}} D_{\mathsf{vg}}\rangle$	$-\frac{1}{\sqrt{2}}\lvert u_{\mathsf{g}}\bar{s}_{\mathsf{v}}c_{\mathsf{v}}\bar{u}_{\mathsf{g}} + d_{\mathsf{g}}\bar{s}_{\mathsf{v}}c_{\mathsf{v}}\bar{d}_{\mathsf{g}}\rangle$

Table 2. Scattering channels for the case of $I = 0$.

for each parameter M, g and Z. In table 1, we show the resulting standard deviations for Z, which give an idea of the expected accuracy in a fit to actual lattice data. The results for the case of the u-quark twisting are very similar. We see that, for $Lm_\pi = 2.5$ where the finite volume effects are the largest, we need lattice errors smaller than 1 MeV in order to obtain an accuracy in Z below 0.1. For larger volumes, the accuracy required in the input lattice data is even bigger. If we increase the number of lattice data points, we get slightly better results but, in general, the dependence on the increase of the size of the data set is very mild. For example, we need to use around 20 data points to achieve an accuracy of order 0.1 in Z, given an input error $\Delta M_L = 2$ MeV and volume $Lm_\pi = 2.5$.

5 Partially twisted boundary conditions in the DK system

The partial twisting, unlike the full twisting, is more affordable in terms of computational cost in lattice simulations, because one does not need to generate new gauge configurations. Thus, it is very interesting to study whether it is possible to extract any physically relevant information from simulations using this kind of boundary conditions. Problems may arise when there are annihilation channels present, as is the case in the DK scattering in the isoscalar channel, where light quarks may annihilate. An analysis of Lüscher approach with partial twisting for scattering problem in the presence of annihilation channels was recently addressed in [46]. Namely, a modified partially twisted Lüscher equation was derived for the $\pi\eta - K\bar{K}$ coupled channel scattering in the framework of non-relativistic EFT.

Here, we address the same problem in the context of the DK scattering. The method is described in ref. [46], to which the reader is referred for further details. Consider first the scattering in the infinite volume. We start from building the channel space by tracking the quarks of different species following through the quark diagrams describing the DK scattering. It is clear that, since only light quarks may annihilate, the possible final states contain *valence*, *sea* or *ghost* light quarks with equal masses, as given in table 2. Omitting channel indices, the resulting *algebraic* Lippmann-Schwinger equation couples 3 different channels

$$T = V + VG_{DK}T\,, \tag{5.1}$$

where T, V and G are given by 3×3 matrices.

The free Green function is given by

$$G_{DK}(s) = G(s)\ \text{diag}\ (1, 1, -1) \tag{5.2}$$

JHEP01(2015)118

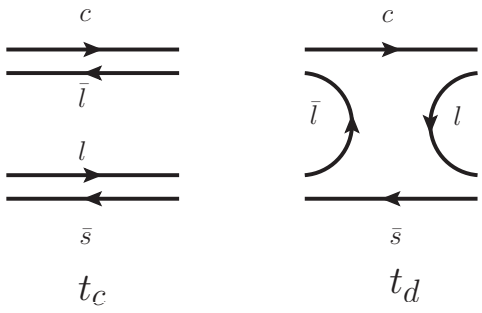

Figure 5. Connected (t_c) and disconnected (t_d) diagrams, emerging in $DK \to DK$ scattering amplitudes with various quark species; l=u, d.

where $G(s)$ is defined in eqs. (2.11) and (2.16), supplemented by the prescription that the integral is performed in dimensional regularization *after* expanding the integrand in powers of 3-momenta (see refs. [46, 73] for details). The minus sign on the diagonal of the matrix G arises due to fermionic nature of D and K mesons composed of valence and (commuting) ghost quarks.

The crucial point now is that there exist linear symmetry relations between various elements of T due to equal valence, sea and ghost quark masses. Note that scattering matrix elements are given by residues of the 4-point Green functions Γ_{ij} of the bilinear quark operators at the poles, corresponding to the external mesonic legs. Decomposing Γ_{ij} into *connected* t_c and *disconnected* t_d pieces through Wick contractions (see figure 5) and noting that quark propagators are the same for all light quark species, we get

$$\Gamma_{11} = \Gamma_{22} = t_c - t_d\,, \quad \Gamma_{33} = -t_c - t_d\,, \quad \Gamma_{12} = \Gamma_{13} = \Gamma_{23} = \Gamma_{21} = \Gamma_{31} = \Gamma_{32} = -t_d\,, \tag{5.3}$$

Since in our case there are no neutral states and thus no mixing occurs, following the argumentation given in ref. [46], it is easy to show that T-matrix obeys the same symmetry relations as Γ

$$T_{11} = T_{22} = t, \quad T_{33} = -t + 2y\,, \quad T_{12} = T_{13} = T_{23} = T_{21} = T_{31} = T_{32} = y\,. \tag{5.4}$$

Here $T_{11} = t$ corresponds to the *physical* elastic DK scattering amplitude, i.e scattering in the sector with valence quarks only. Other diagonal entries are *unphysical* in the sense that they correspond to scattering of particles, composed of sea and ghost light quarks. Non-diagonal elements of T-matrix describe coupling between valence and sea/ghost sectors through *disconnected* diagrams. Furthermore, it is straightforward to check from eq. (5.1) that the elements of potential matrix V satisfy the same symmetry relations as T and can be expressed in the following form

$$V = \begin{pmatrix} \tau & \upsilon & \upsilon \\ \upsilon & \tau & \upsilon \\ \upsilon & \upsilon & -\tau + 2\upsilon \end{pmatrix}, \tag{5.5}$$

JHEP01(2015)118

Let us now turn to the case of a finite volume and derive the Lüscher equation for a couple of particular choices of partially twisted boundary conditions. Note that the potential V remains the same (up to exponentially suppressed in terms L), while in the loop functions the integration is substituted by summation over lattice momenta.

1. Twist the s/c-quark, leaving u and d-quarks to obey periodic boundary condition. In this case, the matrix of the Green functions is diag $\left(\tilde{G}_L^{\vec{\theta}}, \tilde{G}_L^{\vec{0}}, -\tilde{G}_L^{\vec{0}}\right)$. The solution of the Lippmann-Schwinger equation in a finite volume for the *physical* amplitude t is given by

$$t = \frac{\tau}{1 - \tau \tilde{G}_L^{\vec{\theta}}}\,, \tag{5.6}$$

where $\tilde{G}_L^{\vec{\theta}}$ is the loop function $G(s)$ in a finite volume. We see that the finite-volume spectrum in case of the partial twisting is determined from the Lüscher equation

$$1 - \tau \tilde{G}_L^{\vec{\theta}}(s) = 0, \tag{5.7}$$

in the same way as in the full-twisting case. Thus, the results obtained by using of the partially twisted boundary conditions on the c- or s-quark are equivalent to those using full twisting.

2. Twist the valence u- and d-quarks simultaneously, leaving s- and c-quarks obey periodic boundary condition. In this case, the ghost light quarks also need to be twisted, and the matrix of the Green functions is diag $\left(\tilde{G}_L^{\vec{\theta}}, \tilde{G}_L^{\vec{0}}, -\tilde{G}_L^{\vec{\theta}}\right)$.

   The Lüscher equation determining the finite volume spectrum now takes the form

$$\left[1 - \tau \tilde{G}_L^{\vec{0}}(s)\right] \left[1 - (\tau - \upsilon)\tilde{G}_L^{\vec{\theta}}(s)\right]^2 = 0\,. \tag{5.8}$$

   Vanishing of the first bracket on the r.h.s. gives the Lüscher equation with *no twisting*. Note also that the quantity $\tau - \upsilon$ is in fact the connected part of the scattering potential for the isoscalar DK system, which is identical to the DK scattering potential in the isovector channel. Hence, vanishing of the second bracket is equivalent to the fully twisted Lüscher equation for the isovector DK scattering.[4]

6 Summary and conclusions

i) Lattice QCD does not only determine the hadron spectrum. Under certain circumstances, it may provide information about the nature of hadrons, which renders lattice simulations extremely useful for the search and the identification of exotic states. Note that the lattice QCD possesses unique tools at its disposal (e.g., the study of the volume and quark mass dependence of the measured quantities), which are not available to experiment.

[4]Since there is no disconnected Wick contraction for the isovector DK scattering, partial twisting is always equivalent to the full twisting in this case.

JHEP01(2015)118

ii) In the present paper, we concentrate on the identification of hadronic molecules on the lattice. Experimentally, one may apply Weinberg's compositeness condition to the near-threshold bound states, in order to distinguish the molecular states from the elementary ones. To this end, one may use the value of the wave function renormalization constant Z which obeys the inequalities $0 \leq Z \leq 1$. The vanishing value of the parameter Z corresponds to the purely molecular state. In this paper we consider the lattice version of the Weinberg's condition.

iii) It is known that the quantity Z can be extracted from lattice data by studying the volume dependence of the measured energy spectrum. We have shown that the same result can be achieved by measuring the dependence of the spectrum on the twisting angle in case of twisted boundary conditions. Moreover, within the method proposed, the expected effect is approximately twice as large in magnitude and comes at a lower computational cost. Further, we have analyzed synthetic data to estimate the accuracy of the energy level measurement which is required for a reliable extraction of the value of Z on the lattice.

iv) As an illustration of the method, we consider the $D_{s0}^*(2317)$ meson, which is a candidate of a DK molecular state. It is proven that, despite the presence of the so-called annihilation diagrams, one may still use the partially twisted boundary conditions for the extraction of Z from data if the charm or strange quark is twisted. The effects which emerge due to partial twisting, are suppressed at large volumes.

Acknowledgments

The authors thank M. Döring, L. Liu, U.-G. Meißner and S. Sasaki for interesting discussions. This work is partly supported by the EU Integrated Infrastructure Initiative HadronPhysics3 Project under Grant Agreement no. 283286. We also acknowledge the support by the DFG (CRC 16, "Subnuclear Structure of Matter"), by the DFG and NSFC (CRC 110, "Symmetries and the Emergence of Structure in QCD"), by the Shota Rustaveli National Science Foundation (Project DI/13/02), by the Bonn-Cologne Graduate School of Physics and Astronomy, by the NSFC (Grant No. 11165005), and by Volkswagenstiftung under contract No. 86260.

A Formulas for the function $\Delta G_L^{\vec{\theta}}$ below threshold

We compute the scattering amplitude in a finite volume by replacing the loop function G by its finite volume counterpart $\tilde{G}_L^{\vec{\theta}} = G + \Delta G_L^{\vec{\theta}}$ and obtain synthetic data from the poles of the finite volume scattering amplitude. In particular, the pole below threshold gives the mass of the bound state in a finite volume.

For the case of a level below threshold, there exists a fairly simple way to calculate $\Delta G_L^{\vec{\theta}}$ defined by eq. (3.2), so that the equation (3.8) for κ_L can be easily solved. Here, we consider three different cases, one with periodic boundary conditions, and two with twisted boundary conditions. Depending on which quarks are twisted, the momenta of the mesons are modified accordingly.

JHEP01(2015)118

A.1 Periodic boundary conditions

In the case of periodic boundary conditions, the meson momenta in a box are given by

$$\vec{q}_n = \frac{2\pi\vec{n}}{L}, \qquad \vec{n} \in \mathbb{Z}^3. \tag{A.1}$$

We can evaluate the sum in eq. (3.2), using the Poisson summation formula $\sum_n \delta(n-x) = \sum_n e^{2\pi i n x}$. Transforming the sum into the integral gives

$$\frac{1}{L^3}\sum_{\vec{n}} I(\vec{q}_n) = \frac{1}{L^3}\sum_{\vec{n}} \int d^3\vec{q}\; \delta^{(3)}(\vec{q}-\vec{q}_n) I(\vec{q}) = \sum_{\vec{n}} \int \frac{d^3\vec{q}}{(2\pi)^3}\; e^{i\vec{q}\cdot\vec{n}L} I(\vec{q}). \tag{A.2}$$

Next, we note that the integrand $I(\vec{q})$ can be approximated by $\frac{1}{2\sqrt{s}}\frac{1}{k^2-\vec{q}^2}$, since the difference is exponentially suppressed [60]. Here, k^2 is the three-momentum squared of the particles in the center of mass (c.m.) frame. Then, for $k^2 < 0$, $\Delta G_L^{\vec{\theta}}$ reads

$$\Delta G_L^{\vec{0}} = \frac{1}{2\sqrt{s}}\sum_{\vec{n}\neq\vec{0}} \int \frac{d^3\vec{q}}{(2\pi)^3}\,\frac{e^{i\vec{q}\cdot\vec{n}L}}{k^2-\vec{q}^2} = -\frac{1}{8\pi\sqrt{s}L}\sum_{\vec{n}\neq\vec{0}} \frac{1}{|\vec{n}|} e^{-|\vec{n}|\sqrt{-k^2}L}. \tag{A.3}$$

The function $\Delta G_L^{\vec{0}}$ can be expressed in terms of the Lüscher zeta-function $Z_{00}(1,\hat{k}^2)$, as follows [60]:

$$\Delta G_L^{\vec{0}} = \frac{1}{8\pi\sqrt{s}}\left(-\sqrt{-k^2} - \frac{2}{\sqrt{\pi}L} Z_{00}(1,\hat{k}^2)\right), \tag{A.4}$$

$$Z_{00}(1;\hat{k}^2) = \frac{1}{\sqrt{4\pi}} \sum_{\vec{n}\in\mathbb{Z}^3} \frac{1}{\vec{n}^2-\hat{k}^2}\,, \tag{A.5}$$

where $\hat{k} = kL/(2\pi)$.

A.2 Twisted boundary conditions: both momenta shifted

In the case of twisted boundary conditions, when the momenta of both particles are shifted but the particles still are in the c.m. frame, the allowed momenta in a box are:

$$\vec{q}_n = \frac{2\pi}{L}\vec{n} + \frac{\vec{\theta}}{L}, \qquad \vec{n} \in \mathbb{Z}^3\,, \tag{A.6}$$

where $\vec{\theta}$ is the twisting angle. Now, acting in the same way, we can evaluate the sum in eq. (3.2)

$$\frac{1}{L^3}\sum_{\vec{n}} I(\vec{q}_n) = \frac{1}{L^3}\sum_{\vec{n}} \int d^3\vec{q}\; \delta^{(3)}(\vec{q}-\vec{q}_n) I(\vec{q}) = \sum_{\vec{n}} \int \frac{d^3\vec{q}}{(2\pi)^3}\; e^{i\vec{\theta}\cdot\vec{n}} e^{i\vec{q}\cdot\vec{n}L} I(\vec{q}) \tag{A.7}$$

and $\Delta G_L^{\vec{\theta}}$ becomes

$$\Delta G_L^{\vec{\theta}} = -\frac{1}{8\pi\sqrt{s}L}\sum_{|\vec{n}|\neq 0} \frac{1}{|\vec{n}|} e^{i\vec{\theta}\cdot\vec{n}} e^{-|\vec{n}|\sqrt{-k^2}L}. \tag{A.8}$$

JHEP01(2015)118

Again, we can express $\Delta G_L^{\vec{\theta}}$ in terms of the Lüscher zeta-function with twisted boundary conditions, $Z_{00}^{\vec{\theta}}(1,\hat{k}^2)$, as follows,

$$\Delta G_L^{\vec{\theta}} = \frac{1}{8\pi\sqrt{s}}\left(-\sqrt{-k^2} - \frac{2}{\sqrt{\pi}L} Z_{00}^{\vec{\theta}}(1,\hat{k}^2)\right), \tag{A.9}$$

$$Z_{00}^{\vec{\theta}}(1;\hat{k}^2) = \frac{1}{\sqrt{4\pi}} \sum_{\vec{n}\in\mathbb{Z}^3} \frac{1}{\left(\vec{n}+\vec{\theta}/2\pi\right)^2 - \hat{k}^2}\,. \tag{A.10}$$

For the particular case of $\vec{\theta} = (\theta,\theta,\theta)$, the first few terms of the above expansion are given by

$$\Delta G_L^{(\theta,\theta,\theta)}(M) = -\frac{1}{8\pi ML}\Bigg[6\cos\,\theta\, e^{-\kappa L} + 3\sqrt{2}(1+\cos 2\theta)e^{-\sqrt{2}\kappa L} + \frac{2}{\sqrt{3}}(3\cos\theta + \cos 3\theta)e^{-\sqrt{3}\kappa L} + \cdots\Bigg] \tag{A.11}$$

with $\kappa = \sqrt{-k^2}$.

A.3 Twisted boundary conditions: only one momentum shifted

Finally, in the case of twisted boundary conditions, when only the momentum of one of the particles (say, particle 1) is shifted, the allowed momenta in a box are

$$\vec{q}_1 = \frac{2\pi}{L}\vec{n}_1 + \frac{\vec{\theta}}{L}, \qquad \vec{q}_2 = \frac{2\pi}{L}\vec{n}_2, \qquad \vec{n}_1,\vec{n}_2 \in \mathbb{Z}^3\,. \tag{A.12}$$

The particles are not in the c.m. frame any more: the c.m. momentum is equal to $\vec{P} = \vec{\theta}/L$. Hence, we have to evaluate $\Delta G_L^{\vec{\theta}}$ in a moving frame with momentum $\vec{P}$,

$$\Delta G_L^{\vec{\theta}} = \frac{1}{L^3}\sum_{\vec{n}} I(\vec{q}_n) - \int \frac{d^3\vec{q}}{(2\pi)^3} I(\vec{q}), \qquad I(\vec{q}) = \frac{1}{2\omega_1\omega_2}\frac{\omega_1+\omega_2}{P_0^2 - (\omega_1+\omega_2)^2},$$

$$\omega_1^2 = (\vec{P}-\vec{q})^2 + m_1^2, \qquad \omega_2^2 = \vec{q}^{\,2} + m_2^2, \qquad \vec{q}_n = \frac{2\pi\vec{n}}{L}, \qquad P^2 = P_0^2 - \vec{P}^2 = s. \tag{A.13}$$

Again, we can approximate the integrand by [74]

$$I(\vec{q}) = -\frac{1}{2P_0}\frac{1}{(\vec{q}\,')^2 - (\vec{q}\,'\cdot\vec{P})^2/P_0^2 - \vec{k}^2} + \cdots, \qquad \vec{q}\,' = \vec{q} - \mu\vec{P}, \tag{A.14}$$

where $\mu = \frac{1}{2}\left(1 - \frac{m_1^2-m_2^2}{s}\right)$, $\vec{k}$ is the momentum of the particles in the c.m. frame, and the dots denote exponentially suppressed terms. Using the Poisson summation formula, we arrive at

$$\Delta G_L^{\vec{\theta}} = -\frac{1}{2P_0}\sum_{|\vec{n}|\neq 0} e^{-i\mu\vec{P}\cdot\vec{n}L}\int\frac{d^3\vec{q}}{(2\pi)^3}\frac{e^{i\vec{q}\cdot\vec{n}L}}{\vec{q}^{\,2} - \vec{k}^2 - \frac{(\vec{q}\cdot\vec{P})^2}{P_0^2}} \tag{A.15}$$

$$= -\frac{1}{8\pi\sqrt{s}L}\sum_{|\vec{n}|\neq 0}\frac{1}{|\hat{\gamma}\vec{n}|}e^{-i\mu\vec{\theta}\cdot\vec{n}}e^{-|\hat{\gamma}\vec{n}|\sqrt{-k^2}L}, \quad \hat{\gamma}\vec{n} = \gamma\vec{n}_{\parallel} + \vec{n}_{\perp}, \tag{A.16}$$

JHEP01(2015)118

where $\vec{n}_\parallel$ and $\vec{n}_\perp$ are the components parallel and perpendicular to $\vec{P}$ of $\vec{n}$, and $\gamma = P_0/\sqrt{s}$ is the relativistic gamma-factor. Once again, we can relate $\Delta G_L^{\vec{\theta}}$ in this case with the Lüscher zeta function in the moving frame $Z_{00}^{\vec{d}}(1;(q^*)^2)$ [75], see also refs. [74, 76, 77]:

$$\Delta G_L^{\vec{\theta}} = \frac{1}{8\pi\sqrt{s}}\left(-\sqrt{-k^2} - \frac{2}{\sqrt{\pi}L\gamma} Z_{00}^{\vec{d}}(1;\hat{k}^2)\right), \tag{A.17}$$

$$Z_{00}^{\vec{d}}(1;\hat{k}^2) = \frac{1}{\sqrt{4\pi}} \sum_{\vec{r}\in P_d} \frac{1}{\vec{r}^2 - \hat{k}^2},$$

$$P_d = \{\vec{r} = \mathbb{R}^3 \mid r_\parallel = \gamma^{-1}(n_\parallel - \mu|\vec{d}|),\ \vec{r}_\perp = \vec{n}_\perp,\ \vec{n} \in \mathbb{Z}^3\}, \tag{A.18}$$

where $\vec{d} = \vec{P}L/2\pi = \vec{\theta}/2\pi$. For the case of $\vec{\theta} = (\theta,\theta,\theta)$, the first few terms in the above expansion are

$$\Delta G_L^{(\theta,\theta,\theta)}(M) = -\frac{1}{8\pi ML}\left[\frac{6\sqrt{3}\cos(\mu\theta)}{\sqrt{\gamma^2+2}} e^{-\sqrt{\frac{\gamma^2+2}{3}}\kappa L} + 3\sqrt{2}e^{-\sqrt{2}\kappa L} + \frac{3\sqrt{6}\cos(2\mu\theta)}{\sqrt{2\gamma^2+1}} e^{-\sqrt{\frac{2}{3}(2\gamma^2+1)}\kappa L} + \cdots\right]. \tag{A.19}$$

In the case of shallow bound states, the exponential factor κ will be usually quite small, so in order to reproduce accurately the full function, one should take several terms in the expansion for $\Delta G_L^{\vec{\theta}}$ above.

References

[1] R.L. Jaffe, *Multi-quark hadrons. 1. The phenomenology of $Q^2\bar{Q}^2$ mesons*, *Phys. Rev.* **D 15** (1977) 267 [INSPIRE].

[2] D. Black, A.H. Fariborz, F. Sannino and J. Schechter, *Putative light scalar nonet*, *Phys. Rev.* **D 59** (1999) 074026 [hep-ph/9808415] [INSPIRE].

[3] N.N. Achasov and A.V. Kiselev, *The new analysis of the KLOE data on the $\phi \to \eta\pi^0\gamma$ decay*, *Phys. Rev.* **D 68** (2003) 014006 [hep-ph/0212153] [INSPIRE].

[4] J.R. Pelaez, *Light scalars as tetraquarks or two-meson states from large-N_c and unitarized chiral perturbation theory*, *Mod. Phys. Lett.* **A 19** (2004) 2879 [hep-ph/0411107] [INSPIRE].

[5] J.D. WEinstein and N. Isgur, *Do multi-quark hadrons exist?*, *Phys. Rev. Lett.* **48** (1982) 659 [INSPIRE].

[6] J.A. Oller, E. Oset and J.R. Pelaez, *Nonperturbative approach to effective chiral Lagrangians and meson interactions*, *Phys. Rev. Lett.* **80** (1998) 3452 [hep-ph/9803242] [INSPIRE].

[7] J.A. Oller, E. Oset and J.R. Pelaez, *Meson meson interaction in a nonperturbative chiral approach*, *Phys. Rev.* **D 59** (1999) 074001 [*Erratum ibid.* **D 60** (1999) 099906] [*Erratum ibid.* **D 75** (2007) 099903] [hep-ph/9804209] [INSPIRE].

JHEP01(2015)118

[8] J.A. Oller and E. Oset, *N/D description of two meson amplitudes and chiral symmetry*, *Phys. Rev.* **D 60** (1999) 074023 [hep-ph/9809337] [INSPIRE].

[9] G. Janssen, B.C. Pearce, K. Holinde and J. Speth, *On the structure of the scalar mesons $f_0(975)$ and $a_0(980)$*, *Phys. Rev.* **D 52** (1995) 2690 [nucl-th/9411021] [INSPIRE].

[10] Z.-H. Guo and J.A. Oller, *Resonances from meson-meson scattering in* U(3) *ChPT*, *Phys. Rev.* **D 84** (2011) 034005 [arXiv:1104.2849] [INSPIRE].

[11] S. Peris, M. Perrottet and E. de Rafael, *Matching long and short distances in large-N_c QCD*, *JHEP* **05** (1998) 011 [hep-ph/9805442] [INSPIRE].

[12] V. Elias, A.H. Fariborz, F. Shi and T.G. Steele, *QCD sum rule consistency of lowest lying $q\bar{q}$ scalar resonances*, *Nucl. Phys.* **A 633** (1998) 279 [hep-ph/9801415] [INSPIRE].

[13] D. Morgan, *Pole counting and resonance classification*, *Nucl. Phys.* **A 543** (1992) 632 [INSPIRE].

[14] N.A. Törnqvist, *How to parametrize an S wave resonance and how to identify two hadron composites*, *Phys. Rev.* **D 51** (1995) 5312 [hep-ph/9403234] [INSPIRE].

[15] S. Weinberg, *Evidence that the deuteron is not an elementary particle*, *Phys. Rev.* **137** (1965) B672.

[16] D. Morgan and M.R. Pennington, *$f_0(S^*)$: molecule or quark state?*, *Phys. Lett.* **B 258** (1991) 444 [*Erratum ibid.* **B 269** (1991) 477] [INSPIRE].

[17] D. Morgan and M.R. Pennington, *New data on the $K\bar{K}$ threshold region and the nature of the $f_0(S^*)$*, *Phys. Rev.* **D 48** (1993) 1185 [INSPIRE].

[18] V. Baru, J. Haidenbauer, C. Hanhart, Y. Kalashnikova and A.E. Kudryavtsev, *Evidence that the $a_0(980)$ and $f_0(980)$ are not elementary particles*, *Phys. Lett.* **B 586** (2004) 53 [hep-ph/0308129] [INSPIRE].

[19] V. Baru, J. Haidenbauer, C. Hanhart, A.E. Kudryavtsev and U.-G. Meißner, *Flatté-like distributions and the $a_0(980)/f_0(980)$ mesons*, *Eur. Phys. J.* **A 23** (2005) 523 [nucl-th/0410099] [INSPIRE].

[20] C. Hanhart, *Towards an understanding of the light scalar mesons*, *Eur. Phys. J.* **A 31** (2007) 543 [hep-ph/0609136] [INSPIRE].

[21] C. Hanhart, *How and when can one identify hadronic molecules in the baryon spectrum*, *Eur. Phys. J.* **A 35** (2008) 271 [arXiv:0711.0578] [INSPIRE].

[22] T. Hyodo, D. Jido and A. Hosaka, *Compositeness of dynamically generated states in a chiral unitary approach*, *Phys. Rev.* **C 85** (2012) 015201 [arXiv:1108.5524] [INSPIRE].

[23] T. Hyodo, *Structure and compositeness of hadron resonances*, *Int. J. Mod. Phys.* **A 28** (2013) 1330045 [arXiv:1310.1176] [INSPIRE].

[24] J. Nebreda, J.R. Pelaez and G. Rios, *Enhanced non-quark-antiquark and non-glueball N_c behavior of light scalar mesons*, *Phys. Rev.* **D 84** (2011) 074003 [arXiv:1107.4200] [INSPIRE].

[25] J.R. Pelaez and G. Rios, *Nature of the $f_0(600)$ from its N_c dependence at two loops in unitarized chiral perturbation theory*, *Phys. Rev. Lett.* **97** (2006) 242002 [hep-ph/0610397] [INSPIRE].

JHEP01(2015)118

[26] C. Hanhart, J.R. Pelaez and G. Rios, *Quark mass dependence of the ρ and σ from dispersion relations and chiral perturbation theory*, *Phys. Rev. Lett.* **100** (2008) 152001 [arXiv:0801.2871] [INSPIRE].

[27] J.R. Pelaez and G. Rios, *Chiral extrapolation of light resonances from one and two-loop unitarized chiral perturbation theory versus lattice results*, *Phys. Rev.* **D 82** (2010) 114002 [arXiv:1010.6008] [INSPIRE].

[28] V. Bernard, M. Lage, U.-G. Meißner and A. Rusetsky, *Scalar mesons in a finite volume*, *JHEP* **01** (2011) 019 [arXiv:1010.6018] [INSPIRE].

[29] M. Albaladejo and J.A. Oller, *On the size of the sigma meson and its nature*, *Phys. Rev.* **D 86** (2012) 034003 [arXiv:1205.6606] [INSPIRE].

[30] F. Okiharu et al., *Tetraquark and pentaquark systems in lattice QCD*, hep-ph/0507187 [INSPIRE].

[31] H. Suganuma, K. Tsumura, N. Ishii and F. Okiharu, *Lattice QCD evidence for exotic tetraquark resonance*, PoS(LAT2005)070 [hep-lat/0509121] [INSPIRE].

[32] H. Suganuma, K. Tsumura, N. Ishii and F. Okiharu, *Tetra-quark resonances in lattice QCD*, *Prog. Theor. Phys. Suppl.* **168** (2007) 168 [arXiv:0707.3309] [INSPIRE].

[33] A. Martinez Torres, L.R. Dai, C. Koren, D. Jido and E. Oset, *The KD, ηD_s interaction in finite volume and the nature of the $D_{s^*0}(2317)$ resonance*, *Phys. Rev.* **D 85** (2012) 014027 [arXiv:1109.0396] [INSPIRE].

[34] T. Sekihara and T. Hyodo, *Size measurement of dynamically generated hadronic resonances with finite boxes*, *Phys. Rev.* **C 87** (2013) 045202 [arXiv:1209.0577] [INSPIRE].

[35] S. Ozaki and S. Sasaki, *Lüscher's finite size method with twisted boundary conditions: an application to J/ψ-ϕ system to search for narrow resonance*, *Phys. Rev.* **D 87** (2013) 014506 [arXiv:1211.5512] [INSPIRE].

[36] M. Albaladejo, C. Hidalgo-Duque, J. Nieves and E. Oset, *Hidden charm molecules in finite volume*, *Phys. Rev.* **D 88** (2013) 014510 [arXiv:1304.1439] [INSPIRE].

[37] R.A. Briceño, Z. Davoudi, T.C. Luu and M.J. Savage, *Two-baryon systems with twisted boundary conditions*, *Phys. Rev.* **D 89** (2014) 074509 [arXiv:1311.7686] [INSPIRE].

[38] BABAR collaboration, B. Aubert et al., *Observation of a narrow meson decaying to $D_s^+\pi^0$ at a mass of 2.32 GeV/c^2*, *Phys. Rev. Lett.* **90** (2003) 242001 [hep-ex/0304021] [INSPIRE].

[39] CLEO collaboration, D. Besson et al., *Observation of a narrow resonance of mass 2.46 GeV/c^2 decaying to $D_s^{*+}\pi^0$ and confirmation of the $D_{sJ}^*(2317)$ state*, *Phys. Rev.* **D 68** (2003) 032002 [*Erratum ibid.* **D 75** (2007) 119908] [hep-ex/0305100] [INSPIRE].

[40] S.-L. Zhu, *New hadron states*, *Int. J. Mod. Phys.* **E 17** (2008) 283 [hep-ph/0703225] [INSPIRE].

[41] M. Cleven, F.-K. Guo, C. Hanhart and U.-G. Meißner, *Light meson mass dependence of the positive parity heavy-strange mesons*, *Eur. Phys. J.* **A 47** (2011) 19 [arXiv:1009.3804] [INSPIRE].

[42] L. Liu, K. Orginos, F.-K. Guo, C. Hanhart and U.-G. Meißner, *Interactions of charmed mesons with light pseudoscalar mesons from lattice QCD and implications on the nature of the $D_{s0}^*(2317)$*, *Phys. Rev.* **D 87** (2013) 014508 [arXiv:1208.4535] [INSPIRE].

JHEP01(2015)118

CHAPTER 4

Optical Potential on the lattice

4.1 Summary of the project

The project is focused on the extraction of the hadron-hadron scattering parameters in case of multiple inelastic channels, which is often case with exotica and non-exotic resonances. It is well known that the Lüscher formalism becomes too complicated for practical use when the number of channels growths. An alternative approach to deal with this issue, as we suggested, is to extract the complex hadron-hadron potential from lattice calculations, using the partially twisted boundary conditions as a tool to scan the energy region of interest. To that end, we used the causal prescription $E \to E + i\epsilon$ in order to continue into the complex plane. Furthermore, the limits of the lattice size $L \to \infty$ and $\epsilon \to 0$ must be taken in this order to get an infinite-volume potential. However, since lattice calculations at large volumes are barely possible, we suggest to perform a smoothing procedure for the oscillations, arising in the optical potential at finite L and ϵ, which allows to reconstruct the infinite-volume optical potential. We tested our method on synthetic lattice date generated for the $\pi\eta - K\bar{K}$ system. As a consistency check, two smoothing methods were used: the parametric method (LASSO regularization) and the non-parametric one (Gaussian smearing). The fits of synthetic data, performed for uncertainty of the energy eigenvalues equal to 2 MeV and 3 MeV, give reliable results. However, the imaginary part is more sensitive to the input error and for the values of the order 10 MeV the fit is no longer reliable.

JHEP

Published for SISSA by Springer

Received: April 12, 2016
Revised: May 26, 2016
Accepted: May 27, 2016
Published: June 8, 2016

The optical potential on the lattice

Dimitri Agadjanov,[a] **Michael Döring,**[b,c] **Maxim Mai,**[a] **Ulf-G. Meißner**[a,d] **and Akaki Rusetsky**[a]

[a] *Helmholtz-Institut für Strahlen- und Kernphysik (Theorie) and Bethe Center for Theoretical Physics, Universität Bonn, D-53115 Bonn, Germany*

[b] *Institute for Nuclear Studies and APSIS, Department of Physics, The George Washington University, 725 21st St. NW, Washington, DC 20052, U.S.A.*

[c] *Thomas Jefferson National Accelerator Facility, 12000 Jefferson Ave, Newport News, VA 23606, U.S.A.*

[d] *Institute for Advanced Simulation (IAS-4), Institut für Kernphysik (IKP-3) and Jülich Center for Hadron Physics, Forschungszentrum Jülich, D-52425 Jülich, Germany*

E-mail: dagadjanov@hiskp.uni-bonn.de, doring@gwu.edu, mai@hiskp.uni-bonn.de, meissner@hiskp.uni-bonn.de, rusetsky@hiskp.uni-bonn.de

Abstract: The extraction of hadron-hadron scattering parameters from lattice data by using the Lüscher approach becomes increasingly complicated in the presence of inelastic channels. We propose a method for the direct extraction of the complex hadron-hadron optical potential on the lattice, which does not require the use of the multi-channel Lüscher formalism. Moreover, this method is applicable without modifications if some inelastic channels contain three or more particles.

Keywords: Chiral Lagrangians, Effective field theories, Lattice QCD

ArXiv ePrint: 1603.07205

doi:10.1007/JHEP06(2016)043

JHEP06(2016)043

Contents

1 Introduction

The Lüscher approach [1] has become a standard tool to study hadron-hadron scattering processes on the lattice. The use of this approach in case of elastic scattering is conceptually straightforward: besides technical complications, caused by partial-wave mixing, each measured energy level at a given volume uniquely determines the value of the elastic phase shift at the same energy.

In the presence of multiple channels, the extraction of the scattering phase becomes more involved. In case when only two-particle coupled channels appear, one can make use of the coupled-channel Lüscher equation [2–9] and fit a simple pole parameterization for the multi-channel K-matrix elements to the measured energy spectrum in the finite volume [10–12]. A more sophisticated parameterization of the K-matrix elements, which is applicable in a wider range of the energies, can be obtained using unitarized chiral perturbation theory (ChPT) [13–17]. In the one-channel case such an approach has been successfully applied, e.g., in ref. [18] to analyze P-wave $\pi\pi$ scattering and to study the properties of the ρ-meson. However, in order to include the coupled channels $\pi\pi - K\bar{K}$, one has to determine several K-matrix elements (unknowns) from a single measurement of a finite-volume energy level. Hence, using some kind of (phenomenology-inspired) parameterizations of the multi-channel K-matrix elements becomes inevitable in practical applications.

In case when some of the inelastic channels contain three or more particles, the situation is far more complicated. Despite the recent progress in the formulation of the theoretical

JHEP06(2016)043

framework [19–23], it is still too cumbersome to be directly used in the analysis of the data. Moreover, the problem of the choice of the parameterization for three-particle scattering might become more difficult (and lead to even larger theoretical uncertainties) than in two-particle scattering.

From the above discussion it is clear that a straightforward extension of the Lüscher approach through the inclusion of more channels has its limits that are reached rather quickly. On the other hand, many interesting systems, which are already studied on the lattice, may decay into multiple channels. In our opinion, the present situation warrants a rethinking of the paradigm. One may for example explore the possibility to analyze the lattice data without explicitly resolving the scattering into each coupled channel separately. Such a detailed information is usually not needed in practice. Instead, in the continuum scattering problem, the effect of inelastic channels could be included in the so-called optical potential [24–26], whose imaginary part is non-zero due to the presence of the open inelastic channels. In many cases, it would be sufficient to learn how one extracts the real and imaginary parts of the optical potential from the lattice data, without resorting to the multi-channel Lüscher approach. In the present paper, we propose such a method, which relies on the knowledge of a sufficiently large number of eigenvalues measured in lattice simulations. Furthermore, we suggest a method that allows one to obtain this set of eigenvalues by varying a continuous parameter — the twisting angle that defines the boundary conditions set on the quark fields in the simulations [27–32]. The latter has its own limitations, but there exist certain systems, where it could in principle be applied. In particular, we have the following systems in mind:

- The scattering in the coupled-channel $\pi\eta - K\bar{K}$ system in the vicinity of the $K\bar{K}$ threshold and the $a_0(980)$ resonance.

- The spectrum and decays of the XYZ states; namely, $Z_c(3900)^\pm$ that couples to the channels $J/\psi\pi^\pm$, $h_c\pi^\pm$ and $(D\bar{D}^*)^\pm$ (this system was recently studied in ref. [33]) or the $Z_c(4025)$ that couples to the $D^*\bar{D}^*$ and $h_c\pi$ channels (see, e.g., ref. [34]).

There certainly exist other systems where this method can be used. It should also be stressed that the systems, where the partial twisting (i.e., twisting only the valence quarks) can be carried out, are interesting in the first place — for an obvious reason. All examples listed above belong to this class. In general, the partial twisting can always be carried out when the annihilation diagrams are absent. In the presence of annihilation diagrams, each particular case should be analyzed separately, invoking the methods of effective field theories in a finite volume [32]. The present paper contains an example of such an analysis.

Further, there exists an alternative method for the extraction of hadron-hadron interaction potentials from the measured Bethe-Salpeter wave functions on the Euclidean lattice. This method goes under the name of the HAL QCD approach and its essentials are explained in refs. [35–37]. The HAL QCD collaboration claims that this approach can be extended to the multi-channel systems, including the channels that contain three and more-particles [38, 39]. Note also that this approach has already been used to study various systems on the lattice, including the analysis of coupled-channel baryon-baryon scattering

JHEP06(2016)043

(see, e.g., ref. [40–42]). Hence, it would be interesting to compare our method with the HAL QCD approach.

The layout of the present paper is as follows. In section 2 we discuss the theoretical framework for the extraction of the real and imaginary parts of the optical potential and provide an illustration of the method with synthetic data, generated by using unitarized ChPT. Further, in section 3, we discuss the role of twisted boundary conditions for measuring the optical potential. Namely, the possibility of imposing partially twisted boundary conditions is explored in section 3.1. Here, we also discuss the possibility of imposing the different boundary conditions on the quark and antiquark fields. The analysis of synthetic data, including an error analysis, is presented in section 3.2. Finally, section 4 contains our conclusions.

2 Optical potential in the Lüscher approach

2.1 Multichannel potential, projection operators

In the continuum scattering theory, the inelastic channels can be effectively included in the so-called optical potential by using the Feshbach projection operator technique [24, 25]. Namely, let us start from the multi-channel T-matrix which obeys the Lippmann-Schwinger equation

$$T = V + VG_0T\,. \tag{2.1}$$

Here, V is the potential and G_0 denotes the free Green's function . The quantities T, V, G_0 are all $N \times N$ matrices in channel space.

In case when only two-particle intermediate states are present, using dimensional regularization together with the threshold expansion, it can be shown that the Lippmann-Schwinger equation (2.1) after partial-wave expansion reduces to an algebraic matrix equation (see, e.g., ref. [43]). With the proper choice of normalization, the matrix $G_0(E)$ in this case takes the form (E is the total energy in the center-of-mass system)

$$G_0(E) = \mathrm{diag}\,(ip_1(E), \cdots, ip_n(E))\,, \tag{2.2}$$

where $p_k(E)$ denotes the magnitude of the center-of-mass three-momentum, i.e.,

$$p_k(E) = \frac{1}{2E}\sqrt{\left(E^2 - \left(m_1^{(k)} + m_2^{(k)}\right)^2\right)\left(E^2 - \left(m_1^{(k)} - m_2^{(k)}\right)^2\right)} \tag{2.3}$$

and $m_{1,2}^{(k)}$ are the masses of particles in the k^{th} scattering channel. Hence, if dimensional regularization is used in case of two-particle channels, the potential V coincides with the multi-channel K matrix. The latter quantity can always be defined, irrespectively of the used regularization. Our final results are of course independent of the use of a particular regularization. Indeed, the parameterization of T in terms of eq. (2.1) with G_0 from eq. (2.2) is completely general and simply reflects the multi-channel unitarity.

Suppose further that we focus on the scattering in a given two-particle channel. Let us introduce the projection operators P and $Q = 1 - P$, which project on this channel and on

JHEP06(2016)043

the rest, respectively. In the following, we refer to them as the primary (index P) and the secondary (index Q) channels. The secondary channels may contain an arbitrary number of particles. It is then straightforward to show that the quantity $T_P(E) = PT(E)P$ obeys the following single-channel Lippmann-Schwinger equation

$$T_P(E) = W(E) + W(E)G_P(E)T_P(E)\,, \tag{2.4}$$

where

$$W(E) = P\left(V + VQ\frac{1}{E - H_0 - QVQ}QV\right)P \quad \text{and} \quad G_P(E) = PG_0(E)P\,. \tag{2.5}$$

It is easily seen that, while V is Hermitean, $W(E)$ above the secondary threshold(s) is not. The imaginary part of $W(E)$ is expressed through the transition amplitudes into the secondary channels

$$W(E) - W^\dagger(E) = -2\pi i\, PT_Q^\dagger(E)Q\,\delta(E - H_0)\,QT_Q(E)P\,, \tag{2.6}$$

where

$$T_Q(E) = V + VG_Q(E)T_Q(E) \quad \text{and} \quad G_Q(E) = QG_0(E)Q\,. \tag{2.7}$$

For illustration, let us consider scattering in the $\pi\eta - K\bar{K}$ coupled channels. Let $K\bar{K}$ and $\pi\eta$ be the primary and secondary channels, respectively. Then, the formulae for the S-wave scattering take the following form (we suppress the partial-wave indices for brevity):

$$T_{K\bar{K}\to K\bar{K}}(E) = W(E) + ip_{K\bar{K}}\,W(E)T_{K\bar{K}\to K\bar{K}}(E)\,. \tag{2.8}$$

Here,

$$W(E) = V_{K\bar{K}\to K\bar{K}} + \frac{ip_{\pi\eta}V^2_{K\bar{K}\to\pi\eta}}{1 - ip_{\pi\eta}V_{\pi\eta\to\pi\eta}}\,, \tag{2.9}$$

$p_{K\bar{K}}$, $p_{\pi\eta}$ denote the magnitude of the relative three-momenta in the center-of-mass frame in the respective channel, as given in eq. (2.3).

Solving eq. (2.8), one finds an explicit expression of the on-shell T-matrix in terms of the optical potential $W(E)$:

$$T_{K\bar{K}\to K\bar{K}}(E) = \frac{1}{W^{-1}(E) - ip_{K\bar{K}}}\,. \tag{2.10}$$

Note that the form of eq. (2.10) with a complex optical potential W is a completely general expression for the case of the multi-channel and -particle scattering problem.

It is often useful to introduce the so-called M-matrix $M = V^{-1}$, i.e.,

$$M = \frac{1}{\Delta}\begin{pmatrix} V_{\pi\eta\to\pi\eta} & -V_{K\bar{K}\to\pi\eta} \\ -V_{K\bar{K}\to\pi\eta} & V_{K\bar{K}\to K\bar{K}} \end{pmatrix}\,, \qquad \Delta = V_{K\bar{K}\to K\bar{K}}V_{\pi\eta\to\pi\eta} - V^2_{K\bar{K}\to\pi\eta}\,. \tag{2.11}$$

In terms of this quantity, the above formula can be rewritten in the following form:

$$W^{-1}(E) = M_{K\bar{K}\to K\bar{K}} - \frac{M^2_{K\bar{K}\to\pi\eta}}{M_{\pi\eta\to\pi\eta} - ip_{\pi\eta}}\,. \tag{2.12}$$

JHEP06(2016)043

Using the latter form can be justified, when a resonance near the elastic threshold exists that shows up as a pole on the real axis in V. In contrast, the quantity M is smooth in this case and can be Taylor-expanded near threshold.

In a finite volume, one may define a counterpart of the scattering amplitude $T_{K\bar{K}\to K\bar{K}}(E)$. Imposing, e.g., periodic boundary conditions leads to the modification of the loop functions[1]

$$ip_k \to \frac{2}{\sqrt{\pi}L}\, Z_{00}(1;q_k^2) \quad \text{for} \quad q_k = \frac{p_k L}{2\pi}\,, \tag{2.13}$$

whereas the potential V remains unchanged up to exponentially suppressed corrections. In the above expressions, L is the size of the cubic box and Z_{00} denotes the Lüscher zeta-function.

The energy levels of a system in a finite volume coincide with the poles of the modified scattering amplitude. The position of these poles is determined from the secular equation

$$\left(M_{K\bar{K}\to K\bar{K}} - \frac{2}{\sqrt{\pi}L}\, Z_{00}(1;q_{K\bar{K}}^2)\right)\left(M_{\pi\eta\to\pi\eta} - \frac{2}{\sqrt{\pi}L}\, Z_{00}(1;q_{\pi\eta}^2)\right) - M_{K\bar{K}\to\pi\eta}^2 = 0\,. \tag{2.14}$$

The positions of these poles on the real axis are the quantities that are measured on the lattice.

2.2 Continuation to the complex energy plane

The main question, which we are trying to answer, can now be formulated as follows: is it possible to extract the real and imaginary parts of $W(E)$ from the measurements performed on the lattice? We expect that the answer exists and is positive, for the following reason. Let us imagine that all scattering experiments in Nature are performed in a very large hall with certain boundary conditions imposed on its walls. It is *a priori* clear that nothing could change in the interpretation of the results of this experiment, if the walls are moved to infinity. Consequently, there *should* exist a consistent definition of the infinite-volume limit in a finite-volume theory that yields all quantities defined within the scattering theory in the continuum. Since the optical potential is one of these, there should exist a quantity defined in a finite volume, which coincides with the optical potential in the infinite-volume limit.

In order to find out, which quantity corresponds to the optical potential in a finite volume and how the infinite-volume limit should be performed, let us follow the same pattern as in the infinite volume. Namely, we apply the one-channel Lüscher equation for the analysis of data, instead of the two-channel one. As a result, we get:

$$W_L^{-1}(E) := \frac{2}{\sqrt{\pi}L}\, Z_{00}(1;q_{K\bar{K}}^2) = M_{K\bar{K}\to K\bar{K}} - \frac{M_{K\bar{K}\to\pi\eta}^2}{M_{\pi\eta\to\pi\eta} - \frac{2}{\sqrt{\pi}L}\, Z_{00}(1;q_{\pi\eta}^2)}\,. \tag{2.15}$$

The left-hand side of this equation is measured on the lattice at fixed values of $p_{K\bar{K}}$, corresponding to the discrete energy levels in a finite volume. Methods to measure W_L^{-1} are

[1] For simplicity, we restrict ourselves to the S-waves from here on and neglect partial wave mixing. This approximation might not be always well justified phenomenologically. However, the primary goal of the present paper is to explain the essentials of the method without focusing much on the technical details. Including partial-wave mixing within this approach forms a subject of a separate investigation.

JHEP06(2016)043

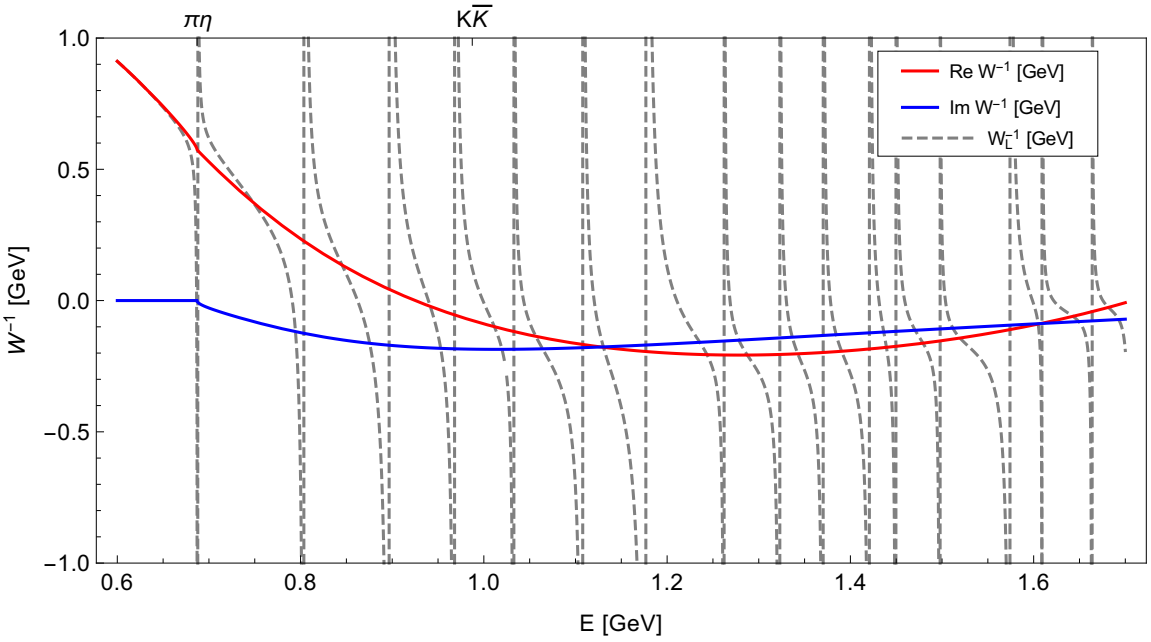

Figure 1. The real and imaginary parts of the quantity $W^{-1}(E)$, as well as its finite-volume counterpart $W_L^{-1}(E)$ for $L = 5M_\pi^{-1}$.

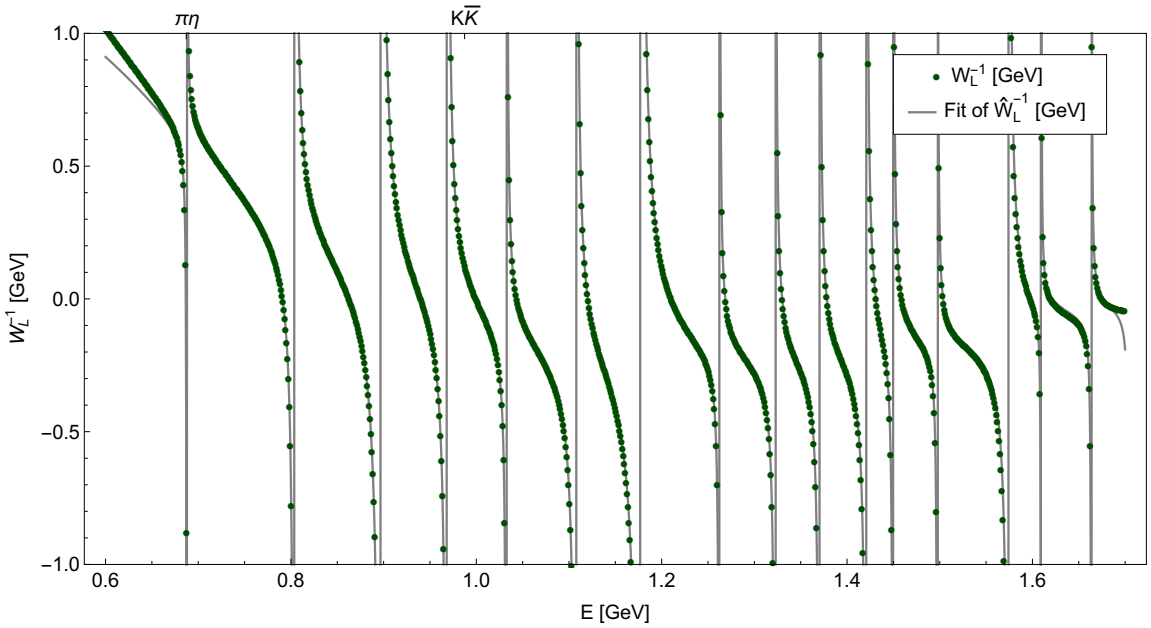

Figure 2. Fit of the function specified in eq. (2.17) to the quantity $W_L^{-1}(E)$ for $L = 5M_\pi^{-1}$ and uniformly distributed values of energy E.

discussed in section 3. The quantity on the right-hand side is proportional to the cotangent of the so-called *pseudophase*, defined as the phase extracted with the one-channel Lüscher equation [2, 3]. It coincides with the usual scattering phase in the absence of secondary channels.

JHEP06(2016)043

Figure 1 shows the real and imaginary parts of the quantity $W^{-1}(E)$ that is constructed by using a simple parameterization of the two-channel T-matrix, based on unitarized ChPT (see ref. [44]). For comparison, the finite-volume counterpart $W_L^{-1}(E)$, which is defined by eq. (2.15), is also shown. If the secondary channels were absent, $W^{-1}(E)$ would be real and equal to $W_L^{-1}(E)$, up to exponentially suppressed contributions. Figure 1 clearly demonstrates the effect of neglecting the secondary channels. While the "true" function $W^{-1}(E)$ is a smooth (and complex) function of energy, the (real) function $W_L^{-1}(E)$ has a tower of poles and zeros. The (simple) zeros of $W_L^{-1}(E)$ (poles of $W_L(E)$) emerge, when E coincides with one of the energy levels in the interacting $\pi\eta$ system. The background, obtained by subtracting all simple poles, is a smooth function of E. It should be stressed that this statement stays valid even in the presence of multiple secondary channels, some of which containing three or more particles. The only singularities that emerge in general are the simple poles that can be traced back to the eigenvalues of the total Hamiltonian restricted to the subspace of the secondary states.[2]

It is important to note that, if L tends to infinity, the optical potential does not have a well-defined limit at a given energy. As the energy levels in the secondary channel(s) condense towards the threshold, the quantity $W_L^{-1}(E)$ at a fixed E oscillates from $-\infty$ to $+\infty$. Thus, the question arises, how the quantity $W^{-1}(E)$ can be obtained in the infinite-volume limit.

It should be pointed out that this question has been already addressed in the literature in the past. In this respect, we find ref. [45] most useful. In this paper it is pointed out that, in order to give a correct causal description of the scattering process, one should consider adiabatic switching of the interaction. This is equivalent to attaching an infinitesimal imaginary part $E \to E + i\varepsilon$ to the energy. Further, as argued in ref. [45], the limits $L \to \infty$ and $\varepsilon \to 0$ are not interchangeable. A correct infinite-volume limit is obtained, when $L \to \infty$ is performed first (see ref. [46] for a more detailed discussion of this issue). Physically, this statement is clear. The quantity ε defines the available energy resolution, and the distance between the neighboring energy levels tends to zero for $L \to \infty$. If this distance becomes smaller than the energy resolution, the discrete levels merge into a cut and the infinite-volume limit is achieved. It is also clear, why the infinite-volume limit does not exist on the real axis: $\varepsilon = 0$ corresponds to an infinitely sharp resolution and the cut is never observed.

The above qualitative discussion can be related to Lüscher's regular summation theorem [47]. On the real axis above threshold, the zeta-function $Z_{00}(1; q_{\pi\eta}^2)$ in eq. (2.15) does not have a well-defined limit. Assume, however, that the energy E gets a small positive imaginary part, $E \to E + i\varepsilon$. The variable $q_{\pi\eta}^2$ also becomes imaginary:

$$q_{\pi\eta}^2 \to q_{\pi\eta}^2 + \frac{i\varepsilon E}{2}\left(\frac{L}{2\pi}\right)^2\left(1 - \frac{(M_\eta^2 - M_\pi^2)^2}{E^4}\right) = q_{\pi\eta}^2 + i\varepsilon'\,. \tag{2.16}$$

It is immediately seen that above threshold, $E > M_\eta + M_\pi$, the quantity ε' is strictly positive. Now, for real energies E, the nearest singularity is located at the distance ε from

[2] Strictly speaking, this argument applies only to $W_L(E)$. However, assuming the absence of accidental multiple zeros in $W_L(E)$, one may extend this argument to $W_L^{-1}(E)$.

JHEP06(2016)043

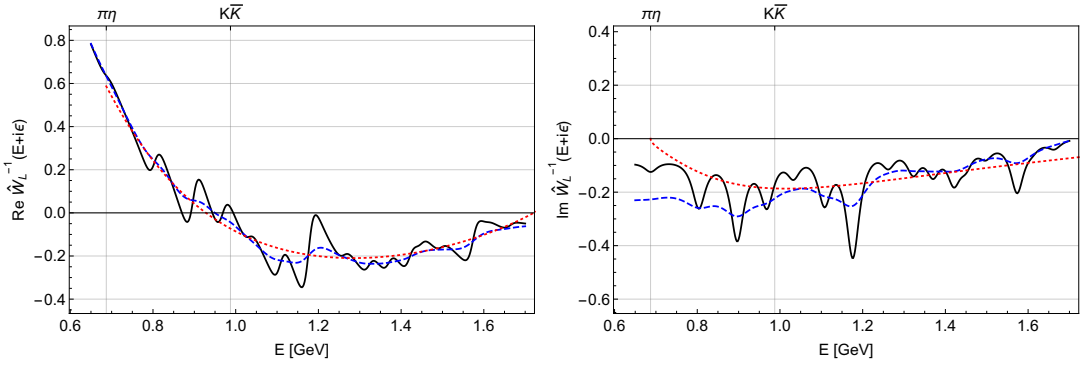

Figure 3. The real and imaginary parts of the quantity $\hat{W}_L^{-1}(E+i\varepsilon)$ for $\varepsilon = 0.02$ GeV (solid black lines) and $\varepsilon = 0.05$ GeV (dashed blue lines) versus the real and imaginary parts of the infinite-volume counterpart $W^{-1}(E)$ (dotted red lines). All quantities are given in units of GeV.

the real axis, so the regular summation theorem can be applied. It can be straightforwardly verified that the remainder term in this theorem vanishes as $\exp(-\varepsilon' L)$ (modulo powers of L), when $L \to \infty$.

The above argumentation can be readily extended to the cases when intermediate states contain any number of particles. Consider a generic loop diagram in the effective field theory where these particles appear as internal lines. It is most convenient to use old-fashioned time-ordered perturbation theory, where the integrand contains the energy denominator $(E + i\varepsilon - w_1(\mathbf{p}_1) \ldots - w_n(\mathbf{p}_n))^{-1}$. Here, $w_i(\mathbf{p}_1)\,,\ i = 1, \ldots, n$ stand for the (real) energies of the individual particles in the intermediate state. It is clear that, if $\varepsilon \neq 0$, the denominator never vanishes, and the regular summation theorem can be applied. The remainder, as in the two-particle case, vanishes exponentially when $\varepsilon \neq 0$.

The analytic continuation into the complex plane can be done as follows. Suppose one can measure the quantity $W_L^{-1}(E)$ on the real axis. Bearing in mind the above discussion, one may fit this function by a sum of simple poles plus a regular background. Figure 2 shows the result of such a fit which was performed by using the function

$$\hat{W}_L^{-1}(E) = \sum_i \frac{Z_i}{E - Y_i} + D_0 + D_1 E + D_2 E^2 + D_3 E^3 \tag{2.17}$$

to fit a sample of the exact W_L^{-1} without errors. The exact values of the fit parameters are not listed here since figure 2 is given for the illustrative purposes only. In the actual numerical simulation of section 3.2, the order of the polynomial is varied.

The continuation into the complex plane is trivial: one uses eq. (2.17) with fixed values of $Z_i,\ Y_i,\ D_i$ and makes the substitution $E \to E + i\varepsilon$. The real and imaginary parts of the quantity $\hat{W}_L^{-1}(E+i\varepsilon)$ for $\varepsilon = 0.02$ GeV and $\varepsilon = 0.05$ GeV are shown in figure 3. For comparison, the real and imaginary parts of the infinite-volume counterpart $W^{-1}(E)$ are also given. As seen, the finite-volume "optical potential" oscillates around the true one and the magnitude of such oscillation grows larger, when ε becomes smaller. On the other hand, the artifacts caused by a finite ε grow, when ε becomes large.

JHEP06(2016)043

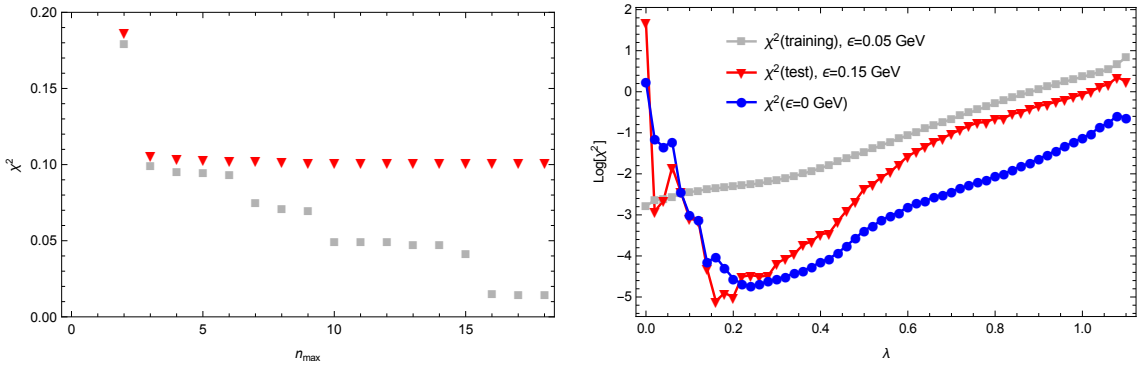

Figure 4. *Left:* the χ^2 as a function of the degree of the fit polynomial, $n_{\max}$. While the χ^2 of the unconstrained fits (gray squares) monotonically decreases, a finite penalty factor of $\lambda = \hat{\lambda}_{\text{opt}} = 0.2$ for P_2 stabilizes the result (red triangles). *Right:* cross validation. The χ^2 of the fits to the training set according to eq. (2.19) are shown with gray squares; the χ^2_V of these fits, evaluated for the test/validation set, are indicated with red triangles; the χ^2_t of these fits evaluated for the (unknown) true optical potential according to eq. (2.22) are displayed with blue circles. The minimum of the $\chi^2_V(\lambda)$ of the test/validation set (red) estimates the penalty factor $\hat{\lambda}_{\text{opt}} \sim 0.15 - 0.2$ which is very close to the truly optimal $\lambda_{\text{opt}} \sim 0.2 - 0.3$ (blue). The absolute and relative scales of the different χ^2's are irrelevant.

2.3 Infinite-volume extrapolation

From the above discussion it is clear that, performing the limit $L \to \infty$ for a fixed ε, and then taking $\varepsilon \to 0$, the infinite-volume limit is restored from $\hat{W}_L^{-1}(E + i\varepsilon)$. For the actual extraction on the lattice, however, taking the large volume limit could be barely feasible. An alternative to this procedure is to "smooth" the oscillations arising from eq. (2.17) if evaluated at complex energies at a finite L and ε. This allows one to perform the extraction of the optical potential at a reasonable accuracy even at sufficiently small values of L. As in the present study the true optical potential is known, the validity of this procedure can be tested. We would like to stress that $LM_\pi = 5$ used in this study is rather small and thus not completely beyond reach.

In the present section we test two different algorithms for smoothing the quantity $\hat{W}_L^{-1}(E + i\varepsilon)$. In both cases, the result is called $\hat{W}^{-1}$, i.e., the estimate of the true infinite-volume potential W^{-1}. The final results of the numerical studies, presented in section 3.2 are evaluated with both methods.

Parametric method. The basic idea of this method is to fit the optical potential $\hat{W}_L^{-1}(E + i\varepsilon)$ from eq. (2.17) at complex energies in the whole energy range with a suitable Ansatz. Model selection is performed with LASSO regularization (as explained in detail later) in combination with cross validation. Such methods have the advantage that basic properties of the optical potential, like Schwartz's reflection principle and threshold behavior, can be built in explicitly. In our problem, this is particularly simple because the only non-analyticity is given by the branch point at the $\pi\eta$ threshold. In more complex problems, additional non-analyticities like resonance poles or complex branch points from multi-channel states [48, 49] have to be included in the parameterization. Yet, all these non-

JHEP06(2016)043

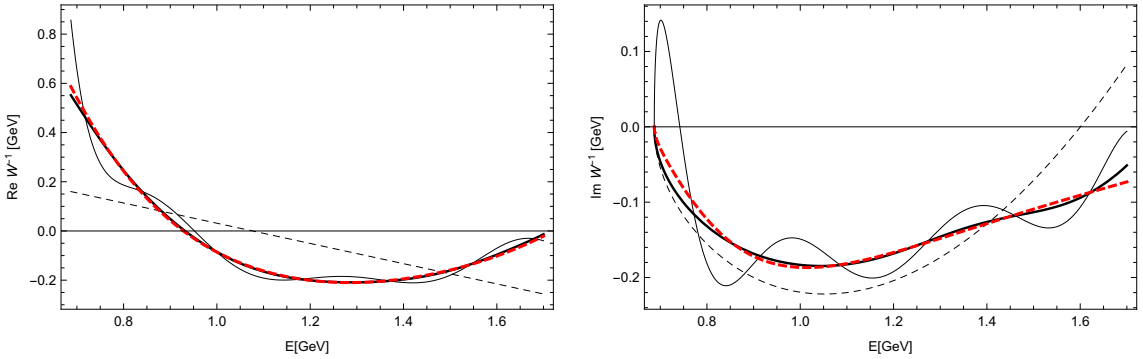

Figure 5. Real and imaginary parts of the optical potential. The thick dashed (red) lines show the true optical potential W^{-1}. The thick solid (black) lines show the reconstructed potential $\hat{W}^{-1}$ with $\hat{\lambda}_{\text{opt}} = 0.2$. The thin lines show a largely under-constrained result (thin solid, oscillating lines) with $\lambda = 0.05$ and a largely over-constrained result (thin dashed lines) with $\lambda = 1$.

analyticities are situated on other than the first Riemann sheet. The parametric and non-parametric methods proposed here use an extrapolation from finite, but positive ε to $\varepsilon \to 0$, i.e., an extrapolation performed on the first Riemann sheet that is analytic by causality.

A suitable yet sufficiently general parameterization of the optical potential is given by

$$\hat{W}^{-1}(E) = \sum_{j=0}^{n_{\max}} \left[(a_j + i\, b_j\, p_{\pi\eta})\, (E - E_0)^j \right] \tag{2.18}$$

with real parameters a_j, b_j. The only non-analyticity of $\hat{W}^{-1}$ is given by the cusp function $i\, p_{\pi\eta}$, evaluated at the complex energy E (see eq. (2.12)), that is therefore explicitly included in the Ansatz; the rest is then analytic and can be expanded in a power series around a real E_0 chosen in the center of the considered energy region, in order to reduce correlations among fit parameters (the actual value of E_0 is irrelevant).

To perform the effective infinite-volume extrapolation through smoothing, we consider the minimization of the χ^2,

$$\chi^2 = \sum_{k=1}^{m} \frac{\left| \hat{W}^{-1}(E_k) - \hat{W}_L^{-1}(E_k) \right|^2}{\sigma_k^2} + P_i(a_j,\, b_j)\,, \tag{2.19}$$

where P_i are penalty functions specified below. The absolute scale of the χ^2 is irrelevant. The quantity $\hat{W}_L^{-1}$ is fitted by sampling at the complex energies $E_k = E_{\min} + k\,\delta E + i\varepsilon$ ($\varepsilon = 0.05\,\text{GeV}$) over the considered energy range $E_{\min} \le E \le E_{\max}$ with a step $\delta E = 10\,\text{MeV}$, and assigning an arbitrary error of $\sigma_k = \sigma = 1\,\text{GeV}$. Note that in cross validation (to be specified later), the position of the minimal χ^2 determines the size of the penalty, i.e., the size of σ is irrelevant. The infinite-volume optical potential is then obtained by simply evaluating $\hat{W}^{-1}$ at real energies, i.e., setting $\varepsilon = 0$.

If we assume for the moment that the penalty function P_i in eq. (2.19) is zero, then it is clear that the minimized χ^2 is a monotonically decreasing function of the degree of the fit polynomial $n_{\max}$. This is demonstrated by the gray squares in figure 4 (left panel).

JHEP06(2016)043

Apparently, the fit stabilizes first for $n_{\max} = 3-6$, which might lead to the wrong conclusion that an optimal smoothing had been obtained. Then, for higher $n_{\max}$, another plateau is reached at $n_{\max} = 7-9$ and then another one for $n_{\max} = 10-14$. Thus, without an additional criterion, one cannot decide which $n_{\max}$ is optimal.

In general, for a small $n_{\max}$, the smoothing will be too aggressive (large χ^2), while for too large values of $n_{\max}$ the fit will start following the oscillations (figure 3), resulting in a low χ^2 but missing the point of smearing the optical potential. These two extreme cases are illustrated in figure 5 with the thin dashed and thin solid lines, respectively.[3] There is obviously a *sweet spot* for $n_{\max}$. Model selection refers to the process of determining this spot as outlined in the following.

Model selection for the fit (2.18) is formally introduced through a penalty $P(a_j, b_j)$ imposed on the fit parameters. The penalty is formulated using the LASSO method developed by Tibshirani in 1996 [50]. See also refs. [51, 52] for an introduction into the topic. The LASSO method has been recently applied in hadronic physics for the purpose of amplitude selection [53].

A natural choice to suppress oscillations is to penalize the modulus of the second derivative [51],

$$P_1(a_j,\, b_j) = \lambda^4 \int_{E_{\min}+i\varepsilon}^{E_{\max}+i\varepsilon} dE \left| \frac{\partial^2 \hat{W}^{-1}(E)}{\partial E^2} \right| , \tag{2.20}$$

where the integral is performed along a straight line in the complex plane. Another choice is to penalize only the polynomial part of the Ansatz (2.18), i.e., removing the $p_{\pi\eta}$ factor that has an inherently large second derivative at the $\pi\eta$ threshold,

$$P_2(a_j,\, b_j) = \lambda^4 \int_{E_{\min}+i\varepsilon}^{E_{\max}+i\varepsilon} dE \left(\left| \frac{\partial^2}{\partial E^2} \sum_{j=0}^{n_{\max}} a_j (E-E_0)^j \right| + \left| \frac{\partial^2}{\partial E^2} \sum_{j=0}^{n_{\max}} b_j (E-E_0)^j \right| \right) . \tag{2.21}$$

Including λ to the fourth power is done in order to have a clearer graphical representation of the penalty factor in subsequent plots. Imposing a penalty, the decrease of χ^2 with $n_{\max}$ is eventually stabilized, as shown by the red triangles in figure 4 (left panel) for some yet to be determined value of λ. Clearly, the minimized χ^2 from eq. (2.19) is a monotonically increasing function of λ as demonstrated by the gray squares in figure 4 (right panel) for the penalty function P_2.

The fitted data ($\varepsilon = 0.05\,\text{GeV}$) form the so-called *training set* [50]. The main idea of cross validation to determine the sweet spot of λ is as follows (for more formal definitions and k-fold cross validation, see refs. [50–52]): after a random division of a given data set into *training* and *test/validation* sets, the fit obtained from the training set is used to evaluate its χ^2 with respect to the test/validation set, called χ^2_V in the following (without changing fit parameters and setting $P_i = 0$). For too large values of λ, both values of χ^2 from training and from test/validation sets will be large. For too small λ, the fit to

[3] These curves are derived in a similar but slightly different context, see below. However, they still may serve as a good illustration for the statement given here.

JHEP06(2016)043

the training set is too unconstrained and sensitive to unwanted random properties such as fluctuations in the training data. However, those unwanted random properties are different in the validation set, leading to a *worse* χ^2_V for too small λ. It is then clear that $\chi^2_V(\lambda)$ exhibits a minimum at the sweet spot $\lambda = \hat{\lambda}_{\text{opt}}$.

Here, we cannot meaningfully divide the data set randomly. Instead, we have to look for data, for which the physical property (infinite-volume optical potential) is unchanged, but the unphysical property (oscillations from finite-volume poles) is changed. This is naturally given by $\hat{W}_L^{-1}$ but evaluated for a substantially different value of ε (we choose $\varepsilon = 0.15\,\text{GeV}$). The analytic form of eq. (2.18) ensures that the infinite-volume optical potential can be analytically continued to different values of ε, and only the unwanted finite-volume oscillations are different for different ε. Indeed, as indicated with the red triangles in figure 4 (right panel), χ^2_V exhibits a clear minimum at $\lambda = \hat{\lambda}_{\text{opt}} \sim 0.2$. The potential dependence of the this value on the chosen ε is discussed below.

Furthermore, in this example, we know the underlying optical potential and can simply determine the (generally unknown) truly optimal value for λ, λ_{opt} by evaluating the χ^2 of the estimate of the optical potential, $\hat{W}^{-1}$, with respect to the true optical potential on the real axis, W^{-1},

$$\chi^2_t(\lambda) = \sum_{k=1}^{m} \frac{\left|\hat{W}^{-1}(\text{Re}\,E_k) - W^{-1}(\text{Re}\,E_k)\right|^2}{\sigma^2}\,. \tag{2.22}$$

Note that the quantity $\chi^2_t(\lambda)$ (implicitly) depends on λ, because the quantity $\hat{W}^{-1}(\text{Re}\,E_k)$ was determined at a fixed value of λ. The quantity χ^2_t is shown with the blue filled circles in figure 4 (right panel). Its minimum at $\lambda = \lambda_{\text{opt}}$ is very close to the minimum of the validation χ^2_V at $\lambda = \hat{\lambda}_{\text{opt}}$, demonstrating that cross validation [51] is indeed capable of estimating the optimal penalty in our case.

Instead of using the penalty function P_2, one can also choose P_1, see eqs. (2.20) and (2.21). The estimated $\hat{\lambda}_{\text{opt}}$ given by the minimum of χ^2_V will, of course, change. But, again, it was checked that the new $\hat{\lambda}_{\text{opt}}$ is very close to the new λ_{opt} given by the minimum of χ^2_t. Similarly, we have checked other forms of penalization, with the same findings: imposing penalty on the third derivative, variation of the value of ε for the training set, and variation of the value of ε for the test/validation set. The only restriction is that the ε of the test/validation set has to be chosen sufficiently larger than ε of the training set for a minimum in χ^2_V to emerge — if the two ε's are too similar, the oscillations are too similar and no minimum in χ^2_V is obtained. Also, n_{max} has to be chosen high enough so that, at a given ε for the training set, the fit is capable of fitting oscillations (for small λ) which is a prerequisite for a minimum in χ^2_V to appear. In all simulations we have chosen $n_{\text{max}} = 18$ although $n_{\text{max}} \sim 7$ would suffice as the left panel of figure 4 shows.

For the initially considered case, using P_2 for the penalty, $\varepsilon = 0.05\,\text{GeV}$ for the training set, and $\varepsilon = 0.15\,\text{GeV}$ for the test/validation set, the resulting optical potential is shown in figure 5 with the thick black solid lines. For comparison, the true optical potential is shown with the thick red (dashed) lines. The optical potential is well reconstructed over the entire energy range. At the $\pi\eta$ threshold, the reconstructed potential reproduces the square-root behavior due to the explicit factor $p_{\pi\eta}$ in the parameterization (2.18). The reconstructed

JHEP06(2016)043

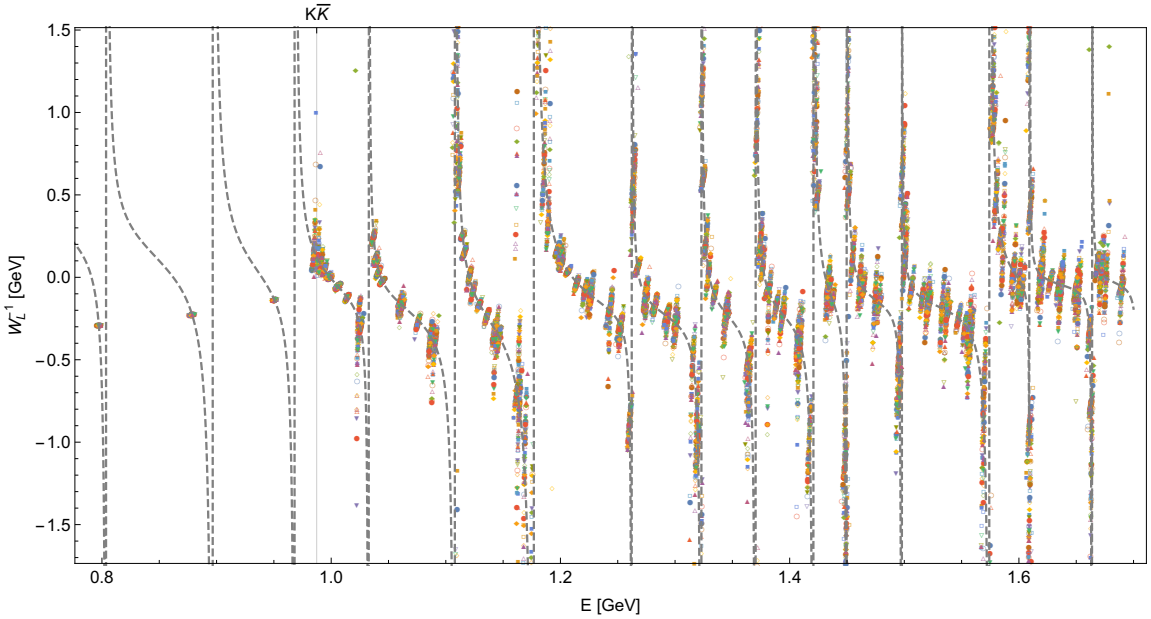

Figure 6. Subset (75 sets) of the re-sampled lattice data, where each type of marker symbols shows the set of 189 energy eigenvalues, randomly distributed with $\Delta E = 1\,\text{MeV}$ around the central energy eigenvalues, extracted from eq. (2.15) imposing twisted boundary condition. The gray dashed line shows the actual amplitude $W_L^{-1}(E)$ to guide the eye.

potential explicitly fulfills Schwartz's reflection principle and its imaginary part is zero below threshold. At the highest energies, small oscillations become visible originating from the upper limit of the fitted region at $E_{\text{max}} = 1.7\,\text{GeV}$. Here, the smoothing algorithm, that is an averaging in energy, has simply no information on $\hat{W}_L^{-1}$ beyond E_{max}. Note that in the numerical simulation of the next section, that uses re-sampling techniques and realistic error bars, these small oscillations themselves average out over the Monte-Carlo ensemble, simply resulting in a widened, but smooth, error band at the highest energies.

For illustration, we also show in figure 5 a largely under-constrained result (too small λ, thin solid lines) in which the oscillations from the finite-volume poles in $\hat{W}_L^{-1}$ survive. The opposite case, i.e., an over-constrained fit with too large λ, is shown with the thin dashed lines exhibiting too large of a penalization on the second derivative.

Non-parametric method. The advantage of non-parametric methods lies in its blindness of analytic structures, which, however, also leads to the fact that threshold behavior and Schwartz' reflection principle cannot be implemented easily. As a particular method, we utilize an approach, commonly used in image processing applications. This approach goes under the name of Gaussian smearing. The basic idea of the Gaussian smearing is quite simple: for a given set of uniformly distributed data, any data point is replaced by a linear combination of its neighboring data points (within a given radius r), with individual weights, $w(x)$ given by

$$w(x) \propto e^{-\frac{x^2}{2\sigma_0^2}}\,. \tag{2.23}$$

JHEP06(2016)043

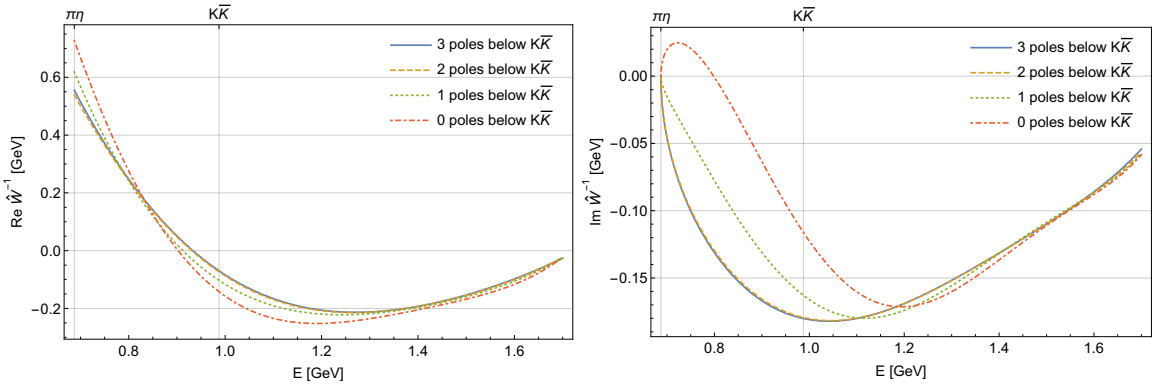

Figure 7. Comparison of different scenarios with respect to the number of poles reconstructed below the primary threshold. The curves were produced by using the parameters of the perfect fit from the section 2, but neglecting a certain number of poles below the $K\bar{K}$ threshold.

Here, x and σ_0 denote the distance of the individual points from the central one and the standard deviation. Typically, the latter value is chosen to match the radius of the smearing by $\sigma_0 = r/2$. Therefore, the only undetermined quantity is given by the smearing radius r.

The general prescription to determine the smearing radius should rely on the properties of the original data only. Recall that the latter is determined by the function $\hat{W}_L^{-1}$ in eq.(2.17), which splits up into a real and an imaginary set, when evaluated at the energy $E + i\varepsilon$ for a fixed $\varepsilon > 0$ and uniformly distributed values of E. Therefore, after the fits to the (synthetic) lattice data are performed, the scale of the structures to be smeared is determined by the distance between two poles, see figure 8. Of course, since the poles are not distributed uniformly over the whole energy range, one could argue in favor of using different values of r for different energies. It is also clear that constraint on the standard deviation $\sigma_0 = r/2$ affects the result of the smoothing. However, in order not to over-complicate the procedure, in the following we choose the smearing radius to be twice as large as the typical (average) distance between two poles. If the radius is much larger than this, physical information (i.e. the functional form of the optical potential) will be smeared out. If, however, the radius is much smaller than this value, then the (unphysical) oscillations will remain, preventing the reconstruction of the underlying optical potential. The situation is in fact very similar to the under- and over-constrained results, discussed in the previous section for the too small and too large values of λ.

After the parameters of the smearing kernel (2.23) are fixed, the method is applied to the sets of real and imaginary parts of $\hat{W}_L^{-1}$ at a fixed $\varepsilon > 0$. Then the procedure is repeated, each time assuming slightly smaller value of ε than before. In the final step, a simple (polynomial) extrapolation is performed to real energies, i.e. $\varepsilon = 0$, to obtain the final result of this procedure, namely $\hat{W}^{-1}(E)$.

In this section, we have demonstrated that the real and imaginary parts of the optical potential can be reconstructed from the pseudophase measured on the lattice for real energies, W_L^{-1}, if the analytic continuation into the complex plane is performed. Two distinct methods are presented to smear the oscillations which emerge from the analytic continuation, and to recover the optical potential for real energies. It remains to be seen,

JHEP06(2016)043

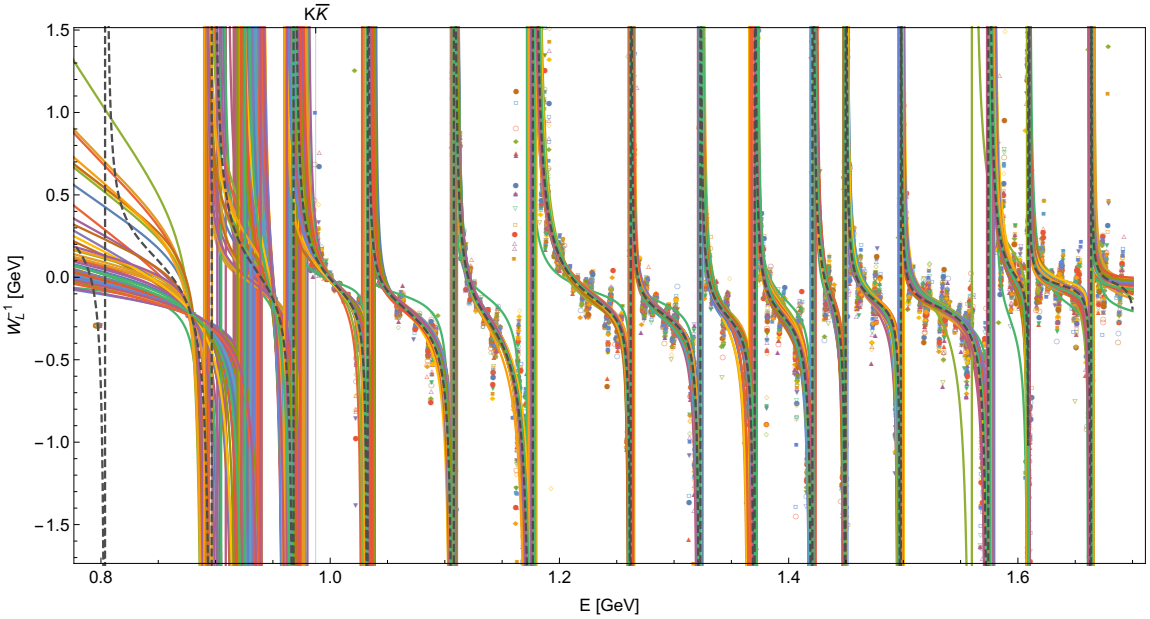

Figure 8. A subset (75 sets) of the fits of eq. (2.15) to the synthetic lattice data as described in the main text. Different curves represent fits to different sets of re-sampled synthetic lattice data corresponding to the notation of figure 6. The gray dashed line shows the actual amplitude $W_L^{-1}(E)$ to guide the eye.

how the pseudophase can be measured in practice. This issue will be considered in the section 3 where a realistic numerical simulation will be carried out as well.

3 Reconstruction of the optical potential

The quantity $W_L^{-1}(E)$, which is used to extract the optical potential, along with the energy E, depends on other external parameters, say, on the box size L, boundary conditions, etc. In the fit to $W_L^{-1}(E)$, the values of these parameters have to be fixed. Otherwise, for example, the position of the poles in $W_L^{-1}(E)$ will be volume-dependent and one does not know, how to perform such a fit. Hence, we are quite restricted in the ability to scan the variable E: the knob, which tunes E, must leave all other parameters in the pseudophase intact.

3.1 Partially twisted boundary conditions

In certain systems, there indeed exists a possibility to scan the energy within a given range in this manner. It is provided by the use of twisted boundary conditions and can be realized, e.g., in the coupled-channel $\pi\eta - K\bar{K}$ scattering. Namely, as was discussed in refs. [3, 32], in this system it is possible to apply (partially) twisted boundary conditions so that, when the twisting angle is changed continuously, the $K\bar{K}$ threshold moves, whereas the $\pi\eta$ threshold stays intact. This can be achieved, for example, by twisting the light u, d quarks by the same angle and leaving the s-quark with periodic boundary conditions. This

JHEP06(2016)043

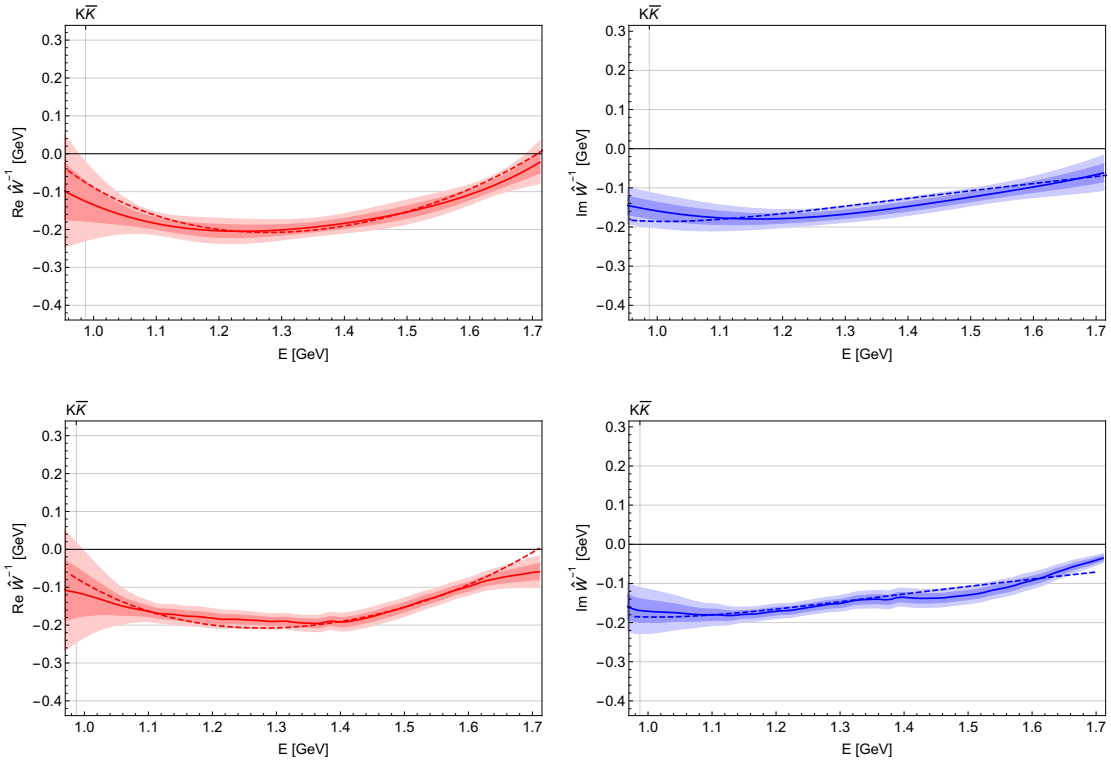

Figure 9. Results of the smearing and extrapolation to real energies using parametric method (top) and Gaussian smearing (bottom). The full lines show the average of the re-sampling of all sets, whereas the darker (lighter) bands show the corresponding 1 (2) σ error bands. The exact infinite volume solution is shown by the dashed lines for comparison.

will lead to the modification of the secular equation (2.14), replacing $Z_{00}(1;q^2_{K\bar{K}})$ by

$$Z^{\theta}_{00}(1;q^2_{K\bar{K}}) = \frac{1}{\sqrt{4\pi}} \sum_{\mathbf{n}\in\mathbb{Z}^3} \frac{1}{(\mathbf{n}+\boldsymbol{\theta}/2\pi)^2 - q^2_{K\bar{K}}}\,. \tag{3.1}$$

The expression for $W_L^{-1}(E)$ remains the same and does not contain the twisting angle $\boldsymbol{\theta}$.

The method can be used to study the isospin $I = 1$ scattering in the $\pi\eta - K\bar{K}$ system. As shown in ref. [32], despite the presence of the annihilation diagrams, the partial twisting in this case is equivalent to the full twisting, if the light quarks are twisted, whereas twisting of the s-quark does not lead to an observable effect. As a rule of thumb, one expects that the partial twisting of a given quark will be equivalent to full twisting, only if this quark line goes through the diagram without being annihilated (of course, a rigorous proof of this statement should follow by using effective field theory methods [32]). In our case, we could choose to work with the state with maximal projection of the isospin, say $I = 1, I_3 = 1$. This state contains one u-quark and one $\bar{d}$-quark, which cannot be annihilated. Choosing the same twisting angle for both quarks, the system stays in the center-of-mass frame and the pseudophase becomes independent from the twisting angle, as required. From the above

JHEP06(2016)043

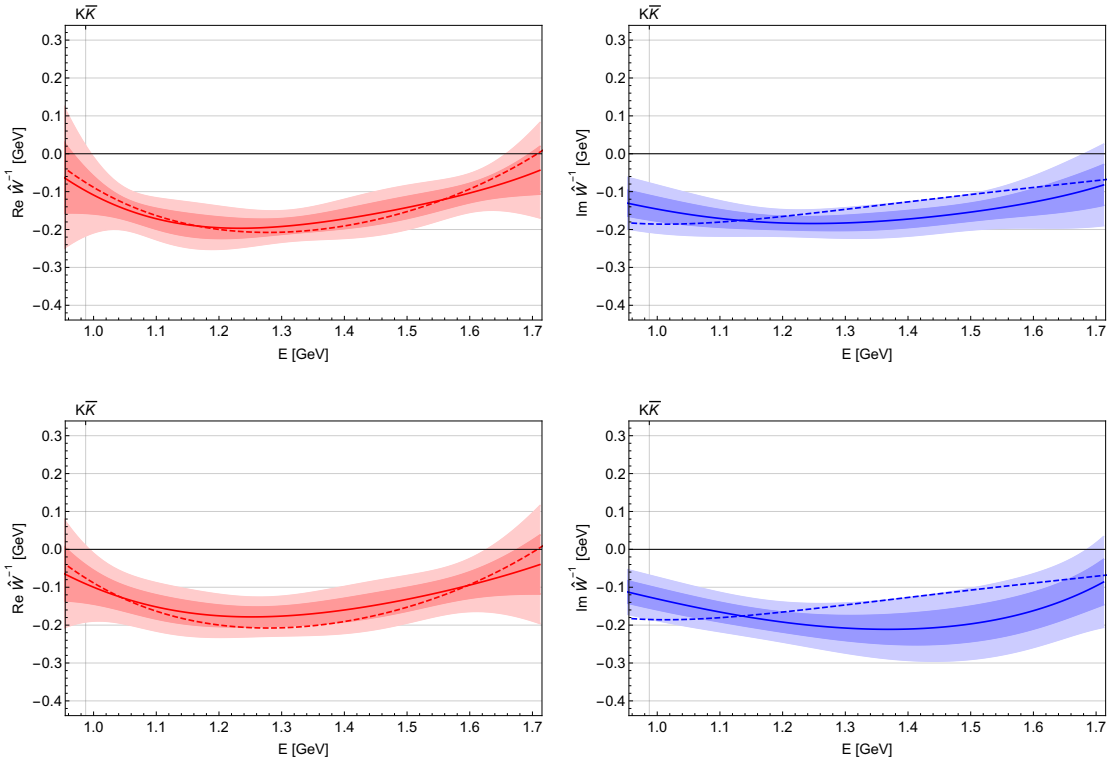

Figure 10. Results of the smearing and extrapolation to real energies using parametric method for synthetic lattice data with $\Delta E = 2\,\mathrm{MeV}$ (top) and $\Delta E = 3\,\mathrm{MeV}$ (bottom). The full lines show the average of the re-sampling of all sets, whereas the darker (lighter) bands show the corresponding 1 (2) σ error bands. The exact infinite volume solution is shown by the dashed lines for comparison.

discussion it is also clear that using our method for the extraction of the optical potential in the channel with isospin $I = 0$ implies the use of full twisting instead of partial twisting.

The same trick can be used to study the $Z_c(3900)$ and $Z_c(4025)$ states, which both have isospin $I = 1$. Twisting u- and d-quarks by the same angle, the D- and D^*-mesons will get additional momenta proportional to the twisting angle, whereas the J/ψ, h_c and π-mesons will not. Consequently, one may choose the channels containing the D and D^* mesons as the primary ones (in our nomenclature) and regard every other channel as secondary. For this choice, the pseudophase will not depend on the twisting angle.

Last but not least, an unconventional twisting procedure was used in the study of the $J/\psi\phi$ scattering from $Y(4140)$ decays [54]. Namely, in that work the c- and s-quarks were twisted by the angles $\boldsymbol{\theta}$ and $-\boldsymbol{\theta}$, respectively, whereas their Hermitean conjugates $\bar{c}$, $\bar{s}$ were subject to periodic boundary conditions. Albeit in the particular case of $J/\psi\phi$ scattering the twisting cannot be used for the extraction of the optical potential, one could not exclude a possibility that this kind of twisting could be applied in other systems for this purpose. For this reason, we consider in detail this case of (unconventional) twisting in appendix B.

JHEP06(2016)043

3.2 Analysis of synthetic data

In the following, we shall reconstruct the optical potential from a synthetic lattice data set generated by the chiral unitary approach of ref. [44]. Twisted boundary conditions are applied as described above, and the box size is taken to be $L = 5M_\pi^{-1}$. In the first stage of our analysis we have observed that more than 100 energy eigenvalues are required[4] to extract the potential in the considered, and quite wide, energy range from $E = 2M_K$ to $E = 1.7\,\mathrm{GeV}$. To produce the synthetic data, we consider the following set of six different twisting angles

$$\boldsymbol{\theta} = \begin{pmatrix}0\\0\\0\end{pmatrix}, \begin{pmatrix}0\\0\\\pi\end{pmatrix}, \begin{pmatrix}0\\\pi\\\pi\end{pmatrix}, \begin{pmatrix}\pi\\\pi\\\pi\end{pmatrix}, \begin{pmatrix}0\\0\\\pi/2\end{pmatrix}, \begin{pmatrix}0\\\pi/2\\\pi/2\end{pmatrix}. \tag{3.2}$$

For these values, $Z_{00}^{\theta}(1;q_{K\bar{K}}^2)$ has the smallest number of poles. This requirement is important, when the energy eigenvalues are measured with a finite accuracy. Then, in proximity of its poles, the function $Z_{00}^{\theta}(1;q_{K\bar{K}}^2)$ will exhibit a very large uncertainty. Solving eq. (2.14) with $Z_{00}(1;q_{K\bar{K}}^2)$ replaced by $Z_{00}^{\theta}(1;q_{K\bar{K}}^2)$ for each of the aforementioned angles we were able to extract 186 energy eigenvalues above and 3 below the $K\bar{K}$ threshold. Further, in any realistic lattice simulation, the eigenvalues will be known only up to a finite precision. To check the feasibility of the proposed method, it is important to account for this error, ΔE, and to see how this uncertainty[5] is reflected in the final result as studied with re-sampling techniques in the following. Therefore, we start from a sufficiently large number (~ 1000) of re-sampled lattice data sets, normally distributed around the (189) synthetic eigenvalues with a standard deviation of ΔE. An example of 75 synthetic lattice data sets with $\Delta E = 1\,\mathrm{MeV}$ is presented in figure 6.

In the next step, we determine the parameters of eq. (2.17) for each of these sets. Prior to doing so, we have to clarify several questions:

- **Range of applicability.** Below the $K\bar{K}$ threshold, the function $Z_{00}^{\theta}(1;q_{K\bar{K}}^2)$ does not depend on $\boldsymbol{\theta}$ up to exponentially suppressed contributions. Therefore, only a limited number of energy eigenvalues can be determined. A reliable extraction of positions and residua of all four lowest poles is not possible because the twisting cannot generate the necessary scan of W_L^{-1} in this energy region. This means that, on the one hand, this approach does not allow one to extract the optical potential below the primary ($K\bar{K}$) threshold. On the other hand, it is crucial to recall that, due to smearing applied in the complex energy plane, this failure will yield the wrong real and especially imaginary parts of the reconstructed $\hat{W}^{-1}(E)$. This is demonstrated in figure 7, which was produced by using the test parameters of the perfect fit from the last section, but neglecting a certain number of poles below the $K\bar{K}$ threshold. It is seen that the imaginary part of $\hat{W}^{-1}$ at the primary threshold deviates by about

[4] Note that this is a total number that includes all measurements at different values of the twist angle. The number of the measured energy levels, of course, is much less, see figure 8.

[5] Since higher excited levels are harder to measure, the uncertainty will presumably increase with the energy. However, in this first study we will assume constant values for ΔE.

JHEP06(2016)043

50%, if no poles are considered below this threshold. However, already the inclusion of the first pole below the primary threshold improves the description drastically. Therefore, all poles above as well as the one below the primary threshold should be considered in the fit to the (synthetic) lattice data. Note also that if the secondary channels open above the primary channel, none of these complications arise.

- **Number of poles — starting values.** We found that, for sufficiently many eigenvalues and ΔE of the order of several MeV, the number of poles above the primary threshold to be fitted can be determined, searching for a rapid sign change of $Z_{00}^{\theta}(1; q_{K\bar{K}}^2)$. The corresponding energy eigenvalues serve us as limits on the pole positions, while the residua are allowed to vary freely.

- **Highest order of the polynomial part.** In principle, the order of the polynomial part of eq. (2.17) is not restricted a priori. We have tested explicitly that adding terms of fourth or fifth order in energy to the fit function yields only a small change of the reconstructed potential. This part may be further formalized by conducting combined χ^2- and F-tests on the χ^2 defined below.

- **Definition of $\boldsymbol{\chi^2}$.** The uncertainty of the (synthetic) lattice data is given by ΔE only. Therefore, a proper definition of $\chi^2_{\text{d.o.f.}}$ should account for the difference between the measured $\{E_i | i = 1, \ldots, N\}$ and fitted eigenvalues $\{E_i^f | i = 1, \ldots, N\}$ compared to ΔE for all N data points. The E_i^f eigenvalues are defined as the solutions of the following equation

$$\frac{2}{\sqrt{\pi} L} Z_{00}^{\theta}(1; q_{K\bar{K}}^2(E)) = \sum_j \frac{Z_j}{E - Y_j} + D_0 + D_1 E + D_2 E^2 + D_3 E^3 \,, \tag{3.3}$$

  which is technically very intricate. The problem of finding such solutions can be circumvented by expanding both sides of the latter equation in powers of $(E_i^f - E_i)$ around E_i for each $i = 1, \ldots, N$. Up to next-to-leading order in this expansion, the correct quantity to minimize reads

$$\chi^2_{\text{d.o.f.}} = \frac{1}{N - n} \sum_{i=1}^{N} \frac{1}{\Delta E^2} \left(\frac{\hat{W}_L^{-1}(E) - Z_{00}^{\theta_i}(1; q_{K\bar{K}}^2(E))}{\left(Z_{00}^{\theta_i}(1; q_{K\bar{K}}^2(E)\right)' - \left(\hat{W}_L^{-1}(E)\right)'} \right)^2_{E=E_i} \,, \tag{3.4}$$

  where n is the number of free parameters and $\boldsymbol{\theta}_i$ is the twisting angle corresponding to the energy eigenvalue E_i. Note that the χ^2 in eq. (3.4) differs from the usual definition by a correction factor in the denominator, given by the difference of the derivatives of the Lüscher and the fit function.

For every member of the data sets, each consisting of 188 energy eigenvalues (186 above and 2 below threshold), we perform a fit, minimizing $\chi^2_{\text{d.o.f.}}$ given in eq. (3.4). Note that the two closest energy eigenvalues below the $K\bar{K}$ threshold, which are included in the fit, are assigned a weight factor of 6, because they are measured at every value of $\boldsymbol{\theta}$ of eq. (3.2) and do not depend on its value up to exponentially suppressed contributions. Further, the

JHEP06(2016)043

number of free parameters n is set to 32, consisting of 13(1) pole positions and 13(1) residua above(below) $K\bar{K}$ threshold, as well as 4 parameters in the polynomial part. The minimization is performed by using the Minuit2 (5.34.14) library from ref. [55]. A representative subset (75 synthetic lattice data sets) of the results of the fits is shown in figure 8. It is seen that the data are described fairly well by all fits in a large energy region starting above the $K\bar{K}$ threshold. At and below this threshold, there is much larger spread of the fit curves describing the data. Especially the pole at $\sim 0.9\,\text{GeV}$ is not fixed very precisely which is quite natural, keeping in mind the small number of synthetic data points in this energy region.

For each of the above fits we proceed as described in section 2. First, the function $\hat{W}_L^{-1}(E)$ is evaluated at the complex energies. Second, using the Gaussian smearing as well as the parametric method discussed in section 2.3, the real and imaginary parts of the potential are smoothened. The penalty factor $\lambda = 0.28$ (see appendix A) and the smearing radius $r = 0.2\,\text{GeV}$ are used in these methods, respectively. Finally, for every energy, we calculate the average and the standard deviation σ. The result of this procedure is presented in figure 9. It is seen that both smearing methods yield very similar results. Overall, the exact solution (the dashed line) in the considered energy region lies within 1 or 2 sigma bands around the reconstructed potential. The error band appears to be comfortably narrow, but becomes broader around the $K\bar{K}$ threshold and $E_{\text{max}} = 1.7\,\text{GeV}$. This effect is a natural consequence of the missing information outside the energy region, which influences the prediction within the energy region via smearing during the intermediate steps of the potential reconstruction.

Furthermore, we have repeated the whole procedure of synthetic lattice data generation, fitting and recovering of the optical potential for higher uncertainty of the energy eigenvalues, $\Delta E = 2\,\text{MeV}$ and $\Delta E = 3\,\text{MeV}$. The results are presented in figure 10 and show that the error bars grow roughly linearly with ΔE and that the real part of the reconstructed amplitude remains quite stable. The imaginary part is more sensitive to the value of ΔE. Further, at even higher values of $\Delta E \sim 10\,\text{MeV}$, the fit is not reliable anymore and the imaginary part becomes very small.

4 Conclusions

i) In the present paper, we formulate a framework for the extraction of the complex-valued optical potential, which describes hadron-hadron scattering in the presence of the inelastic channels, from the energy spectrum of lattice QCD. An optical potential, defined in the present article, is obtained by using causal prescription $E \to E + i\varepsilon$ for the continuation into the complex energy plane. It converges to the "true" optical potential in the limit $L \to \infty$, $\varepsilon \to 0$. A demonstration of the effectiveness of the method has been carried out by utilizing synthetic data.

ii) The approach requires the precise measurement of the whole tower of the energy levels in a given interval. The optical potential is then obtained through averaging over all these levels.

JHEP06(2016)043

iii) Moreover, the availability of this approach critically depends on our ability to take the lattice data at neighboring energies without changing the interaction parameters in the secondary channels. This can be achieved, e.g., by using (partially) twisted boundary conditions that affects the primary channel only. In the paper, we consider several systems, where the method can be applied. It is remarkable that some candidates for the QCD exotica are also among these systems.

We would like to emphasize that the use of twisted boundary conditions is only a tool, which is used to perform a continuous energy scan of a certain interval. Whatever method is used to measure the dependence of the pseudophase on energy (all other parameters fixed), our approach, based on the analytic continuation into the complex plane, could be immediately applied.

iv) The approach could be most useful to analyze systems, in which the inelastic channels contain three or more particles. Whereas direct methods based on the use of multi-particle scattering equations in a finite volume will be necessarily cumbersome and hard to use, nothing changes, if our approach is applied. The reason for this is that, in case of an intermediate state with any number of particles, the single poles are the only singularities in any Green's function in a finite volume.

Acknowledgments

We would like to thank S. Aoki, G. Schierholz and C. Urbach for helpful discussions. Financial support by the Deutsche Forschungsgemeinschaft (CRC 110, "Symmetries and the Emergence of Structure in QCD"), the Volkswagenstiftung under contract no. 86260, the National Science Foundation (CAREER grant No. 1452055, PIF grant No. 1415459), GWU (startup grant), The Chinese Academy of Sciences (CAS) President's International Fellowship Initiative (PIFI) (Grant No. 2015VMA076), and by the Bonn-Cologne Graduate School of Physics and Astronomy is gratefully acknowledged.

A Penalty factor for a realistic set of the synthetic data

In section 2.3, where the parametric method for the smearing was introduced, we assumed that the quantity W_L^{-1} can be measured with no uncertainties and at all energies from $E_{\min} = M_\pi + M_\eta$ to $E_{\max} = 1.7\,\text{GeV}$. We now turn to a more realistic case, studied in the numerical simulation in section 3. For this, the search for $\hat{\lambda}_{\text{opt}}$ is adapted to the interval from $E_{\min} = 2M_K$ to $E_{\max} = 1.7\,\text{GeV}$, using several $\hat{W}_L^{-1}$'s from the Monte-Carlo ensemble (see description there). Figure 11 shows the χ^2 behavior for the training set, the test/validation set χ^2_V, and the true χ^2_t for one arbitrarily chosen fit of the Monte-Carlo ensemble of different $\hat{W}_L^{-1}$'s. Both variants of the penalty, P_1 and P_2 from eqs. (2.20), (2.21), are shown in the left and right panels, respectively.

As figure 11 shows, the minima of χ^2_V (red triangles) are even more pronounced than in the previously discussed, idealized case, leading to $\hat{\lambda}_{\text{opt}} = 0.34$ for P_1 and $\hat{\lambda}_{\text{opt}} = 0.28$ for P_2 (minima of the curves shown with red triangles). The minima of the χ^2_t occur almost at the

JHEP06(2016)043

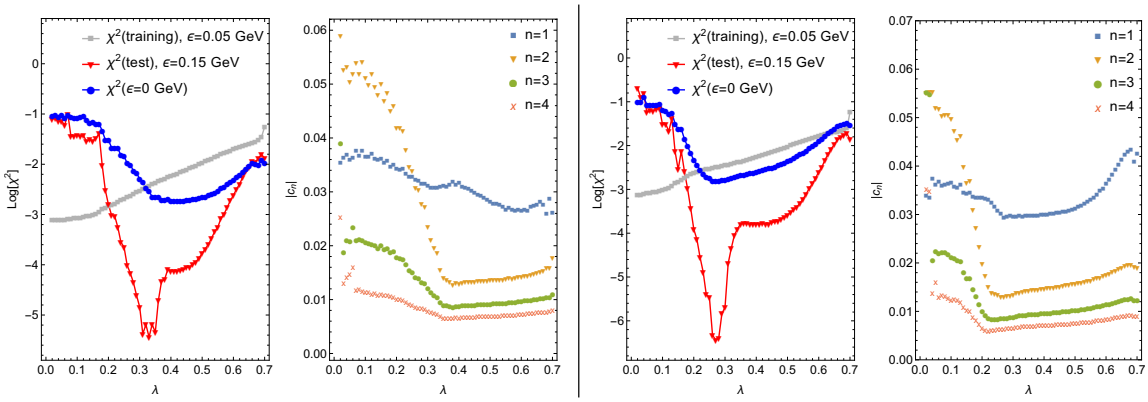

Figure 11. Determination of $\hat{\lambda}_{\text{opt}}$ for a realistic numerical simulation. Notation as in figure 4. Left two graphs: using the penalization P_1 of eq. (2.20). Right two graphs: using the penalization P_2 of eq. (2.21). For each case, the χ^2 (training set), χ^2_V (test/validation set) and χ^2_t (true χ^2) are displayed. Additionally, the moduli of the Fourier coefficients $|c_n|$, $n = 1, \ldots, 4$ are shown for each case. For further explanations, see text.

same respective values of λ (blue filled circles) which again demonstrates the applicability of the method. For both penalties, we also show the moduli of the Fourier coefficients $|c_n|$, $n = 1, \ldots, 4$ in the respective right panels, where

$$c_n(\lambda) = \frac{1}{E_{\text{max}} - E_{\text{min}}} \int_{E_{\text{min}}}^{E_{\text{max}}} dE\, \hat{W}^{-1}(E)\; e^{-i\,\frac{2\pi n E}{E_{\text{max}} - E_{\text{min}}}}\,. \tag{A.1}$$

Here, the infinite-volume quantity $\hat{W}^{-1}(E)$ implicitly depends on λ. These coefficients indicate the weight of the available frequencies to built up the optical potential over a finite energy range. As long as the potential is smooth, we expect the lowest $|c_n|$ to dominate. For decreasing values of λ, eventually a point is reached at which the oscillations will become noticeable and coefficients $|c_n|$ with larger n will become more relevant. Indeed, the figure shows that, close to the respective $\hat{\lambda}_{\text{opt}}$'s, the coefficients $|c_2|$ to $|c_4|$ exhibit a very pronounced rise. In all simulations, which were carried out, we have observed this behavior. This suggests that the λ-dependence of the Fourier coefficients can be used as a tool to cross-check the results from cross validation.

As a final remark, the value of $\hat{\lambda}_{\text{opt}}$ itself carries uncertainty that can be estimated by k-fold cross validation [51, 52]. Using this uncertainty, the simplest model is in principle obtained by the 1-σ rule, i.e., the maximal λ compatible with the uncertainty of $\hat{\lambda}_{\text{opt}}$ [51, 52]. For the numerical simulations, we simply choose one value of $\hat{\lambda}_{\text{opt}} = 0.28$ for the penalty P_2, because uncertainties are dominated by the statistics of the lattice measurements. As mentioned above, the value $\hat{\lambda}_{\text{opt}} = 0.28$ corresponds to one randomly chosen fit from the Monte-Carlo ensemble, but we have made sure that this value is representative.

JHEP06(2016)043

B Partial twisting

In this section, we would like to examine in detail the unconventional twisting prescription, which was introduced in ref. [54], in the context of studying $J/\psi\phi$ scattering from $Y(4140)$ decays. We remind the reader that, within this prescription, only quark fields are twisted, whereas the antiquark fields are subject to the periodic boundary conditions. One could ask whether such a prescription is rigorously justified.

We address this problem by using the same methods as in ref. [32]. In order to simplify things, we restrict ourselves to the case of elastic $J/\psi\phi$ scattering and neglect the coupling to the inelastic channels. In order to treat the partial twisting, we introduce valence (v), sea (s) and ghost (g) quarks for each quark flavor, subject to twisting. Only valence and ghost quarks are twisted, whereas the sea quarks are not. In total, 9 different $J/\psi\phi$ states are possible

$$\begin{array}{lll} 1)\ (c_{\mathsf{v}}\bar{c}_{\mathsf{v}})\,(s_{\mathsf{v}}\bar{s}_{\mathsf{v}}) & 2)\ (c_{\mathsf{v}}\bar{c}_{\mathsf{v}})\,(s_{\mathsf{s}}\bar{s}_{\mathsf{s}}) & 3)\ (c_{\mathsf{v}}\bar{c}_{\mathsf{v}})\,(s_{\mathsf{g}}\bar{s}_{\mathsf{g}}) \\ 4)\ (c_{\mathsf{s}}\bar{c}_{\mathsf{s}})\,(s_{\mathsf{v}}\bar{s}_{\mathsf{v}}) & 5)\ (c_{\mathsf{s}}\bar{c}_{\mathsf{s}})\,(s_{\mathsf{s}}\bar{s}_{\mathsf{s}}) & 6)\ (c_{\mathsf{s}}\bar{c}_{\mathsf{s}})\,(s_{\mathsf{g}}\bar{s}_{\mathsf{g}}) \\ 7)\ (c_{\mathsf{g}}\bar{c}_{\mathsf{g}})\,(s_{\mathsf{v}}\bar{s}_{\mathsf{v}}) & 8)\ (c_{\mathsf{g}}\bar{c}_{\mathsf{g}})\,(s_{\mathsf{s}}\bar{s}_{\mathsf{s}}) & 9)\ (c_{\mathsf{g}}\bar{c}_{\mathsf{g}})\,(s_{\mathsf{g}}\bar{s}_{\mathsf{g}})\ . \end{array} \tag{B.1}$$

The free Green's function is given by a a diagonal 9×9 matrix. Taking into account the sign convention for the mesons containing ghost quarks, this matrix can be written in the following form

$$G = \mathrm{diag}\,(G^{\theta}, G^{+}, -G^{\theta}, G^{-}, G^{0}, -G^{-}, -G^{\theta}, -G^{+}, G^{\theta})\,. \tag{B.2}$$

Here,

$$\begin{aligned} G^{\theta}(\mathbf{p}_1,\mathbf{p}_2) &= \frac{1}{2w_{J/\psi}(\mathbf{p}_1+\mathbf{p}_\theta)2w_{\phi}(\mathbf{p}_2-\mathbf{p}_\theta)}\,\frac{1}{w_{J/\psi}(\mathbf{p}_1+\mathbf{p}_\theta)+w_{\phi}(\mathbf{p}_2-\mathbf{p}_\theta)-E}\,, \\ G^{+}(\mathbf{p}_1,\mathbf{p}_2) &= \frac{1}{2w_{J/\psi}(\mathbf{p}_1+\mathbf{p}_\theta)2w_{\phi}(\mathbf{p}_2)}\,\frac{1}{w_{J/\psi}(\mathbf{p}_1+\mathbf{p}_\theta)+w_{\phi}(\mathbf{p}_2)-E}\,, \\ G^{-}(\mathbf{p}_1,\mathbf{p}_2) &= \frac{1}{2w_{J/\psi}(\mathbf{p}_1)2w_{\phi}(\mathbf{p}_2-\mathbf{p}_\theta)}\,\frac{1}{w_{J/\psi}(\mathbf{p}_1)+w_{\phi}(\mathbf{p}_2-\mathbf{p}_\theta)-E}\,, \\ G^{0}(\mathbf{p}_1,\mathbf{p}_2) &= \frac{1}{2w_{J/\psi}(\mathbf{p}_1)2w_{\phi}(\mathbf{p}_2)}\,\frac{1}{w_{J/\psi}(\mathbf{p}_1)+w_{\phi}(\mathbf{p}_2)-E}, \end{aligned} \tag{B.3}$$

where $\mathbf{p}_\theta = \boldsymbol{\theta}/L$ and $\mathbf{p}_i = 2\pi/L\,\mathbf{n}_i\,,\ \mathbf{n}_i\in\mathbb{Z}^3\,,\ i=1,2.$

The matrix elements that describe the transition of a state i to state j, $i,j=1,\ldots,9$

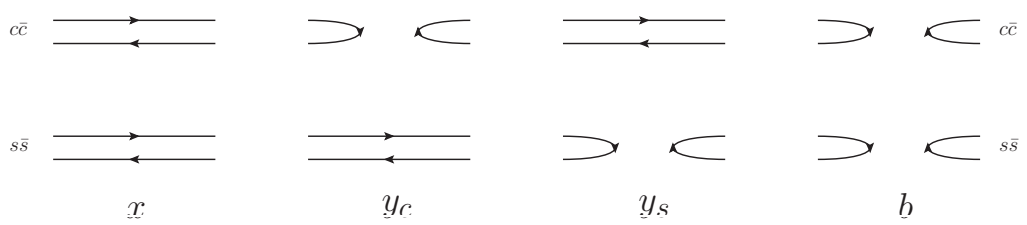

Figure 12. The fully connected piece (x), the partially connected pieces (y_c and y_s) and the fully disconnected piece (b) of the $J/\psi\phi$ scattering amplitude.

are given by

$$T = \begin{pmatrix} a & s & s & c & b & b & c & b & b \\ s & a & s & b & c & b & b & c & b \\ s & s & -a+2s & b & b & -c+2b & b & b & -c+2b \\ c & b & b & a & s & s & c & b & b \\ b & c & b & s & a & s & b & c & b \\ b & b & -c+2b & s & s & -a+2s & b & b & -c+2b \\ c & b & b & c & b & b & -a+2c & -s+2b & -s+2b \\ b & c & b & b & c & b & -s+2b & -a+2c & -s+2b \\ b & b & -c+2b & b & b & -c+2b & -s+2b & -s+2b & a-2c-2s+4b \end{pmatrix}, \tag{B.4}$$

where

$$a = x + y_c + y_s + b\,, \qquad s = y_s + b\,, \qquad c = y_c + b\,. \tag{B.5}$$

The quantities x, y_c, y_s, b denote the fully connected, partially connected and fully disconnected contributions, see figure 12. It is straightforward to verify that the potential matrix V in the infinite volume has exactly the same symmetries as the scattering matrix and is also given by eq. (B.4) with the replacement $a, b, c, s \to \tilde{a}, \tilde{b}, \tilde{c}, \tilde{s}$.

The Lüscher equation is given by

$$\begin{aligned} \det(1 - VG) &= \ell_1^4 \ell_2^2 \ell_3^2 \ell_4 = 0\,, \\ \ell_1 &= 1 - \langle G^\theta \rangle (\tilde{a} + \tilde{b} - \tilde{c} - \tilde{s})\,, \\ \ell_2 &= 1 - \langle G^- \rangle (\tilde{a} - \tilde{s})\,, \\ \ell_3 &= 1 - \langle G^+ \rangle (\tilde{a} - \tilde{c})\,, \\ \ell_4 &= 1 - \langle G^0 \rangle \tilde{a}\,, \end{aligned} \tag{B.6}$$

where

$$\langle G^\theta \rangle = \frac{1}{L^3} \sum_{\mathbf{p}} G^\theta(\mathbf{p}, -\mathbf{p})\,, \qquad \langle G^0 \rangle = \frac{1}{L^3} \sum_{\mathbf{p}} G^0(\mathbf{p}, -\mathbf{p}) \tag{B.7}$$

and $\langle G^\pm \rangle = 0$ due to the conservation of the total momentum, if $\boldsymbol{\theta}$ is not equal to a multiple of 2π.

JHEP06(2016)043

As seen from eq. (B.6), the finite-volume scattering matrix at $\boldsymbol{\theta} \neq \mathbf{0}$ contains two towers of poles, determined by the equations $\ell_1 = 0$ and $\ell_4 = 0$, respectively, where the former depends on the parameter $\boldsymbol{\theta}$ and the latter does not. The explicit expression of the scattering matrix element in the valence sector is given by

$$\begin{aligned}\big(V(1-GV)^{-1}\big)_{\mathsf{vv},\mathsf{vv}} = &\frac{\tilde{a}+\tilde{b}-\tilde{s}-\tilde{c}}{\ell_1} + \frac{\tilde{b}^2}{\tilde{a}}\,\frac{1}{\ell_1^2\ell_4} + \frac{2(\tilde{b}-\tilde{c})(\tilde{b}-\tilde{s})}{\tilde{a}+\tilde{b}-\tilde{c}-\tilde{s}}\,\frac{1}{\ell_1^3} \\ &+\frac{-\tilde{b}^3+(\tilde{c}+\tilde{s})\tilde{b}^2-\tilde{a}^2\tilde{b}+\tilde{a}^2(\tilde{c}+\tilde{s})-\tilde{a}(\tilde{c}^2+\tilde{s}^2)-4\tilde{a}(\tilde{b}-\tilde{c})(\tilde{b}-\tilde{s})}{\tilde{a}(\tilde{a}+\tilde{b}-\tilde{c}-\tilde{s})}\,\frac{1}{\ell_1^2}\,.\end{aligned} \tag{B.8}$$

It is also clear that the $\boldsymbol{\theta}$-dependent singularities are determined by the fully connected part of the scattering amplitude, whereas the $\boldsymbol{\theta}$-independent part contains the full amplitude. Consequently, the approach of ref. [54] can be safely used if and only if the contribution of the disconnected diagrams is much smaller than the connected one (in fact, this was mentioned already in ref. [54]). In this case, i.e., when $\tilde{b} = \tilde{c} = \tilde{s} = 0$, the double and triple poles in eq. (B.8) vanish and one arrives at the expression that was expected from the beginning

$$\big(V(1-GV)^{-1}\big)_{\mathsf{vv},\mathsf{vv}} = \frac{\tilde{a}}{1-\langle G^\theta\rangle\tilde{a}}\,. \tag{B.9}$$

For the particular problem, considered here, one expects that the disconnected contributions will be strongly suppressed, according to the OZI rule. Consequently, the justification of the method, proposed in ref. [54], heavily rests on the effectiveness of the OZI suppression.

References

[1] M. Lüscher, *Two particle states on a torus and their relation to the scattering matrix*, *Nucl. Phys.* **B 354** (1991) 531 [INSPIRE].

[2] M. Lage, U.-G. Meißner and A. Rusetsky, *A method to measure the antikaon-nucleon scattering length in lattice QCD*, *Phys. Lett.* **B 681** (2009) 439 [arXiv:0905.0069] [INSPIRE].

[3] V. Bernard, M. Lage, U.-G. Meißner and A. Rusetsky, *Scalar mesons in a finite volume*, *JHEP* **01** (2011) 019 [arXiv:1010.6018] [INSPIRE].

[4] S. He, X. Feng and C. Liu, *Two particle states and the S-matrix elements in multi-channel scattering*, *JHEP* **07** (2005) 011 [hep-lat/0504019] [INSPIRE].

[5] C. Liu, X. Feng and S. He, *Two particle states in a box and the S-matrix in multi-channel scattering*, *Int. J. Mod. Phys.* **A 21** (2006) 847 [hep-lat/0508022] [INSPIRE].

[6] M.T. Hansen and S.R. Sharpe, *Multiple-channel generalization of Lellouch-Lüscher formula*, *Phys. Rev.* **D 86** (2012) 016007 [arXiv:1204.0826] [INSPIRE].

[7] R.A. Briceno and Z. Davoudi, *Moving multichannel systems in a finite volume with application to proton-proton fusion*, *Phys. Rev.* **D 88** (2013) 094507 [arXiv:1204.1110] [INSPIRE].

JHEP06(2016)043

[8] N. Li and C. Liu, *Generalized Lüscher formula in multichannel baryon-meson scattering*, *Phys. Rev.* **D 87** (2013) 014502 [arXiv:1209.2201] [INSPIRE].

[9] P. Guo, J. Dudek, R. Edwards and A.P. Szczepaniak, *Coupled-channel scattering on a torus*, *Phys. Rev.* **D 88** (2013) 014501 [arXiv:1211.0929] [INSPIRE].

[10] HADRON SPECTRUM collaboration, J.J. Dudek, R.G. Edwards, C.E. Thomas and D.J. Wilson, *Resonances in coupled πK-ηK scattering from quantum chromodynamics*, *Phys. Rev. Lett.* **113** (2014) 182001 [arXiv:1406.4158] [INSPIRE].

[11] D.J. Wilson, J.J. Dudek, R.G. Edwards and C.E. Thomas, *Resonances in coupled πK, ηK scattering from lattice QCD*, *Phys. Rev.* **D 91** (2015) 054008 [arXiv:1411.2004] [INSPIRE].

[12] HADRON SPECTRUM collaboration, J.J. Dudek, R.G. Edwards and D.J. Wilson, *An a_0 resonance in strongly coupled $\pi\eta$, $K\overline{K}$ scattering from lattice QCD*, *Phys. Rev.* **D 93** (2016) 094506 [arXiv:1602.05122] [INSPIRE].

[13] M. Döring, U.-G. Meißner, E. Oset and A. Rusetsky, *Unitarized chiral perturbation theory in a finite volume: scalar meson sector*, *Eur. Phys. J.* **A 47** (2011) 139 [arXiv:1107.3988] [INSPIRE].

[14] M. Döring, U.-G. Meißner, E. Oset and A. Rusetsky, *Scalar mesons moving in a finite volume and the role of partial wave mixing*, *Eur. Phys. J.* **A 48** (2012) 114 [arXiv:1205.4838] [INSPIRE].

[15] A. Martinez Torres, L.R. Dai, C. Koren, D. Jido and E. Oset, *The KD, ηD_s interaction in finite volume and the nature of the $D_{s^*0}(2317)$ resonance*, *Phys. Rev.* **D 85** (2012) 014027 [arXiv:1109.0396] [INSPIRE].

[16] M. Döring and U.-G. Meißner, *Finite volume effects in pion-kaon scattering and reconstruction of the $\kappa(800)$ resonance*, *JHEP* **01** (2012) 009 [arXiv:1111.0616] [INSPIRE].

[17] M. Döring, M. Mai and U.-G. Meißner, *Finite volume effects and quark mass dependence of the $N(1535)$ and $N(1650)$*, *Phys. Lett.* **B 722** (2013) 185 [arXiv:1302.4065] [INSPIRE].

[18] D.R. Bolton, R.A. Briceno and D.J. Wilson, *Connecting physical resonant amplitudes and lattice QCD*, *Phys. Lett.* **B 757** (2016) 50 [arXiv:1507.07928] [INSPIRE].

[19] K. Polejaeva and A. Rusetsky, *Three particles in a finite volume*, *Eur. Phys. J.* **A 48** (2012) 67 [arXiv:1203.1241] [INSPIRE].

[20] R.A. Briceno and Z. Davoudi, *Three-particle scattering amplitudes from a finite volume formalism*, *Phys. Rev.* **D 87** (2013) 094507 [arXiv:1212.3398] [INSPIRE].

[21] M.T. Hansen and S.R. Sharpe, *Relativistic, model-independent, three-particle quantization condition*, *Phys. Rev.* **D 90** (2014) 116003 [arXiv:1408.5933] [INSPIRE].

[22] M.T. Hansen and S.R. Sharpe, *Expressing the three-particle finite-volume spectrum in terms of the three-to-three scattering amplitude*, *Phys. Rev.* **D 92** (2015) 114509 [arXiv:1504.04248] [INSPIRE].

[23] U.-G. Meißner, G. Ríos and A. Rusetsky, *Spectrum of three-body bound states in a finite volume*, *Phys. Rev. Lett.* **114** (2015) 091602 [arXiv:1412.4969] [INSPIRE].

[24] H. Feshbach, *Unified theory of nuclear reactions*, *Annals Phys.* **5** (1958) 357 [INSPIRE].

[25] H. Feshbach, *A unified theory of nuclear reactions. 2*, *Annals Phys.* **19** (1962) 287 [*Erratum ibid.* **281** (2000) 519] [INSPIRE].

JHEP06(2016)043

[26] A.K. Kerman, H. McManus and R.M. Thaler, *The scattering of fast nucleons from nuclei*, *Annals Phys.* **8** (1959) 551 [*Erratum ibid.* **281** (2000) 853][INSPIRE].

[27] P.F. Bedaque, *Aharonov-Bohm effect and nucleon nucleon phase shifts on the lattice*, *Phys. Lett.* **B 593** (2004) 82 [nucl-th/0402051] [INSPIRE].

[28] C.T. Sachrajda and G. Villadoro, *Twisted boundary conditions in lattice simulations*, *Phys. Lett.* **B 609** (2005) 73 [hep-lat/0411033] [INSPIRE].

[29] G.M. de Divitiis, R. Petronzio and N. Tantalo, *On the discretization of physical momenta in lattice QCD*, *Phys. Lett.* **B 595** (2004) 408 [hep-lat/0405002] [INSPIRE].

[30] G.M. de Divitiis and N. Tantalo, *Non leptonic two-body decay amplitudes from finite volume calculations*, hep-lat/0409154 [INSPIRE].

[31] P.F. Bedaque and J.-W. Chen, *Twisted valence quarks and hadron interactions on the lattice*, *Phys. Lett.* **B 616** (2005) 208 [hep-lat/0412023] [INSPIRE].

[32] D. Agadjanov, U.-G. Meißner and A. Rusetsky, *Partial twisting for scalar mesons*, *JHEP* **01** (2014) 103 [arXiv:1310.7183] [INSPIRE].

[33] M. Padmanath, C.B. Lang and S. Prelovsek, $X(3872)$ *and* $Y(4140)$ *using diquark-antidiquark operators with lattice QCD*, *Phys. Rev.* **D 92** (2015) 034501 [arXiv:1503.03257] [INSPIRE].

[34] CLQCD collaboration, Y. Chen et al., *Low-energy scattering of* $(D^*\bar{D}^*)^{\pm}$ *system and the resonance-like structure* $Z_c(4025)$, *Phys. Rev.* **D 92** (2015) 054507 [arXiv:1503.02371] [INSPIRE].

[35] HAL QCD collaboration, N. Ishii et al., *Hadron-hadron interactions from imaginary-time Nambu-Bethe-Salpeter wave function on the lattice*, *Phys. Lett.* **B 712** (2012) 437 [arXiv:1203.3642] [INSPIRE].

[36] S. Aoki, *Nucleon-nucleon interactions via lattice QCD: methodology*, *Eur. Phys. J.* **A 49** (2013) 81 [arXiv:1309.4150] [INSPIRE].

[37] S. Aoki, *Hadron interactions from lattice QCD*, PoS(LATTICE 2007)002 [arXiv:0711.2151] [INSPIRE].

[38] S. Aoki, B. Charron, T. Doi, T. Hatsuda, T. Inoue and N. Ishii, *Construction of energy-independent potentials above inelastic thresholds in quantum field theories*, *Phys. Rev.* **D 87** (2013) 034512 [arXiv:1212.4896] [INSPIRE].

[39] HAL QCD collaboration, K. Sasaki et al., *Coupled-channel approach to strangeness* $S = -2$ *baryon-bayron interactions in lattice QCD*, *Prog. Theor. Exp. Phys.* **2015** (2015) 113B01 [arXiv:1504.01717] [INSPIRE].

[40] S. Aoki, B. Charron, T. Doi, T. Hatsuda, T. Inoue and N. Ishii, *Construction of energy-independent potentials above inelastic thresholds in quantum field theories*, *Phys. Rev.* **D 87** (2013) 034512 [arXiv:1212.4896] [INSPIRE].

[41] T. Kurth, N. Ishii, T. Doi, S. Aoki and T. Hatsuda, *Phase shifts in* $I = 2\pi\pi$*-scattering from two lattice approaches*, *JHEP* **12** (2013) 015 [arXiv:1305.4462] [INSPIRE].

[42] T. Kawanai and S. Sasaki, *Potential description of charmonium and charmed-strange mesons from lattice QCD*, *Phys. Rev.* **D 92** (2015) 094503 [arXiv:1508.02178] [INSPIRE].

[43] V. Bernard, M. Lage, U.-G. Meißner and A. Rusetsky, *Resonance properties from the finite-volume energy spectrum*, *JHEP* **08** (2008) 024 [arXiv:0806.4495] [INSPIRE].

JHEP06(2016)043

CHAPTER 5

Summary

The nature and properties of the recently discovered exotic states cannot be explained within the quark model. Various interpretations have been suggested, such as hadronic molecules, tetraquarks, etc. There is an active ongoing research in this field, both in phenomenology and theory. In the present thesis we developed the finite-volume methods suitable for the study of the exotic states in the framework of Lattice QCD. These methods are also tested for synthetic lattice data. The application of twisted boundary conditions plays the central role. The future applications of these methods in real lattice simulations will potentially reveal more information about exotics. Below we list the main results of the thesis

- In Chapter 2, we explored the possible way to impose twisted boundary conditions in the scalar sector of lattice QCD. It was shown that it is possible to derive a modified Lüscher equation in the presence of quark annihilation diagrams. Although, we focused specifically on the S-wave $\pi\eta - K\bar{K}$ scattering, qualitatively, the result holds true in general case. It can be formulated as a rule of thumb: if a twisted valence quark may annihilate than the corresponding partial twisting is equivalent to no twisting; if the twisted quark propagates through all quark diagrams without annihilating, then the partially twisted Lüscher equation is identical to the fully twisted one.

- In Chapter 3, we developed the method which allows, in principle, to estimate the compositeness of the exotic states. The original idea behind this method goes back to Weinberg, who established the connection between the wave-function renormalization constant Z with the compositeness of the system in question. The value $Z = 0$ corresponds to the predominantly molecular state, whereas $Z = 1$ signals a loosely bound one. We formulated the lattice version of this criterion, using partially twisted boundary conditions, which in principle allows to study the compositeness content of the exotic states in lattice simulations. The method was tested for the $D^*_{s0}(2317)$ meson, which favours a molecular picture due to closeness to the DK threshold, using synthetic lattice data generated from the leading order heavy flavour chiral Lagrangian. The resulting finite-volume effect from twisting is twice as large as the one without twisting. We further performed an error analysis to estimate the accuracy of extraction of Z for different lattice sizes, input lattice errors and the number of data points.

- In Chapter 4, we suggested and tested the new method, suitable for the study of the exotic states, such as XYZ states as well as $a_0(980)$ resonance, etc. Our method solves in principle the problem associated with the solution of the multi-channel Lüscher equation, which is relevant for the exotic systems. The key idea of the approach is to extract the complex hadron-hadron potential from lattice simulations, applying the twisted boundary conditions. We tested the procedure of extraction of the optical potential with synthetic lattice data, generated for the $\pi\eta - K\bar{K}$ system.

Furtheremore, we checked that, for input uncertanties of the energy levels equal to 2 MeV and 3 MeV, the imaginary and real parts can be reliably extracted. In addition, the imaginary part is more sensitive to the input error and, at a higher error values of 10 MeV, the fit is not reliable anymore.